National Library
of Canada

Bibliothèque nationale
du Canada

Canadian Theses Service

Services des thèses canadiennes

Ottawa, Canada
K1A 0N4

CANADIAN THESES

THÈSES CANADIENNES

NOTICE

The quality of this microfiche is heavily dependent upon the quality of the original thesis submitted for microfilming. Every effort has been made to ensure the highest quality of reproduction possible.

If pages are missing, contact the university which granted the degree.

Some pages may have indistinct print especially if the original pages were typed with a poor typewriter ribbon or if the university sent us an inferior photocopy.

Previously copyrighted materials (journal articles, published tests, etc.) are not filmed.

Reproduction in full or in part of this film is governed by the Canadian Copyright Act, R.S.C. 1970, c. C-30.

AVIS

La qualité de cette microfiche dépend grandement de la qualité de la thèse soumise au microfilmage. Nous avons tout fait pour assurer une qualité supérieure de reproduction.

S'il manque des pages, veuillez communiquer avec l'université qui a conféré le grade.

La qualité d'impression de certaines pages peut laisser à désirer, surtout si les pages originales ont été dactylographiées à l'aide d'un ruban usé ou si l'université nous a fait parvenir une photocopie de qualité inférieure.

Les documents qui font déjà l'objet d'un droit d'auteur (articles de revue, examens publiés, etc.) ne sont pas microfilmés.

La reproduction, même partielle, de ce microfilm est soumise à la Loi canadienne sur le droit d'auteur, SRC 1970, c. C-30.

THIS DISSERTATION
HAS BEEN MICROFILMED
EXACTLY AS RECEIVED

LA THÈSE A ÉTÉ
MICROFILMÉE TELLE QUE
NOUS L'AVONS REÇUE

NL-339 (r.86/06)

Canada

THE UNIVERSITY OF ALBERTA

Sedimentology of the Lower Cambrian Gog Group, British Columbia,: An early Cambrian tidal deposit

by

Andrew Charles Wolberg

A THESIS
SUBMITTED TO THE FACULTY OF GRADUATE STUDIES AND RESEARCH
IN PARTIAL FULFILMENT OF THE REQUIREMENTS FOR THE DEGREE
OF Master of Science

Geology

EDMONTON, ALBERTA
Spring, 1986

Permission has been granted to the National Library of Canada to microfilm this thesis and to lend or sell copies of the film.

The author (copyright owner) has reserved other publication rights, and neither the thesis nor extensive extracts from it may be printed or otherwise reproduced without his/her written permission.

L'autorisation a été accordée à la Bibliothèque nationale du Canada de microfilmer cette thèse et de prêter ou de vendre des exemplaires du film.

L'auteur (titulaire du droit d'auteur) se réserve les autres droits de publication; ni la thèse ni de longs extraits de celle-ci ne doivent être imprimés ou autrement reproduits sans son autorisation écrite.

ISBN 0-315-30238-0

Geological Association of Canada
Association géologique du Canada

Geological Survey of Canada
601 Booth Street
Ottawa, Ontario K1A 0E8

Andrew Wolberg
Department of Geology
University of Alberta
Edmonton, Alberta
T6G 2E3

25 March 1986

Dear Mr. Wolberg:

Your letter requesting permission to reproduce a figure from one of our publications has been forwarded to me. I am pleased, on behalf of the Geological Association of Canada, to grant permission for you to reproduce Figure 32 on page 161 of Geoscience Canada Reprint Series No.1, *Facies Models* in your thesis on Lower Cambrian tidal deposits.

Yours sincerely,

Godfrey S. Nowlan

Godfrey S. Nowlan
Chairman, Publications Committee

President
J.A. Coope
Newmont Exploration of Canada Ltd.
33 Yonge Street, Suite 370
Toronto, Ontario
M5E 1T2
(416) 362-1688

Vice-President
G.D. Mossop
Alberta Geological Survey
Alberta Research Council
4445 Calgary Trail South
Edmonton, Alberta T6H 5R7
(403) 438-0555

Secretary-Treasurer
J.G. Malpas
Department of Earth Sciences
Memorial University of Newfoundland
St. John's, Newfoundland
A1B 3X5
(709) 737-7660

THE UNIVERSITY OF ALBERTA

RELEASE FORM

NAME OF AUTHOR Andrew Charles Wolberg

TITLE OF THESIS Sedimentology of the Lower Cambrian Gog Group, British Columbia,:
An early Cambrian tidal deposit

DEGREE FOR WHICH THESIS WAS PRESENTED Master of Science

YEAR THIS DEGREE GRANTED Spring, 1986

Permission is hereby granted to THE UNIVERSITY OF ALBERTA LIBRARY to reproduce single copies of this thesis and to lend or sell such copies for private, scholarly or scientific research purposes only.

The author reserves other publication rights, and neither the thesis nor extensive extracts from it may be printed or otherwise reproduced without the author's written permission.

(SIGNED) Andrew Wolberg

PERMANENT ADDRESS:
4018 Manitou Way
Madison, Wisconsin
53711 United States

DATED April 21st 1986

THE UNIVERSITY OF ALBERTA

FACULTY OF GRADUATE STUDIES AND RESEARCH

The undersigned certify that they have read, and recommend to the Faculty of Graduate Studies and Research, for acceptance, a thesis entitled Sedimentology of the Lower Cambrian Gog Group, British Columbia,: An early Cambrian tidal deposit submitted by Andrew Charles Wolberg in partial fulfilment of the requirements for the degree of Master of Science.

Francis J. Hein

Supervisor

Stelck

Date April 21st 1986

Dedication

This thesis is dedicated
to the loving memory of my grandfather
Dr. Otto A. Mortensen

ABSTRACT

The Lower Cambrian Gog Group comprises a laterally extensive, quartzite-dominated sequence up to 3 km thick which unconformably overlies the Upper Miette (Hadrynian-age) sediments of the Hector Formation. Exposures of the Gog Group located near Sink Lake consist of thickly-bedded, medium- to coarsely-crystalline quartzites with slaty shale and shale interbeds. At this locality the Gog Group shows excellent examples of bidirectional cross-bedding in sets between 20 to 80 cm thick. In addition, the Gog Group shows well preserved master bedding sequences, sandwave complexes and thin graded layers interbedded within slaty shales.

The Lower Cambrian Gog sediments at Sink Lake are thought to have been deposited on a tidally-dominated, open continental shelf between the distal inner and proximal middle shelf regions. This is supported by a suite of sedimentary structures suggestive of tidal environments, the textural and mineralogical maturity of the sediments, the absence of both foreshore-shoreface features and evidence of emergence structures, and by a trace fossil assemblage (*Cruziana* ichnofacies) characteristic of a shallow marine setting.

The most important evidence supporting a tidal interpretation is the presence of adjacent sets of cross-stratification showing bimodal-bipolar paleocurrent patterns. Further substantiation of a tidal origin is indicated by the occurrence of reactivation surfaces and thin mud drapes in sets of cross-bedding. In addition, the presence of sandwave complexes and master bedding sequences are characteristic of ancient and modern tide-dominated shelves. Consequently, these observations support the interpretation that the Lower Cambrian Gog Group located in Yoho National Park near Sink Lake represents an offshore, open marine, tidally-dominated stratigraphic unit.

Acknowledgements

Appreciation is expressed to Dr. Fran J. Hein, especially her patience and understanding throughout the course of this thesis. Financial assistance from the Natural Sciences and Engineering Research Council of Canada along with permission to collect samples from Parks Canada is gratefully acknowledged. Also, I would like to thank Grant Millner and Lisa Brattland for very capable and spirited field assistance.

I gratefully recognize the never-ending encouragement, invaluable support and thoughtful suggestions of my true friend R. William Arnott. His knowledge in sedimentology contributed immeasurably to this thesis. In addition, he never seemed to grow impatient after the daily barrage of questions or ideas, and for this my sincere thanks. Most importantly, I am deeply indebted to Dr. S.G. Pemberton, for without his constant encouragement, generosity and interest in sedimentology over the years, this thesis would not have been possible.

Endlich möchte ich meiner geliebten Frau Linda Aschenbrenner herzlich danken. Mit grosser Geduld und tiefem Verständnis hat sie die letzten strapazierenden Jahre "mitgelitten." Noch einmal aufrichtigen Dank.

Table of Contents

Chapter Page

1. INTRODUCTION 1
   - 1.1 LOCATION AND ACCESS 1
   - 1.2 PURPOSE OF STUDY 1
   - 1.3 METHODS 3
   - 1.4 PREVIOUS WORK: LOWER CAMBRIAN STRATIGRAPHIC UNITS IN THE SOUTHERN CANADIAN ROCKY MOUNTAINS 3
   - 1.5 REGIONAL STRATIGRAPHY 7
   - 1.6 LOCAL STRATIGRAPHY 15
   - 1.7 REGIONAL AND TECTONIC SETTING 16
   - 1.8 STRUCTURAL GEOLOGY 17
2. CURRENTS AND SEDIMENTATION ON MODERN CONTINENTAL SHELVES 21
   - 2.1 CONTINENTAL SHELF CURRENTS 21
     - 2.1.1 OCEANIC CURRENTS 21
     - 2.1.2 TIDES 23
     - 2.1.3 METEOROLOGICAL FORCES 25
     - 2.1.4 SEDIMENT GRAVITY FLOWS 26
   - 2.2 RECENT CONTINENTAL SHELF SEDIMENTATION 28
     - 2.2.1 OCEANIC CURRENT SEDIMENTATION 28
     - 2.2.2 STORM-DOMINATED SHELF SEDIMENTATION 29
     - 2.2.3 TIDE-DOMINATED SHELF SEDIMENTATION 32
3. FACIES DESCRIPTIONS AND INTERPRETATIONS 39
   - 3.1 FACIES SCHEME 39
     - 3.1.1 FACIES OUTLINE 44
     - 3.1.2 FACIES 1: INTERBEDDED SLATY SHALE AND VERY-FINE TO MEDIUM-CRYSTALLINE QUARTZITES 46
     - 3.1.3 SUBFACIES 1A: INTERBEDDED SLATY SHALE AND MASSIVE QUARTZITES 48
     - 3.1.4 SUBFACIES 1B: INTERBEDDED SLATY SHALE AND STRATIFIED VERY-FINE- TO MEDIUM-CRYSTALLINE QUARTZITES 48
     - 3.1.5 SUBFACIES 1C: INTERBEDDED SLATY SHALE AND GRADED QUARTZITES 48

3.1.6 SUBFACIES 1D: INTERBEDDED SLATY SHALE AND BIOTURBATED / BURROWED QUARTZITES 50

3.1.7 SUBFACIES 1E: FINE- TO MEDIUM-CRYSTALLINE QUARTZITE WITH THIN ARGILLACEOUS INTERBEDS 50

3.1.8 FACIES 2: SHALE AND SLATY SHALE 52

3.1.9 FACIES 3: GRADED MATRIX-SUPPORTED PEBBLE CONGLOMERATE 52

3.1.10 FACIES 4: SMALL-SCALE TROUGH AND PLANAR CROSS-STRATIFIED QUARTZITES 55

3.1.11 FACIES 5: PLANAR CROSS-STRATIFIED QUARTZITES 55

3.1.12 SUBFACIES 5A: PLANAR CROSS-BEDDED SETS (0.05 - 0.4 M THICK) 57

3.1.13 SUBFACIES 5B: PLANAR CROSS-BEDDED SETS (0.4 - 2 M THICK) 57

3.1.14 FACIES 6: TROUGH CROSS-BEDDED QUARTZITES 59

3.1.15 SUBFACIES 6A: TROUGH CROSS-BEDDED SETS (0.05 - 0.4 M THICK) 59

3.1.16 SUBFACIES 6B: TROUGH CROSS-BEDDED SETS (0.4 - 1 M THICK) 61

3.1.17 FACIES 7: LOW ANGLE AND HORIZONTALLY STRATIFIED QUARTZITES 61

3.1.18 FACIES 8: MASSIVE QUARTZITES 64

3.2 FACIES INTERPRETATIONS 64

3.2.1 FACIES 1 64

3.2.2 SUBFACIES 1A: INTERBEDDED SLATY SHALE AND MASSIVE QUARTZITES 65

3.2.3 SUBFACIES 1B: INTERBEDDED SLATY SHALE AND STRATIFIED VERY-FINE-TO MEDIUM-CRYSTALLINE QUARTZITES 65

3.2.4 SUBFACIES 1C: INTERBEDDED SLATY SHALE AND GRADED QUARTZITES 68

3.2.5 SUBFACIES 1D: INTERBEDDED SLATY SHALE AND BIOTURBATED / BURROWED QUARTZITES 68

3.2.6 SUBFACIES 1E: FINE- TO MEDIUM-CRYSTALLINE QUARTZITE WITH THIN ARGILLACEOUS INTERBEDS 69

3.2.7 FACIES 2: SHALE AND SLATY SHALE 69

3.2.8 FACIES 3: GRADED MATRIX-SUPPORTED PEBBLE CONGLOMERATE 70

3.2.9 FACIES 4: SMALL-SCALE CROSS-STRATIFIED QUARTZITES 71

3.2.10 SUBFACIES 5A: PLANAR CROSS-BEDDED SETS (0.05 - 0.4 M THICK) 73

3.2.11 SUBFACIES 5B: PLANAR CROSS-BEDDED SETS (0.4 - 2 M THICK) 74

3.2.12 SUBFACIES 6A: TROUGH CROSS-BEDDED SETS (0.05 - 0.4 M THICK) 77

3.2.13 SUBFACIES 6B: TROUGH CROSS-BEDDED SETS (0.4 - 1 M THICK) 78

3.2.14 FACIES 7: LOW ANGLE AND HORIZONTALLY STRATIFIED QUARTZITES 79

3.2.15 FACIES 8: MASSIVE QUARTZITES 82

4. PALEOCURRENT ANALYSIS OF THE GOG SEDIMENTS AT SINK LAKE, BRITISH COLUMBIA 84

4.1 METHODS OF PALEOCURRENT ANALYSIS 84

4.2 PALEOCURRENT DATA FOR OUTCROP A 85

4.3 PALEOCURRENT DATA FOR OUTCROP B 87

4.4 PALEOCURRENT DATA FOR OUTCROP C 89

4.5 PALEOCURRENT DATA FOR OUTCROP D 92

5. VERTICAL FACIES RELATIONSHIPS AND ASSOCIATIONS 93

5.1 INTRODUCTION 93

5.2 EMBEDDED AND NON-EMBEDDED MARKOVIAN METHODS 93

5.3 FACIES ASSOCIATIONS 95

5.3.1 COARSE-GRAINED FACIES ASSOCIATION 99

5.3.2 COARSE/FINE-GRAINED INTERCALATED FACIES ASSOCIATION 105

5.4 INTERPRETATION OF THE COARSE-GRAINED FACIES ASSOCIATION 109

5.5 INTERPRETATION FOR THE COARSE/FINE-GRAINED INTERCALATED FACIES ASSOCIATION 112

6. DEPOSITIONAL MODEL FOR THE LOWER CAMBRIAN GOG GROUP 114

6.1 TRACE FOSSILS OF THE LOWER CAMBRIAN GOG GROUP 120

6.2 PALEOGEOGRAPHY OF THE LOWER CAMBRIAN GOG GROUP 121

7. REFERENCES CITED 126

8. APPENDIX I 135

9. APPENDIX II 166

10. APPENDIX III 175

LIST OF TABLES

Table 3.1. Table showing the percentages of facies and average bed thickness comprising the four outcrops 45

Table 3.2. Summary of facies 63

Table 5.1. Interpretations of the salient facies transitions occurring within the four outcrops .98

Table 5.2. Table showing the precentages of facies and average bed thickness comprising the two facies associations 100

Table 5.3. Non-embedded tally matrix for the Coarse-grained Facies Association 176

Table 5.4. Non-embedded observed probability matrix for the Coarse-grained Facies Association 177

Table 5.5. Non-embedded random probability matrix for the Coarse-grained Facies Association 178

Table 5.6. Non-embedded difference matrix for the Coarse-grained Facies Association 179

Table 5.7. Embedded tally matrix for the Coarse/Fine-grained Intercalated Facies Association 180

Table 5.8. Embedded observed probability matrix for the Coarse/Fine-grained Intercalated Facies Association 181

Table 5.9. Embedded random probability matrix for the Coarse/Fine-grained Intercalated Facies Association 182

Table 5.10. Embedded difference matrix for the Coarse/Fine-grained Intercalated Facies Association 183

Table 5.11. Non-embedded tally matrix for outcrop A 184

Table 5.12. Non-embedded observed probability matrix for outcrop A 185

Table 5.13. Non-embedded random probability matrix for outcrop A 186

Table 5.14. Non-embedded difference matrix for outcrop A 187

Table 5.15. Embedded tally matrix for outcrop B 188

Table 5.16. Embedded observed probability matrix for outcrop B.................................. 189

Table 5.17. Embedded random probability matrix for outcrop B.................................... 190

Table 5.18. Embedded difference matrix for outcrop B 191

Table 5.19. Embedded tally matrix for outcrop C 192

Table 5.20. Embedded observed probability matrix for outcrop C 193

Table 5.21. Embedded random probability matrix for outcrop C.................................... 194

Table 5.22. Embedded difference matrix for outcrop C 195

Table 5.23. Non-embedded tally matrix for outcrop D.. 196

Table 5.24. Non-embedded observed probability matrix for outcrop D 197

Table 5.25. Non-embedded random probability matrix for outcrop D 198

Table 5.26. Non-embedded difference matrix for outcrop D... 199

LIST OF FIGURES

Figure 1.1. Location of the four major outcrops at Sink Lake 2

Figure 1.2. Regional location map 4

Figure 1.3. Table of Formations for the late Proterozoic and early Paleozoic strata in the Canadian Rocky Mountains 8

Figure 1.4. Location of areas between the Kicking Horse Pass and Mount Assiniboine.......... 11

Figure 1.5. Structural subprovinces in the southern Cordilleran region 18

Figure 1.6. Generalized structure map of the Sink Lake region 20

Figure 2.1. Diagram illustrating the horizontal component of the tide-producing forces acting on the ocean surface and the corresponding tidal bulges 24

Figure 2.2. Phases of the moon and their associated spring and neap tides.. 24

Figure 2.3. Block diagram of the main tidal bedform zones on a tidally-dominated continental shelf 33

Figure 3.1. Histogram indicating the percentages of facies comprising outcrop A 40

Figure 3.2. Histogram indicating the precentages of facies comprising outcrop B................ 41

Figure 3.3. Histogram indicating the precentages of facies comprising outcrop C 42

Figure 3.4. Histogram indicating the precentages of facies comprising outcrop D 43

Figure 3.5. Photograph of Subfacies 1a: Interbedded slaty shale and massive quartzites........ 47

Figure 3.6. Photograph of Subfacies 1b: Interbedded slaty shale and stratified quartzites...... 47

Figure 3.7. Photograph of Subfacies 1c: Interbedded slaty shale and graded quartzites 49

Figure 3.8. Photograph of Subfacies 1c showing small-scale cross-lamination located in the upper portion of the bed 49

Figure 3.9. Photograph of Subfacies 1d: Interbedded slaty shale and bioturbated/burrowed quartzite 51

Figure 3.10. Photograph of Subfacies 1e: Fine- to medium-crystalline quartzite with thin argillaceous interbeds 51

Figure 3.11. Photograph of Facies 2: Shale and slaty shale 53

Figure 3.12. Photograph of Facies 3: Graded matrix-supported pebble conglomerate 54

Figure 3.13. Photograph of Facies 3 showing small-scale trough cross-lamination located in the upper portion of the bed 54

Figure 3.14. Photograph of Facies 4: Small-scale trough and planar cross-stratified quartzites 56

Figure 3.15. Photogragh of Subfacies 5a: Planar cross-bedded sets (0.05 - 0.4 m thick) 56

Figure 3.16. Photograph of subfacies 5a showing lateral variation in crystallinity between adjacent foresets 58

Figure 3.17. Photograph of Subfacies 5b: Planar cross-bedded sets (0.4 - 2 m thick) 58

Figure 3.18. Photograph of Subfacies 6a: Trough cross-bedded sets (0.05 - 0.4 m thick) 60

Figure 3.19. Photograph of Subfacies 6b: Trough cross-bedded sets (0.4 - 2 m thick) 60

Figure 3.20. Photograph of Facies 7: Low angle and horizontally stratified quartzites 62

Figure 3.21. Photograph of Facies 8: Massive quartzites 62

Figure 3.22. Depth-velocity diagram for fine-grained sand 67

Figure 3.23. Bedform stability plots on a size-velocity diagram 72

Figure 3.24. Schematic diagram of flow pattern and resulting deposition of backflow ripples in the lee face of a bedform 76

Figure 3.25. Block diagram of hummocky cross-stratification 80

Figure 4.1. Rose diagram recording the rotated paleocurrent data for outcrop A 86

Figure 4.2. Rose diagram recording the rotated paleocurrent data for outcrop B 86

Figure 4.3. Photograph showing bidirectional cross-stratification of Subfacies 5a beds at outcrop B........88

Figure 4.4. Rose diagram recording the rotated paleocurrent data for outcrop C........91

Figure 4.5. Photograph showing bidirectional cross-bedding at outcrop C........90

Figure 4.6. Rose diagram recording the rotated paleocurrent data for outcrop D........91

Figure 5.1. Facies relationship diagram for outcrop A........96

Figure 5.2. Facies relationship diagram for outcrop B........96

Figure 5.3. Facies relationship diagram for outcrop C........97

Figure 5.4. Facies relationship diagram for outcrop D........97

Figure 5.5. Photograph of a master bedding surface........101

Figure 5.6. Lithologic correlation diagram for outcrop A........(in pocket)

Figure 5.7. Sandwave complex at outcrop D........103

Figure 5.8. Facies relationship diagram for the Coarse-grained Facies Association........104

Figure 5.9. Lithologic correlation diagram for outcrop B........(in pocket)

Figure 5.10. Lithologic correlation diagram for the sections at outcrop B which are perpendicular to the east-west outcrop face........(in pocket)

Figure 5.11. Lithologic correlation diagram for outcrop C........(in pocket)

Figure 5.12. Lithologic correlation diagram for outcrop D........(in pocket)

Figure 5.13. Photograph showing the lateral transition of planar cross-bedding into trough cross-bedding........107

Figure 5.14. Photograph of the lateral facies relationship between a planar cross-stratified quartzite bed and small-scale cross-stratified quartzites........107

Figure 5.15. Facies relationship diagram for the Coarse/Fine-grained Intercalated Facies Association........104

Figure 5.16. Diagram of Allen's theoretical sandwave model 110

Figure 6.1. Block diagram of the Lower Cambrian tidally-dominated continental shelf illustrating the depositional provinces corresponding to the two facies associations....... 116

Figure 6.2. 10° rose diagram for the Coarse-grained Facies Association 118

Figure 6.3. 10° rose diagram for the Coarse/Fine-grained Intercalated Facies Association ... 118

Figure 6.4. Cambrian paleogeographic map 123

Figure 7.1. Lithologic symbols and sedimentary structures 136

1. INTRODUCTION

1.1 LOCATION AND ACCESS

The study area is located in Yoho National Park, near Sink Lake, 51° 28' North latitude and 116° 18' West longitude, in the Main Ranges of the Canadian Rocky Mountains. Sink Lake is situated approximately two kilometers west of the Alberta-British Columbia border in terrain dominated by grassy slopes and moderately forested areas.

In this study, four Lower Cambrian outcrops were selected for detailed measurement. They occur along the north side of the Trans-Canada Highway as small cliff-forming sequences generally 5 to 15 meters high and several tens of meters long. These exposures are excellent with no vegetation cover and show minimal tectonic disturbance other than a gentle westward tilting. Most of the outcrops are not laterally continuous and are cut by possible small-scale normal faults, which prevent the lateral traceability of individual beds between outcrops.

Outcrops A and B are located just a few meters north of the Trans-Canada Highway and are readily accessible by foot (Fig. 1.1). Vehicles can be parked directly across from the exposures at the Sink Lake pinic area on the south side of the Trans-Canada Highway. The other two main outcrops, C and D, selected for detailed facies analysis, are located a few hundred meters from the culvert running underneath the highway. Access is by a short walk up a small avalanche chute filled with talus consisting of large quartzite boulders.

1.2 PURPOSE OF STUDY

In the geological record there are only a few examples of ancient tide-dominated outer shelf sand bodies. Outcrops of the Lower Cambrian Gog Group located in Yoho National Park near Sink Lake, B.C., appear to support another example of an offshore, open marine, tidally-dominated stratigraphic unit. In recent years, the presence of tidal and storm deposits has been increasingly recognized, but detailed information regarding their internal structures and lateral relationships have yet to be well documented.

Most ancient examples for tide-dominated shelves are from either nearshore or inshore environments. This research on the Lower Cambrian Gog Group provides an example and important insight into tidally-controlled offshore sand bodies and also our understanding of the depositional processes on tidally-dominated offshore shelves during a time of continuous rapid

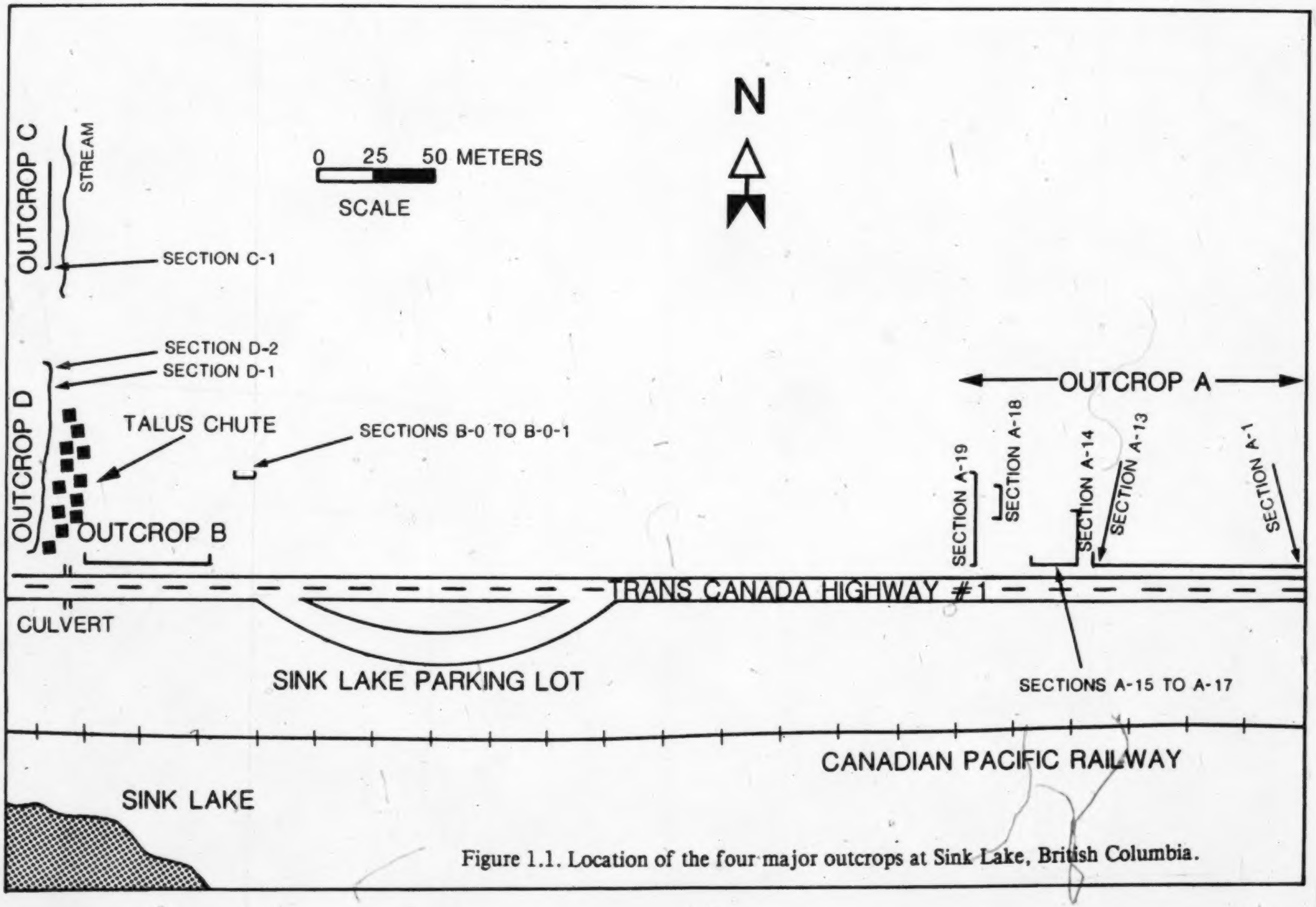
N
0
25
50 METERS
SCALE
OUTCROP C
STREAM
SECTION C-1
SECTION D-2
SECTION D-1
OUTCROP D
TALUS CHUTE
SECTIONS B-0 TO B-0-1
OUTCROP B
OUTCROP A
SECTION A-19
SECTION A-18
SECTION A-14
SECTION A-13
SECTION A-1
TRANS CANADA HIGHWAY #1
CULVERT
SINK LAKE PARKING LOT
SECTIONS A-15 TO A-17
CANADIAN PACIFIC RAILWAY
SINK LAKE

Figure 1.1. Location of the four major outcrops at Sink Lake, British Columbia.

subsidence.

The purpose of this study is to conduct a detailed facies analysis of the various tidal and storm deposits observed in the transgressive offshore Gog sediments. In addition, detailed studies were conducted on the facies relationships within preserved sandwave complexes. Emphasis is placed on a careful examination of the internal structures, three-dimensional geometry and characteristic associations of sedimentary structures. Large-scale vertical and lateral facies relationships will be studied in detail in order to develop a model for tidally-controlled outer shelf deposition.

1.3 METHODS

The Lower Cambrian Gog outcrops located near Sink Lake, B.C., were studied during the summer of 1984. The study approach used in this analysis consisted of detailed description of individual beds at four selected outcrops located along the north side of the Trans-Canada Highway. Here the Gog Group outcrops as small cliff-forming sequences and approximately 500 meters of vertical section was measured on a bed-by-bed basis as 47 vertical transits along the four major outcrops. Particular emphasis was placed on describing the sedimentary structures, bed thickness, bed geometries, basal bed contacts, crystallinity, and biogenic structures. The beds were divided into 8 facies based largely on sedimentary structures, bed thickness and apparent grain size. The lateral and vertical facies relationships were mapped at each study location. In addition, trough-axis orientations and maximum foreset dip directions were measured to determine paleocurrent patterns. The paleocurrent data was corrected for tectonic tilt and restored back to the original horizontal attitude using a FORTRAN 77 program (H.A.K. Charlesworth, 1986, personal communication).

1.4 PREVIOUS WORK: LOWER CAMBRIAN STRATIGRAPHIC UNITS IN THE SOUTHERN CANADIAN ROCKY MOUNTAINS

Early geological reconnaissance of the Lower Cambrian sediments within the Bow Valley and Kicking Horse Pass region of the southern Canadian Rocky Mountians (for regional correlation locations refer to Figures 1.2, 1.4 and 1.5) was first attempted by McConnell in 1887. He measured a generalized section in the vicinity of Castle Mountain and proceeded to subdivide the rocks into the following two groups. The Castle Mountain Group, consisting

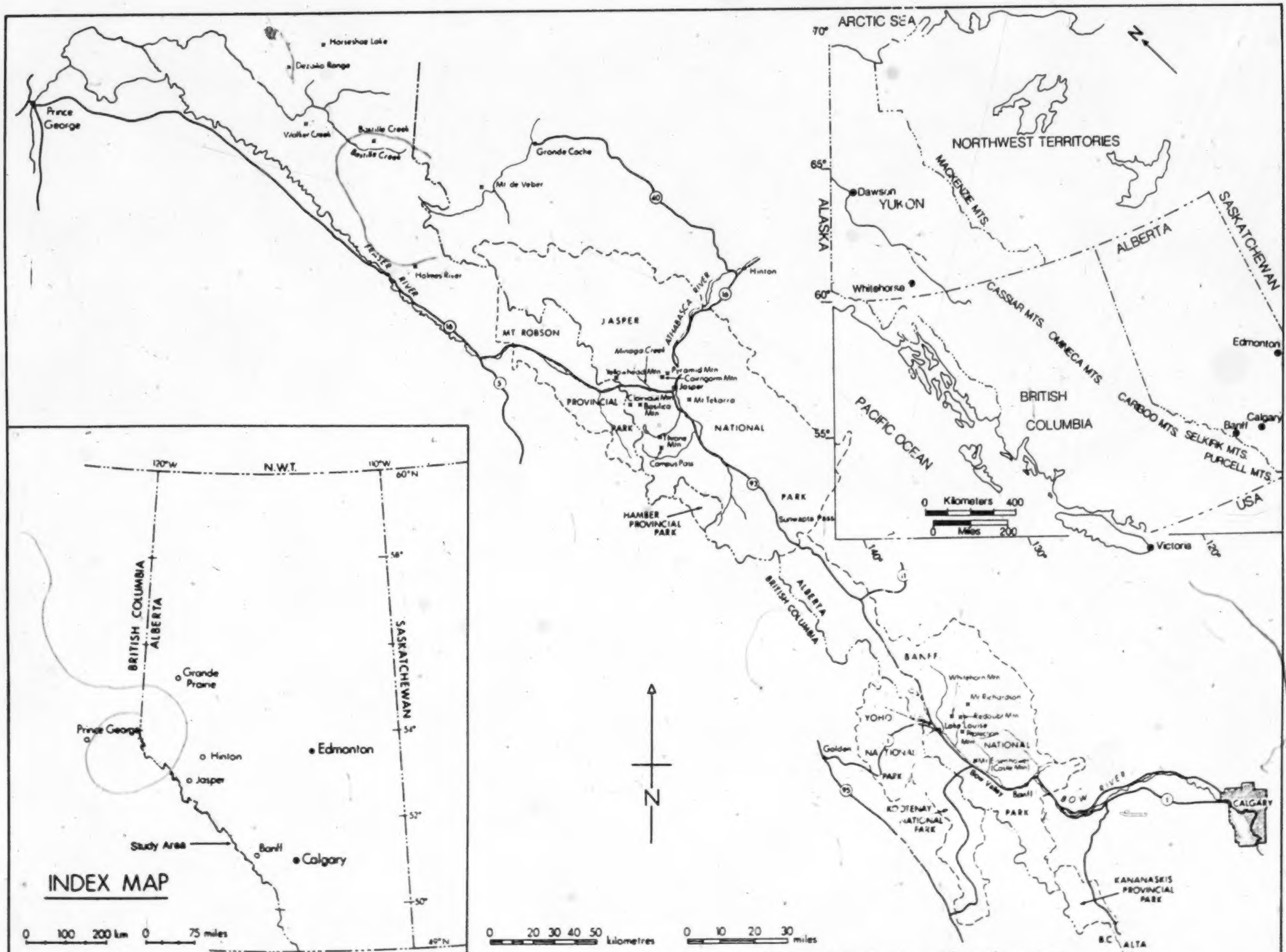
Prince George
Horseshoe Lake
Dezaiko Range
Walker Creek
Bastille Creek
Bastille Creek
Grande Cache
Mt de Veber
Holmes River
FRASER RIVER
16
5
MT ROBSON
JASPER
ATHABASCA RIVER
Hinton
16
Minaga Creek
Yellowhead Mtn
Pyramid Mtn
Cairngorm Mtn
Jasper
Clairvaux Mtn
Basilica Mtn
Mt Tekarra
PROVINCIAL
PARK
NATIONAL
Throne Mtn
Cavell Pass
HAMBER PROVINCIAL PARK
93
PARK
Sunwapta Pass
ALBERTA
BRITISH COLUMBIA
11
BANFF
Whitehorn Mtn
Mt Richardson
Redoubt Mtn
Lake Louise
Protection Mtn
NATIONAL
Mt Eisenhower (Castle Mtn)
YOHO
NATIONAL
PARK
Golden
1
95
KOOTENAY NATIONAL PARK
Bow Valley
Banff
BOW RIVER
PARK
1
CALGARY
KANANASKIS PROVINCIAL PARK
B.C.
ALTA
N
0 20 30 40 50 kilometres
0 10 20 30 miles
ARCTIC SEA
70°
N
NORTHWEST TERRITORIES
MACKENZIE MTS.
65°
Dawson
YUKON
ALASKA
Whitehorse
60°
SASKATCHEWAN
ALBERTA
CASSIAR MTS.
OMINECA MTS.
Edmonton
BRITISH COLUMBIA
CARIBOO MTS.
SELKIRK MTS.
PURCELL MTS.
Banff
Calgary
55°
PACIFIC OCEAN
0 Kilometers 400
0 Miles 200
USA
140°
130°
120°
Victoria
120°W
N.W.T.
110°W
60°N
58°
BRITISH COLUMBIA
ALBERTA
SASKATCHEWAN
Grande Prairie
Prince George
54°
Hinton
Edmonton
Jasper
52°
Study Area
Banff
Calgary
INDEX MAP
50°
0 100 200 km
0 75 miles
49°N
U.S.A.

Figure 1.2. Regional location map.

mostly of limestone and dolomites (which are now assigned to the Cambrian and Ordovician) and the underlying clastic sediments belonging to the Bow Valley Group which contained quartzites and argillites (presently assigned to the Lower Cambrian and late Hadrynian). McConnell in 1889 extended the terminology westward to Mount Stephen near Field, British Columbia. In the following years Dawson (1901) reexamined the Cambrian strata at Mount Stephen and Castle Mountain and revised the descriptions of the Bow River and Castle Mountain groups.

In 1907 Walcott measured the Castle Mountain, Mount Bosworth and the lower portion of the Mount Stephen and Mount Whyte sections. The following year Walcott (1908a, 1908b) published a detailed measured section of Mount Bosworth which contained more than 12,000 feet (3657 m) of conformable strata. Consequently, the section was often cited in the literature dealing with Cambrian stratigraphy as one of the most complete sections of Cambrian strata in the Canadian Cordillera. After measuring Cambrian sections in the vicinity of the 51° North parallel, Walcott (1908a, 1908b) was the first to subdivide and establish a sequence of formations for the Lower Cambrian sediments in the Bow Valley and Kicking Horse Pass region. He recognized four formations for the basal Cambrian clastic sediments, which are, from oldest to youngest: Fairview, Lake Louise, St. Piran and Mount Whyte.

Walcott in 1912 reviewed the Mount Bosworth section and changed the lowest Cambrian formation from Fairview to Fort Mountain (Walcott, 1912) because of its prior usage in American stratigraphic nomenclature. He also changed the "type" locality to Fort Mountain, presently known as Redoubt Mountain. Walcott never published a stratigraphic succession of the rocks on Redoubt Mountain, however,he did measure a generalized section 3 miles (4.8 km) to the north on the eastern side of Ptarmigan Peak. In 1914 Allan (1914) reviewed the Cambrian stratigraphy near Field, B.C. and compiled the first geological map of the Cambrian rocks of the area using Walcott's formational terminology for rocks corresponding to the Lower and Middle Cambrian.

In 1928 Resser compiled all Walcott's original measured sections in the southern Canadian Rockies, including the first detailed stratigraphic sections from Castle Mountain and Ptarmigan Peak (Walcott, 1928). This comprehensive summary of early Paleozoic type sections measured by Walcott in Alberta and British Columbia along with an unfinished manuscript by Walcott was published posthumously by Resser.

Deiss (1939) remeasured Castle Mountain, Ptarmigan Peak and Ross Lake which were originally defined by Walcott. He amended the definitions of the Fort Mountain, St. Piran and Mount Whyte formations of the Lower Cambrian and the Ptarmigan, Cathedral and Eldon Formations of the Middle Cambrian. Unfortunately, when revising the original Fort Mountain Formation, Deiss erred in the stratigraphic position of the Lower Cambrian basal contact in the vicinity of Ptarmigan Peak and Redoubt Mountain. The thin basal conglomerate believed to be part of the Lower Cambrian Fort Mountain Formation is actually a conglomerate lens within slates of the Precambrian (late Hadrynian) Hector Formation (Aitken, 1969).

In the following year, Deiss (1940) continued to remeasure and amend several of Walcott's original type sections in the southern Cordilleran region. The Mounts Bosworth and Assiniboine sections were examined and remeasured in order to compare with the original sections. Deiss noted a major discrepancy dealing with the thickness of the Lower Cambrian Fort Mountain, Lake Louise and St. Piran Formations when comparing the original and amended Mount Bosworth section. When the lower part of the original section was measured by Walcott (1908a, 1908b), the thickness of the last unit was 503 feet (153 m) of exposed St. Piran quartzite. The underlying formations were not measured because of the isolated nature of the outcrops and therefore, prohibiting a continuous stratigraphic sequence. However, the published Mount Bosworth section contained 2705 feet (824 m) of St. Piran quartzite, 105 feet (32 m) of Lake Louise shale and over 600 feet (183 m) of Fort Mountain quartzite. This confusion over the Lower Cambrian stratigraphy in the original section resulted because Walcott added beds from the Lake Louise and Lake Agnes section, located 8 km southeast, which contain a complete and well exposed sequence through the Lower Cambrain Lake Louise and Fort Mountain formations. Therefore, the lower part of Walcott's original Mount Bosworth section was actually a composite section from two separate localities, published under the single heading of Mount Bosworth. This error was finally corrected in Deiss's amended section and the total measured thickness of strata on Mount Bosworth was corrected to slightly over 6300 feet (1920 m) instead of 12,353 feet (3765 m) originally measured by Walcott.

Mountjoy and Aitken (1963) measured the prominent cross-bedding within the Lower Cambrian clastic sediments in Jasper National Park. The corresponding paleocurrents indicated that during the Lower Cambrian the direction of sedimentary transport was towards the west and southwest, suggesting that the Precambrian basement rocks of the Canadian Shield formed an eastern landmass which was the major source of sediment during Lower Cambrian time.

Palonen (1976) studied the sedimentology and stratigraphy of the Gog Group sandstones in the southern Canadian Rockies between Lake Louise and Jasper. He divided the Lower Cambrian Gog Group into seven units based on the resistant and recessive nature of the exposure. These alternating units corresponded to three large-scale transgressive and regressive shallow marine cycles. The study included a comprehensive summary of the regional stratigraphy of the Lower Cambrian Gog Group within the Main Ranges of the southern Canadian Rockies.

Recently, a detailed sedimentologic study of the Lower Cambrian St. Piran quartzites was conducted by Hein (1982, 1986) and Hein and Arnott (1983) near the Spiral Tunnels Lookout in Yoho National Park. The research concentrated on a detailed facies analysis of the various shallow marine deposits and paleocurrent patterns recorded by the prominent cross-bedding within the quartzite beds.

1.5 REGIONAL STRATIGRAPHY

Regional stratigraphic correlation and the establishment of formal nomenclature is very difficult in the southern Canadian Cordillera because of the local distribution and the wide variations in thickness and lithology of the Lower Cambrian sediments along with the absence of diagnostic fossil assemblages (Mountjoy, 1962; Young, 1979; Palonen, 1976). Despite this, numerous studies have attempted to regionally correlate the clastic sediments located above the late Precambrian Miette Group and stratigraphically beneath the Middle Cambrian carbonate succession within the Canadian Rocky Mountains (Fig. 1.3).

The contact with the underlying Precambrian (Hadrynian-age) sedimentary rocks has long been a source of controversy. Part of the confusion surrounding the nature and stratigraphic position of the Cambrian-Precambrian contact was caused by previous workers experiencing difficulty in distinguishing the basal conglomerates of the Gog Group from the underlying feldspathic, vein-quartz pebble conglomerates in the Miette Group. The upper portion of the Hector Formation (highest recognized stratigraphic formation within the Miette Group) contains discontinuous conglomerate lenses interbedded within purple and green slates. The delineation of the Miette-Gog contact is extremely difficult when these conglomerate-bearing lenses directly underlie the basal pebble conglomerates of the Lower

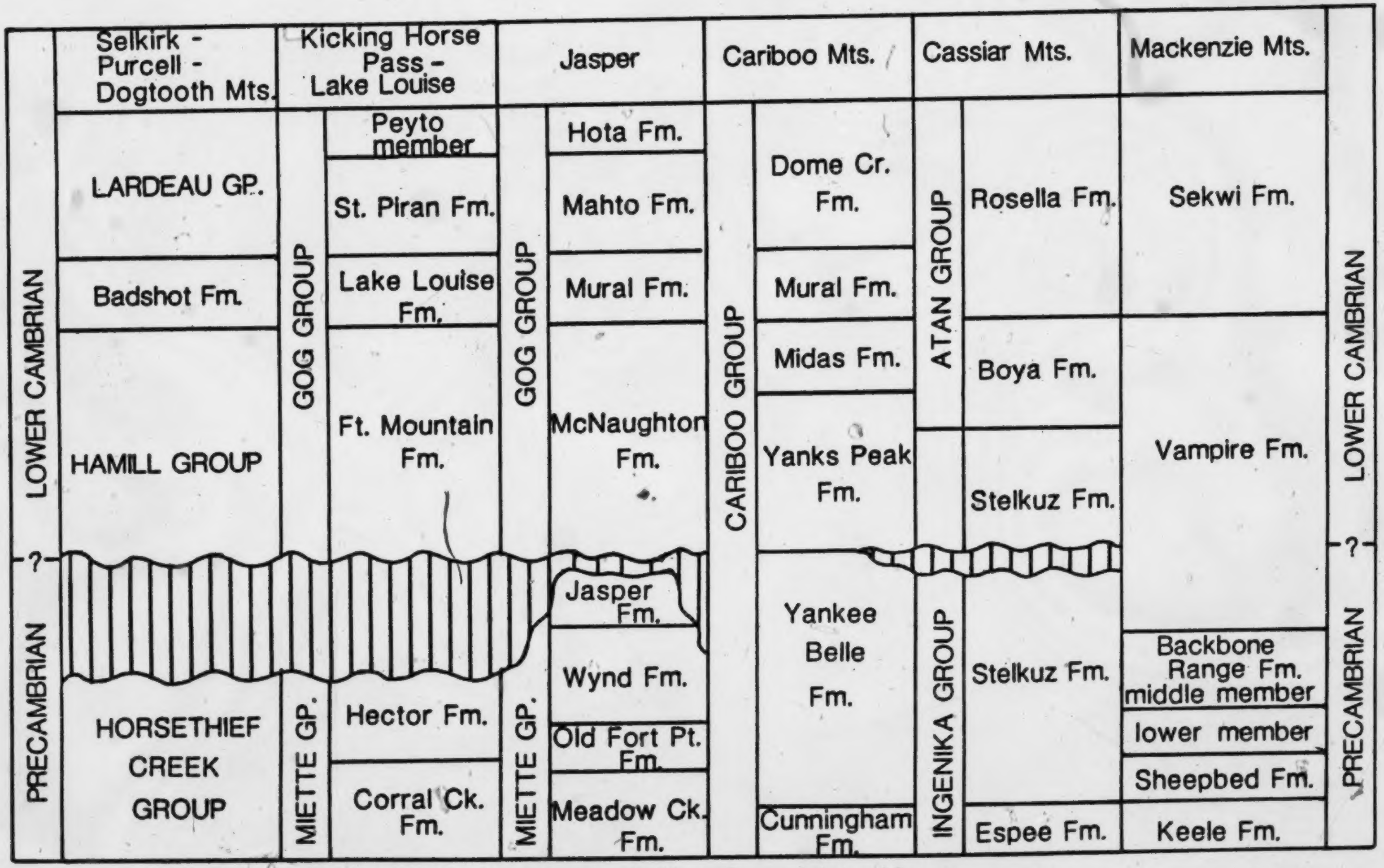
LOWER CAMBRIAN
?
PRECAMBRIAN
Selkirk - Purcell - Dogtooth Mts.
LARDEAU GP.
Badshot Fm.
HAMILL GROUP
HORSETHIEF CREEK GROUP
GOG GROUP
MIETTE GP.
Kicking Horse Pass - Lake Louise
Peyto member
St. Piran Fm.
Lake Louise Fm.
Ft. Mountain Fm.
Hector Fm.
Corral Ck. Fm.
GOG GROUP
MIETTE GP.
Jasper
Hota Fm.
Mahto Fm.
Mural Fm.
McNaughton Fm.
Jasper Fm.
Wynd Fm.
Old Fort Pt. Fm.
Meadow Ck. Fm.
CARIBOO GROUP
Cariboo Mts.
Dome Cr. Fm.
Mural Fm.
Midas Fm.
Yanks Peak Fm.
Yankee Belle Fm.
Cunningham Fm.
ATAN GROUP
INGENIKA GROUP
Cassiar Mts.
Rosella Fm.
Boya Fm.
Stelkuz Fm.
Stelkuz Fm.
Espee Fm.
Mackenzie Mts.
Sekwi Fm.
Vampire Fm.
Backbone Range Fm. middle member
lower member
Sheepbed Fm.
Keele Fm.
LOWER CAMBRIAN
?
PRECAMBRIAN

Figure 1.3. Regional correlation chart showing the Upper Precambrian and Lower Cambrian strata in the Canadian Rocky Mountains (modified from correlation charts given by Fritz, 1985 and Hein and Arnott, 1983).

Cambrian Gog Group.

Walcott (1910) was the first to describe the Lower Cambrian-Precambrian boundary in the vicinity of Redoubt Mountain and Ptarmigan Peak, where the contact between the Fort Mountain quartzites and the underlying Hector shales is well exposed. He concluded that the contact was unconformable and represented a significant stratigraphic and erosional break between the two formations. Unfortunately, Walcott (1910) and Deiss (1939) failed to correctly locate the base of the Lower Cambrian quartzite sequence because they placed the Cambrian-Precambrian contact at the base of a series of Miette conglomeratic lenses. However in the "type" Gog section at Mount Assiniboine, Deiss (1940) correctly noted a major erosional surface at the base of the Lower Cambrian Gog quartzite.

In the Jasper area early work by Walcott (1913) presented evidence that the contact between the Gog and Miette Group sediments was unconformable and separated by a distinct erosional surface. Subsequent work by Charlesworth *et al.* (1967) concluded that the contact separating the Lower Cambrian and Precambrian sediments was locally conformable and apparently gradational.

Aitken (1969) extensively examined the Lower Cambrian- Precambrian contact in the Bow Valley and Lake Louise region and resolved the problems surrounding the correct stratigraphic placement and nature of the contact. He documented the existence of a major regional unconformity separating the Miette and Gog groups sediments in the Main Ranges of the southern Canadian Rocky Mountains. The nature of the Cambrian-Precambrian contact was examined in the Jasper area and evidence was cited which indicated the presence of a unconformity at the base of the Lower Cambrian. This was futher substantiated in the Yellowhead Pass region by Teitz and Mountjoy (1985) who observed a distinct disconformity (unconformity between parallel strata) in the form of a karst surface between the Gog Group and the carbonate unit located at the top of the upper Miette group.

Directly overlying the Cambrian-Precambrian boundary in the southern Rocky Mountains is a laterally extensive and vertically thick sequence of thickly-bedded quartzites or clean quartz sandstone with slaty shale and shale interbeds. As previously mentioned, in the area between Castle Mountain (Mt. Eisenhower) and Yoho National Park, Walcott (1908a, 1908a, 1912) subdivided this Lower Cambrian terrigenous clastic succession into four formations. These formations are, in ascending stratigraphic order, the Fort Mountain, Lake

Louise, St. Piran and Mount Whyte which forms the basis of the present nomenclature applicable to the stratigraphic succession of the Lower Cambrian Gog Group in the Bow Valley- Lake Louise- Kicking Horse Pass region.

The Middle-Lower Cambrian boundary, originally placed at the top of the carbonate-bearing Mount Whyte Formation, was questioned by Burling (1914, 1922) based on paleontologic evidence. He demonstrated that the Mount Whyte Formation contains trilobite fossils which are Middle Cambrian in age, except in the lower part. Consequently, the Middle-Lower Cambrian boundary should have been placed at a lower position within the Mount Whyte Formation. This controversy was settled by Rasetti (1951) who transfered the boundary to a stratigraphically lower position and assigned the Peyto Limestone Member to the Lower Cambrain. The overlying carbonate sequence of Walcott's original Mount Whyte Formation still retained the same formational nomenclature and was assigned to the Middle Cambrian (Rasetti, 1951).

Walcott (1928) extended the application of the Lower Cambrian terminology from the original "type" locality located in the vicinity of Lake Louise, southeastward to the Mount Assiniboine region. However, Deiss (1940) recognized that the rocks originally assigned to the Mount Whyte Formation by Walcott were actually basal Middle Cambrian in age based upon the occurrence of Middle Cambrian trilobites. Therefore, he suggested that the basal Cambrian clastic sequence at the Mount Assiniboine section was stratigraphically equivalent to the Mount Whyte and St. Piran formations in the Bow Valley- Lake Louise region. This correlation was based on the presence of *Olenellus* located several hundred feet below the Middle-Lower Cambrian boundary and the absence of the Mount Whyte Formation in the Assiniboine area. Deiss advocated that the formerly assigned terms "St. Piran, Lake Louise and Fort Mountain" in the original Mount Assiniboine section (Walcott, 1928) be discarded and these basal clastic sediments be placed in a new formation called the "Gog". The Gog Formation is named after Gog Lake located at the north edge of Naiset Point and the "type" locality is on the north side of the Assiniboine Massif at the base of Mount Towers (Fig. 1.4).

Early stratigraphic classification of the Lower Cambrian sediments in the Jasper region was first attempted by Walcott (1913). He recognized the following four formations: the McNaughton (basal quartzitic sandstone), Tah (limestone), Mahto (quartzitic sandstone), and the Hota (upper arenaceous limestone). The Lower Cambrian to Middle Cambrian boundary

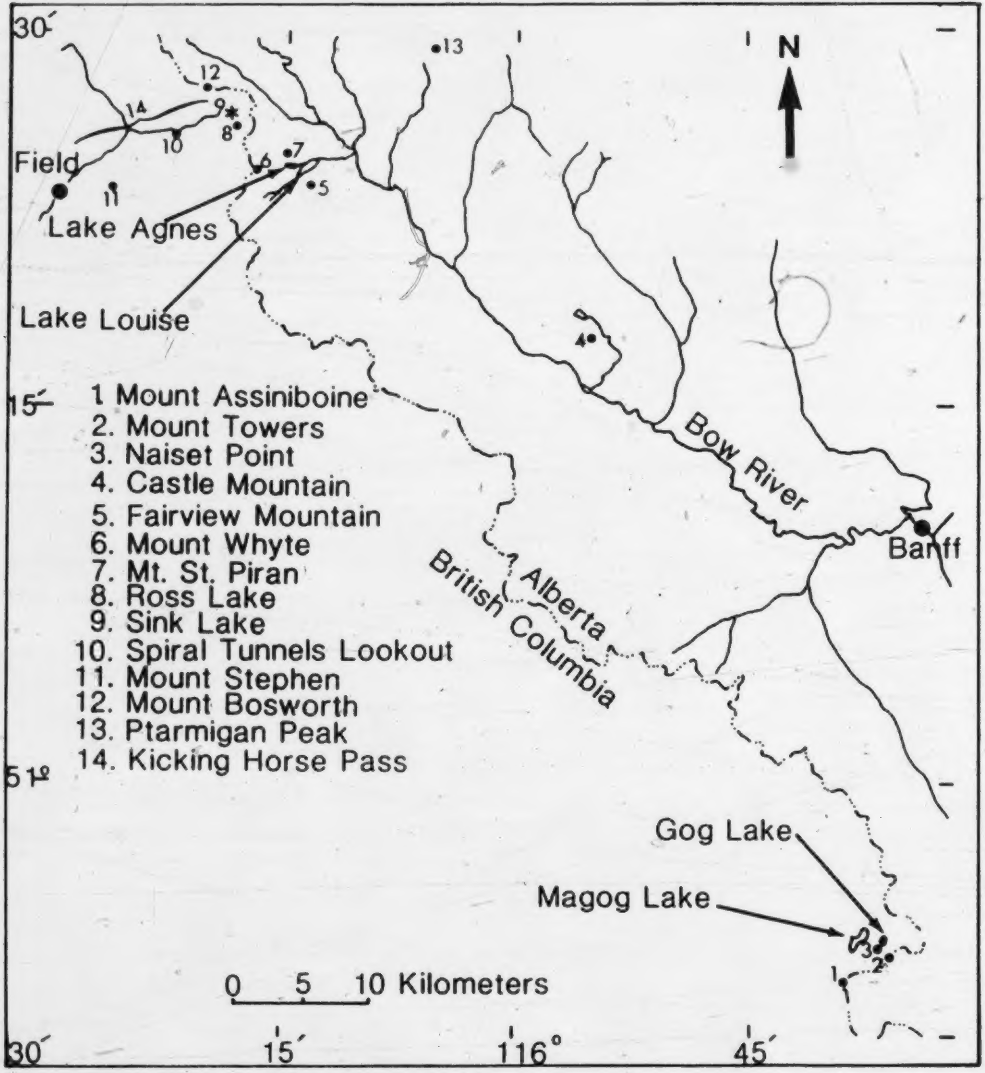
30′
•13
N
12
14
9
8
10
Field
•7
6
•5
11
Lake Agnes
Lake Louise
4
15′
1 Mount Assiniboine
2. Mount Towers
3. Naiset Point
4. Castle Mountain
5. Fairview Mountain
6. Mount Whyte
7. Mt. St. Piran
8. Ross Lake
9. Sink Lake
10. Spiral Tunnels Lookout
11. Mount Stephen
12. Mount Bosworth
13. Ptarmigan Peak
14. Kicking Horse Pass
Bow River
Banff
Alberta
British Columbia
51°
Gog Lake
Magog Lake
3
2
1
0 5 10 Kilometers
30′
15′
116°
45′

Figure 1.4. Location map of the southern Canadian Rockies between the Kicking Horse Pass area and Mount Assiniboine.

was placed at the contact separating the Hota and overlying Chetang formations. Burling (1923) reexamined the paleontology of the Hota Formation and suggested that the Lower-Middle Cambrian boundary be transferred to the base of the Hota Formation. He advocated that the Hota be assigned to the Middle Cambrian and renamed the Adolphus Formation, and that the Tah Formation be discarded in favor of the Mural Formation.

Mountjoy (1962) investigated the age relationships and stratigraphy concerning the Lower Cambrian rocks in the Jasper area and consequently raised the thick succession of fine to coarse clastic sediments occupying the Lower Cambrian within the southern Canadian Mountains to group status. The newly proposed "Gog Group" incorporates the quartzite-dominated sequence occurring stratigraphically above the Hector slates of the Miette Group and directly beneath the Middle Cambrian carbonates. The terminology proposed by Hughes (1955) for the Lower Cambrian strata in the Sunwapta Pass region (the Jonas Creek Formation) was discarded because the previous terminology advocated by Walcott was found acceptable in the Jasper region.

Fritz and Mountjoy (1975) reviewed the age, stratigraphy and nomenclature of the Lower Cambrian formations in Jasper National Park. According to Fritz and Mountjoy the Lower-Middle Cambrian boundary was correctly placed by Walcott (1913) at the top of the Hota. They noted that Burlings attempt to change the position of the boundary was incorrect because he misinterpreted the age of Lower Cambrian fauna within the Hota Formation by assigning the fossils to the Middle Cambrian. Fritz and Mountjoy advocated that the terms "McNaughton, Mural, Matho, and Hota" be the formational nomenclature assigned to the Lower Cambrian succession in the Jasper region.

Over the last few decades many regional correlation attempts have been made on the Lower Cambrian rocks in the Main Ranges of the Canadian Rockies. However, regional stratigraphic correlations are often difficult in the Canadian Mountains because of the lack of Early Cambrian fossils, confusion over the basal contact and the wide variations in thickness and lithology of the Lower Cambrian strata.

In the Jasper area, Charlesworth *et al.* (1967) suggested, based on lithological similarity, that the Upper Precambrian Meadow Creek, Old Fort Point and Wynd Formations occupy the same stratigraphic position as the Hector and Corral Creek Formations (Miette Group) in the Lake Louise region. In addition they suggested that the Jasper Formation was stratigraphically equivalent to the lower part of the Gog Group in the vicinity of Lake Louise. Young (1979) also correlated the conglomeratic, feldspathic quartzite of the Jasper Formation with the basal feldspathic sediments of the McNaughton Formation, the lowest formation of the Gog Group. Thus the Jasper Formation was assigned to the Gog Group in Jasper National Park and localities in west-central Alberta.

However, Palonen (1976) questioned this regional correlation of the Jasper Formation with the Fort Mountain Formation because of the absence of feldspathic quartzite in the basal portion of the Gog Group at Lake Louise. He points out that there is no southern lithologic equivalent of the Jasper Formation and that either the deposition of the feldspathic sediments did not occur at Lake Louise or that the feldspathic unit was eroded before the subsequent deposition of the Gog Group.

As a result of a study on the Lower Paleozoic and Proterozoic sediments exposed between Jasper, Alberta and Pine River, British Columbia, Slind and Perkins (1966) extended the Lower Cambrian strata westward using the three-fold subdividison McNaughton, Mural and Mahto. Evidence of an erosional contact between the McNaughton Formation and the Precambrian Miette Group was observed in the vicinity of Horseshoe Lake B.C. and they suggested that the contact was unconformable throughout the study area.

On the east side of the Rocky Mountain Trench the Lower Cambrian terrigenous clastic succession comprising the Gog Group is exposed in the Canadian Rockies from Mount Assiniboine to the Pine River district. To the northwest, in north-central British Columbia the Gog Group is equivalent to the upper part of the Misinchinka Group and an unnamed overlying Lower Cambrian unit (Gabrielse, 1975).

Young (1979) studied the stratigraphy, sedimentology and age relationships of the Lower Cambrian McNaughton Formation located northwest of Jasper National Park and the equivalent strata of the Cariboo Group in the northern Cariboo Mountains, east of Prince George. In this study Young correlated the lowest formation of the Gog Group -the McNaughton Formation- westward across the Rocky Mountain Trench to the stratigraphically equivalent upper Yankee Belle, Yanks Peak, and Midas Formations of the Cariboo Group.

In the vicinity of Field, B.C. the quartzite-dominated sequence of the Gog Group disappears beneath the Middle Cambrian Chancellor Formation and is not exposed at the surface in the western Main Ranges and the Western Ranges of the Rockies. Farther west, in the mountainous region of the southeastern British Columbia these Lower Cambrian quartzites reappear west of the Rocky Mountain Trench as the Hamill Group in the Selkirk-Purcell-Dogtooth Mountains, and as the Cranbrook Formation in the vicinity of Cranbrook (Evans, 1933; Okulitch, 1949, 1956). The Lower Cambrian Hamill Group and overlying Badshot Formation and Lardeau Group rest unconformably on the Hadrynian Horsethief Creek Group (Fig. 1.3)(Poulton and Simony, 1980). This regional correlation of the Lower Cambrian Hamill Group and Cranbrook Formation with the Gog Group of the southern part of the Rockies was based on lithologic similarity and the occurrence of Olenellid trilobites in the upper carbonate units in both localities.

In the Cassiar Mountains of north-central British Columbia, the early Paleozoic and late Proterozoic strata are contained within the Boya and Rosella formations of the Atan Group (Lower Cambrian) and the Espee and Stelkuz formations of the Ingenika Group (Upper Precambrian and early Lower Cambrian)(Fritz, 1980a, 1985). The Precambrian-Cambrian boundary is tentatively located in the upper part of the Stelkuz Formation (Fritz, 1980a). The regional correlation between the Atan Group and the Stelkuz Formation with equivalent strata in the Jasper area (Fig. 1.3) suggests that the Rosella Formation is correlated with the Mural, Mahto and Hota formations while the Boya and Stelkuz (uppermost part) formations are equated with the McNaughton Formation (Fritz, 1980a).

North of the Cariboo Mountains, in the west-central Mackenzie Mountains, the stratigraphic succession of late Precambrian and Lower Cambrian sediments has recently been studied (Fritz, 1980b, 1982, 1985). The predominantly clastic sequence is divided into the early Lower Cambrian Vampire Formation and the overlying Sekwi Formation. The Precambrian-Cambrian boundary is placed within the lower part of the Vampire Formation (Fritz, 1982). Stratigraphic correlations between the Mackenzie and Cassiar Mountains (Fig. 1.3) indicates that the Sekwi Formation is equivalent to the Rosella Formation, whereas the Boya Formation correlates to the upper portion of the Vampire Formation (Fritz, 1980a).

The thick clastic succession of mountain-forming Gog Group, abruptly thins eastward in the subsurface of central Alberta. These early Paleozoic Gog sediments of the Main Ranges are tentatively correlated to the "Basal Sandstone" unit of the Alberta Plain. The "Basal Sandstone" rests unconformably on the Precambrian igneous and metamorphic rocks of the

Canadian Shield and eventually pinch out against rocks of the Hudsonian basement in southeastern Alberta (Aitken, 1968; Pugh, 1971, 1973, 1975).

1.6 LOCAL STRATIGRAPHY

In the Bow Valley-Lake Louise region of the southern Canadian Rockies the Lower Cambrian is dominated by a laterally extensive and vertically thick accumulation of quartzites with slaty shale or shale interbeds. In this area, the rocks comprise a terrigenous clastic succession which attains a maximum thickness of 1,273 meters (Walcott, 1928). They rest on a major regional unconformity eroded into the underlying rocks of the Windermere Supergroup consisting largely of non-fossiliferous conglomerate, quartzite and slate. This thick, monotonous succession of the Lower Cambrian quartzite in the Bow valley-Lake Louise region was stratigraphically sub-divided into four formations based primarily on lithology (Walcott, 1908a, 1908b, 1912).

The lowermost formation of the Gog Group is the Fort Mountain, composed predominantly of thickly-bedded quartzites with slaty shale interbeds and subsidiary conglomerates. The most noticeable feature of this formation is the ubiquitous cross-stratification within the quartzite beds. The Fort Mountain Formation is overlain by the Lake Louise Formation, consisting of pale-green and maroon non-fossiliferous shale with less common thin-bedded quartzitic sandstone. The Lake Louise shale varies considerably in thickness from 105 feet (32 m) at the type locality near Lake Louise to 28 feet (8.5 m) in the Mount Assiniboine area, a distance of 97 kilometers. Consequently, Deiss (1939) among others questioned the formational status given to the Lake Louise "Formation" and believes the unit is only a locally developed shale lentil and therefore should be considered a member of the Fort Mountain Formation. The overlying St. Piran Formation is predominantly a cliff-forming quartzite succession with shale interbeds. Prominent cross-stratification occurs within the quartzite beds. Conformably overlying this quartzite-dominated sequence and representing the top of the Lower Cambrian is the Peyto Limestone Member of the Mount Whyte Formation. The Peyto Limestone contains abundant Olenellid fauna and drastically varies in thickness from 60 meters thick, to being locally absent (Cook, 1975). This evidence suggests an erosional unconformity at the top of the Peyto Limestone Member.

1.7 REGIONAL AND TECTONIC SETTING

The Lower Cambrian sedimentary sequence of the Gog Group forms part of a narrow, sinuous belt of late Proterozoic and early Paleozoic strata extending for 4050 km along the western coast of North America. These Upper Precambrian and Lower Cambrian sediments confined within this linear trough setting are made up mainly of non-volcanic supracrustal rocks. This miogeoclinal setting (volcanism is not associated with sedimentation) drastically thickens in a westward direction from being regionally absent on the craton to the east to more than 7,500 meters thick, over a distance of a few hundred kilometers. This vertically thick accumulation of coarse clastic sediments present in the early Paleozoic Cordilleran miogeocline represents a westwardly thickening sedimentary prism of shallow marine shelf to slope deposits (Monger *et al.*, 1972; Stewart, 1972; Bond and Kominz, 1984). The existence of the thick accumulation of continental shelf to deep-water slope assemblages composing the miogeoclinal wedge were interpreted as evidence for continental separation during the latest Precambrian or earliest Cambrian (600 Ma to 555 Ma)(Monger *et al.*, 1972; Stewart, 1972; Bond and Kominz, 1984). The Gog sediments represent deposition along the western trailing edge of the Cambrian passive continental margin during the post-rift or drift phase (Bond and Kominz, 1984). The major stratigraphic hiatus separating the Miette and Gog Group sediments in the southern Canadian Rockies is probably similar to the breakup unconformity separating the syn-rift and post-rift sediments on modern continental margins (Bond and Kominz, 1984). Arnott and Hein (1986) suggest that this sub-Cambrian unconformity is associated with the spreading of the proto-Pacific ocean during the pre-Drift phase. Consequently the actual rift unconformity which represents an early episodic rift orogenic phase is at the base of the Hector Formation. The coarse clastic detritus was shed along the extensive proto-Pacific continental platform during a time of continuous and uniform tectonic subsidence (Stewart, 1972). This clastic deposition, once initiated, kept pace with the continuous subsidence resulting in the accumulation of up to 3 kilometers (Young, 1979) of shallow marine sandstone and shale comprising the Lower Cambrian Gog Group.

The continental shelf during the Lower Cambrian was orientated in a north-south direction and extended westward past the present day Rocky Mountain Trench (Stelck and Hedinger, 1975). Outcrops of the Lower Cambrian shoreline deposits are very rare in the southern Canadian Rockies. However, stratigraphically the Gog Group thins laterally in the subsurface near Banff suggesting the relative position of the paleoshoreline (C.R. Stelck, 1985, personal communication). Paleodispersal within the Gog Group is reflected by the prominent cross-bedding within the quartzite beds. This indicates that the Lower Cambrian sediments of the Cordilleran miogeocline were probably derived from the erosion of the Precambrian crystalline basement rocks of the Canadian Shield to the east and transported to the proto-Pacific continental margin by southwest flowing currents (Mountjoy and Aitken, 1963).

A topographically positive area, referred to as "Montania" was situated near the Columbia River region of British Columbia and Washington. The amount of coarse clastic sediment this landmass supplied to the passive margin during Cambrian time is still in question (Walcott, 1927, 1928; Mountjoy and Aitken, 1963; Young, 1979). However, it appears Montania had no major influence on the deposition of clastics except locally along its western edge (Mountjoy and Aitken, 1963).

1.8 STRUCTURAL GEOLOGY

The Canadian Rockies is a linear belt of castellated mountain ranges which rise to elevations between 2,100 and 3,600 meters above sea level. This distinctive and narrow physiographic province is composed of a north-easterly tapering Helikian to Late Jurassic miogeocline-platform assemblage reaching a maxium thickness of 12 km to 14 km. This sequence is succeeded by a 6 km thick clastic wedge of late Mesozoic to Early Tertiary sediments. The deposition of clastic wedges along the foreland margin of the Cordillera which initiated in the Late Jurassic indicates the onset of a large-scale orogeny. This sequence of Late Jurassic to Early Tertiary clastic wedge deposits records the thrusting and folding associated with the major mountain building event of the Laramide phase of the Columbian Orogeny (Taylor *et al.*, 1964).

The Rocky Mountain System which is located between the Interior Plains and the Rocky Mountain Trench is divided into four distinctive, subparallel structural subprovinces based on changes in the topographic and structural style and lithology. The series of subprovinces in the southern Canadian Rocky Mountains are from east to west: the Foothills, Front Ranges, Main Ranges, and Western Ranges (North and Henderson, 1954)(Fig. 1.5).

The location of the study area lies entirely within the eastern part of the Main Ranges subprovince. The Main Ranges structural subprovince represents the topographic and structural

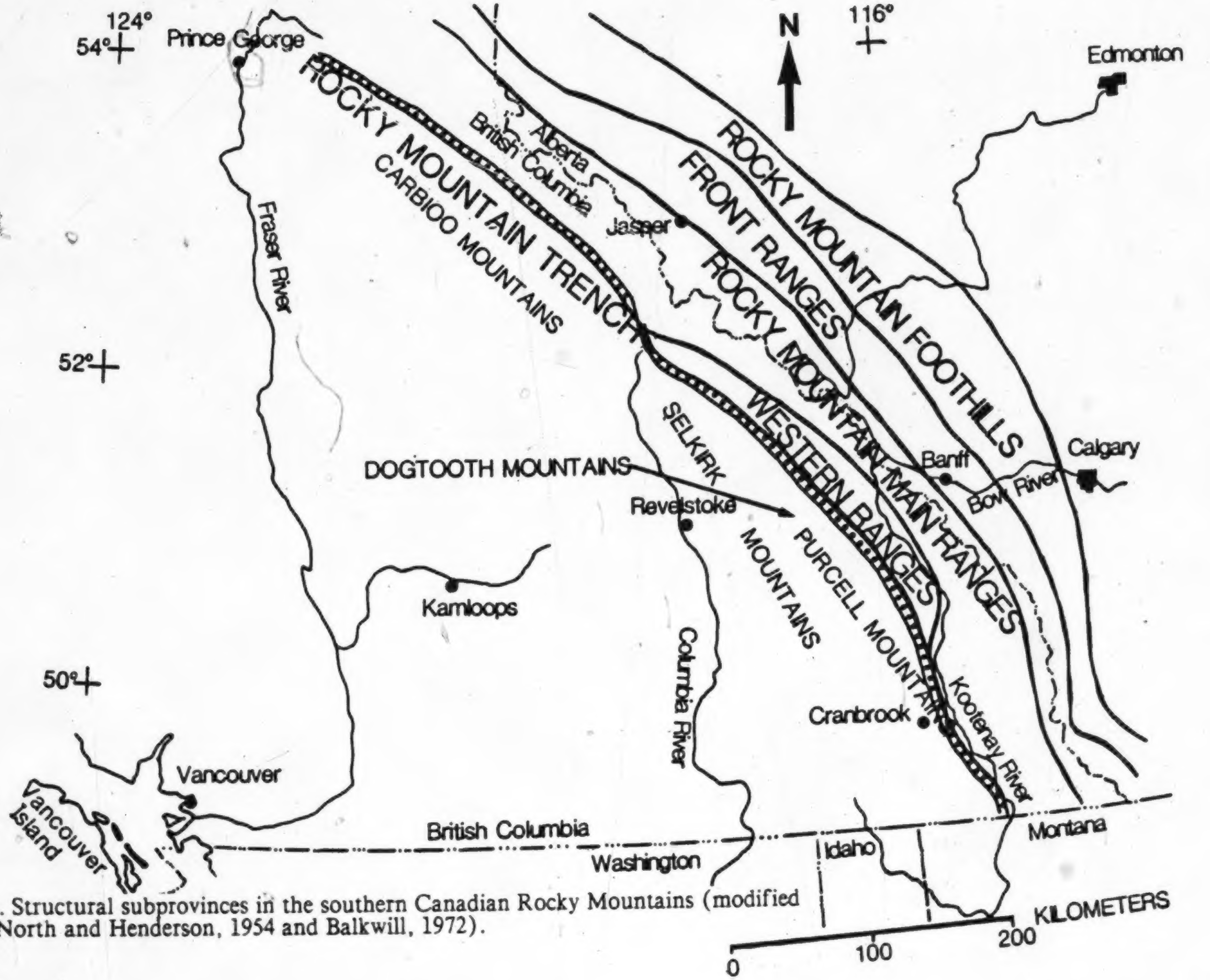
124°
54°
116°
N
52°
50°
Prince George
Edmonton
Fraser River
ROCKY MOUNTAIN TRENCH
CARBIOO MOUNTAINS
Alberta
British Columbia
Jasper
ROCKY MOUNTAIN FOOTHILLS
FRONT RANGES
ROCKY MOUNTAIN MAIN RANGES
WESTERN RANGES
SELKIRK
DOGTOOTH MOUNTAINS
Revelstoke
Banff
Calgary
Bow River
Kamloops
MOUNTAINS
PURCELL MOUNTAINS
Columbia River
Cranbrook
Kootenay River
Vancouver
Vancouver Island
British Columbia
Washington
Idaho
Montana
0
100
200
KILOMETERS

Figure 1.5. Structural subprovinces in the southern Canadian Rocky Mountains (modified after North and Henderson, 1954 and Balkwill, 1972).

culmination within the Rockies. The eastern sector of the Main Ranges is characterized by relatively flat-lying beds, broad open folds and flat, simple thrust sheets (Price and Mountjoy, 1970). The structural style in the eastern Main Ranges is related to the competence and anisotropic character of the Upper Precambrian to Middle Cambrian strata. Consequently, the thick, competent, quartzite-dominated sequence of the Lower Cambrian Gog Group strongly influences the geometry of the folds which are characteristically broad and open (Balkwill, 1972). The broadly folded Upper Precambrian and Lower to Middle Cambrian strata within the eastern Main Ranges are cut by a set of northly-trending *en echelon* normal gravity faults which generally dip to the west (Price and Mountjoy, 1970; Cook, 1975). One of the major contributors to the structural style in the eastern Main Ranges are the southwest dipping thrust faults which are generally concave upwards in profile and are infered not to intersect the Hudsonian crystalline basement beneath the Rocky Mountains (Price *et al.*, 1972). In the vicinity of Sink Lake the Simpson Pass Thrust underlies the mountain-forming rocks of this study area (Fig. 1.6). The surface trace of this remarkable thrust fault extends for more than 320 km along the length of the eastern Main Ranges from Mount Assiniboine to near Jasper (Price *et al.*, 1972).

The Sink Lake section lies on the easterly-dipping limb of the Sherbrooke Lake Syncline. The measured sections only show a slight variation in bedding plane orientations and average 262°/12° SW. The Lower Cambrian Gog Group at Sink Lake is exposed as a series of gently westwardly-dipping ridges which show minimal tectonic deformation. The slaty shale interbeds commonly exhibit well developed slaty cleavage, however, penetrative deformation within the quartzite beds is virtually absent. The ridges are not laterally continuous but are disrupted by series of sub-parallel, possible small-scale normal faults which trend north or north-northwesterly. However, the local structure is poorly documented in the area and the size and displacement of the faults are difficult to determine.

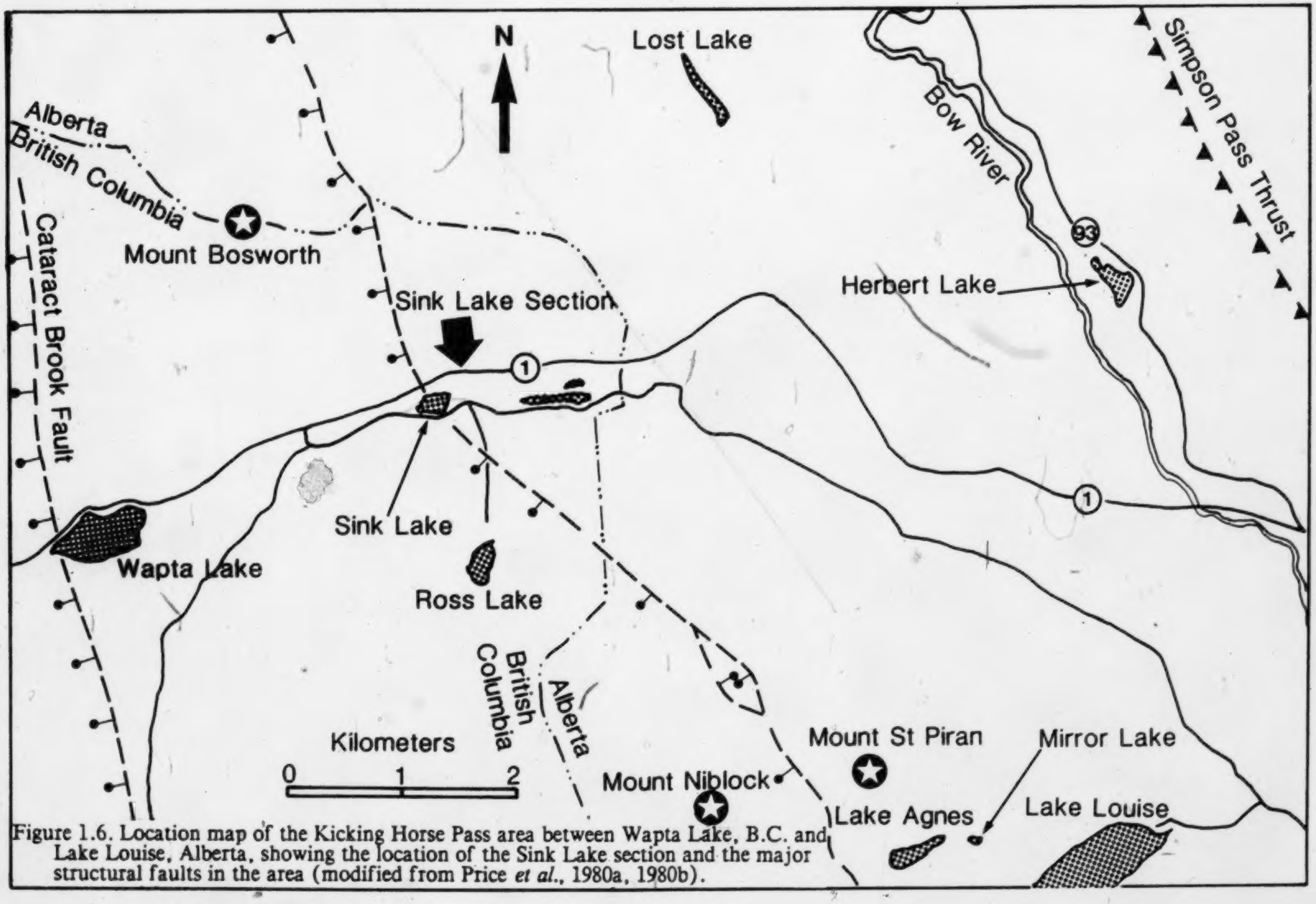
N
Lost Lake
Bow River
Simpson Pass Thrust
93
Herbert Lake
Alberta
British Columbia
Mount Bosworth
Cataract Brook Fault
Sink Lake Section
1
Sink Lake
Wapta Lake
Ross Lake
British Columbia
Alberta
Kilometers
0
1
2
Mount Niblock
Mount St Piran
Mirror Lake
Lake Agnes
Lake Louise

Figure 1.6. Location map of the Kicking Horse Pass area between Wapta Lake, B.C. and Lake Louise, Alberta, showing the location of the Sink Lake section and the major structural faults in the area (modified from Price *et al.*, 1980a, 1980b).

2. CURRENTS AND SEDIMENTATION ON MODERN CONTINENTAL SHELVES

During the past decade there has been a renewed interest in offshore shelf depositional environments and the diverse oceanographic phenomena which are affecting sediment dynamics on modern continental shelves. Numerous workers have recognized the importance of these continental shelf processes, which include oceanic currents (Flemming, 1978, 1980a, 1980b), meterologically-induced currents (Walker, 1984; Johnson, 1978), sediment gravity flows (Middleton and Hampton, 1976) and tidal currents (Stride, 1982). Consequently, we are just starting to understand the diverse range of unsteady and quasi-steady water movements that influence sediment entrainment and dispersal in offshore marine environments.

Despite this upsurge in interest in the sedimentary dynamics of continental shelves, many of the details of the inner and outer shelf processes and their resulting deposits remain unclear. As a result, a facies model for the shallow marine environment has not yet been developed that can adequately describe the complex interactions of various shelf processes and the vast array of shelf deposits. This is particularity true for offshore shelf settings where the extreme financial costs and technical difficultly of even securing the simplest of measurements are enhanced. This section will review the four main types of currents that influence the erosion, transportation, and deposition of material on the continental shelf. These currents are: 1) oceanic currents, 2) tidal currents, 3) meteorological currents (wind, wave and storm currents) and 4) sediment gravity flows. Shallow marine sedimentation will be examined on oceanic-, storm- and tide-dominated continental shelves.

2.1 CONTINENTAL SHELF CURRENTS

2.1.1 OCEANIC CURRENTS

Our knowledge of oceanic currents stems mostly from physical oceanographers studying the marine world and their continuing integration of oceanography with marine geology. Only recently have advances been made in the importance of ocean currents in sediment transport and development of bedforms at the shelfbreak (Flemming, 1978, 1980a, 1980b; Karl *et al.*, 1983; Pietrafesa, 1983). The recent improvements in acoustic methods including side-scan sonor techniques, with resolution down to 0.5 m have allowed scientists to study and map bedforms on the outer shelf.

The two vertically juxtaposed components of ocean currents namely, wind-driven and thermohaline currents are responsible for generating oceanic current circulation.

Wind-driven (or surface currents) currents are directly influenced by atmospheric circulation patterns and effect surface waters with currents progressively deepening with time due to the turbulent mixing of the water column (Ekman spiral effect). The global wind patterns are controlled primarily by heat differences produced by radiation from the sun. The Coriolis forces developed by the earth's rotation causes air to be deflected towards the right in the Northern Hemisphere and towards the left in the Southern Hemisphere. Consequently, the resulting latitudinally-defined global wind patterns consist of prevailing westerlies and trade winds. The low latitude trade winds travel from the east diagonally towards the equator while the midlatitude westerlies move from the west diagonally away from the equator. This wind system exerts a direct shear stress on the ocean's surface and produces the wind-driven circulation of the ocean which follow the prevailing global wind patterns described above. This global atmospheric circulation pattern will become more important in Chapter 6. At which time it will be shown that steady southeast trade winds blowing towards the equator influenced the depositional processes of clastic sediments in the Cambrian shallow epeiric sea covering the North American craton.

Thermohaline circulation currents are the result of density variations caused by salinity and temperature changes in the oceans. These currents are considerably deeper and slower (ranging from the normal 1-2 cm/sec to 10 cm/sec for western boundary currents at depths of 1500 to 2000 m) than the surface currents (Gross, 1977). Typically, the deep-sea circulation currents move in a great complexity of directions due to the rotation of the earth and the presence and geometric shape of the continents and ocean floor.

The oceanic currents consisting of the relatively shallow wind-driven component and the deep water thermohaline component are typically located on the oceanward side of the continental shelf edge. Major ocean currents (e.g. Gulf Stream System) are typically not confined, narrow subsurface flows but actually consist of a complex of filamentary flows, meanders, and eddies. When the series of large meanders become to large, it can detach off the main current to form large eddies. Consequently, there is an active interchange between oceanic and outer continental shelf waters.

The Gulf Stream is a western boundary current flowing along the continental margin of the eastern U.S. which attains near surface velocities ranging from 100 cm/sec to almost 300 cm/sec (Karl *et al.*, 1983). The meandering of the Gulf Stream interacts with the waters at the shelf edge and influences the sediment entrainment and dispersal along the outer continental shelf (Karl *et al.*, 1983; Pietrafesa, 1983).

2.1.2 TIDES

Oceanic tides are caused by the gravitational attraction of the moon and sun on the surface waters of the earth, and the centrifugal forces resulting from the revolution of the earth-moon system. The gravitational and centrifugal forces acting on a water particle augment or oppose each other, resulting in tide-producing forces which act tangentially to the earth's surface, pulling the water to form tidal bulges (Fig. 2.1). The distribution of the two tidal bulges, assuming an ocean of uniform depth covering the earth, consists of a tidal bulge on the side of the earth nearest the moon and on the side opposite the moon. This equilibrium tide occurs semi-diurnally, when there are two high and low tides daily; diurnally, when there is one high and one low tide per day; or they may be mixed showing characteristics of both diurnal or semi-diurnal within the lunar cycle. Superimposed on these daily sea level fluctuations are fortnightly variations which effect the size and strength of tidal currents. These longer term fluctuations are the result of the tidal influence from the sun, which are similar to those produced by the moon but only about half as great (Stride, 1982). When the sun and moon are aligned with the earth, the solar and lunar tide-generating forces act together causing a maximum the spring tide (Fig. 2.2); when the sun and moon act in opposition to each other (at right angles), relatively weak neap tides occur.

The equilibrium theory of the tides which assumed an idealized ocean can not offer a complete explanation of tidal phenomena. In reality, tides are extremely more complex because of the distribution of continents which interrupt the free movement of the tides across the ideal unobstructed ocean water surface. In additon oceanic tides are effected by Coriolis forces along with the local variations of the shape and depth of the basins.

Tidal currents on the continental shelves are the result of tidal waves propagating from deep ocean basins onto adjacent shelves. This is because the continental shelf seas are too small, in shape and depth, to generate a significant response to the tidal producing forces.

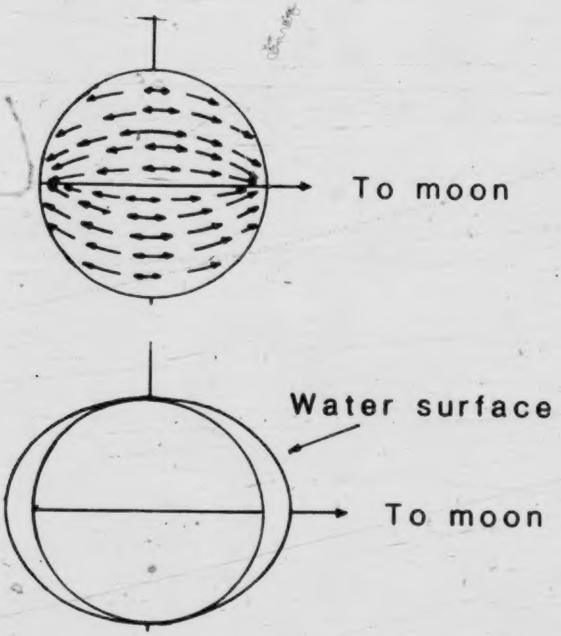
To moon
Water surface
To moon

Figure 2.1. Tide-producing forces with arrows indicating the direction of tide-generating forces which procduces two bulges on the ocean surface (modified after Gross, 1977).

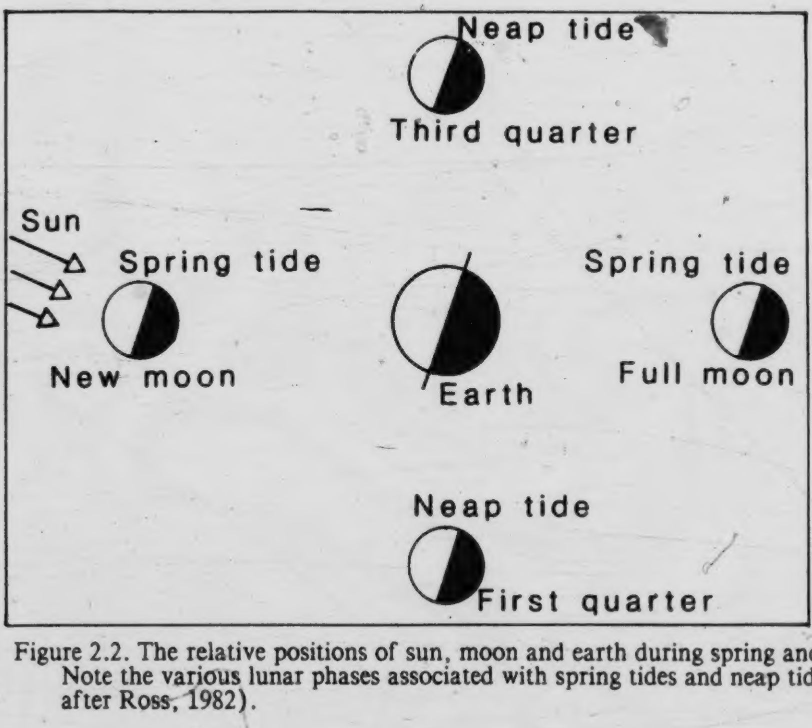
Neap tide
Third quarter
Sun
Spring tide
Spring tide
New moon
Earth
Full moon
Neap tide
First quarter

Figure 2.2. The relative positions of sun, moon and earth during spring and neap tides. Note the various lunar phases associated with spring tides and neap tides (modified after Ross, 1982).

Therefore, enclosed seas or those with only a narrow connection with the deep oceans generally have nonexistent or low tidal ranges.

In the open ocean, tidal currents are not restricted by the coastline, and they follow rotary paths; that is a water particle would move in an elliptical path in a horizontal plane during one complete tidal cycle. The open rotary currents continually change direction and typically obtain velocities of about 30 cm/sec (Thurman, 1981). As one approaches the shoreline from the sea, the rotary currents are changed to an alternating or a rectilinear reversing currents. The currents associated with tides in most coastal areas are inherently unsteady, with flood currents directed towards the shore and the returning ebb flows moving away from the coast. The intervening slack water conditions occur each time the tidal current changes direction.

2.1.3 METEOROLOGICAL FORCES

Currents on the continental shelf are strongly influenced by meteorological forces. The two most notable components to the meterological forcing are wind- and wave-induced processes. They are especially effective agents of sediment transport in shallow shelf seas with a negligible or minimum tidal range.

Wind-driven currents form on the water surface by the transfer of energy from the surrounding air to the water, as a result of direct wind shear stress on the water surface. Prevailing wind systems are seasonally variable and can be intimately associated with seasonal storms. During severe winter storms on the Washington continental shelf, Smith and Hopkins (1972) have recorded near-bottom currents ranging from 25 cm/sec to a maximum of 80 cm/sec at water depths of 50 to 80 meters. Such currents caused significant sediment transport, especially for suspended fine-grained material, into the outer parts of the continental shelf. The effectiveness of surface currents generated by wind stress in moving bottom sediments generally increases with decreasing depth because the near bottom flows respond more rapidly to direct surface wind stresses in shallow water.

The movements of water particles caused by the passage of waves in deep water is essentially a circular orbit which becomes smaller with depth. The diameter of these orbits at the surface is about equal to the wave height. At depths greater than one-half the wavelength water motion is almost nonexistent. The orbital motion of the water particle is not entirely closed and the small amount of forward movement associated with a water particle during orbital motion causes wave-drift currents. The most dramatic change in surface waves occurs as waves enter shallow water. In shallow water interference with the sea bottom causes the particles to move in progressively more elliptical paths which become flatter with depth. A purely oscillatory particle motion resulting in little or no net sediment transport is theoretically possible but does not appear to occur in nature. The two directions of orbital wave motion can vary in strength resulting in an asymmetry in the sediment motion. Consequently, a preferred direction of flow and sediment transport is established indicating that surface waves can cause unidirectional as well as oscillatory motions.

Another type of water movement which is greatly influenced by meteorological forces is storm-surge. This phenomena is the result of atmospheric pressure fluctuations causing large volumes of water to pile up on a coastline by storm winds blowing the water towards shore. A substantial rise in sea level may occur if the storm surge is coincident with a high tide, with water rising sometimes to heights of more than 6 meters (McCormick and Thiruvathukal, 1976). These augmented storm surges are particularly significant in enclosed coastal bays where the sea water is funneled into the embayment and temporarily trapped. The resulting coastal set-up creates a seaward-oriented pressure gradient causing the relaxation currents (returning bottom flow) or if this coastal set up coincides with high tide, a storm-surge ebb currents. These seaward directed currents are important transporting agents in redepositing coastal sediments farther offshore (Hayes, 1967; Reineck and Singh, 1972; Nelson, 1982).

2.1.4 SEDIMENT GRAVITY FLOWS

Sediment gravity flows are the result of unstable sediment moving downslope under the direct influence of gravity. These flows are very important in transporting coarse, nearshore clastics into a deeper water, offshore environments. In general, sediment gravity flows can be discussed in terms of the mechanics of sediment failure and the geologic phenomena that causes slope failure.

Subaqueous mass-gravity transport is initiated when the stresses exerted by gravity are greater than the shear strength of the marine sediment. Sediment strength at a potential failure surface is a function of the cohesion between grains and the intergranular friction. The initiation of marine slope instability and incipient failure can result from an increase in shear stress or a reduction in shear strength. The circumstances leading to shear stress increases can be either from oversteepening of the slope or progressive thickening of the sediment. The conditions that decrease the sediment strength properties are primarily the increase in pore fluid pressure, which reduces the effective strength of the sediment.

Some of the geologic conditions which can trigger slope failure include earthquakes or shock waves, rapid deposition of underconsolidated sediment on oversteepened slopes, or fluidization or gas-charging resulting in a decrease in effective sediment strength (Karlsrud and Edgers, 1982).

Cyclic loading of sediment by surface waves is worthy of further mention because it is a possible mechanism in the clastic resedimentation of the graded matrix-supported pebble conglomerates of Facies 3. The stability of bottom sediments can be altered by the passage of storm waves which causes cyclic increases and decreases of pressure on the ocean floor and the sediment column. Clukey *et al.* (1980) studied the susceptibility of modern Yukon prodelta deposits to wave-induced liquefaction during high-intensity storm events. They determined that the cyclic loading by severe storms with 6 meter wave heights can cause sediment liquefaction to a depth of about 3.5 m in one hour. Since the cyclic wave loading acts within the upper few meters of the deposit a larger volume of sediment can be displaced by this mechanism than by bottom currents just acting on the sediment-water interface. They state that the occurrence of thick sand-storm layers located within 50 km of the Yukon prodelta shoreline suggest sediment liquefaction and sediment gravity flows may be important processes in transporting sediment farther offshore.

One of the best-documented examples of cyclic loading of bottom sediments by surface waves is from the modern Mississippi delta (Henkel, 1970; Prior and Coleman, 1982). Henkel (1970) has shown that wave-induced pressure changes on underconsolidated deltaic sediments are able to cause cyclic shear stresses and resulting sediment failure in water depths up to 400 feet. Likewise, the investigations on the Mississippi prodelta front by Prior and Coleman (1982) revealed that active mass movement down slope was occurring in the form of subaqueous slides and flows. They have found that instability in underconsolidated marine sediments can occur on extremely low prodelta slopes, ranging from 0.7° to 1.5°, in water depths of 10 to 80 m. The resulting slope instability is due to an interaction of excessive pore-water pressures, localized slope oversteepening, cyclic wave loading, and the rapid generation of *in situ* methane gas. In the case of wave-induced stresses, Prior and Coleman (1982) have stated that the Mississippi delta is mainly affected by severe winter storms and hurricanes.

Sediment gravity flows are divided into four individual types based on the mechanism of grain support. They are as follows: (1) turbidity currents, (2) grain flows, (3) liquefied sediment flows, and (4) debris flows. Turbidity currents are distinguished from the other types of flows by the upward component of fluid turbulence. In grain flows the direct grain-to-grain interactions (collisions or close approaches) lifts the sediment up against the force of gravity. The sediment support mechanism for liquefied sediment flows is caused by the upward flow of fluid escaping from between the grains as the grains are settled by gravity. In debris flows the larger clasts are supported by a matrix; usually a mixture of interstitual fluid and fine sediment, which has a finite yield strength (Middleton and Hampton, 1976). Although these grain-support end members are conceptually distinct processes, it is very likely that they are not distinct in nature and that during a single mass gravity event they occur and interact together (Middleton and Hampton, 1976).

2.2 RECENT CONTINENTAL SHELF SEDIMENTATION

2.2.1 OCEANIC CURRENT SEDIMENTATION

Approximately 3% of continental shelves are dominated by strong, one-dimensional oceanic currents (Walker, 1984). When these ocean currents impinge on the outermost part of the continental shelf they can influence sediment transport and the development of continental margin bedforms. Ocean currents appear to play a role in shelf-edge sedimentation on extremely narrow shelves and on continental margins which are situated to receive invading boundary currents. As mentioned earlier, open-ocean circulation is dominated by east-west currents. The presence and geometric shape of continents causes these currents to be deflected and split into boundary currents that flow more or less north-south along the outer regions of the continental shelf.

One of the best examples of large-scale sediment movement by intruding ocean currents was the work done by Flemming (1978, 1980a, 1980b) along the southeast African continental margin. He documented that the strong western boundary flow of the Agulhas Current is the single most important factor controlling the sediment dispersal along the narrow southeastern shelf of South Africa. Flemming recognized that the southward flowing Agulhas Current provided the mechanism for transporting sediment from the inner shelf to the central shelf. This sediment dispersal is initiated by the unsteadiness of the Agulhas Current which tends to periodically shift laterally and meander from the mean flow path. When the current migrates to a position closer to the shelf, consequently shifting its shoreward margin onto the inshore sand prism, it can entrain the bedload sediment and transport it to the central shelf. Flemming observed on side-scan sonar a wide variety of current-generated longitudinal and tranverse bedforms on this central shelf zone which is situated 4 to 8 km offshore, in 40 to 60 m of water. This zone of major sand transport is 20 km long and 10 km wide and contains continuous dune fields of variable height. The most common are dunes with heights of up to 8 m and wavelenghts stretching over several hundred meters. The largest individual dune recorded by Flemming reached a maximum height of 17 m and a corresponding wavelength of about 700 m. Walker (1979) indicates that the angle of the lee face for this particular dune is greater than 25°. He states that this single observation is very important because it is the only documented angle of repose slipface several meters high known in the modern shallow marine environment. Walker postulated that since the Agulas Current only reworks and redistributes relict shelf sediments and does not supply the southeast African shelf with new material, that it will only form a stratigraphic thickness of a few meters.

Another example of oceanic currents affecting the sediment transport and development of bedforms is noted by Field and Roy (1984). They have documented several linear sand bodies off the southeastern coast of Australia which appear to be maintained and modified by the East Australian boundary currents.

2.2.2 STORM-DOMINATED SHELF SEDIMENTATION

Storm-induced sedimentation is very prominent on many shelf seas that are tideless or only weakly tidal. The dominant source of energy is provided by wind- and wave-induced currents. The shelf hydraulic regime is characterized by these meteorological forces which exhibit strong seasonal variability. Intense wave and wind action occurs on continental shelves (Washington-Oregon shelf) that face the prevailing westerly winds and have a large oceanic connection to receive the waves generated in the adjacent ocean basins. These conditions are considerably less intense on continental shelves that are situated in the lee of prevailing winds, such as the Atlantic shelf of eastern U.S. and in partially enclosed shelf seas, as in the Gulf of Mexico (Johnson, 1978).

The importance of storm-related processes has been widely recognized (Hayes, 1967; Reineck and Singh, 1972; Kumar and Sanders, 1976; Morton, 1981). These episodic events are responsible for transporting sand in offshore shelf environments and forming graded sequences in water depths of up to 40 m and distances as far as 45 km from the shoreline (Reineck and Singh, 1972). Deposits typically have sharp and erosive bases with burrowed or diffuse upper contacts indicating a rapid emplacement of sediment with the eventual recolonization by benthonic fauna. Under waning storm conditions the deposit may be normally graded and contain a sequence of sedimentary structures illustrating a progressive decrease in current energy. Hayes (1967) was the first to propose, storm surge ebb as a post-storm process resulting from seaward moving, wind-forced bottom-return flows developed during major storms. He introduced the concept as an explanation for the presence of graded beds that were cored in water depths up to 36 meters from the Texas shelf following Hurricane Carla. He concluded that storm surge ebb is a possible mechanism for developing graded and well-sorted sandy sediment on the inner shelf. The potential of storm-associated bottom currents combined with storm-wave liquefaction processes in transporting nearshore sediment seaward has been addressed by Nelson (1982). He observed that severe storms effecting the modern Yukon Delta shoreline in the northern Bering Sea can create storm surges upwards to 5 meters. These major coastal set-ups generate unidirectional storm surge ebb currents that transported inshore sediments more than 100 km offshore. The resulting graded sand layers contained a sequence of sedimentary structures resembling those of turbidites.

The presence of graded sequences and well-sorted sand beds (Hayes, 1967; Reineck and Singh, 1972; Kumar and Sanders, 1967; Morton, 1981) illustrates that significant widespread changes in shelf sedimentation occurs during episodic high-energy storm events. The nature and details of the storm-related physical processes involved in their formation remains unclear. Presented above is a storm-surge ebb mechanism, but other viable physical processes include: sediment suspension clouds generated by waves (Reineck and Singh, 1972); deposition from geostrophic bottom flows produced by wind forcing (Morton, 1981) and *in situ* reworking of shell debris and sand by cyclic pressure fluctuations from surface waves (Powers and Kinsman, 1953).

No discussion of storm-related bottom currents is complete without some reference to the influence of the Coriolis force which affects the initial seaward bottom flow as it crosses the shoreface and inner shelf. In the northern hemisphere the returning storm-induced bottom flow is deflected to the right and eventually moves parallel to isobars created by the coastal set-up. This flow resulting from the balance between gravitational forces and the Coriolis effect is called a geostrophic current which flows predominantly along the shelf. To date there is very little information on the marine geostrophic currents and direct correlation between geostrophic currents and specific processes has not been achieved. However, Swift (in Walker, 1984) suggests that sustained alongshore geostrophic currents during storms are much more important for sediment transport than the relaxation currents (storm surge ebb). He believes that for a storm lasting for a period of 2 days the resultant geostrophic bottom discharge may be 2000 to 3000 times the discharge of the seaward directed relaxation flow. The graded and well-sorted sand layers initially believed by Hayes (1967) to be deposited by seaward flowing storm-surge ebb currents following Hurricane Carla is under question. Morton (1981) re-evaluated the information and suggests that the graded bed deposited during Carla is the result of geostrophic currents travelling southward along the Texas coast and not from storm-surge ebb currents as originally defined by Hayes (1967).

Another structure which has been linked genetically to storm-wave processes is hummocky cross-stratification. This particular structure has become generally accepted as a feature reflecting sedimentation of fine sand entrained by storm-wave induced currents, giving evidence of deposition below fair-weather wave base. Currently there is a dispute over the origin of hummocky cross-stratification, particularly whether it is produced by random scour and drape, or by the result of regular bedform development (Dott and Bourgeois, 1982). Harms *et al.* (1982) suggest that hummocky cross-stratification forms by deposition of fine sand during oscillatory flow produced by large surface waves. As the wave action impinges on the ocean floor the resulting oscillatory flow with periods of several seconds and fairly high orbital velocities essentally moulds the depositing sand into hummocks and swales. Storm waves generate not only bidirectional oscillatory, but also multidirectional flows on continental shelves which may be important in the formation of hummocky cross-stratification (Harms *et al.*, 1982).

2.2.3 TIDE-DOMINATED SHELF SEDIMENTATION

Large areas of modern continental shelves are swept by strong tidal currents. These tidal conditions affect approximately 17% of the present day continental shelves and exercise a fundamental control over sediment transport and formation of bedforms (Walker, 1984). Within tide-dominated shelf settings, a variety of sedimentary features occur which appear to be related to the prevailing tidal currents.

The feature which is considered probably most characteristic of tidal environments is herringbone cross-stratification, a bidirectional current-formed sedimentary structure. The adjacent layers of oppositely dipping foreset laminae appear to preserve the reversal of currents during an ebb/flood tidal cycle. This feature indicates that typically both the ebb and flood flows are effective in transporting bed-material. The occurrence of herringbone cross-stratification is rare in unidirectional bedforms which respond to the large predominance of one tide over the other (Klein, 1970). Herringbone cross-stratification, however, is common in bedforms formed under the bipolarity of current flow reflecting the ebb and flood current flow. Herringbone cross-stratification is particularly common in intertidal and subtidal environments where the intensity of current flow is highly variable, a result of the oscillatory flow pattern of tidal currents and from the neap/spring-tide cycle.

In many tidally-dominated continental shelves large-scale unidirectional bedforms occur such as linear sand ridges and sandwaves. These bedforms reflect the predominance of the tidal currents in one direction over the currents in the opposite direction (Terwindt, 1971). This predominance may seem unusual for a tidal environment where rectilinear, bidirectional or rotary tidal currents are present. However, unidirectional sediment transport paths commonly develop because of the following reasons: ebb and flood tidal currents may follow separate transport paths, the strength and duration of ebb and flood tidal velocities are usually not equal, and wind-driven currents may enhance a single tidal direction (Johnson, 1978).

The southern North Sea is one of the most intensively studied tidal basins (Stride, 1963; Belderson and Stride, 1966; Caston, 1972; Stride, 1982). From this area Belderson and Stride (1966) show that certain bedforms are located in specific regions along the tidal current transport path (Fig. 2.3). These sediment transport paths contain a sequence of zones with the following bedforms characterizing a particular depositional zone: sand ribbons, sandwaves, sand patches, and mud. These continental shelf bedforms are in partial equilibrium with the

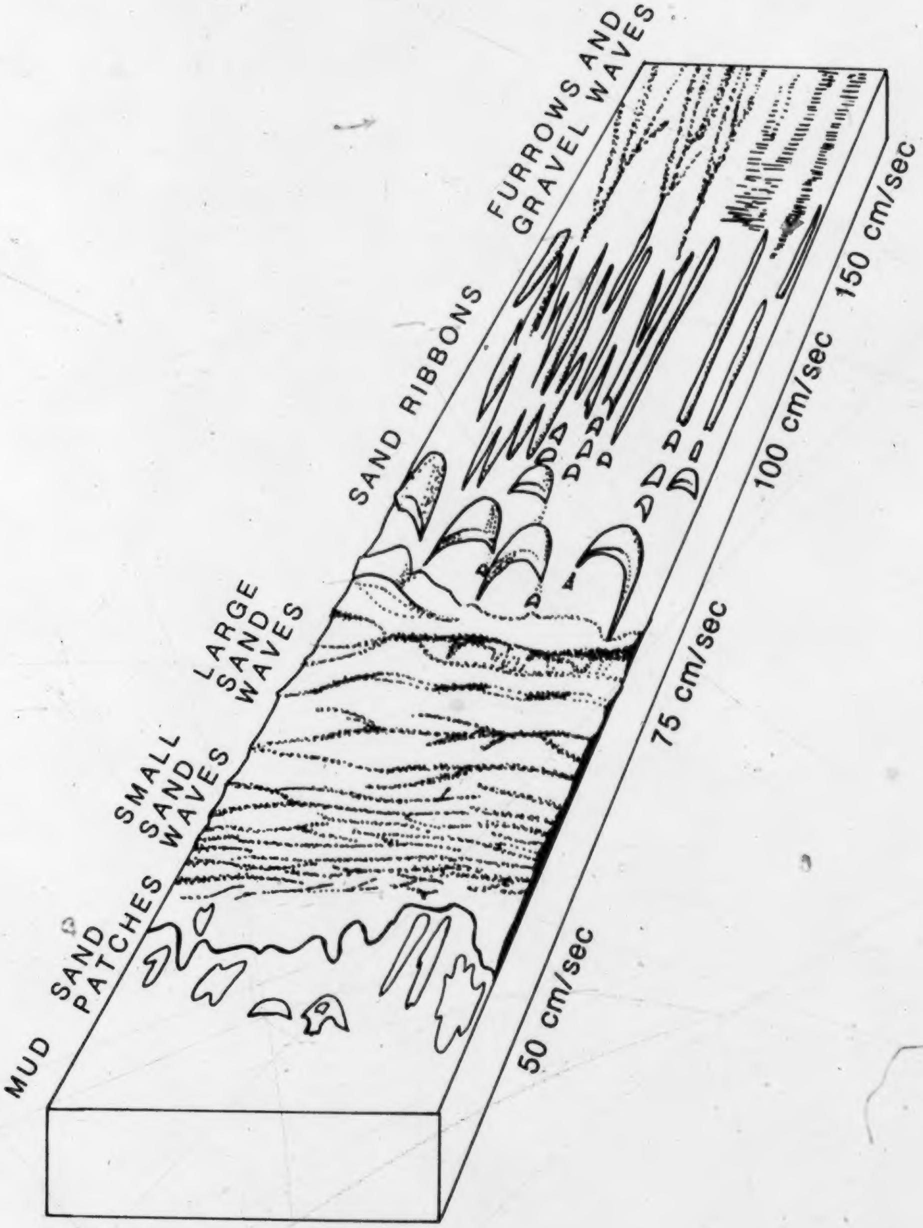
MUD
SAND PATCHES
SMALL SAND WAVES
LARGE SAND WAVES
SAND RIBBONS
FURROWS AND GRAVEL WAVES
50 cm/sec
75 cm/sec
100 cm/sec
150 cm/sec

Figure 2.3. Block diagram of bedforms produced by tidal currents on the continental shelf. Illustrates the succession of depositional provinces along a tidal transport path, with the corresponding mean spring near-surface tidal velocities (modified after Stride, 1982).

controlling tidal currents and reflect the local strength of the tidal currents (Stride, 1982).

Sand ribbons are essentially linear bedforms that are spread over a coarser, immobile sediment that is exposed between the ribbons of sand. They are aligned parallel to both the maximum tidal current velocities and the bed load transport path of the tidal currents. Typically, this sand ribbon zone is located along a tidal transport path between a zone of erosion and a sandwave zone (Belderson and Stride, 1966), although sand ribbons are known to co-exist within the sand deficient regions of the sandwave zone. They are generally formed on continental shelves where the tidal currents reach an excess of 100 cm/sec, in water depths ranging from 20 m to a maximum of 150 m (Kenyon, 1970). These longitudinal sand ribbons with sharp and parallel boundaries are known to reach up to 15 km long and 200 m wide, with thicknesses rarely exceeding 1 m. Their length to width ratio is typically more than 40 to 1 (Kenyon, 1970). These ribbons or strips of sand have a low preservation potential because they would typically be replaced by other less transitory tidal features as the sand supply or current strength changes with time (Kenyon, 1970; Stride, 1982).

Sand waves are straight crested, flow-transverse features which have been widely recognized as a major bedform in modern tidal environments. They are widely distributed in a variety of tidal environments, but appear to be particularly abundant in restricted, tidally influenced seas and seaways with connections to open oceans. For example, sandwaves have been known to occur in several kinds of tidal environments ranging from estuaries to open continental shelves in water depths up to about 200 m (Stride, 1982). This discussion will restrict itself to sandwaves formed under tidally oscillating flows (Allen, 1980a) and not from intervening, unidirectional oceanic currents (Flemming, 1978, 1980a, 1980b) or in modern river systems (Coleman, 1969).

The best studied areas for tidal sandwaves is in the partially enclosed tide-swept shelf seas of Northwest Europe (Houbolt, 1968; McCave, 1971; Terwindt, 1971; McCave and Langhorne, 1982). The available data indicates that sandwaves usually have wavelengths between 30 to 500 m and vary in height from 1.5 to 15 m (Johnson, 1978). The length to height ratio of sandwaves is generally above 30, and may reach values up to 100 (Reineck and Singh, 1980). The sandwaves range in cross-sectional shape from symmetrical to strongly asymmetrical. Allen (1980a) suggests that the asymmetrical form of sandwaves is linked to the asymmetry of the tidal flow, with the steeper side in the direction of the stronger tidal current and therefore in the direction of net bedload transport.

Sand waves are generally distributed within a particular depositional zone that is between the proximal sand ribbons and the more distal sand patches (Belderson and Stride, 1966)(Fig. 2.3). This sandwave province occurs along the tidal transport path where the near-surface tidal velocities are around 65 cm/sec, with the smaller sandwaves requiring a slightly lower current velocities (Stride, 1982).

The majority of sandwaves have superimposed megaripples actively migrating on the stoss and lee sides. Consequently, the internal structures of the sandwave should reflect these surface morphological features. However, at present the internal structures of sandwaves are poorly understood and restricted to two studies (Reineck, 1963; Houbolt, 1968) which systematically cored sandwaves in the southern North Sea. Largely on the basis of these two studies and additional work on sandwave morphology (Twichell, 1983) the internal structure of sandwaves is inferred to consist of gently inclined set boundaries (master bedding surfaces) with high angle cross-stratification recording the migration megaripples on the master bedding surfaces.

Beyond the zone of sandwaves is a patchy development of flat, well-sorted, fine sand sheets which may fine upwards or grade laterally into poorly-sorted muddy sand (Belderson and Stride, 1966). These sand patches vary considerably in size and shape, with rather irregular and non-parallel boundaries. Sand patches are typically longer than broad, with the direction of elongation roughly parallel to tidal current transport paths. These fairly extensive sand sheets can range in thickness from a few centimeters up to 3 meters (Stride, 1982) and occur in zones where near-surface tidal velocities are around 50 cm/sec (Stride, 1982). The surface of these sand patches are covered with sinuous crested ripples along with a diverse fauna. (Flemming and Stride, 1967).

Another distinctive feature of tide-swept shelf seas are linear tidal sand ridges. These tidal sand ridges or banks are large-scale, longitudinal features whose long axes are oriented at a small oblique angle relative to the strongest tidal current flow direction. These bedforms are characteristic of many tide-dominated seas and should not be confused with the shoreface connected sand ridges of continental shelves that are associated with storm wave activity and storm driven currents. The best documented tidal sand ridges are found in the southern North Sea and are in the order of 60 km long, 1 to 2 km wide and range in height from 10 m to 40 m.

They are considered the largest bedforms of tidally-influenced seas, occurring in water depths ranging from 30-50 m, while their topographically high crests lie submerged at water depths of only 3-13 m below the surface (Johnson, 1978). These tidal ridges tend to occur in clusters, both offshore and in estuaries, or else as small solitary ridges near the coast developed in the lee of headlands or islands (Kenyon *et al.*, 1981).

The world-wide occurrence of these linear, large bedforms on tidal-dominated continental shelves has been noted by Off (1963) and has led to a deductive correlation between these features and the presence of strong, prevailing, tidal currents, such as those in the North Sea. Off (1963) originally thought that the tidal sand ridges were orientated parallel to the strongest tidal currents, but recently it has been shown that the long axes are somewhat obliquely orientated between about 7° and 15°, to the regional peak tidal-flow direction (Kenyon *et al.*, 1981).

Many of the tidal sand ridges have superimposed sandwaves and megaripples migrating obliquely to the ridge crestline with their steeper slopes directed towards the crestline from either side of the tidal sand ridge (Houbolt, 1968; Caston, 1972). This crestward migration of these superimposed bedforms from both flanks is the result of bedload transport of sand by tidal currents flowing obliquely across the sides of the ridge towards the ridge crest (Caston, 1972). These actively maintained tidal ridges in the North Sea are believed to be in dynamic equilibrium with the existing tidal conditions (Caston, 1972) and are found in areas where the near-surface tidal currents exceed 50 cm/sec (Kenyon *et al.*, 1981). Caston (1972) noted that the ridges tended to be asymmetric in cross-section with the steeper face, approaching a maximum angle of 7°, orientated to the northeast. In such cases the steeper slope is considered to be the side of the ridge that faces obliquely to the regional direction of peak tidal flow and to the resulting net sand transport direction (Kenyon *et al.*, 1981). The long term growth and migration of some North Sea linear tidal sand ridges in the direction of the steeper side was documented by Houbolt (1968) and Caston (1972).

The seismic sparker sections and cores of such asymmetric tidal ridges indicate large-scale internal bedding planes aligned roughly parallel to their steep "lee" slope, with smaller sets of high-angle cross-bedding associated with the migrating megaripples on the slope (Houbolt, 1968). Walker (1984) has reviewed the two documented studies (Reineck, 1963; Houbolt, 1968) on internal ridge morphology based from core. He suggests that tidal sand ridges can be characterized by large-scale low-angle surfaces (corresponding to the 4 to 7° steep "lee" side) with relatively small-scale, high-angle cross-stratification dipping either up or down the low-angle accretion surfaces (master bedding surface).

These linear tidal sand ridges are anomalous with respect to the depositional sequence of the tidal transport path, because they appear to occupy no preferred postion within tidal current transport paths. The two types of ridge fields, namely those occurring in embayments and those found offshore, tend to be elongated parallel to the axis of the embayment and parallel to the regional trend of the shoreline, respectively. There is no doubt that modern tidal ridges are being actively built or maintained by present tidal currents (Houbolt, 1968; Caston, 1972). However, Swift (1975) believes that they were probably formed by shoreline detachment during the course of the Holocene transgression. Therefore, the distribution of tidal ridges on tide-dominated continental shelves is more closely related to the transgressive history of the adjacent nearshore regions than to the succession of depositional provinces along a tidal transport path (Swift, 1975).

Along the inferred tidal current transport path there is a progressive decrease in grain size which ultimately leads to the final depositional zone, which is characterized by mud accumulation (Stride, 1963; Belderson and Stride, 1966). On continental shelf settings there are three factors which appear to influence the deposition of mud : wave activity, suspended sediment concentration and current velocity (McCave, 1971). In the southern North Sea the wave activity tends to inhibit fine-grained deposition, although with suitable suspended sediment concentrations and relatively low wave activity mud deposition can occur under quite high tidal current velocities (McCave, 1971). As mentioned wave action is a controlling factor in the deposition of mud. McCave (1971) has shown that in the southern North Sea, mud deposits commonly occur in offshore areas at water depths below 30 m, because of the low wave effectiveness in these shelf settings. The absence of mud in offshore areas of the North Sea is most reasonably attributed to the fact that the wave action is sufficient to counteract the slow mud deposition. One such place occurs in the St. Georges Channel where in water depth of over 100 m the deposition of mud is prevented by strong tidal currents in excess of 100 cm/sec which scour the sea floor (Johnson, 1978). Mud is deposited in a wide variety of marine environments but since wave action principally controls fine-grained sedimentation most of the extentive mud accumulation occurs at the ends of transport paths in moderately deep water where the wave and current activity is relatively low.

3. FACIES DESCRIPTIONS AND INTERPRETATIONS

3.1 FACIES SCHEME

Beds were measured individually on a bed by bed basis within 47 vertical sequences (measured sections are in Appendix I). Detailed descriptions of the internal sedimentary structures, set thickness, basal bedding contacts, apparent grain size (crystallinity) and biogenic structures were conducted on each bed. The main distinguishing features in grouping the various beds into 8 sedimentary facies were the apparent grain size and physical sedimentary structures. This thesis uses facies as a descriptive term. The eight facies recognized at Sink Lake are distinguished by the physical characteristics (internal sedimentary structures, apparent grain size and set thickness) of the Gog sediments. This usage is consistent with de Raaf *et al.* (1965) definition of facies as the "lithological, structural and organic aspects detectable in the field." Figures 3.1-3.4 show the percentages of facies comprising the four outcrops.

Basal contacts of beds were described as planar, undulating or scoured and refers to the depth of erosion into the immediately underlying beds. Planar basal bedding contacts are non-erosional and form very flat lower bed boundaries. Undulating contacts are gently irregular to wavy with the basal erosion surface showing a relief of less than 5 cm. Scoured contacts are characteristically irregular with a relief of 5 cm to 15 cm, these surfaces are rare, but when present they often truncate the structures in the underlying bed(s). In addition, loaded contacts are commonly observed on the underneath side of quartzite horizons overlying slaty shale or shale. These non-erosional features vary in relief from a few centimeters to several decimeters.

In this study, crystallinity is described in terms of inferred grain size at the time of deposition. Apparent grain size was determined by using the Wentworth grain size scale. The size of the individual grains were visually estimated with reference to a Amstrat field card of known Wentworth grain sizes.

The relative amount of biogenic reworking was documented in the sequence of clastic sedimentary beds. Bioturbated and/or burrowed quartzite layers, in which 75% or more of the substrate has been modified by biogenic reworking were placed in a special subfacies. It should be noted, that formal nomenclature was not assigned to all biogenic structures, only the trace fossils which had features that were sufficiently distinctive or easily recognizable were given

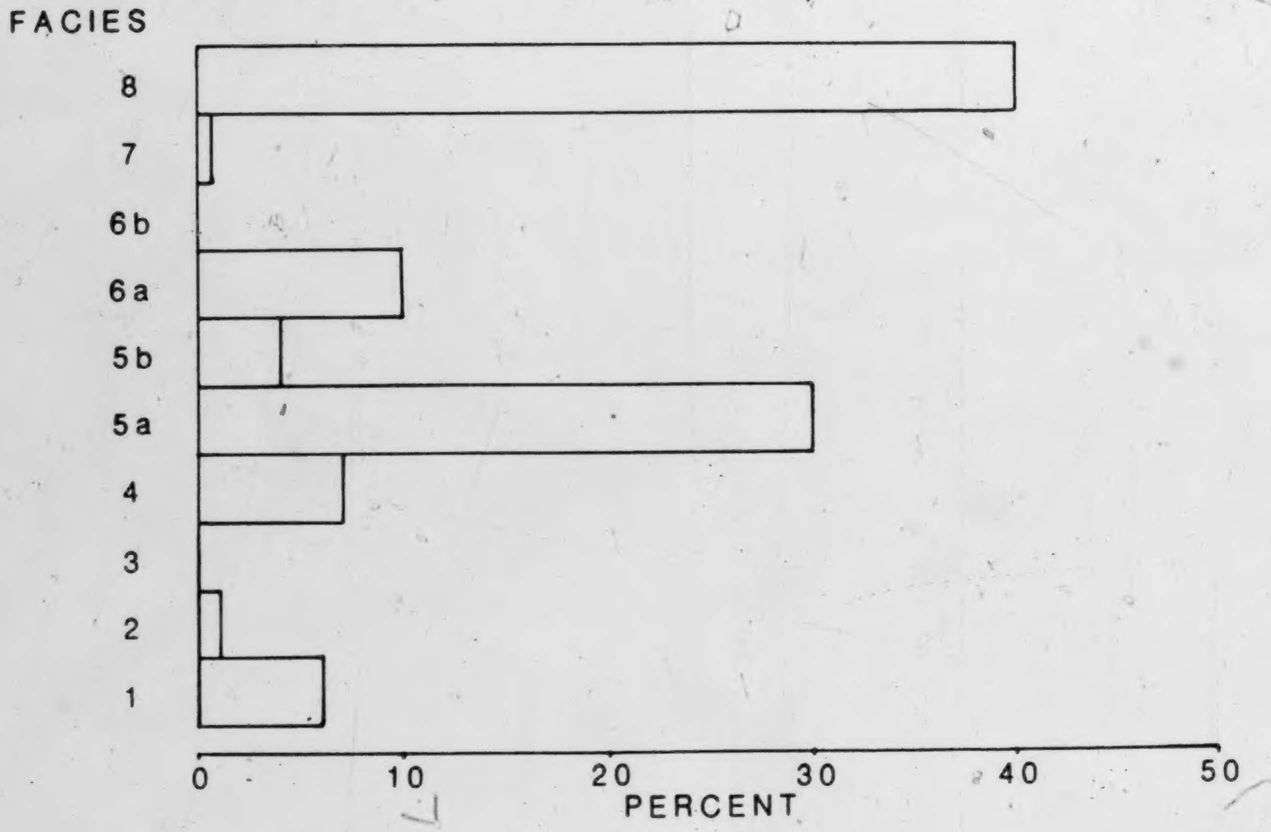

Figure 3.1. Histogram showing the percentages of facies which comprise outcrop A.

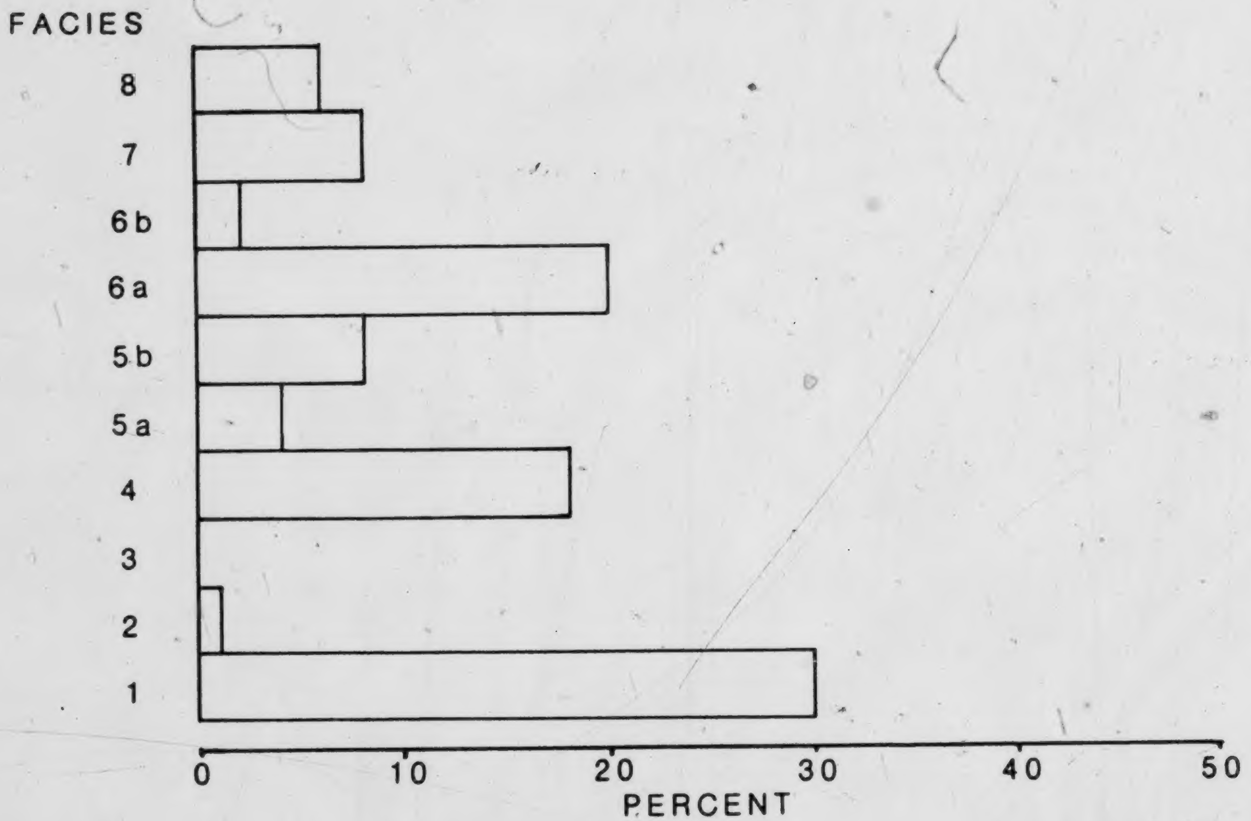

Figure 3.2. Histogram showing the precentages of facies which comprise outcrop B.

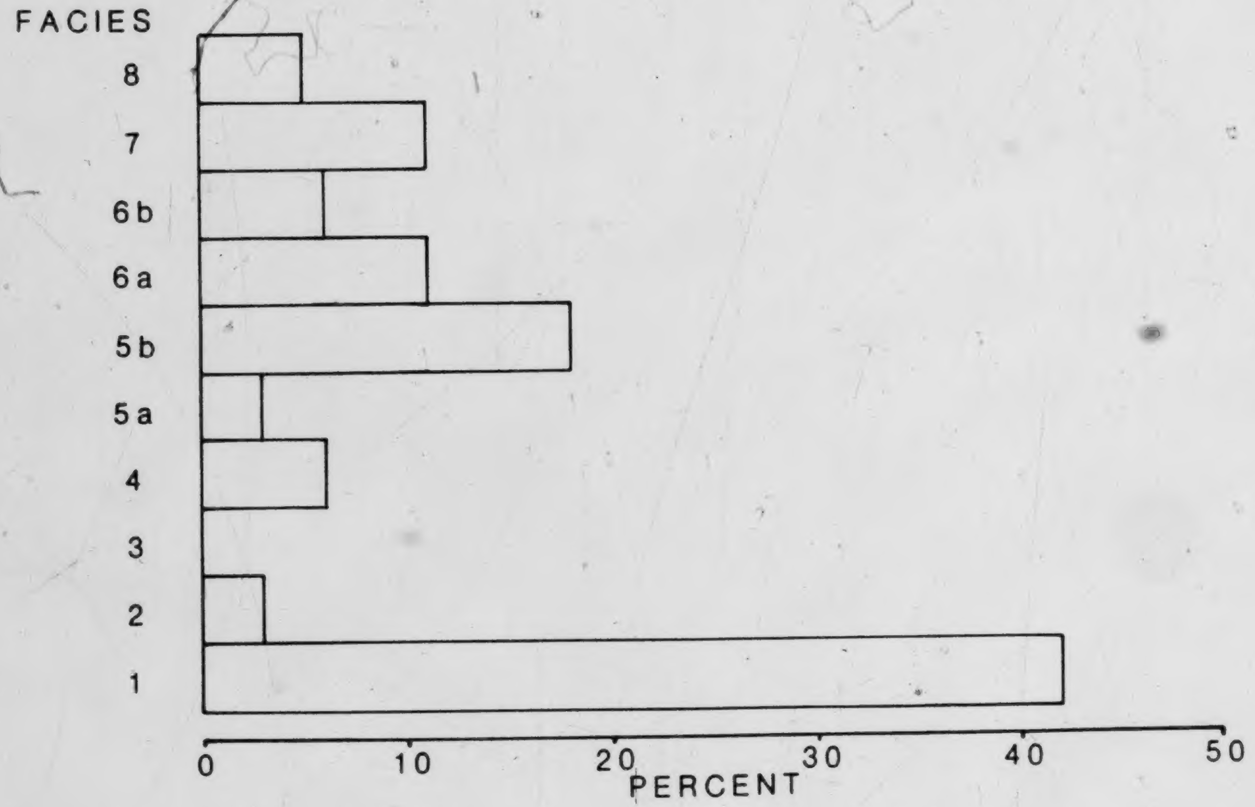

Figure 3.3. Histogram showing the precentages of facies which comprise outcrop C.

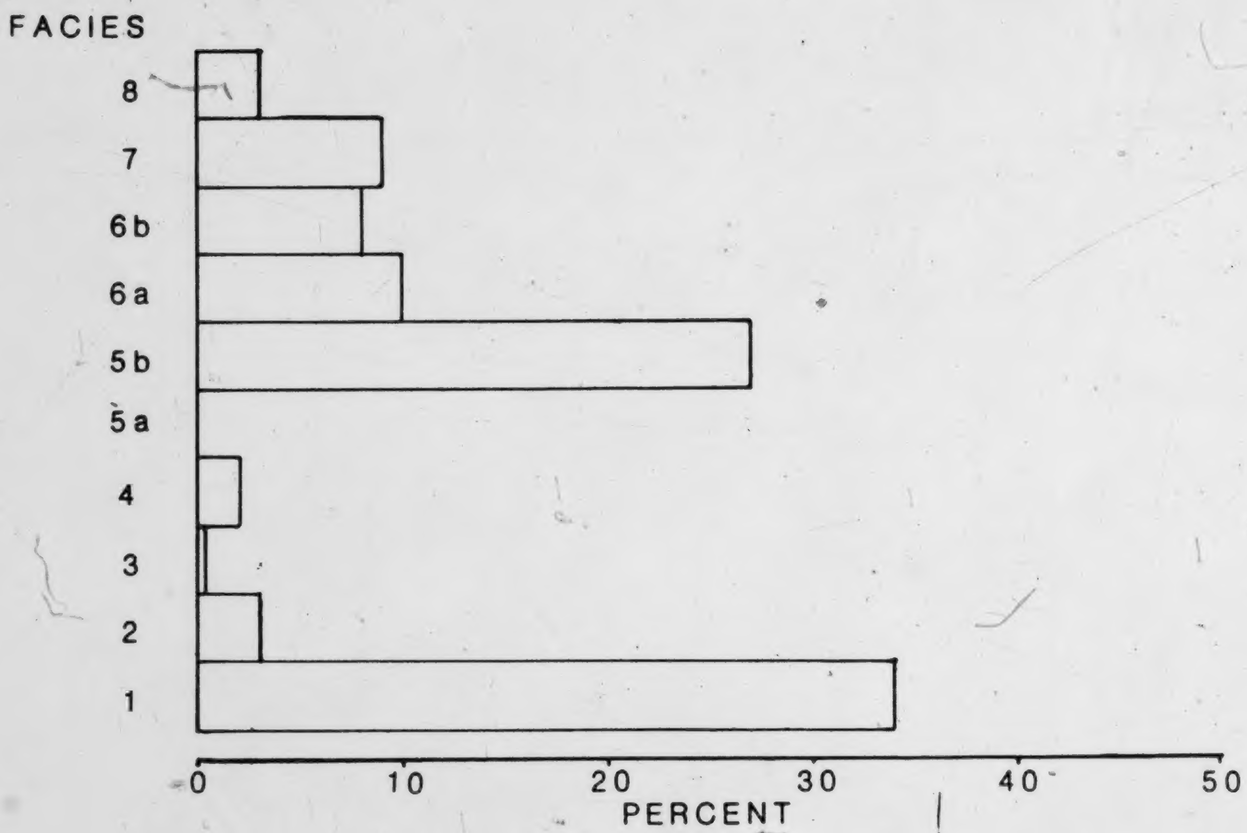

Figure 3.4. Histogram showing the precentages of facies which comprise outcrop D.

scientific names.

In this study particular emphasis was placed on primary sedimentary structures. Detailed descriptions were recorded for the primary sedimentary features, the internal arrangement of stratification and bed configurations. However, at times it was difficult to distinguish primary sedimentary structures because some of the internal sedimentary features have been destroyed by a combination of synsedimentary deformation, diagenesis, metamorphic recrystallization and fracturing. Two main types of internal cross-stratification were recognized based on the angle at which the cross-laminae meet the lower bounding surface of the set. Planar cross-stratification is characterized by angular foresets with sharp based truncations and trough cross-stratification is recognized on the basis of well-developed toesets which intersect the base tangentially. The trough and planar cross-bedded facies were arbitrarily divided into two subfacies on the basis of set thickness. For low angle cross-stratification it is often difficult to determine the amount of curvature and the angle at which the laminae meets the lower surface of the bed. This is primarily due to the difficulty in tracing individual laminae laterally within the bed. The distinction of planar-tangential foresets was difficult because many of the exposures did not permit an accurate determination of the changing curvature of individual foresets along strike.

It should be noted, that the orientation of the outcrop face in relation to the strike and dip of bedding only allowed the two-dimensional strike orientations of beds to be visible. Therefore, because of the rarity of exposures showing three-dimensional (strike and dip) surfaces the various types of cross-stratification were identified based on the two-dimensional strike surfaces of the beds.

3.1.1 FACIES OUTLINE

Facies 1: Interbedded slaty shale and very-fine to medium-crystalline quartzites.

1a Massive quartzite interbeds.

1b Stratifed / cross-stratified quartzite interbeds.

1c Graded quartzite interbeds.

1d Bioturbated / burrowed quartzite interbeds.

1e Argillaceous quartzite interbeds.

OUTCROP A

FACIES	% OF TOTAL MEASURED SECTION	AVERAGE BED THICKNESS
1	6%	6 cm
2	0.9%	1 cm
3	0%	0 cm
4	7%	12 cm
5a	30%	34 cm
5b	4%	53 cm
6a	10%	26 cm
6b	0%	0 cm
7	0.6%	24 cm
8	40%	31 cm

OUTCROP B

FACIES	% OF TOTAL MEASURED SECTION	AVERAGE BED THICKNESS
1	30%	29 cm
2	1%	3 cm
3	0%	0 cm
4	18%	18 cm
5a	4%	23 cm
5b	8%	63 cm
6a	20%	22 cm
6b	2%	46 cm
7	8%	18 cm
8	6%	20 cm

OUTCROP C

FACIES	% OF TOTAL MEASURED SECTION	AVERAGE BED THICKNESS
1	42%	49 cm
2	3%	5 cm
3	0%	0 cm
4	6%	15 cm
5a	3%	19 cm
5b	18%	65 cm
6a	11%	20 cm
6b	6%	60 cm
7	11%	20 cm
8	5%	16 cm

OUTCROP D

FACIES	% OF TOTAL MEASURED SECTION	AVERAGE BED THICKNESS
1	34%	36 cm
2	3%	4 cm
3	0.3%	7 cm
4	2%	6 cm
5a	0%	0 cm
5b	27%	71 cm
6a	10%	20 cm
6b	8%	66 cm
7	9%	19 cm
8	3%	13 cm

Table 3.1.

Table showing the precentages of facies and average bed thickness comprising the 4 major outcrops at Sink Lake.

Facies 2: Slaty shale and shale.
Facies 3: Graded matrix-supported pebble conglomerates.
Facies 4: Small-scale cross-stratified quartzites.
Facies 5: Planar cross-bedded quartzites.
    5a Planar cross-bedded sets, 0.05 - 0.4 m thick.
    5b Planar cross-bedded sets, 0.4 - 2 m thick.
Facies 6: Trough cross-bedded quartzites.
    6a Trough cross-bedded sets, 0.05 - 0.4 m thick.
    6b Trough cross-bedded sets, 0.4 - 2 m thick.
Facies 7: Low angle to horizontally stratified quartzites.
Facies 8: Massive quartzites.

3.1.2 FACIES 1: INTERBEDDED SLATY SHALE AND VERY-FINE TO MEDIUM-CRYSTALLINE QUARTZITES

This facies is characterized by very-fine to medium-crystalline reddish-purple quartzite layers separated by interbeds of slaty shale and shale. In this facies the slaty shale and shale range in thickness from individual laminae to beds up to 35 cm thick. The thicker interbeds of slaty shale in outcrops B, C and D often show well developed slaty cleavage. In outcrop A, slaty cleavage is rare and generally not well developed. The very-fine to medium-crystalline quartzites range in thickness from individual laminae to beds 22 cm thick. The thicker intervals of facies 1 located at outcrop B, C and D typically contain interbeds of quartzites ranging in thickness from 0.5 to 1.5 cm and are separated by 5 to 10 cm of slaty shale. In general, these quartzite layers are laterally continuous and traceable for several meters along strike. Amalgamation of the thin quartzite beds is common and typically consists of 2 to 4 stacked beds. This facies is the most common at outcrops B, C and D; it is of lesser importance at outcrop A. This facies only comprises approximately 6% of the total measured section at outcrop A, compared with 30%, 42% and 34% at outcrops B, C and D respectively. The average bed thickness is 6 cm at outcrop A, 29 cm at outcrop B, 49 cm at outcrop C and 36 cm at outcrop D. Facies 1 is divided into the following six subfacies based on the nature of the individual quartzite layers.

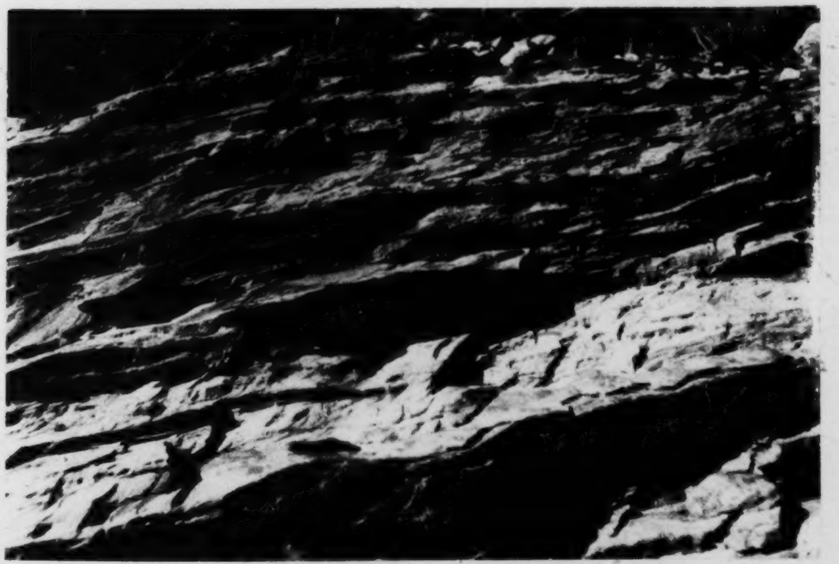

Figure 3.5. Subfacies 1a: Interbedded slaty shale and massive quartzites. Notice the lateral thickening and thinnig of individual quartzite interbeds.

Figure 3.6. Subfacies 1b: Interbedded slaty shale and stratified quartzites. Photograph shows a trough cross-stratified quartzite interbed.

3.1.3 SUBFACIES 1A: INTERBEDDED SLATY SHALE AND MASSIVE QUARTZITES

In this subfacies the thin quartzite beds are characteristically massive, showing no internal stratification or grading and range in thickness from individual laminae to beds 12 cm thick (Fig. 3.5). Basal contacts are typically sharp and planar to slightly undulating with no observed load structures. Bioturbation is minor and typically occurs at the base of the interbedded quartzites. Subfacies 1a at outcrop A consists of thin massive quartzite laminae (0.1 to 0.5 cm in thickness) interbedded with slaty shale. The very-fine to fine-crystalline quartzite laminae account for slightly more than 10% of the beds and are characteristically wispy to parallel-sided. At outcrops B, C and D this subfacies contains thin quartzite beds generally ranging in thickness between 1 to 3 cm.

3.1.4 SUBFACIES 1B: INTERBEDDED SLATY SHALE AND STRATIFIED VERY-FINE- TO MEDIUM-CRYSTALLINE QUARTZITES

This subfacies consists of quartzite interbeds containing internal small-scale trough and planar cross-lamination and rare parallel lamination (Fig. 3.6). The average thickness for the individual stratified interbeds of quartzites range between 0.5 to 4 cm. Discrimination between small-scale trough and planar cross-lamination was very difficult due to the nature of the outcrops. The basal contacts of the thin quartzite beds are typically undulating to planar and slightly erosional. The upper set boundaries of the quartzite beds are typically undulating to planar. These quartzite interbeds are laterally persistent and traceable for several meters along strike. In the cases where lateral terminations occur as pinch outs, these quartzite layers re-emerge a few tens of centimeters along strike. Subfacies 1b shows minor bioturbation along the basal surfaces of the thin quartzite interbeds. Only one thin quartzite bed (2 cm thick) observed at outcrop C contained definite parallel lamination. However, certain quartzite interbeds with planar and sharp set boundaries show vague parallel lamination.

3.1.5 SUBFACIES 1C: INTERBEDDED SLATY SHALE AND GRADED QUARTZITES

This subfacies occurs at outcrop C and D, where it comprises less than 1% and 3% of the total measured section. Average thickness of the interbedded graded quartzites is 2.6 cm (range: 1 - 4.5 cm). The thin quartzite beds are normally graded and display transitions from coarsely-crystalline quartzites to siltstones, which are graditional with the overlying slaty shales

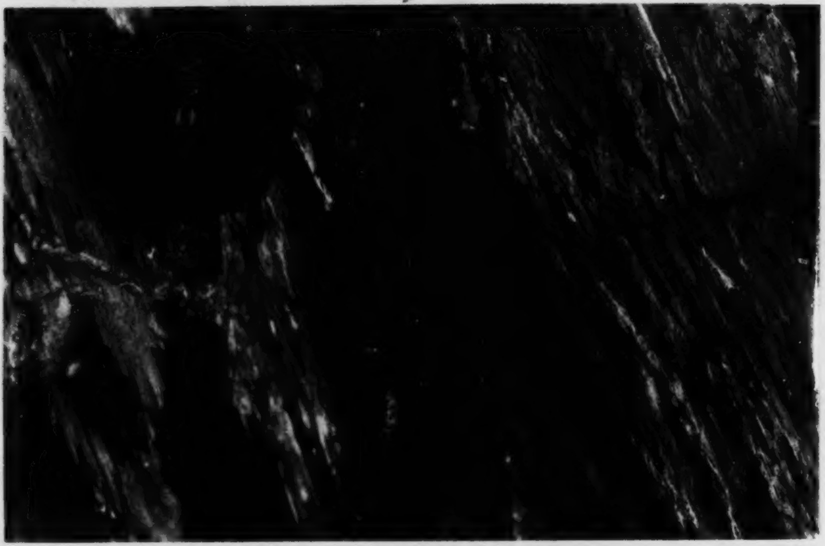

Figure 3.7. Subfacies 1c: Interbedded slaty shale and graded quartzites.

Figure 3.8. Photograph of a thin graded quartzite interbed (Subfacies 1c) with a sharp basal contact and small-scale cross-lamination located in the upper portion of the interbed.

(Fig. 3.7). In general the beds of this subfacies show no internal sedimentary structures; however, rare cases of small-scale trough cross-lamination are located in the upper portions of the graded beds (Fig. 3.8). Upper bed boundaries are undulating to planar. Basal contacts are erosional and planar or gently undulating surfaces. Scour and tool marks are rarely observed perhaps partly due to outcrop exposure, which rarely shows the basal bedding planes of beds. The slaty shale interbeds typically show well developed slaty cleavage which commonly penetrates the underlying thinly-bedded quartzites, forming refractive cleavage, suggestive of normally graded beds. The graded quartzite beds of this subfacies are typically laterally persistent and can be traced for several meters along strike.

3.1.6 SUBFACIES 1D: INTERBEDDED SLATY SHALE AND BIOTURBATED / BURROWED QUARTZITES

This subfacies consists of bioturbated and burrowed quartzites interbedded with slaty shales (Fig. 3.9). Most of the interbedded quartzite layers (>75%) have been modified by biogenic reworking. In general, the homogenization by burrowing has completely destroyed any evidence of internal primary sedimentary structures. The nature of the upper and lower bed surfaces are commonly obscured and difficult or impossible to distinguish. Vertical burrows (0.1 to 0.3 cm in diameter) are rare; however, horizontal to slightly sub-horizonal burrows (0.1 to 1.3 cm in diameter) are very common. These are simple cylindrical horizontal burrows which occur both at the base of bioturbated quartzite layers and as discrete burrows within the slaty shale interbeds.

3.1.7 SUBFACIES 1E: FINE- TO MEDIUM-CRYSTALLINE QUARTZITE WITH THIN ARGILLACEOUS INTERBEDS

This subfacies represents an end-member to the previous subfacies, and is characterized by fine- to medium-crystalline quartzites containing thin argillaceous laminae and silty shale stringers (Fig. 3.10). The argillaceous laminations are generally horizontal to slightly wavy, with individual argillaceous laminae ranging in thickness from 1 to 3 mm. The beds of this subfacies range in thickness from 1 to 11 cm. Subfacies 1e contains basal bed contacts which are sharp and planar to gently undulating and slightly erosional. Bioturbation is virtually absent.

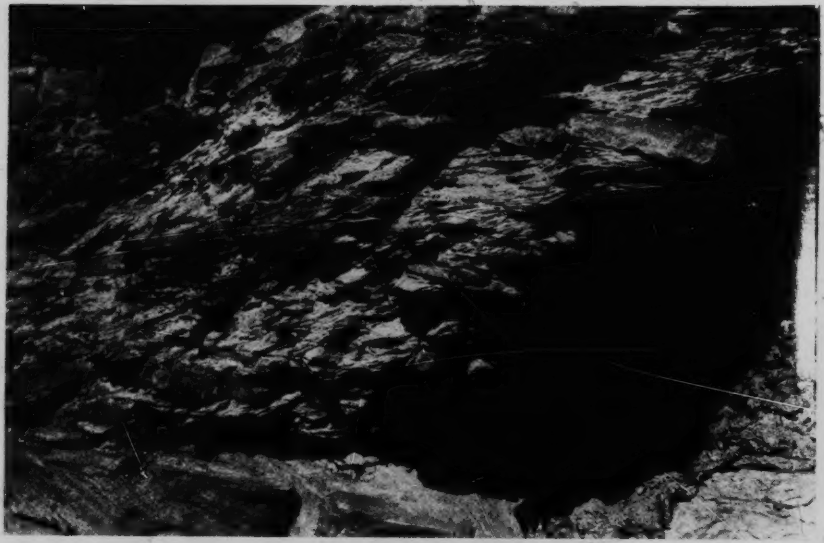

Figure 3.9. Subfacies 1d: Interbedded slaty shale and bioturbated/burrowed quartzite. Note the discrete horizontal burrows located directly above the lens cap. This very broad U-shaped trace is identified as *Trichophycus* which is a intrastratal feeding burrow, possibly produced by a trilobite-like organism burrowing and dwelling within the sediment.

Figure 3.10. Subfacies 1e: Fine- to medium-crystalline quartzite with thin argillaceous interbeds.

3.1.8 FACIES 2: SHALE AND SLATY SHALE

This facies is characterized by black to green shale and slaty shale with minor thin quartzite stringers (Fig. 3.11). Facies 2 is differentiated on the basis of the shale content (shale >90%). The shale and slaty shales are typically massive with flat, non-erosional basal contacts. The very-fine to fine-crystalline quartzite interlaminae are massive, wispy or parallel-sided horizons ranging in thickness from 1 to 7 mm. The black shales of Facies 2 exhibit no slaty cleavage and are only found at outcrop A, where it accounts for 0.9% of the total measured section. The average bed thickness at outcrop A is 2 cm (range: 0.2 - 8 cm). The olive green slaty shales locally show well developed slaty cleavage and are found at outcrops B, C and D where it comprises 1%, 3% and 4%, respectively, of the total measured sections. The average bed thickness is 3 cm at outcrop B, 5 cm at outcrop C, and 4 cm at outcrop D. Bioturbation is present and typically occurs in the upper portion of the bed; in some cases discrete burrows may be preserved.

3.1.9 FACIES 3: GRADED MATRIX-SUPPORTED PEBBLE CONGLOMERATE

This facies is rare and only occurs at outcrop D where it comprises 0.68% of the total measured section. Average bed thickness is 6.5 cm (range: 4.5 - 11 cm). In the beds of this facies the basal layers are matrix-supported pebble conglomerates that grade upward into horizontally stratified quartzites followed abruptly by ripple cross-laminated finely-crystalline quartzites (Fig. 3.12). The horizontally stratified quartzites are medium- to coarsely-crystalline and vary in thickness from being locally absent to 6 cm thick. The thickest intervals of horizontal stratification generally occur when the underlying basal pebble conglomerate is relatively thin. The overlying ripple set thickness is typically less than 5 cm. Internally, the small-scale cross-stratification consists of asymptotically-dipping cross-laminae and is interpreted as trough cross-lamination (Fig. 3.13). Basal contacts are sharp, planar and erosional. Upper bed boundaries are undulating to slightly planar. Beds are laterally persistent and can be traced for several meters with slight variations in thickness. The chert-pebble clasts (2 - 6 mm in diameter) are generally elongated and subrounded. The matrix consists of well sorted and subrounded, medium- to coarse-crystalline quartzite grains. Internally the chert pebble clasts are not uniformly distributed throughout the bed along strike. The bed contains scattered pockets of massive matrix void of coarse clasts. Sole marks are difficult to distinguish

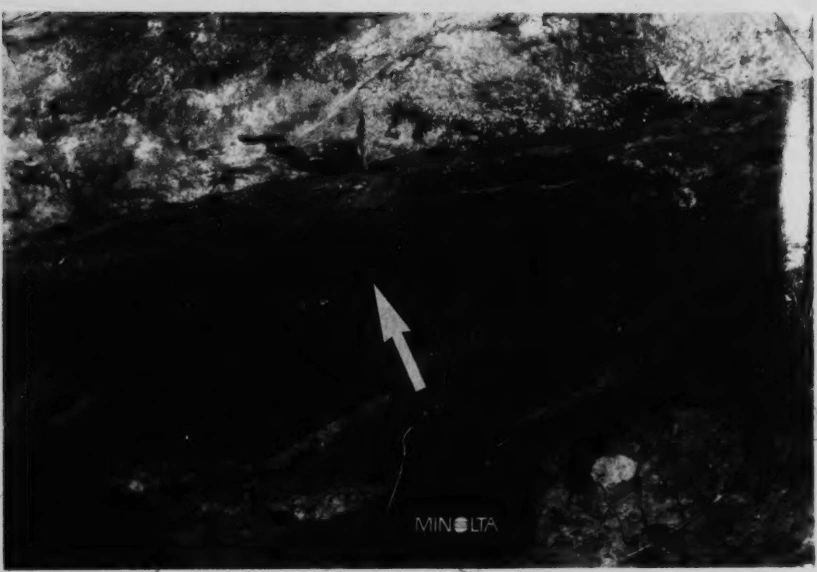

Figure 3.11. Facies 2: Shale and slaty shale. Arrow points to a bioturbated interval occurring in the upper portion of the bed.

Figure 3.12. Facies 3: Graded matrix-supported pebble conglomerate.

Figure 3.13. Photograph of Facies 3 showing small-scale trough cross-lamination within the upper portion of the bed.

due to the limited erosional relief of the basal bedding planes of beds.

3.1.10 FACIES 4: SMALL-SCALE TROUGH AND PLANAR CROSS-STRATIFIED QUARTZITES

This facies consists of fine- to medium-crystalline quartzites which contain small-scale trough and planar cross-stratification (set thickness is less than 5 cm). Although rarely visible the wavelengths of the ripple sets varies from 8 to 18 cm. The nature of the upper set boundary is characteristically undulating to slightly planar and non-erosional. Basal contacts are generally undulating and non-erosional to erosional. No climbing ripple cross-lamination was observed in any of the measured outcrops. This facies comprises 7%, 18%, 6%, and 2% of the total measured sections at outcrops A, B, C, and D, respectively. The average bed thickness is 12 cm at outcrop A, 18 cm at outcrop B, 15 cm at outcrop C and 6 cm at outcrop D. Within this facies two types of cross-stratification are recognized. The dominant type of cross-stratification shows cross-laminae which asymptotically dip towards the base (Fig. 3.14). These are interpreted as trough cross-stratification. The other less common type is planar cross-stratification, characterized by angular bottomset contacts. Bioturbation is minor and typically occurs at the base of the cross-stratified layers. Discrimination between small-scale trough and planar cross-stratification is difficult or impossible. This is due to the susceptibility of fine grained sandstone to metamorphic recrystallization and thus destroying internal sedimentary structures. In cases where the cross-laminae are obscured or only vaguely defined, this facies was identified on the basis of the undulating upper and lower set boundaries, suggesting that the units were originally cross-laminated. Amalgamation of sets is very common in this facies. The thickness of the individual cross-stratified sets is between 2 and 5 cm. However, sets occur in stacked units with an average thickness of 13 cm (range: 5 - 48 cm). Thin slaty shale drapes commonly occur between ripple sets. The thickness of the drapes varies between 0.1 to 1 cm and generally decrease in thickness and abundance upward within the bed.

3.1.11 FACIES 5: PLANAR CROSS-STRATIFIED QUARTZITES

This facies consists of fine- to coarsely-crystalline beds of planar cross-stratified quartzites. This facies is characterized by angular contacts of bottomsets within the cross-strata. This facies is divided into the following two subfacies based on set thickness.

Figure 3.14. Facies 4: Small-scale trough and planar cross-stratified quartzites. The arrow indicates a interval of small-scale trough cross-stratification.

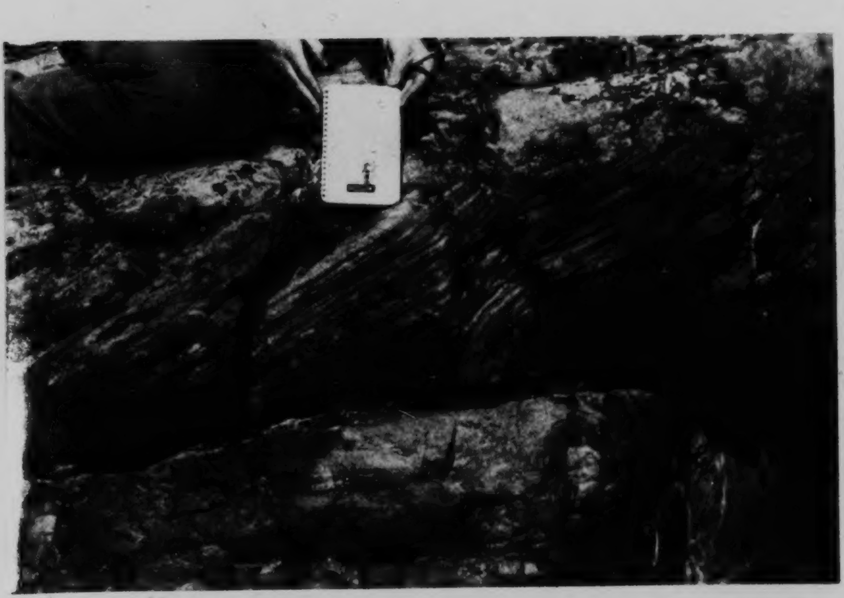

Figure 3.15. Subfacies 5a: Planar cross-bedded sets (0.05 - 0.4 m thick). Photograph shows a 36 cm bed of planar cross-stratification.

3.1.12 SUBFACIES 5A: PLANAR CROSS-BEDDED SETS (0.05 - 0.4 M THICK)

Subfacies 5a consists of fine- to medium-crystalline beds with planar cross-stratification, occurring in sets 0.05 - 0.4 m thick (Fig. 3.15). This facies is the second most common at outcrop A where it accounts for approximately 30% of the total measured sections compared with only 4%, 3% and 0% at outcrops B, C and D, respectively. The average bed thickness is 34 cm at outcrop A, 23 cm at outcrop B and 19 cm at outcrop C. Basal contacts are slighty erosional, planar to gently undulating. Beds of this subfacies are often laterally persistent and can be traced along strike for several meters. This subfacies contains slaty shale intraclasts which range from 0.1 to 2 cm in diameter. Bioturbation is minor and generally occurs at the base of the beds. Rare examples of reactivation surfaces are present and are usually draped by a thin layer of slaty shale. Amalgamation of beds, in which sets are stacked one above the other to make successions of a few meters thick, is extremely common and best illustrated at outcrop A. The interesting feature of this subfacies at outcrop A is the uniformity of cross-bedding and set size within vertically contiguous sets. (set thickness ranges between 6 to 12 cm). At outcrop A, the beds of this subfacies often contain stratification which is only vaguely defined. When visible, the angular foresets show lateral variations in crystallinity, from fine- to medium-crystalline with sucrosic textures to adjacent foresets which are coarsely-crystalline, with non-sucrosic, clear textures (Fig. 3.16). The basal contacts of the sets are sharp and planar with no evidence of scouring. This subfacies is often difficult to distinguish due to the lack of variation in crystallinity between adjacent sets and metamorphic recrystallization. The lower boundaries of the sets are often recognized by the slightly darker coloration and, less commonly, by the occurrence of a coarsely- to very-coarsely crystalline basal lag.

3.1.13 SUBFACIES 5B: PLANAR CROSS-BEDDED SETS (0.4 - 2 M THICK)

Subfacies 5b consists of medium- to coarsely-crystalline planar cross-stratification in sets 0.4 - 2 m thick (Fig. 3.17). This subfacies is the second most common at outcrops C and D, where it comprises 18% and 27% of the total measured section, compared with only 4% and 8% at outcrops A and B. The average bed thickness is 53 cm, 63 cm, 65 cm and 71 cm at outcrops A, B, C and D, respectively. This subfacies is characterized by angular cross-laminae which have sharp-based truncations. The cross-laminae are a maximum of 2.5 cm thick and are

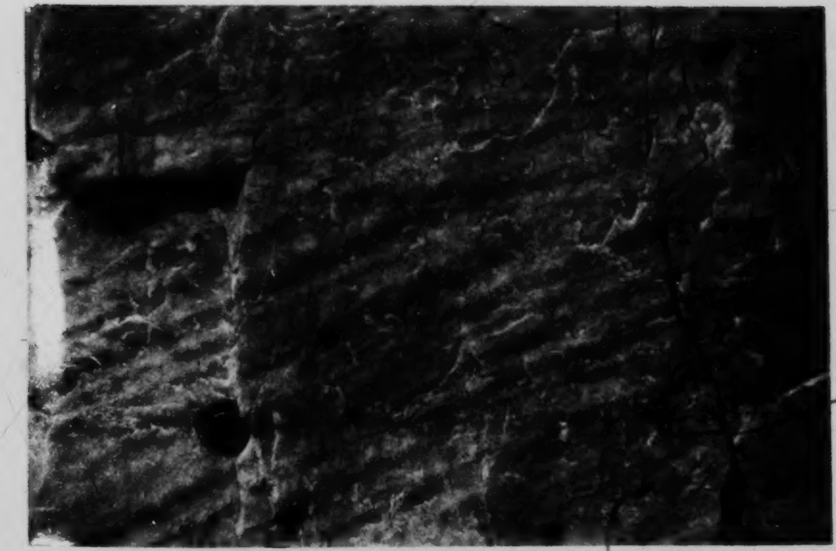

Figure 3.16. Planar cross-stratified bed (8 cm thick) of Subfacies 5a. Note the lateral varations in crystallinity between angular foresets from fine- to medium-crystalline with sucrosic textures to adjacent foresets which are coarsely-crystalline, with non-sucrosic, clear textures.

Figure 3.17. Subfacies 5b; Planar cross-bedded sets (0.4 - 2 m thick). The planar cross-stratified bed shown in the photograph is 52 cm thick.

defined by the variation in color and crystallinity of adjacent cross-laminae. Typically the internal cross-laminae varies laterally in crystallinity from medium- to coarsely-crystalline between adjacent cross-laminae. The thicker beds are laterally persistent and can be traced up to 30 m along strike. Basal contacts are typically slightly erosional, planar to slightly undulating. At outcrop B, scoured basal contacts containing scour-fill cross-lamination are fairly common. Slaty shale intraclasts (0.1 cm to 3 cm in diameter) are common. These clasts are subangular and are often partially weathered out. The slaty shale intraclasts were probably derived from the scouring of the underlying muddy substrate. This subfacies also contains reactivation surfaces which are commonly draped by slaty shale. Less commonly, small-scale ripple cross-lamination occurs along the reactivation surfaces. Outcrop C shows one case of finely-crystalline small-scale ripple cross-stratification occurring in the lower portions of each foreset of the planar cross-stratified bed. The occurrence of soft sediment deformational features (load structures) and bioturbation is rare.

3.1.14 FACIES 6: TROUGH CROSS-BEDDED QUARTZITES

This facies consists of fine- to coarsely-crystalline beds of trough cross-stratification. Internal structures consist of asymptotically-dipping cross-lamination which intersect the base of the bed at a tangental angle. Festoon cross-lamination showing symmetrical basal scour surfaces and concentric infilling foreset laminae is rare. Typically the basal contacts are erosional and planar to gently undulating. Soft sediment deformation features and bioturbation structures rarely occur. Facies 6 is divided into two subfacies based on the thickness of the trough cross-bedded sets.

3.1.15 SUBFACIES 6A: TROUGH CROSS-BEDDED SETS (0.05 - 0.4 M THICK)

This subfacies is the second most common at outcrop B, where it accounts for 20% of the total measured section compared with 10%, 11% and 10% at outcrops A, C and D. The average bed thickness is 26 cm at outcrop A, 22 cm at outcrop B, and 20 cm at outcrops C and D. Internally subfacies 6a consists of fine- to medium-crystalline beds of trough cross-stratification (Fig. 3.18). The bases of cross-laminae are asymptotic to tangental to the base of the bed. These basal contacts are generally erosional, planar to slightly undulating. Scoured bases rarely incise greater than 15 cm. They are usually less than 5 cm in depth.

Figure 3.18. Subfacies 6a: Trough cross-bedded sets (0.05 - 0.4 m thick). The photograph shows a trough cross-stratified bed which varies in thickness from 29 cm to 38 cm.

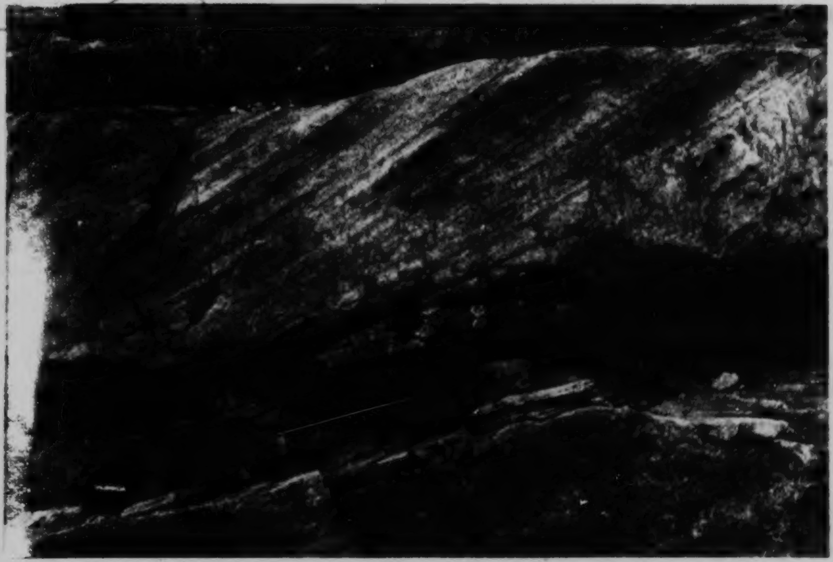

Figure 3.19. Subfacies 6b: Trough cross-bedded sets (0.4 - 2 m thick). The trough cross-stratified bed shown in the photograph is 45 cm thick.

Amalgamation of sets is very common. Individual sets are recognized by thin (0.1 to 0.6 cm thick) coarsely-crystalline basal lag deposits which occur along with basal truncations of trough cross-laminae. In general the set thickness varies from 6 cm to 12 cm, and with the exception of outcrop A, are commonly draped by a thin layer of slaty shale. Slaty shale intraclasts (0.1 to 2 cm in diameter) are fairly common and are usually partially weathered out.

3.1.16 SUBFACIES 6B: TROUGH CROSS-BEDDED SETS (0.4 - 1 M THICK)

This subfacies is not present at outcrop A, but accounts for 2%, 6%, and 8% of the total measured sections at outcrops B, C and D, respectively. The average bed thickness is 46 cm at outcrop B, 60 cm at outcrop C and 66 cm at outcrop D. Subfacies 6a is characterized by medium- to coarsely-crystalline beds of trough cross-strata (Fig. 3.19). The distinctive feature of the cross-laminae are their curved, tangential intersections with the base of the bed. These cross-laminae are 1 cm thick and are defined by the variation in color of adjacent cross-laminae. Basal contacts of beds are planar to gently undulating and slightly erosional. Basal scour surfaces (scour depths between 5 and 15 cm) rarely occur. The beds of this subfacies are laterally continuous and can be traced for up to 15 meters along strike. Reactivation surfaces occur and are commonly draped by 0.1 to 0.7 cm thick slaty shales.

3.1.17 FACIES 7: LOW ANGLE AND HORIZONTALLY STRATIFIED QUARTZITES

This facies is characterized by low angle to horizontal internal stratification which is usually not laterally continuous. Where observable, the cross-laminae are generally planar to slightly concave upwards, with inclinations between 5 - 15° (Fig. 3.20). The basal bedding contacts are sharp, gently undulating to slightly planar and typically non-erosional. The low angle to horizontally stratified quartzites vary in crystallinity from fine- to coarsely-crystalline. This facies comprises only 0.6% of the total measured sections at outcrop A compared with 8% at outcrop B, 11% at outcrop C and 9% at outcrop D. Average bed thickness is 24 cm at outcrop A, 18 cm at outcrop B, 20 cm at outcrop C and 19 cm at outcrop D. The interesting feature of this facies is that the beds are not laterally persistent and commonly can be traced several meters along strike to planar or trough cross-stratified beds of Facies 5 and 6. Silty shale intraclasts are fairly common. These clasts are typically subangular and average 1 cm in diameter. Reactivation surfaces and bioturbation structures are virtually absent. There is no

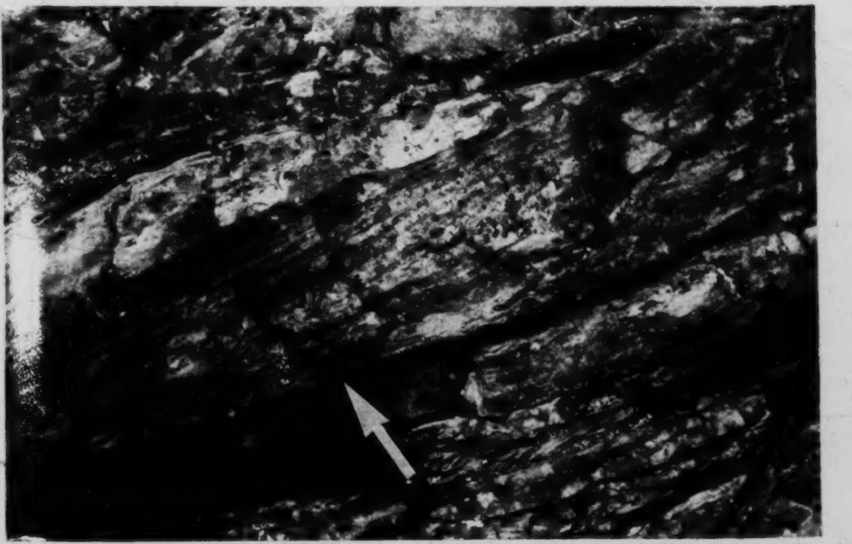

Figure 3.20. Facies 7: Low angle and horizontally stratified quartzites. Photograph shows a quartzite bed with internal low angle stratification. Arrow indicates the inclined bedding plane.

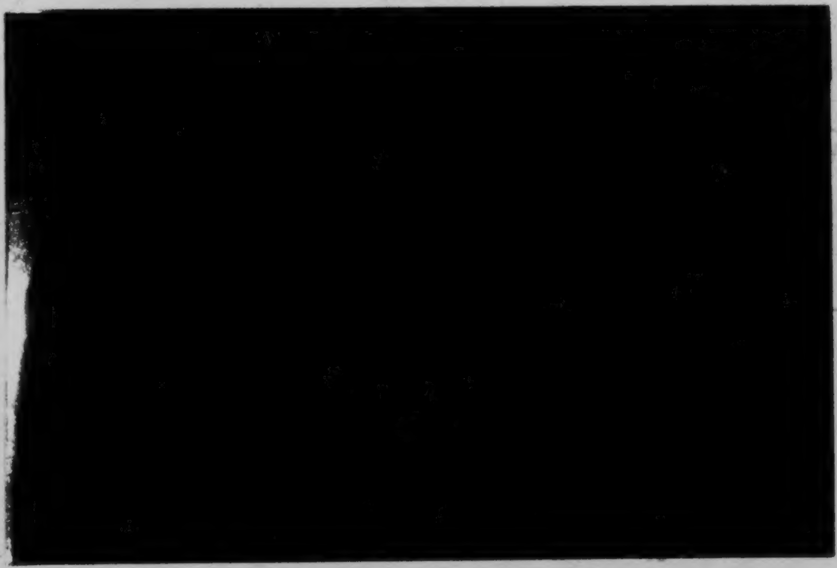

Figure 3.21. Facies 8: Massive quartzites.

TABLE 3.2 Summary of the Lower Cambrian Gog Group facies.

a = abundant c = common r = rare

Facies	1a	1b	1c	1d	1e	2	3	4	5a	5b	6a	6b	7	8
Bed base														
erosive	—	—	c	—	—	—	c	r	c	c	c	c	c	—
sharp, planar	a	c	c	c	—	c	c	c	c	c	c	c	c	c
wavy	r	c	—	—	r	—	—	a	—	—	—	—	—	—
Set thicknesses														
small scale (5cm thick)	c	a	c	c	—	—	c	a	—	—	—	—	—	—
medium scale (0.05-0.4m thick)	r	—	r	—	c	—	r	—	a	—	a	—	a	a
large scale (0.4-2m thick)	—	—	—	—	—	—	—	—	—	a	—	a	—	—
Structures														
parallel lamination	—	r	—	—	—	—	—	—	—	—	—	—	—	—
planar cross-bedding	—	c	—	—	—	—	—	c	a	a	—	—	—	—
trough cross-bedding	—	c	r	—	—	—	r	a	—	—	a	a	—	—
low angle to horizontal strat.	—	—	—	—	—	—	—	—	—	—	—	—	a	—
massive	a	—	—	—	—	c	c	r	—	—	—	—	—	a
matrix-supported	—	—	—	—	—	—	a	—	—	—	—	—	—	—
normal grading	—	—	a	—	—	—	a	—	—	r	—	—	—	—
amalgamation of sets	r	r	—	—	—	—	—	a	a	—	—	—	—	a
shale intraclasts	r	—	—	—	—	—	—	a	c	c	a	c	c	c
slaty cleavage	c	c	c	—	—	c	—	—	—	—	—	—	—	—
shale stringers	—	—	—	—	a	—	—	—	—	—	—	—	—	—
bioturbation	r	r	r	a	—	—	—	c	r	r	r	—	—	—
reactivation surfaces	—	—	—	—	—	—	—	r	r	c	c	c	—	—
soft sediment deformation	r	—	r	—	—	—	—	—	—	r	—	—	r	r
quartzite stringers	—	—	—	—	—	a	—	—	—	—	—	—	—	—
Mean grain size (Φ)	← clay to 1 →					clay	-4-3	2-3	2-3	1-3	2-3	1-3	1-2	0-3

evidence of internal surfaces showing parting lineations. Load structures are sometimes found and in a few cases affect the underlying quartzite interbeds within Facies 1.

3.1.18 FACIES 8: MASSIVE QUARTZITES

This facies consists of fine- to coarsely-crystalline quartzites showing no visible sedimentary structures or grading (Fig. 3.21). The lack of visible internal stratification may be partially due to the homogenous nature of the crystallinity. This facies is the most common facies at outcrop A, where it accounts for 40% of the total measured sections. Facies 8 is of lesser importance at outcrops B, C and D comprising only 6%, 5% and 3%, respectively of the total measured section. The average bed thickness at the various outcrops are 31 cm at A, 20 cm at B, 16 cm at C and 13 cm at D. Basal contacts are slightly erosional and vary from gently undulating to planar. This facies at outcrop A consists of amalgamated sets of massive beds with no shale interbeds. The lack of internal stratification and the uniformity of grain size makes the recognition of each set difficult. Less commonly coarse- to very-coarsely-crystalline basal lags, a few millimeters thick, were the only criteria preserved to distinguish the various sets. The average thickness of these sets is between 6 to 12 cm. Basal contacts appear planar and slightly erosive. At outcrop A, beds of this facies can be traced a few meters along strike to beds of Facies 5a which contain amalgamated sets of planar cross-stratification, 5 to 12 cm thick.

3.2 FACIES INTERPRETATIONS

3.2.1 FACIES 1

This facies which consists of alternating quartzite layers and slaty shale represents an environment with fluctuating energy conditions. The interbedded slaty shales were deposited directly from mud suspension fall-out during quiet water conditions and represents normal mud accumulation in a tranquil environment. The thin quartzite beds are associated with higher energy conditions, probably generated by periodic meteorological disturbances, causing an episodic supply of sand. After the periodic short-lived event which introduced siliciclastic sediments into a otherwise quiet environment the "normal" slow hemipelagic sedimentation resumes and eventually buries the isolated sand horizon.

Facies 1 is divided into six subfacies and the difference between the various subfacies depend on the hydrodynamics of the current during deposition, which ultimately determines the type of internal stratification, and the relative amount of modification by biological activity.

3.2.2 SUBFACIES 1A: INTERBEDDED SLATY SHALE AND MASSIVE QUARTZITES

This subfacies is interpreted as being deposited rapidly from suspension with no tractional movement, thus preventing the formation of internal sedimentary structures. Alternatively, the massive nature of these quartzites may be due to obliteration of recognizable sedimentary structure during metamorphism. Another possible contributing factor is the uniform nature of the grain size. In very well-sorted sands there is only a slight variation in grain size and this minor textural variation between grains makes it difficult to recognize internal sedimentary structures. In some cases the intense iron staning derived from the chemical weathering of ferrous minerals obscures the sedimentary features and contributes to the massive appearence of the quartzite interbeds. One important conspicuous feature of this subfacies is the lateral thickening and thinning of individual quartzite interbeds and the undulating appearence of the upper and lower form set surface. This possibly suggests that the massive quartzite interbeds were originally cross-laminated but subsequent metamorphism destroyed the internal sedimentary structures and consequently only the ripple profile is preserved (Fig. 3.5). The interbedded slaty shale is interpreted as mud suspension fall-out during hydraulically quiet times and represents the "normal" state of sedimentation in the tranquil, mud-floored environment.

3.2.3 SUBFACIES 1B: INTERBEDDED SLATY SHALE AND STRATIFIED VERY-FINE-TO MEDIUM-CRYSTALLINE QUARTZITES

This subfacies is interpreted as the result of bedload transport of sand causing the development of small-scale cross-lamination and rare parallel lamination. The existence of internal primary cross-lamination indicates that current velocities were relatively low but sufficient enough for the tractional transport of sand. According to Figure 3.23 the current strength needed to form small ripples in fine sand (0.2 mm) is about 18 cm/sec to 60 cm/sec. However, it should be noted that the sequence of bed configurations with increasing flow velocity that is shown in Figure 3.23 is experimentally produced in relatively shallow flow depths. Because of the obvious limitations to the size of flumes, it is difficult to model and study the hydraulics of bed configurations in deeper flows. Harms *et al.* (1982) discusses the problems associated with extrapolating laboratory generated data to deeper natural flows.

The internal laminations of many interbedded quartzites layers are often very faint and not laterally persistent along the outcrop. However, in conjuction with the faintly recognizable laminations is the pronounced undulations of the upper and lower set boundaries which adds additional information that the quartzite interbeds contain internal primary stratification resulting from the tractional movement of sediment.

The two depositional regimes which characterize this subfacies is related to the interaction of relatively low and high energy conditions. Each quartzite interbed is apparently the result of tractional transport of sand by unidirectional bottom currents generated by either meteorological (wind-wave) currents or by a tidal current system. In this subfacies the presence of stacked cross-laminated quartzite interbeds suggests that each coset, which typically consists of 2 to 6 amalagmated beds, represents the deposits of a single flow-transverse ripple field.

The relatively coarse crystallinity and well sorted nature of the parallel lamination suggests that it is the result of upper-flow regime plane-bed transport. This indicates that the controlling hydrodynamic conditions were in the lower part of the upper-flow regime and not achieved by slow lamina-by-lamina accretion typical of lower-regime plane beds generated by fairly low flow velocities. The different sequences of bed phases with increasing flow velocity, for grain sizes finer than 0.15 mm is shown in Figure 3.22. For a given flow depth the sequence of bed configurations with increasing current velocity is; no movement, small ripples, upper plane bed, and antidunes. Current velocities of about 62 cm/sec to 130 cm/sec are needed to develop upper plane beds in 0.15 mm sand (Fig. 3.23). Such parallel laminated structures could be formed by sediment transported in suspension and deposited under relatively high flow velocities in the form of parallel laminae, without subsequent traction transport, as the current waned.

The slaty shale intervals represent the passage back into the slow hemipelagic rain which characterizes the "normal" emplacement of fine-grained sediments in the low-energy tranquil environment.

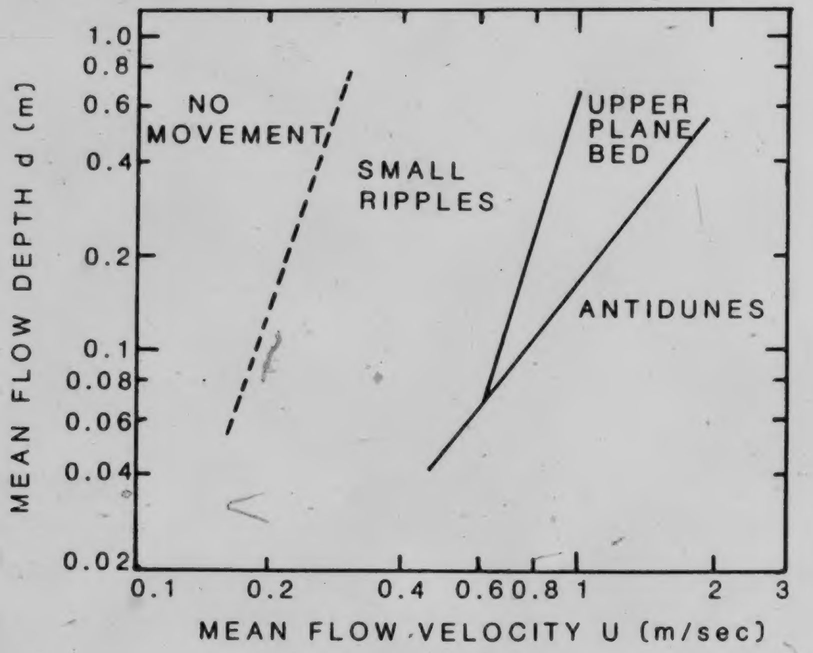

Figure 3.22. Depth-velocity diagram for fine-grained sand (0.01-0.15 mm)(modified after Harms *et al.*, 1982).

3.2.4 SUBFACIES 1C: INTERBEDDED SLATY SHALE AND GRADED QUARTZITES

The interbedded slaty shale and normally graded quartzites represent an environment with fluctuating energy conditions. The thin graded quartzite layers suggest an episodic high energy depositional event, in which suspended sand is rapidly deposited into a tranquil environment, normally characterized by the accumulation of fine-grained sediments. The sequence of graded quartzites with the associated overlying ripple-lamination is interpreted to represent deposition under progressively decreasing current velocities. These thin graded layers which show succeeding sedimentary structures related to reduced flow power represents conditions in which sediment was probably deposited by decelerating suspension-laden currents.

Several physical processes have been attributed to the origins of these graded and laminated quartzites layers as found in Subfacies 1c. These include sediment suspension clouds generated by waves (Reineck and Singh, 1972), density gravity flows formed by storm-surge ebb (Hayes, 1967), and deposition from geostrophic bottom flows produced by wind forcing (Morton, 1981). However, since there is no direct correlation between thin graded sequences and specific processes, it is difficult to determine the exact physical process involved in the formation of Subfacies 1c.

The interbedded nature of this subfacies where the slaty shale alternates with thin graded quartzites reflects the interaction of storms and fair-weather processes. The quartzite beds which show various waning flow sequences suggest that periodic meteorological disturbances were responsible for their formation. The slaty shale interbeds represent a reinstatement of "normal" mud suspension fall-out which buries the high-energy storm event(s) which were introduced into this otherwise tranquil environment characterized by fine-grained sedimentation.

3.2.5 SUBFACIES 1D: INTERBEDDED SLATY SHALE AND BIOTURBATED / BURROWED QUARTZITES

Subfacies 1d represents the flourishing of a benthic community after an influx of sediment from a depositional event. The majority of the quartzite beds are extensively reworked and modified by biological activity which suggests the reinstatement back to normal mud sedimentation. This return to the extremely slow rates of hemipelagic accumulation allows sufficient time for the benthonic organisms to recolonize after the catastrophic event. This subfacies illustrates the alternating interplay of deposition occurring during periodic short-lived events, probably generated by storms, and biological activities during fair-weather periods. The benthic organisms could burrow extensively into the substrate during these fair-weather periods until the occurrence of the next rapid emplacement of sand from a high-intensity episodic event.

3.2.6 SUBFACIES 1E: FINE- TO MEDIUM-CRYSTALLINE QUARTZITE WITH THIN ARGILLACEOUS INTERBEDS

This subfacies is interpreted as being deposited in an environment where current or wave action alternates with periods of quiet water conditions. The relative abundance of quartzite indicates that the conditions were more favorable for the deposition of sand than for muds.

3.2.7 FACIES 2: SHALE AND SLATY SHALE

This facies represents deposition from mud suspension fall-out during periods of normal quiescence, forming a predominately muddy substrate. This very uniform sedimentation over a period of time from hemipelagic fall-out results in the vertical accretion of predominately massive silts and clays. After deposition these very fine grained sediments are not subjected to futher transport and form a muddy bottom environment. This slow accumulation of fine-grained hemipelagic cohesive sediments is occassionally interrupted by periodic short-lived, high-energy conditions which result in the deposition of very thin horizons, a few millimeters thick, of coarse silt or very-fine grained sand. Thus the minor thin quartzite stringers intercalated within this facies are interpreted as the result of very-fine grained sand and silt which are resuspended and transported seaward into deeper areas of shelf muds. Blatt *et al.* (1980) suggested that in shallow marine environments the laminae may be produced in muds by seasonal fluctuations in the sediment supply or periodic stirring of the bottom by wave action. The massive nature of the thin quartzite interlaminae is attributed to the insufficient quantity of coarse grained sediment available in which to generate internal sedimentary structures. Alternatively, the absence of internal stratification within the quartzite stringers and the massive appearence of the slaty shales maybe the result of burrowing organisms which churn-up the substrate and consequently destroy internal sedimentary structures and bedding.

3.2.8 FACIES 3: GRADED MATRIX-SUPPORTED PEBBLE CONGLOMERATE

This facies is interpreted as being rapidly emplaced by transient subaqueous flows of appreciable magnitude because of the distinctive suite of preserved sedimentary structures. This suite includes a sharp, abrupt basal erosional contact, a large grain-size variation from chert pebble clasts to finely-crystalline quartzites, a normal size grading within the bed and a vertical sequence of primary sedimentary structures indicating a decreasing flow intensity.

From this information it appears that the sequence of structures was deposited by sediment gravity flows, more specifically turbidity currents in which sediment is supported in suspension by the upward component of fluid turbulence (Middleton and Hampton, 1976). In general, most turbidity currents deposit beds showing some evidence of size grading and a sequence of internal structures showing progressively reducing flow regimes. The diagnostic sedimentary features of Facies 3 compare similarly to the Bouma sequence of an idealized turbidite bed. This Bouma sequence contains a characteristic sequence of structures that reflect the variations in the rate of deposition, flow regime and grain size of the depositing turbidity current.

The sharp, basal erosional contact of Facies 3 indicates the erosional capacity and nature of the turbidity current surge. Immediately overlying this erosional contact, the basal layer of matrix-supported pebble conglomerate which grades upwards into horizontal stratification and then ripple cross-lamination reflects deposition from a gradually decreasing turbidity current. Not only does the sequence of structures in Facies 3 indicate a turbidity current undergoing gradually decreasing flow conditions but also a change in the rate of deposition. This change is from very rapid deposition resulting in poorly sorted pebble conglomerates at the base to reduced deposition facilitating the generation of tractional structures such as parallel lamination and cross-lamination towards the top of the bed.

According to Walker (1975), mean flow velocities varying from 120 cm/sec to 165 cm/sec are needed to tractionally move pebbles (0.4 mm in diameter) and maintain low concentrations of medium grained sand in suspension. A slight velocity fluctuation below this estimated range would result in a deposit similar to beds of Facies 3. In which a basal layer of matrix supported pebble conglomerates grades upwards into medium grained sand.

The well rounded shape of the chert pebble clasts suggests a multi-cycle origin and that the initial rounding did not occur within the depositional setting of this facies. The rounding of the pebble clasts probably occurred closer to shore in a higher energy setting presumably in a nearshore environment. These rounded clasts were subsequently removed from the nearshore area and deposited futher offshore by unconfined turbulent sediment-transporting systems.

Several episodic high energy events have been attributed to the generation of turbidity current surges. These include earthquakes (Heezen and Ewing, 1952), spontaneous failure of bottom sediments (Walker, 1984), and cyclic wave loading by major storms (Henkel, 1970; Cluckey *et al.* , 1980; Prior and Coleman, 1982; Walker, 1984). However, since there is no direct correlation between turbidite deposits and specific processes, it is often difficult to determine the exact physical process involved in generating the subaqueous turbidity currents.

It should be noted that although Facies 3 is volumetrically less abundant than other facies, it still suggests that turbidity currents are a recognizable mechanism for transporting coastal sediment into more offshore shelf environments.

3.2.9 FACIES 4: SMALL-SCALE CROSS-STRATIFIED QUARTZITES

The internal small-scale cross-stratification which characterizes this facies is interpreted as the migration of small-scale three-dimensional and straight-crested ripples. The processes of tractional movement on noncohesive sediment causes individual grains to migrate up the back of the ripple and under gravity, avalanche down its sloping face. This grain-by-grain avalanching of material over the ripple crest results in the formation of lee side laminae plunging in the "downcurrent" direction. The existence of small-scale cross-lamination which records the migration of flow-transverse ripples indicates that the controlling hydrodynamic conditions existing at the time of deposition were in the lower part of the lower-flow regime.

The current speed-grain size phase diagram (Fig. 3.23) shows that the lowest velocity capable of producing small ripples in fine sand (0.2 mm) is about 18 cm/sec, while the upper limit of current strenght values is roughly 60 cm/sec. This diagram along with Simons *et al.*, (1965) indicate that small ripples cannot form in sand of mean diameter greater than about 0.6 mm.

However, it should be noted that the small-scale stratified structures of this facies are only observed in two dimension as viewed in cross-section on the face of the measured outcrop,

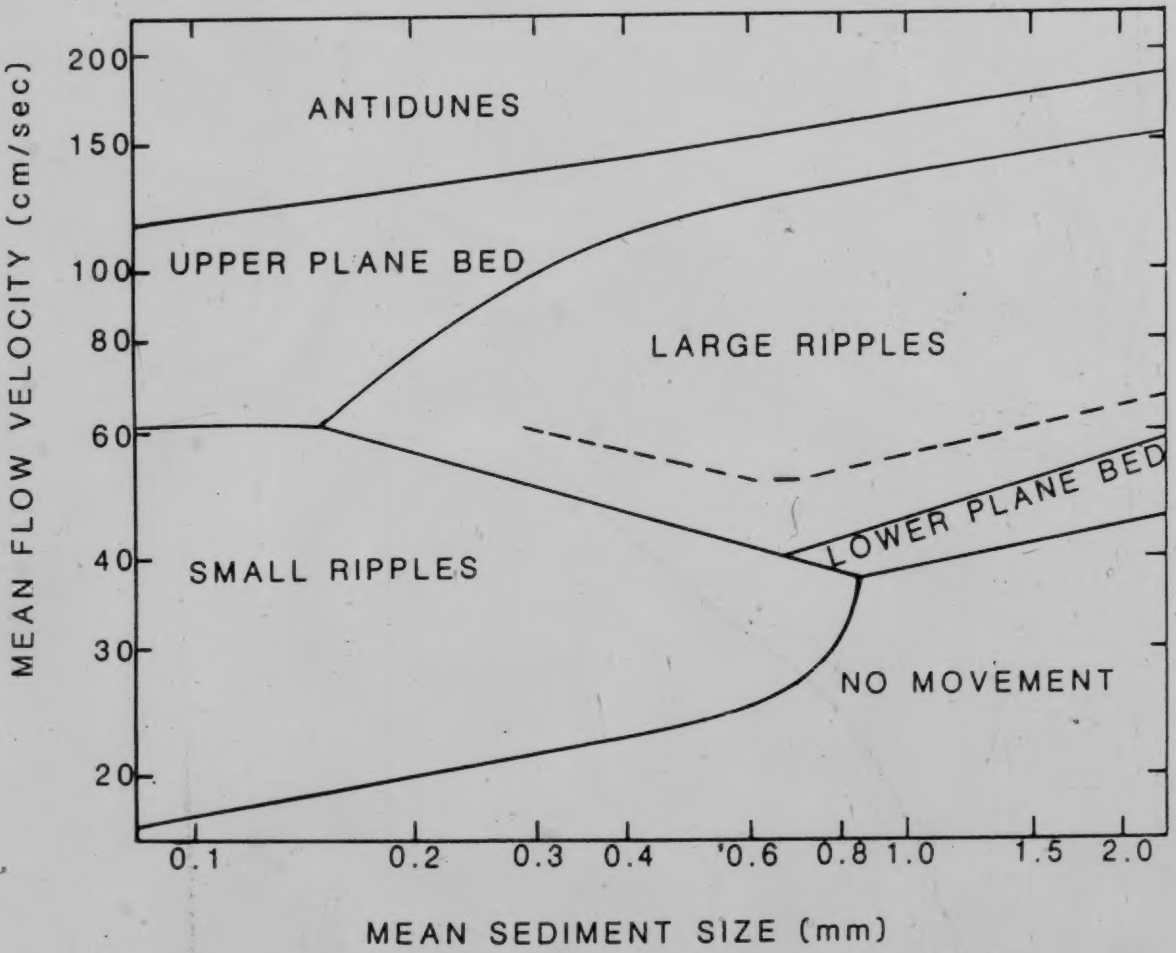

Figure 3.23. Size-velocity diagram with the corresponding bedform stability plots (modified from Harms *et al.*, 1982).

thus preventing a plan view of the crestline and the external geometry of the bedform. This makes it difficult to reconstruct the entire three-dimensional pattern of the bedform and leads to extreme difficulty in inferring from the preserved two-dimensional structure the kinematics of its formation. The advancing trains of ripples suggests that bottom currents were effecting the loose granular bed-material making up the substrate. These bottom currents were possibly driven by a variety of shelf current systems which include oceanic circulation currents, tidal currents and meteorological (wind-wave) currents. The presence of the superimposed sets showing oppositely dipping cross-stratification suggests a possible tidal influence in which the migration of ripples was periodically interrupted by reversing currents.

It is possible that some of the cross-stratified sets and intervals may be the result of remoulding or reworking during higher energy periods of oscillatory wave motions or strong bottom currents which postdate the initial depositional event. The presence of thin shale drapes suggests a slight fluctuation in energy conditions, in which during short-lived quiet water conditions the deposition of fine-grained sediments occurs from mud suspension fall-out. The amalgamation of individual cross-stratified sets which is common in this facies probably represents the migration and aggradation of a sand bed covered by flow-transverse ripple fields.

3.2.10 SUBFACIES 5A: PLANAR CROSS-BEDDED SETS (0.05 - 0.4 M THICK)

This subfacies is a result of bedload transport by the migration of small straight-crested megaripples or sandwaves. The high angle foresets indicate a progression of well developed slip faces from advancing trains of megaripples with straight and parallel crestlines that are elongated transversely to the flow. The non-scoured, planar basal contacts along with the lateral continuity of the beds indicates the lack of scour pits in the troughs and that the wavelenghts of these transverse megaripples are long relative to the height.

The stability fields of two-dimensional megaripples is shown in Figure 3.23. The current strength needed to develop straight-crested megaripples in 0.4 mm sand is approximately 47 cm/sec to 57 cm/sec. The formation of two-dimensional megaripples appears to be related to grain size, because for sands finer than 0.175 mm this bedform configuration is absent. It is important to note that within Facies 5 there is no differentiation genetically between the straight-crested megaripples of Subfacies 5a and that of Subfacies 5b. This is because the sediment transport for both is dominated by bedload movement and the internal cross-stratification is identical. The difference is only in the scale of bed thickness. These two-dimensional lower flow regime megaripples are produced by relatively strong bottom currents generated by possible meteorological currents (wave- and wind-induced processes), circulatory tidal current systems or oceanic circulation currents.

The unimodal paleocurrent pattern at section A suggests that the sediment dispersal was dominated by unidirectional currents. However, the presence of a coarser crystalline basal lag can possibly record erosion surfaces produced by reversing, or at least reworking currents. In the other sections the stacked planar cross-bedded sets often show adjacent units of oppositely dipping foreset laminae. The presence of bidirectional current formed sedimentary structures suggests that sediment dispersal and the migration of the two-dimensional bedforms was dominated mainly by tidal currents. The reactivation surfaces suggests that the migration of the two-dimensional megaripples was periodically interrupted by a reduced sand supply or by reworking or possibly reversing currents. Therefore, the presence of reactivation surfaces are a possible indicator of opposing tidal currents. This is because the asymmetry of the tidal ellipse often results in unidirectional sediment transport only during one tidal phase. The subordinate tidal current may be below the threshold to reverse the megaripple form and consequently the reactivation surface may record the slight reworking of megaripple crests during tidal current reversals. The thin slaty shales drapes occurring on the reactivation surfaces indicate an alternation of slack, quiet water conditions prior to renewed higher energy conditions of bedload transport. The stacked nature of this subfaces along with the uniformity of crystallinity, well developed sorting and constant set thickness suggests a migrating megaripple field.

3.2.11 SUBFACIES 5B: PLANAR CROSS-BEDDED SETS (0.4 - 2 M THICK)

This subfacies is interpreted as being deposited by laterally migrating two-dimensional, straight-crested megaripples or sandwaves with well-defined avalanche faces. In terms of genesis, with increasing flow velocity and grain size the small two-dimensional megaripples characterized by Subfacies 5a are succeeded by large straight-crested sandwaves represented by Subfacies 5b. These large flow transverse bedforms are typically produced at moderate current velocities between those forming small ripples (Facies 4) and of large three-dimensional dunes (Subfacies 6b). According to Figure 3.23, current velocities of about 40 cm/sec to 55 cm/sec are capable of producing straight-crested megaripples in 0.6 mm sand. These larger bedforms of Subfacies 5b are probably developed towards the upper limit of the given current flow values.

One of the most salient features of this subfacies is the lateral traceability and uniform thickness of individual beds along strike. This feature indicates the absence of scour pits in the troughs and the low height to spacing ratio of these larger two-dimensional bedforms. Consequently, the uniform bed thickness suggest bedforms migrating with straight crests of near constant elevation.

These two-dimensional large megaripples are formed by the interaction of strong tractional bottom currents on loose, coarse-grained sediment. The presence of bipolar paleocurrent patterns in outcrops B, C and D suggests reversing sediment transport associated with periodic bidirectionality of the bottom currents suggesting a tide-dominated current regime. However, it is possible that these large two-dimensional megaripples are not exclusively indicative of tidal currents and that strong unidirectional wind- and wave-driven currents and/or oceanic currents also play a role in their formation.

The origin of the small-scale ripple cross-lamination occurring within and between the lower portion of individual foresets is problematical because the direction of migration is unknown. The unidirectional bottom currents may be the source of energy forming the small-scale cross-stratification in the lower part of straight and angular bottomsets. In this case the occurrence of small-scale ripple structures in the bottomset may record low velocity modifications in which small ripples are advancing down the lee slope of the large straight-crested bedform. Conversely, if the backflow current eddies are strong enough, it may remobilize the sediments at the lower portions of the large two-dimensional sandwave producing counter current or backflow ripples which migrate along the bottomset and up the lee slope, building reverse cross-stratification (Fig. 3.24).

Alternatively, the ripple cross-lamination associated with lower foreset planes of the large-scale planar cross-strata could be formed by subordinate tidal currents. In this case the formation of the large straight-crested sandwave is related to the dominate tidal current direction and the reversing subordinate current is sufficiently powerful enough to generate up-slope migrating ripples or ripples moving along the lee face of the sandwave. The presence of reactivation surfaces suggests some unsteadiness of the currents where the migration of the

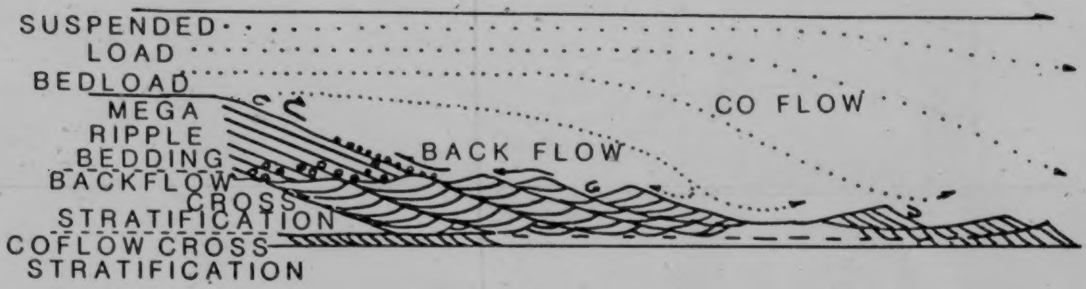
SUSPENDED
LOAD
BEDLOAD
MEGA
RIPPLE
BEDDING
BACKFLOW
CROSS
STRATIFICATION
COFLOW CROSS
STRATIFICATION
CO FLOW
BACK FLOW

Figure 3.24. Backflow ripples occurring on the lower portion of the bedform lee face due to strong backflow current eddies. Backflow ripples forming at the same time as active bedform migration results in the backflow cross-lamination being interwoven within the large-scale foresets (modified from Reineck and Singh, 1980).

bedform was occasionally interrupted by the lower energy conditions allowing mud suspension fall-out or wave reworking. This suggests a partial tidal influence in the deposition of beds of this subfacies.

3.2.12 SUBFACIES 6A: TROUGH CROSS-BEDDED SETS (0.05 - 0.4 M THICK)

This subfacies represents deposits formed from the lateral migration of small three-dimensional megaripples. The internal laminae which are typically curved and tangental to the underlying basal scour surface indicates that the advancing megaripples have undulating to sinuous crestlines with erosional scour surfaces in the troughs. The morphological similarities between the sinuous-crested megaripples of this subfacies and Subfacies 6b are almost identical. This stems primarily from the fact that both subfacies are genetically related, resulting from tractional transport, with Subfacies 6a being a smaller-scale equivalent of Subfacies 6b. In terms of hydrodynamic conditions, these undulating to lunate megaripples producing the trough cross-stratified sets are formed under lower-flow regime conditions at slightly higher current velocities than the small straight-crested megaripples of Subfacies 5a. These small three-dimensional bedforms are orientated transversely to flow, with sediment transport mainly dominated by tractional bedload.

Based on flume work, Harms *et al.* (1982) have stated that the height and spacing of three-dimensional megaripples increases with increasing flow velocity until the transition into upper plane bed at which time the height decreases. The stability field plot of three-dimensional megaripples in the velocity/grain-size diagram (Fig. 3.23) shows that current velocities of about 57 cm/sec to 114 cm/sec are needed to form these three-dimensional megaripples in 0.4 mm sand. Therefore, the smaller sinuous-crested megaripples of Subfacies 6a are probably in equilibrium towards the lower limits of the estimated values. Three-dimensional megaripples are not developed in sands with a mean diameter less than about 0.20 mm.

The multiple sets within this subfacies are formed by the migration and aggradation of a bed formed by megaripple fields. This process of slow net aggradation is important, because when the advancing megaripples climb upwards at a small angle the internal laminae of the bedform is not eroded by subsequent migrating megaripples. This results in a larger precentage of the original height of the three-dimensional bedform to be preserved. The thin slaty shale drapes which commonly occur on the upper set surfaces suggests an alternation of quiet water conditions, resulting in hemipelagic fallout, with more intense higher energy conditions of bedload transport.

The stacked trough cross-stratified sets representing a laterally migrating megaripple field are probably formed by relatively strong unidirectional bottom currents driven by meteorological (wind-wave) currents and/or semi-permanent currents. However, the sediment dispersal for the amalgamated intervals with sets of oppositely dipping cross-strata, that are diametrically opposed to each other, are probably dominated mainly by rectilinear tidal currents. Again, the bimodal-bipolar paleocurrent patterns appears to confirm that the circulatory tidal currents were an important component in the formation of the trough cross-stratified sets representing this subfacies.

3.2.13 SUBFACIES 6B: TROUGH CROSS-BEDDED SETS (0.4 - 1 M THICK)

This subfacies is interpreted as being deposited by laterally migrating large three-dimensional, undulating to sinuous crested bedforms. The presence of curved cross-stratification intersecting lower set boundaries tangentally, in conjunction with basal erosional surfaces, appears to suggest deposition from large three-dimensional dunes. These large flow-transverse bedforms are the result of tractional bedload transport in the upper part of the lower-flow regime. The current velocities governing the formation of these thick trough cross-bedded sets are at slightly greater than those needed to produce the planar cross-bedded sets of subfacies 5b.

As mentioned before, Harms *et al.* (1982) indicated that there was a relationship between dune height and increasing flow velocities. Figure 3.23 shows that the current strength needed to form three-dimensional megaripples in 0.6 mm sand is about 52 cm/sec to 125 cm/sec. The flow velocities characteristic of the larger sinuous-crested dunes of Subfacies 6b are probably represented by the upper limits of the estimated values.

Instances where the beds of this subfacies are laterally persistent along strike suggests that bedform height remained relatively constant with time, in which no noticeable irregularities occurred along the crestline. Jopling (1965) has shown that the shape of the internal laminae is controlled by the amount of sediment in suspension and the velocity and depth of flow. It is shown in the geologic literature (Jopling, 1965) that there appears to be a correlation between these three fundamental parameters and the geometric characteristics of the bedform. However,

CANADIAN THESES THESES CANADIENNES	AUTHOR / AUTEUR	ISBN
	WOLBERG, A.C. SEDIMENTOLOGY OF THE...	0-315-30238-0

2

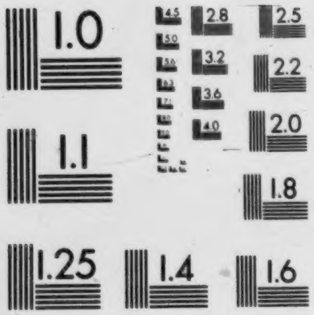
1.0
4.5
5.0
5.6
2.8
3.2
3.6
4.0
2.5
2.2
2.0
1.1
1.8
1.25
1.4
1.6

MICROCOPY RESOLUTION TEST CHART
NATIONAL BUREAU OF STANDARDS
STANDARD REFERENCE MATERIAL 1010a
(ANSI and ISO TEST CHART No. 2)

caution should be used in determining the morphology of bedforms from the shape of the laminae. This is because it is possible to have straight-crested, two-dimensional megaripples forming well-defined attenuated toeset laminae in relatively fine-grained sediment. However, since the size characteristic and spatial distribution of sediments along the preserved cross-laminae in Subfacies 6b is often difficult to distinguish, it may prove difficult to determine the influence of suspension transport on the shape of the laminae. From inferential and dedutive reasoning that the uniform thickness of the set along strike is genetically related to the bedform morphology. It appears that the curved, tangental foresets are the result of deposition from large nearly three-dimensional dunes with relatively continuous crestlines that are distinctly undulatory to smoothly sinuous in plan. Dalrymple *et al.* (1978) have documented similar type three-dimensional dunes with relatively straight crestlines in the eastern arm of the Bay of Fundy. These straight-crested bedforms, vary from 5 to 70 cm in thickness, have small sinuous irregularities along the crestline and contain internal trough cross-stratification. The marked absence of scoured basal contacts in this subfacies is possibly attributed to the relatively straight crestline geometries which do not produce the intense turbulent eddies that result in deep scour pits.

Thick trough cross-stratified sets of Subfacies 6b indicate that strong tractional bottom currents were affecting the loose granular bed material, generating laterally migrating three-dimensional dunes. The processes associated with generating the strong bottom currents are possibly unidirectional currents induced by winds and waves or related to oceanic circulation patterns. Direct wind-drift currents which can be generated by meteorological disturbances can generate strong bottom currents and when intervening oceanic currents are present they might consistently reinforce the wind-driven currents. Alternatively, the strong bottom currents may be driven by rotary tidal currents. The close stratigraphic association of trough cross-bedded sets showing foreset laminae dipping in opposite directions suggests a possible influence of bidirectional tidal currents in the formation of these large three-dimensional dunes.

3.2.14 FACIES 7: LOW ANGLE AND HORIZONTALLY STRATIFIED QUARTZITES

The internal stratification of this facies indicates that the noncohesive clastic sediments were deposited approximately parallel to the depositional surface and that no major topographic features of any sufficient relief existed on the bed during deposition. This facies

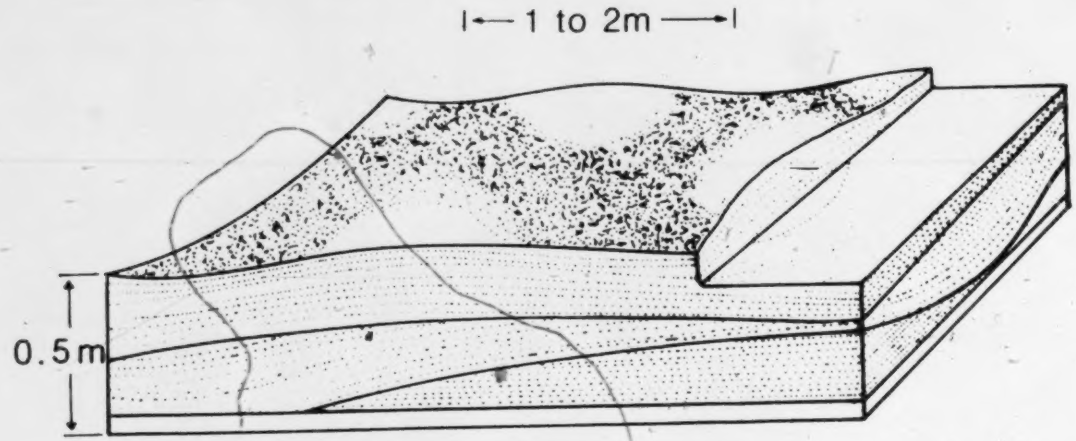

Figure 3.25. Schematic block diagram of hummocky cross-stratification. The diagnostic traits of hummocky cross-stratification are; (1) erosional lower bounding surfaces of sets with the typical slope angles of less than 10°, (2) laminae are parallel or subparallel to the lower erosional bounding surface, (3) laminae can systematically thicken laterally into swales, (4) erosional set boundaries and the overlying laminae show scattered dip directions, and (5) irregularly spaced swales and intervening hummocks at intervals of one to several meters with reliefs generally of 5 to 30 cm (modified from Harms *et al.*, 1982).

lacks the large-scale undulations with gentle (less than 10°) dip inclinations and erosional lower contacts which characterizes hummocky cross-stratification (Harms *et al.*, 1982) (Fig. 3.25). The relatively well sorted, coarsely-crystalline nature of the beds of this facies suggests that the planar lamination is the result of bed-plane transport generated during high flow velocities. Figure 3.23 illustrates that the current strength needed to produce upper plane beds in 0.6 mm sand is approximately 130 cm/sec to 150 cm/sec. Under this set of hydraulic and grain size conditions, upper plane beds are the only stable bed configuration developed.

However, the origin of planar stratification is often difficult to interpret because the internal horizontal laminae can be generated from a number of current conditions and in various sediment sizes. Harms *et al.* (1982) state that under steady unidirectional currents planar laminations are the result of traction over an aggrading upper flow regime plane bed. For all sizes of loose granular material this bed geometry, with no elevations or depressions, is the only stable bed configuration under such strong unidirectional currents. Another possible hydrodynamic condition producing planar lamination is generated from oscillatory flows. These bidirectional or multidirectional currents form oscillatory-flow plane beds when the maximum orbital velocities are sufficiently large. This is the only stable bed phase for all sizes of noncohesive sediments under symmetrical oscillatory flow conditions.

In some cases the internal horizontal stratification may not be genetically related to strong currents but attributed to the two-dimensional aspect of the outcrop. Often when a measured section is orientated at angles not parallel to current or wave direction the visible two-dimensional surface will show horizontal stratification. A true three-dimensional cross-section will reveal that perpendicular to the internal planar stratification are foreset laminae which are inclined to the principal surface of sedimentation. Evidence for this is supported by several beds which can be traced laterally into planar or trough cross-stratified beds and the occasional fracture orientated perpendicular to planar lamination or parallel to flow and allows the recognition of the distinctive cross-laminae.

Typically in shallow marine environments, most notably in foreshore areas, the predominant structure is swash cross-stratification which consists of a series of parallel laminations in sets that intersect at low angles to each other along straight erosional contacts (Thompson, 1937; Reineck and Singh, 1980). These parallel laminations are produced under high flow power conditions and are created by plane bed sediment transport during swash-backswash flow. When subsidence rates are fairly high relative to the rate of foreshore erosion a relatively thick beach deposit of swash cross-stratification is preserved. However, the internal arrangement of parallel lamination deposited in swash-backswash zones does not resemble the type of horizontal stratification characterized by beds of Facies 7. This facies lacks the subtle truncation planes which form straight erosional surfaces and divides the laminations into discrete sets which is typical of swash cross-stratification (Harms *et al.* 1982). In addition this facies does not contain the trace fossil assemblage characteristic of foreshore marine settings. More importantly the beds of this facies are not amalgamated to form a thick sequence of planar lamination typical of the beach face under swash-backswash processes. Rather, the horizontal stratified beds of Facies 7 are in close vertical association with interbedded slaty shale and thin quartzites of Facies 1. This suggests that the planar laminated beds are not deposited by wave swash in the beach environment. Instead it appears that strong currents produced by shoaling solitary waves in a more offshore environment are responsible for producing the beds of this facies. Therefore, deposition of this facies was controlled by offshore currents of high flow velocities (upper flow regime) which formed upper plane beds and very low amplitude bedforms.

3.2.15 FACIES 8: MASSIVE QUARTZITES

Beds ascribed to Facies 8 rarely show any direct evidence pertaining to their mode of deposition because of the characteristic lack of any discernible internal sedimentary structures. However, the absence of internal stratification suggests that the massive quartzites were rapidly deposited from suspension with no subsequent bedform transport. This lack of a tractional phase during the deposition of sands of Facies 8 would invariably lead to the absence of internal lamination because grain-by-grain deposition characteristically results in the formation of primary stratification.

The absence of visible stratification in beds of Facies 8 may not necessary be attributed to the depositional process but may in fact be related to the uniformity of grain size throughout the bed. Typically in very well sorted sands the internal sedimentary structures cannot be delineated by textural variations and appear structureless. This is due to the fact that often in the sedimentary record the recognization of internal sedimentary features is manifested in slight changes in the grain size along stratification planes.

In some cases the massive nature of these quartzites may be a consequence of metamorphic recrystallization and diagenetic changes, which destroyed original stratification. Evidence for this is shown petrographically, in which some metamorphic recrystallization is observed along grain boundaries. This appears to be prevalent in outcrop A where massive beds are traced laterally along bedding contacts to vertically stacked planar cross-stratified beds (Facies 5).

Other inorganic processes which can contribute to the massive appearance of Facies 8 is post-depositional liquefaction which can obliterate internal stratification soon after deposition and also intense ferruginous staining which masks primary sedimentary structures. The heavy iron staining is due to the chemical weathering of ferrous minerals within the associated slaty shales and is an important factor contributing to the massive character of the quartzite beds in outcrops B, C and D.

Another agent which successfully obscures internal structures is the extensive lichen covering the outcrop surface. This organic phenomenon is particularly important at certain areas in outcrop A, where it completely masks any visible sedimentary structures and only shale breaks are recognizable.

Massive bedding can also result from the extensive modification by biological activity in which quartzite beds are thoroughly homogenized by burrowing organisms. However, this special case was placed in a separate category (Subfacies 1c).

4. PALEOCURRENT ANALYSIS OF THE GOG SEDIMENTS AT SINK LAKE, BRITISH COLUMBIA

4.1 METHODS OF PALEOCURRENT ANALYSIS

The importance of paleocurrent indicators in interpreting the prevailing sediment dispersal direction and in reconstructing the paleogeography of a region has been recognized for over forty years. The most reliable and most widely used sedimentary structures for paleocurrent reconstruction are planar and trough cross-stratification. Other paleocurrent indicators such as flute cast orientations, gutter casts and other linear scour features were not measured because of the limited erosional relief beneath the beds. The basic assumption made when using planar cross-stratification for paleocurrent studies is that the controlling currents flowed in the direction of maximum foreset inclination. As for trough cross-stratification the trough-axis orientations provides a more accurate indication of the paleoflow direction than that from dip azimuths of their curving trough foresets (Dott, 1973; Michelson and Dott, 1973; High and Picard, 1974).

The ubiquitous cross-bedding contained within the vertical sections of Gog orthoquartzites at Sink Lake provided an excellent opportunity to make a detailed investigation of trough-axis and cross-set orientations. Every adequately-exposed cross-stratified set was measured, resulting in over 250 paleocurrent readings taken at 47 vertical sections. Every cross-stratifed bed is represented by only one measurement and in the case of composite cosets, every individual set was measured. The lack of well-exposed, three-dimensional cross-stratification was the primary limiting factor in determining paleocurrent measurements. On certain fortuitous two-dimensional vertical outcrops surfaces the orientation of the outcrop face was parallel to the mean trough axial direction and apparent trough-axis plunge directions were able to be measured. In cases of insufficient exposure, an apparent paleocurrent measurement was recorded by measuring the trough cross-strata dip direction which was viewed to have a mean direction coincident with trough axial direction. The lack of three-dimensional exposures for planar cross-stratified sets usually hindered the accuracy in measuring the maximum foreset dip direction. As was often the case the resistive nature of the outcrop caused a two-dimensional exposure in which only an apparent paleocurrent measurement could be recorded for planar cross-stratified beds. On certain beds the foresets weathered out such that you could get an accurate measurement of the dip and strike of the foreset plane. This allowed the direct obtainment of the true dip direction.

The paleocurrent data was corrected for tectonic rotation and restored back to the original horizontal position using a computer program provided by Dr. H.A.K. Charlesworth. The nearest bedding plane orientation was used to restore the cross-stratified beds to horizontality. The tectonically corrected paleocurrent measurements are presented by two-dimensional rose diagrams generated by a program provided by Dr. H.A.K. Charlesworth. These rose diagrams, with 10° class angles, record the rotated paleocurrent dip directions. On all the rose diagrams, north is orientated towards the top of the page and the number of paleocurrent measurements is denoted by N. The rose diagrams combine both planar and trough paleocurrent data because there is no sufficient evidence to indicate that there are significant differences in paleocurrent directions derived from planar and trough cross-stratification.

The tecontically corrected paleocurrent data for each outcrop was analyzed statistically by a method developed by Curray (1956). This method of vector analysis is applied to the cross-set orientation measurements and calculates the two-dimensional vector mean for each individual outcrop. The direction of this vector mean represents the preferred dip direction of the foreset which reflects the average paleocurrent direction. The reliability of the vector was determined by using the Rayleigh test of significance with a minimum significance level of 95%. For the rose diagrams showing bimodal paleocurrent patterns, a separate vector mean was determined for each of the oppositely-directed modes. The average paleocurrent direction for the eastern mode was calculated by analyzing the data between 0° to 180° and conversely the western mode was determined by analyzing the data between 180° and 360°.

4.2 PALEOCURRENT DATA FOR OUTCROP A

The paleocurrent data collected from outcrop A shows a unimodal pattern reflecting a strongly preferential southwesterly transport direction (Fig. 4.1). The average paleocurrent direction is 230°, which compares similarly to the average paleoflow direction (235°) given by Mountjoy and Aitken (1963). The paleoflow directions were derived from Facies 4 and Subfacies 5a, 5b, 6a beds which all show a dominant southwest direction of transport with a relatively low degree of scatter and deviation from the primary flow direction. The paleoflow

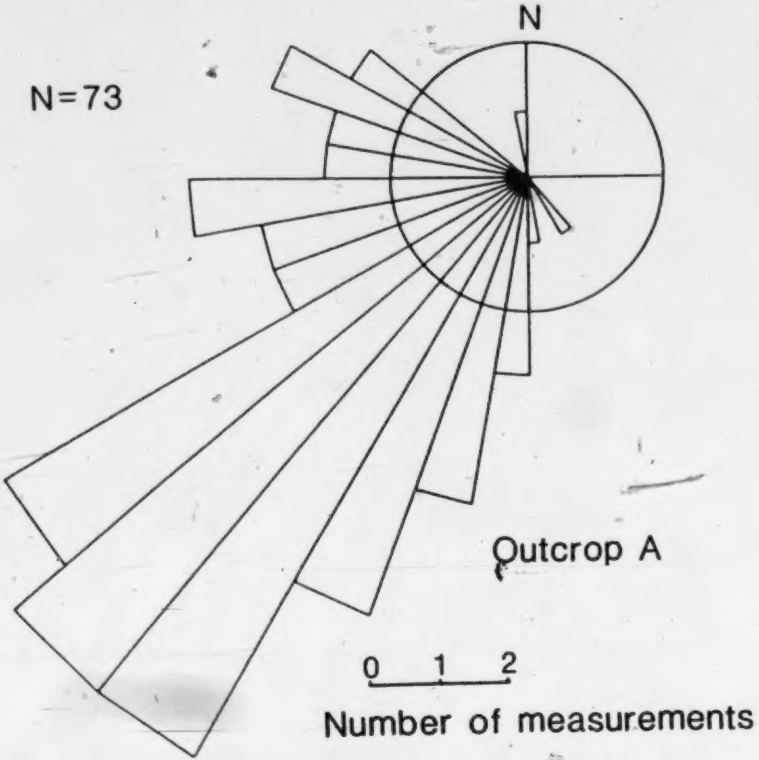

Figure 4.1. 10° rose diagram recording the rotated paleocurrent data for outcrop A. Note the distinct southwest paleocurrent direction at outcrop A, compared to the bimodal-bipolar paleocurrent pattern at outcrops B, C and D.

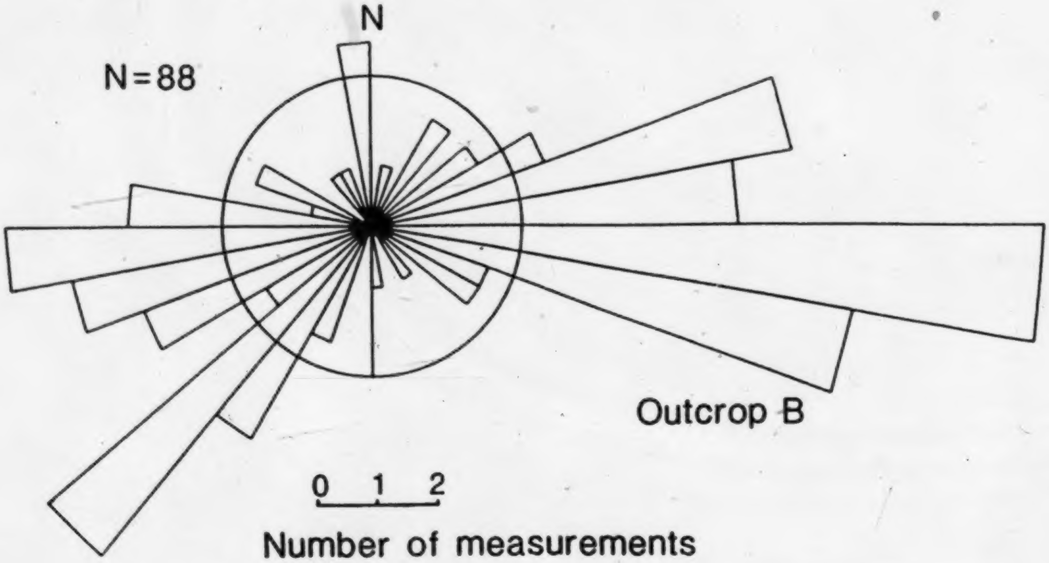

Figure 4.2. 10° rose diagram showing the rotated paleocurrent data for outcrop B.

data collected from these various facies and subfacies are plotted on the columnar sections and are represented as two-dimensional rose diagrams in Appendices I and II respectively. The predominant amount of paleocurrent data at outcrop A was derived from the planar cross-stratified beds of Subfacies 5a. The rose diagram for this subfacies (Appendix II) shows a preferred orientation pattern indicating that the dominate direction of transport was towards the southwest. The anomalous westward paleocurrent direction shown in the rose diagram for outcrop A does not appear to represent a local variation in paleoflow direction because comparison of the rose diagrams for the other facies and subfacies described above reveals a predominately unidirectional paleocurrent pattern with a southwest transport direction. Therefore, this anomalous westward direction is probably attributed to a certain degree of scatter in the measured paleocurrent directions. Throughout the measured vertical sections there is relatively little stratigraphic variation in the prefered southwest orientation of cross-sets. This is illustrated in the columnar sections shown in Appendix I where the plotted paleocurrent directions show a predominately southwesterly orientation throughout all the measured sections at outcrop A.

4.3 PALEOCURRENT DATA FOR OUTCROP B

The results of the paleocurrent data for outcrop B shows a distinct bimodal distribution pattern with a preferred east and west direction of transport. This is clearly shown in the rose diagram which indicates a bimodal distribution, reflecting a predominance of east-west reversing paleocurrents and a general separation angle exceeding 150° between the two subdirections (Fig. 4.2). Applying the vector analysis to the two bipolar modes of cross-set orientation measurements indicates that the central tendency of the eastern mode is 91°, compared to the paleflow 246° for the western mode. An excellent example of bidirectional cross-stratification of adjacent planar cross-bedded quartzites is shown in Figure 4.3. The paleoflow directions were derived from Facies 7, 4 and Subfacies 1b, 5a, 5b, 6a, 6b beds. Plots of rose diagrams for all the lithofacies except 1b show bimodal directional subpopulations with Subfacies 1b illustrating a greater diversity in paleocurrent directions (Appendix II). The anomalous paleocurrents orientated to the north are not facies or section specific because the measurements are collected from three separate lithofacies (1b, 4, 7) and occur within three different sections. This suggests that the anomalous northern paleocurrent trend merely

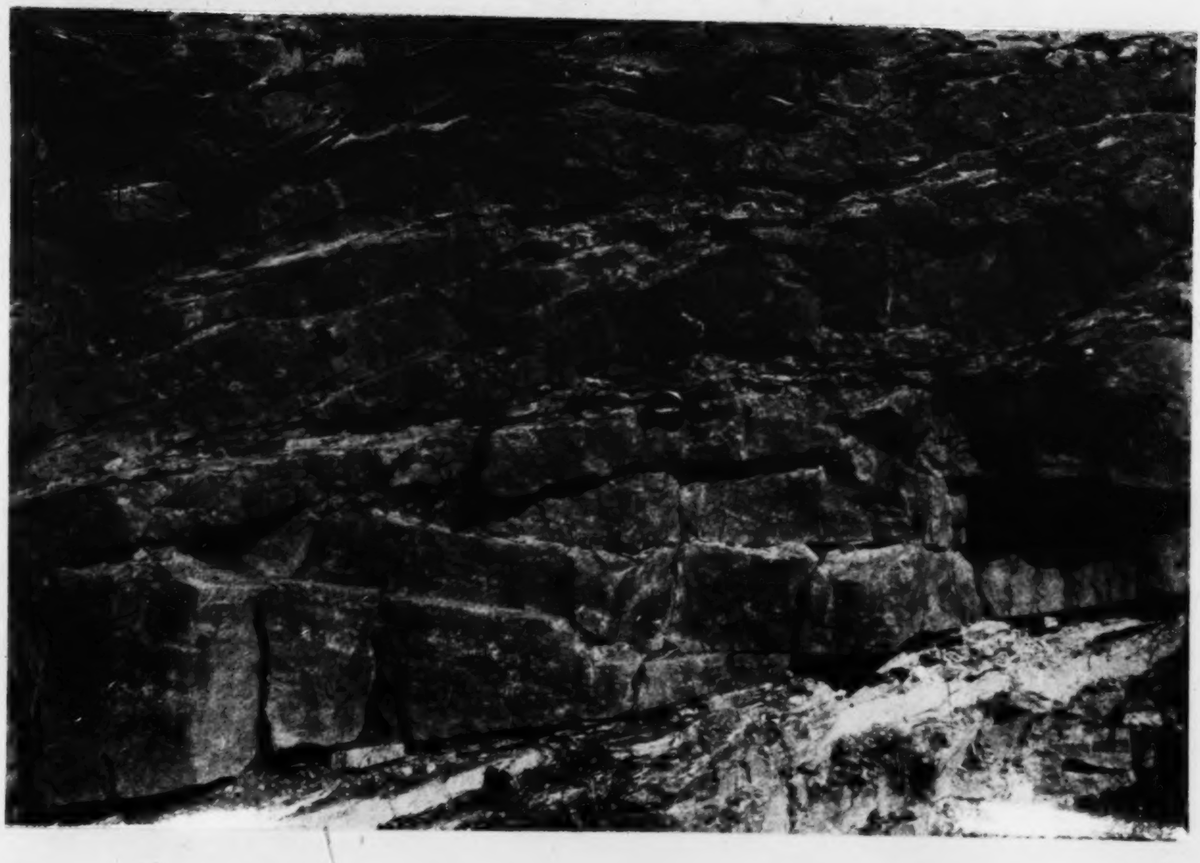

Figure 4.3. Planar cross-stratified quartzites (Subfacies 5a) at outcrop B showing bidirectional paleocurrent trends. Arrow indicates a reactivation surface consisting of a thin slaty shale drape followed by a thin interval of small-scale cross-stratified quartzites (Facies 4) extending along the length of the reactivation surface.

represents a certain amount of scatter of the paleocurrent directions. Throughout the vertical sections there appears to be no systematic change or preferred orientation of the paleocurrent directions stratigraphically.

4.4 PALEOCURRENT DATA FOR OUTCROP C

The paleoflow data collected from outcrop C shows a strikingly low degree of scatter. The rose diagram shows that the bimodal paleocurrent distributions are composed of bipolar, mutually opposed modes rather than of obliquely to perpendicularly oriented parts (Fig. 4.4). The vector mean was calculated for both bipolar modes, with the average paleocurrent direction being 36° for the northeastern mode and 222° for the southwestern mode. Figure 4.5 shows an example of bidirectional cross-bedding at outcrop C. The paleocurrent directions derived from beds of Facies 4, 7 and Subfacies 1b, 5a, 5b, 6a 6b show a northeast and southwest direction of transport. These preferred transport directions are best illustrated by the bimodal-bipolar paleocurrent pattern of Subfacies 6a. Futher examination of the rose diagram for outcrop C reveals that the southwestern orientated mode appears to be slightly more dominant than the northeastern directed mode. This preferred direction appears to be partically attributed to Subfacies 5a and 5b. Although the two subfacies display a bimodal paleocurrent direction the two opposing modes are not symmetrical. The dominant mode is orientated to the southwest, reflecting a preferred southwesterly tranport direction over the reversing transport direction. Similarly this preferred southwestern modality is strengthened by the unimodal paleoflow pattern for Facies 4 and 7 appears to be an artifact of the extremely small sample size. In contrast, the bimodal paleocurrent distribution of Subfacies 1b and 6b reveal a dominant mode orientated to the northeast suggesting a dominantly northeast with less common southwest direction of transport. Within the measured sections at outcrop C there is not a noticeable stratigraphic change in the transport direction with time. The plotted paleocurrent directions in the columnar sections (Appendix I) show that the orientations fluctuate randomly between the two subpopulations throughout the vertical section.

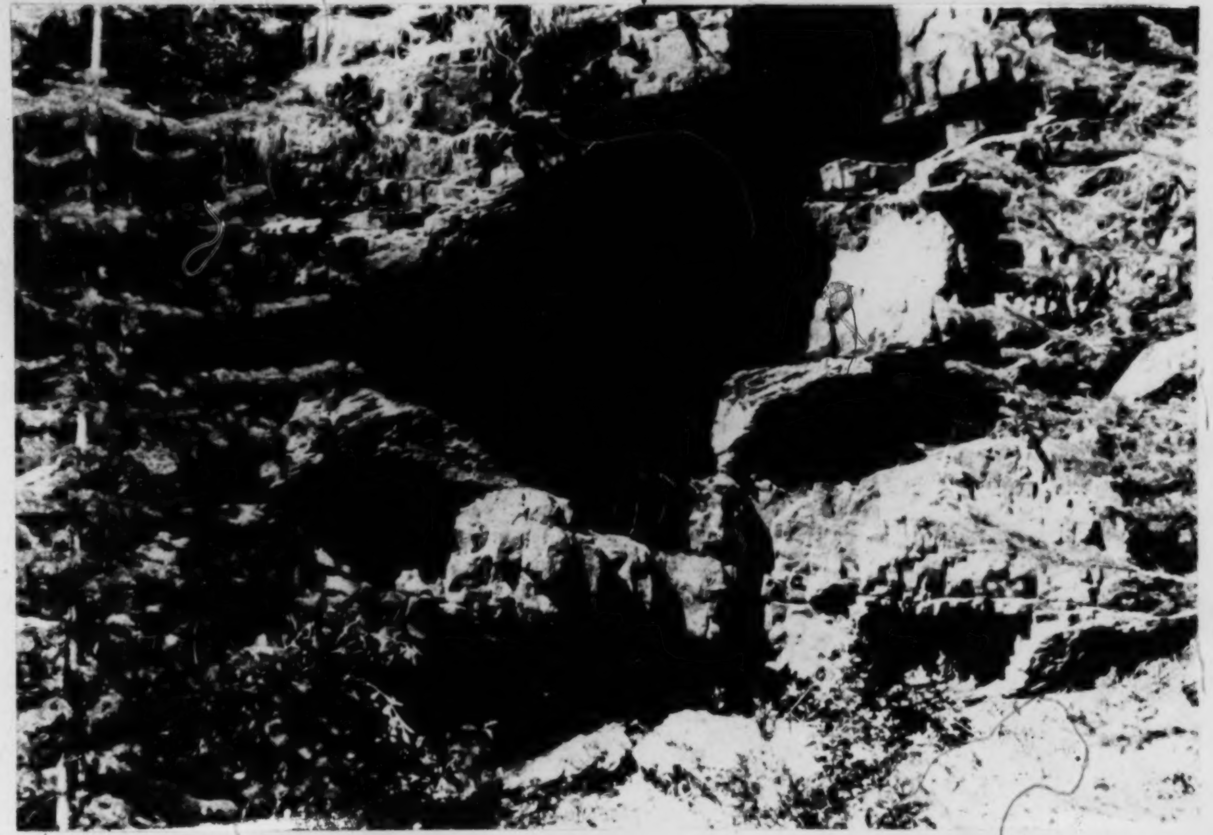

Figure 4.5. Bidirectional cross-bedding at outcrop C. Note that the foresets within the lowermost bed of Subfacies 6b are opposed nearly 180° from the overlying angular foresets of the planar cross-bedded quartzites (Subfacies 5b). The two cross-stratified units with oppositely dipping foresets are separated by an interval of slaty shale (next to rock hammer).

Figure 4.4. 10° rose diagram showing the rotated paleocurrent data for outcrop C.

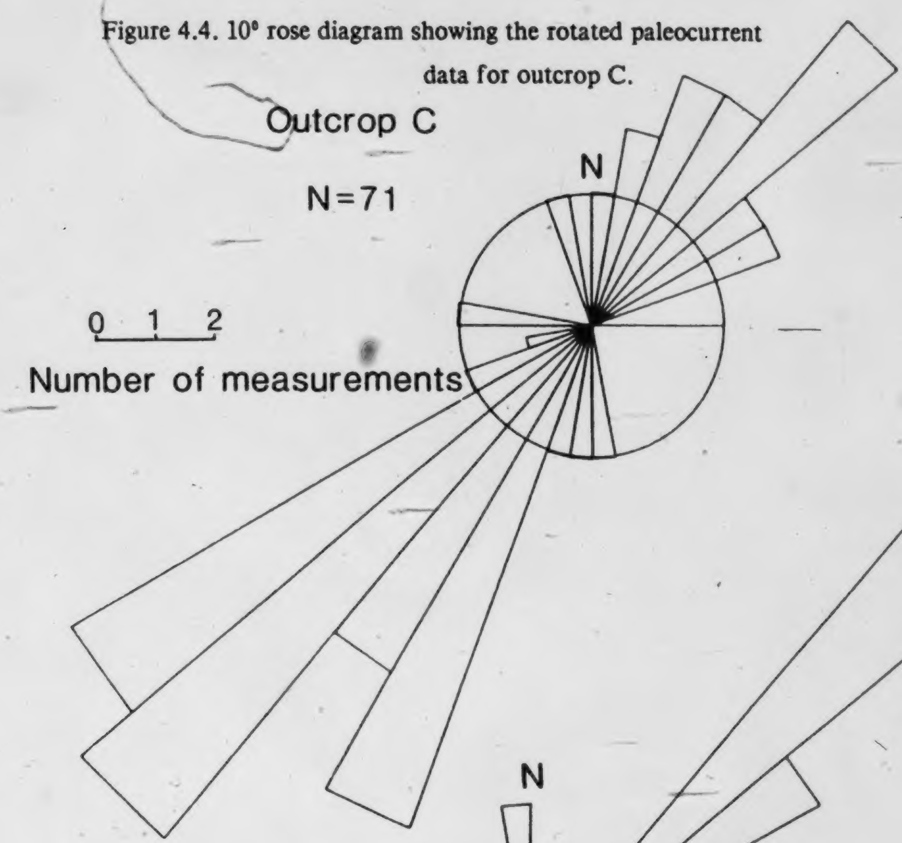

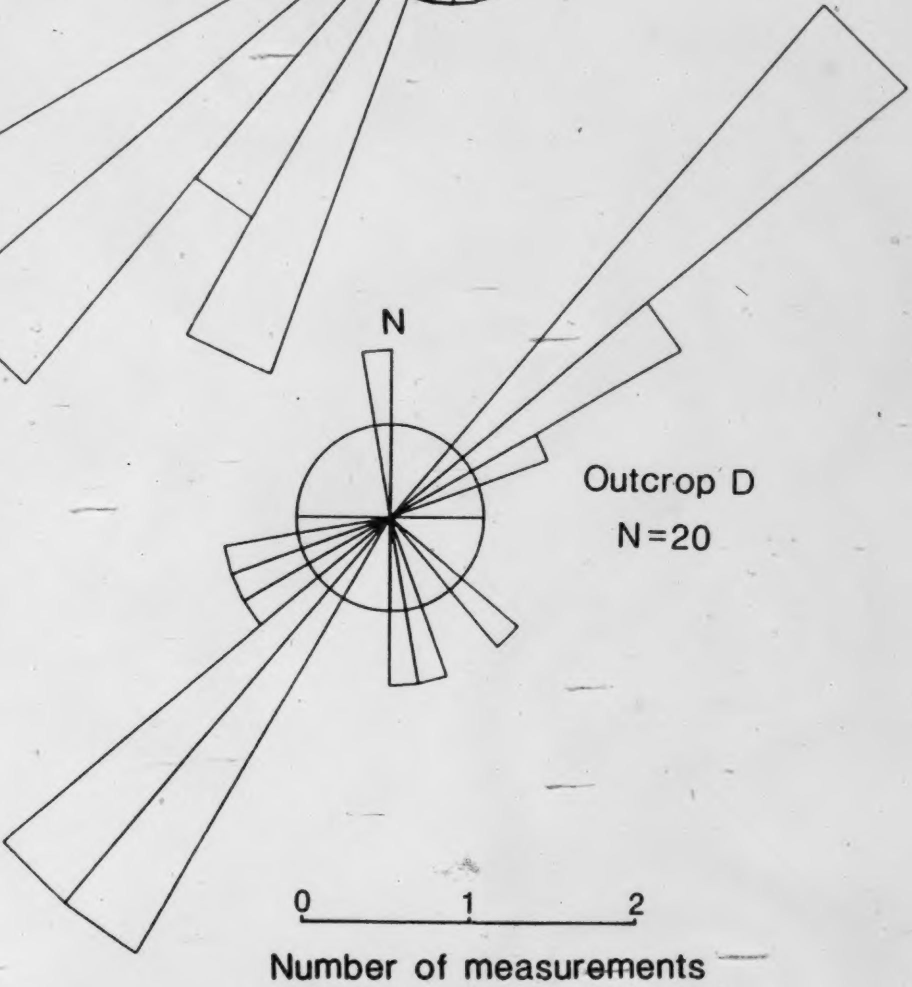

Figure 4.6. 10° rose diagram showing the rotated paleocurrent data for outcrop D.

4.5 PALEOCURRENT DATA FOR OUTCROP D

The collection of paleocurrent data at outcrop D shows a bimodal paleocurrent pattern with the two major modes diametrically opposed to each other. The rose diagram for this outcrop shows a predominately northeast and southwest paleotransport direction (Fig. 4.6). From the two-dimensional vector analysis the average paleocurrent direction for the northeastern orientated mode is 43°, in contrast to 226° for the southwestern directed mode. This bimodal directional distribution is similar to the pattern observed at outcrop C. This is not surprising because these two outcrops represent a continuous stratigraphic sequence separated by a covered interval less than 1 meter thick. The paleoflow data at outcrop D was obtained from Subfacies 1b, 5a, 5b, 6a, and 6b. In the case of Subfacies 5a and 1b the unimodal patterns are due to the single paleocurrent measurement. The other subfacies (5b, 6a and 6b) reveal a more bimodal paleocurrent distribution. Although the rose diagram for outcrop D is bimodal the two oppositely directed paleocurrent modes are not equal. The slightly more dominant mode is orientated to the southwest with the subordinate mode directed towards the northeast. Subfacies 5b appears to be one of the major contributing factors leading to the predominance of this southwesterly orientated mode.

The vertical sections at outcrop D appear not to contain any preferred paleocurrent direction or modality. This is shown in the columnar sections for outcrop D (Appendix I) where the plotted paleocurrents randomly fluctuate between the two opposing modes. The only noticeable discrepancy occurs about 2.5 meters from the base of section D-1, where the stacked beds of Subfacies 5b contain cross-stratification directions orientated towards the southwest.

5. VERTICAL FACIES RELATIONSHIPS AND ASSOCIATIONS

5.1 INTRODUCTION

In the study of stratigraphic sequences, sedimentologists are becoming increasingly interested in the presence of order in a succession of facies and thus the detection of repetition of process and cyclicity in sedimentary systems through time. Certain sedimentary successions such as, Pennsylvanian coal measure cyclothems or fluvial fining-upward cycles are excellent examples of sedimentary sequences which show evidence of recurrent or cyclic repetitions of various facies (Johnson, 1984; Cant and Walker, 1976). In the past the vertical arrangement of facies in sedimentary sequences was largely recognized by subjective visual appraisal of measured outcrop. Invariably this subjective approach leads to personal bias entering into the delineation of significant vertical facies transitions. Markov chain analysis has been widely used to study vertical facies transitions in sedimentary sequences in order to objectively detect sedimentary processes which had logical and determinable relationships in space or time (Gingerich, 1969; Read, 1969; Selley, 1970; Miall, 1973; Ethier, 1975).

5.2 EMBEDDED AND NON-EMBEDDED MARKOVIAN METHODS

In this chapter a single-dependency, first-order Markov chain process is used to determine the preferred facies transitions within the four measured Gog Group sections and the two facies associations at Sink Lake, British Columbia. A first-order Markov chain is a relatively simple analysis in which the nature of the lithological state is determined or dependent only by the lithological state that immediately preceeds it (Carr, 1982). For the purpose of this analysis the vertical lithologic transitions or states refer to the facies present within the stratigraphic succession. Two methods are described in this chapter for handling the vertical juxtaposition of lithological states within a sedimentary sequence. The first technique is the embedded Markov chain analysis, in which any given facies cannot pass upward into the same facies. This method emphasizes the actual lithological change and therefore focuses on the temporal evolution of the depositional processes occurring in the given sedimentary basin. The second method of analysis is the non-embedded Markov chain. This technique is concerned about the upward transition of lithological states and emphasizes the relationship between a given facies and the next facies immediately succeeding it. This alternative method of analysis allows for the recognition of transitions between identical facies or "multistorey" lithologies. This non-embedded Markov chain procedure was conducted at outcrops A and D, and on the Coarse-grained Facies Association because the stacked beds of identical facies contributed to the major portion of the stratigraphic sequences.

The starting point in any Markov chain analysis is the tally matrix or transition count matrix. This is a two-dimensional array in which all the possible vertical lithologic transitions in a given stratigraphic succession are tabulated. The computational procedure used to determine the transition count matrix and subsequent conversion into observed probabilities is given by Miall (1973) and Davis (1973).

The next step is to calculate a "random matrix" which can be compared with the observed transition matrix. This matrix is determined under the assumption that the succession of facies is in a purely random order so that each lithological state is completely independent of the preceding lithological states. The probability of occurrence of any facies depends only on the relative abundance of that particular facies in the sequence. In the case of the non-embedded Markov chain analysis the random matrix is determined by the computational technique given by Miall (1973). However, one of the main obstacles in developing a random probability matrix for the embedded Markov chain analysis is the presence of previously defined zero entries in the principle diagonal of the tally matrix. Carr (1982) states that matrices containing diagonal frequencies that are forced to be zero cannot result from a simple independent random process. To account for this difficulty Powers and Easterling (1982) and Harper (1984, 1985) provide a statistically valid method for generating the expected cell values for the random matrix. This technique of iterative proportional fitting preserves observed column as well as row totals. The technique was applied using a computer software package called SAS (Statistical Analysis Systems) at the University of Alberta.

A difference matrix for both Markov chain methods is calculated by subtracting the random probability matrix from the observed transition probability matrix. The positive values in the difference matrix emphasizes the Markovian tendencies present within the sedimentary sequence by indicating which transitions have occurred with greater than random frequency. In order to test if the difference values are significant and not due to random chance, Harper's (1984) binomial probability method was used for both the non-embedded and embedded Markov chain analysis. The chosen level of significance was 0.15 for the binominal expansion technique. A statistical computer program called "minitab" was used to assist the binomial probability analysis. From the significant levels obtained from Harper's binomal expansion technique, a summary graphic presentation, called a "facies relationship diagram" is constructed. The results of these analysis (Figures 5.1-5.4), indicate that several facies relationships occur. However, the facies relationship diagrams fail to reveal any overall cyclic patterns of sedimentation within any of the measured sections. Therefore, from a Markovian point of view there is no evidence to suggest that there were cyclic changes through time of the depositional environment. However, it is not valid to state that Markovian analysis is of little or no assistance in the interpretation of these rocks because the technique assists in the detection and definition of facies relationships. Furthermore, these facies transition diagrams accurately illustrate the significant facies relationships which are seen in the Gog sediments. For the sake of brevity the geological significance of certain facies relationships, shown in the facies transition diagrams for the four measured outcrops(Figures 5.1-5.4), are discussed in Table 5.1.

The facies transition diagrams for outcrops A and D were determined using a non-embedded Markov chain procedure, while an embedded Markov chain analysis was used to determine the significant facies transitions at outcrops B and C. In the various facies relationships diagrams for the individual outcrops (Fig. 5.1-5.4) and the two facies associations (Fig. 5.8-5.15) the facies types are numbered as in Chapter 3. Transitions which are significant to the 0.05 level are shown with solid arrows, dashed arrows show facies transitions significant to the 0.1 level. Dotted arrows indicate transitions significant to the 0.15 level. Any facies transitions that have a significant level exceeding 0.15 are not listed. The Markovian matrices (tally, observed probability, random and difference) which are tabulated for the four major outcrops and two facies associations are presented in Tables 5.3-5.26 (Appendix III).

5.3 FACIES ASSOCIATIONS

After determining the various facies and identifying the significant facies relationships within the Gog Group, a larger scale classification was defined to describe the distribution of groups of facies occurring in the measured sections. Two main facies associations can be recognized in these Lower Cambrian sediments outcroping near Sink Lake, British Columbia. These two facies associations are distinguished mainly upon the percentage of coarse and fine

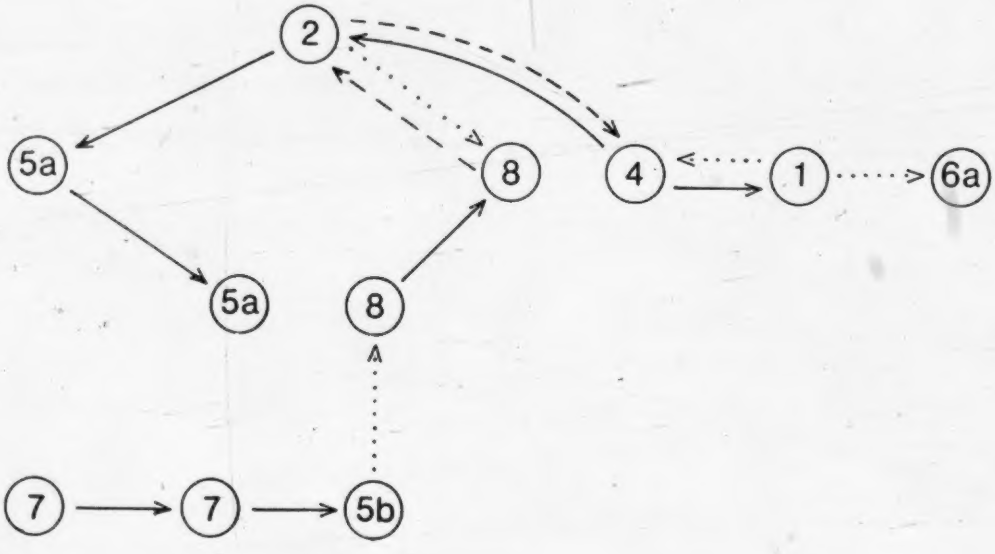
2
5a
8
4
1
6a
5a
8
7
7
5b

Figure 5.1. Facies relationship diagram for outcrop A.

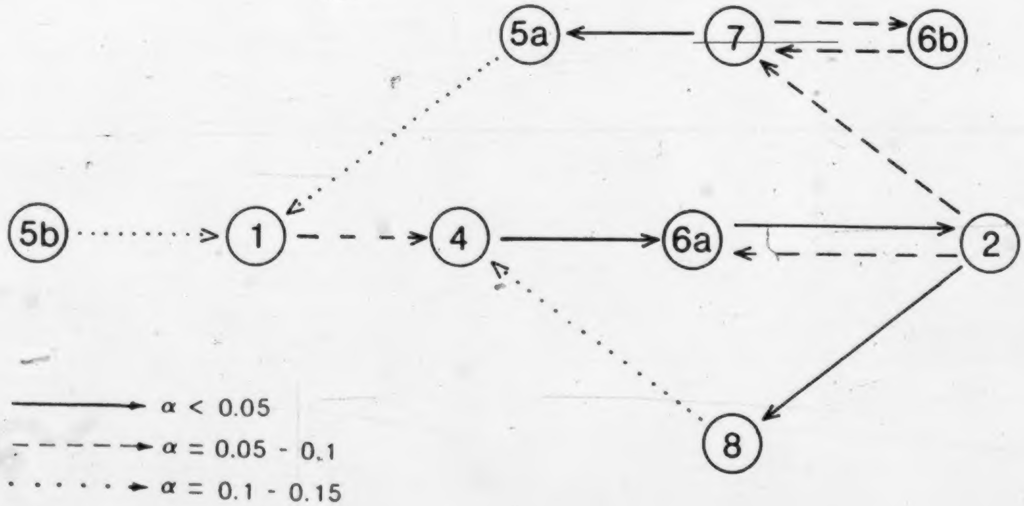
5a
7
6b
5b
1
4
6a
2
8
α < 0.05
α = 0.05 - 0.1
α = 0.1 - 0.15

Figure 5.2. Facies relationship diagram for outcrop B.

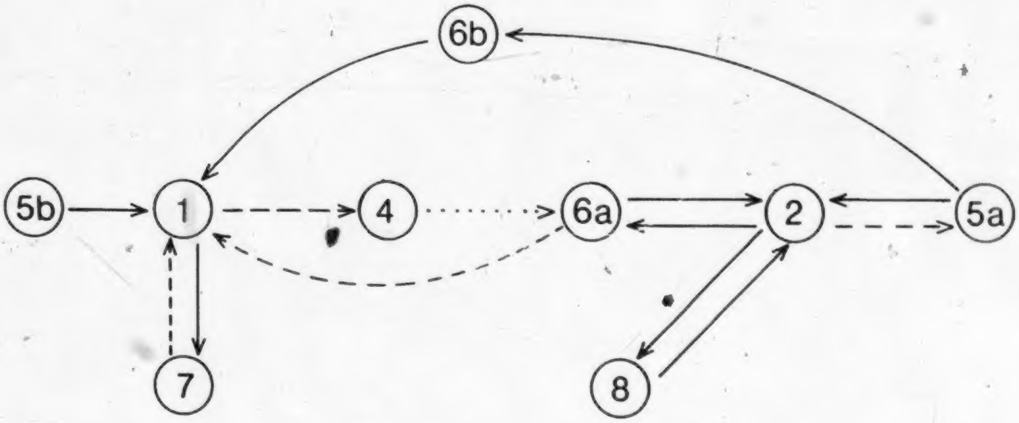
6b
5b
1
4
6a
2
5a
7
8

Figure 5.3. Facies relationship diagram for outcrop C.

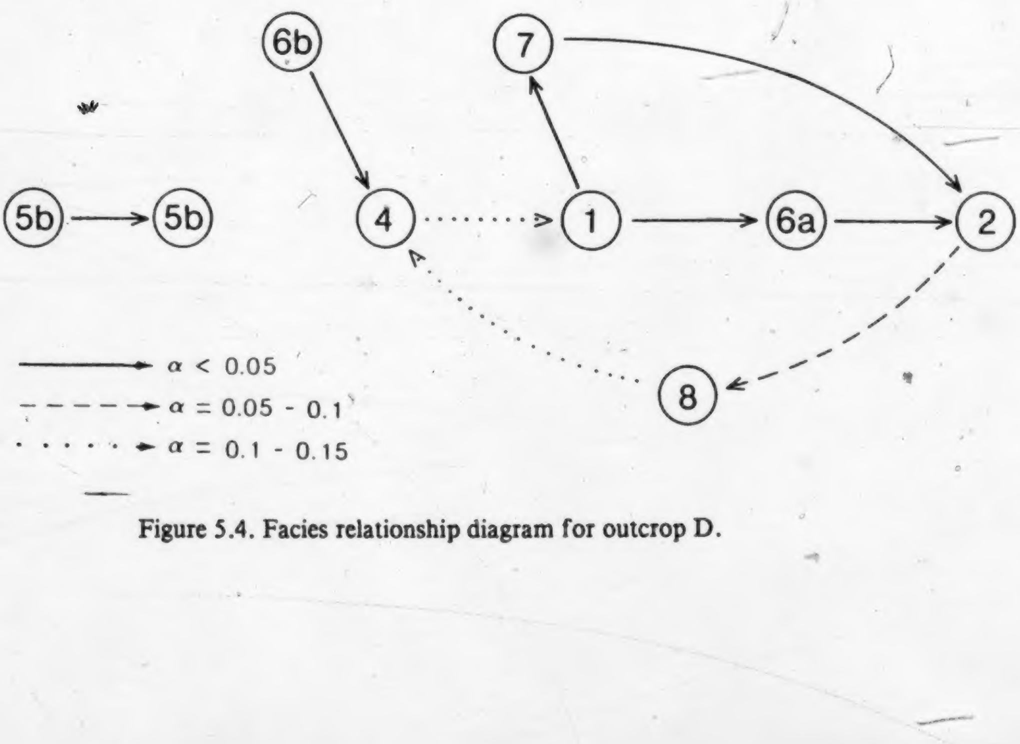
6b
7
5b
5b
4
1
6a
2
8
α < 0.05
α = 0.05 - 0.1
α = 0.1 - 0.15

Figure 5.4. Facies relationship diagram for outcrop D.

Table 5.1. Interpretations of the salient facies transitions shown in the facies relationship diagrams.

Outcrop	Facies transitions	Interpretation
A	5a --- 5a	Represents the lateral migration and the aggration of multiple straight-crested megaripple fields.
A	8 --- 8	Records the migration and up-building of probable straight-crested megaripple fields.
A	4--- 1--- 6a	Represents the successive migration of a series of ripple trains which are draped by mud from suspension fall-out during a period of lower energy conditions. With the reinstatement of higher flow conditions the migration of sinuous-crested megaripples occurs.
B	5b --- 1	Migrating straight-crested dune or sandwave which was buried by a predominately muddy substrate representing a passage into quite water conditions facilitating mud suspension fall-out.
B	4 --- 6a	Indicates a period of progressively increasing flow strengths where laterally shifting ripple fields are superimposed by an aggrating and migrating sinuous-crested megaripple field or individual bedform.
C	6b --- 1	Represents an advancing sinuous-crested dune which is buried by an episode of mud deposition which occurred during a period of lower energy conditions.
C	1--- 4--- 6a	Represents an increase in energy conditions, resulting in the cessation of mud suspension fall-out and the initiation of laterally shifting ripples followed by a migrating sinuous-crested megaripple field or solitary bedform.
D	1 --- 6a	Indicates a period of fine-grained sedimentation succeeded by a migrating sinuous-crested megaripple field or individual bedform.
D	5b --- 5b	Migrating straight-crested dunes or sandwaves which override each other to form a larger-scale sandwave complex.

facies members within the sections and are expressed in terms of the quartzite: shale ratio. Table 5.2 shows the various facies and corresponding precentages comprising the two facies associations.

5.3.1 COARSE-GRAINED FACIES ASSOCIATION

The Coarse-grained Facies Association 1 is characterized by a quartzite:shale ratio of > 25:1. It consists mainly of planar cross-bedded quartzites (Subfacies 5a and 5b), massive quartzites (Facies 8) and trough cross-stratified quartzites (Subfacies 6a). The remainder of the facies occur in minor amounts. This facies association is predominately found at outcrop A, but also occurs within a 2 meter interval at outcrop D.

At outcrop A, the Coarse-grained Facies Association contains sets of planar cross-strata that are enclosed within larger cross-stratified cosets forming compound cross-stratification (Subfacies 5a). These compound cross-stratified sets are characterized by sets of planar cross-stratification with non-horizontal set boundaries which define master bedding surfaces, or E_2 surfaces (Fig. 5.5). These gently inclined set boundaries (master bedding surfaces) consistently dip towards the west at angles less than 15^0 relative to regional bedding. Typically the inclined lower set boundaries of the individual planar stratified sets contain a coarsely-crystalline lag, a few millimeters thick, resting on planar erosional surfaces. The individual sets of planar cross-stratification vary in thickness from 5 cm to 12 cm. The angular foresets show lateral varations in crystallinity from fine- to medium-crystalline with sucrosic textures to adjacent foresets which are coarsely-crystalline, with non-sucrosic, clear textures. In addition, there is no evidence of bioturbation, slaty shale drapes or shale intraclasts along the master bedding surfaces.

Two major lateral facies relationships are recognized within the Coarse-grained Facies Association. The first lateral facies trend occurs at outcrop A where massive quartzites beds (Facies 8) can be traced laterally along bedding contacts to amalgamated sets of planar cross-stratification (Subfacies 5a) which are discussed above. This lateral facies relationship is shown in the correlation diagram for outcrop A (Fig. 5.6, in pocket), which clearly illustrates that the massive quartzites merge laterally into planar cross-stratified cosets. This suggests that the massive character of the quartzites is probably attributed to post-depositional modification occurring during metamorphism or diagenesis and not neccessarily a consequence of primary

COARSE-GRAINED FACIES ASSOCIATION

FACIES	% OF TOTAL MEASURED ASSOCIATION	AVERAGE BED THICKNESS
1	3%	4 cm
2	0.9%	1 cm
3	0%	0 cm
4	7%	12 cm
5a	30%	34 cm
5b	10%	62 cm
6a	10%	26 cm
6b	0%	0 cm
7	0.6%	24 cm
8	40%	31 cm

COARSE/FINE-GRAINED INTERCALATED FACIES ASSOCIATION

FACIES	% OF TOTAL MEASURED ASSOCIATION	AVERAGE BED THICKNESS
1	38%	33 cm
2	2%	4 cm
3	0.1%	7 cm
4	9%	13 cm
5a	4%	21 cm
5b	11%	68 cm
6a	14%	21 cm
6b	6%	57 cm
7	10%	19 cm
8	5%	16 cm

Table 5.2. Table showing the precentages of facies and average bed thickness comprising the Coarse-grained Facies Association and the Coarse/Fine-grained Intercalated Facies Association.

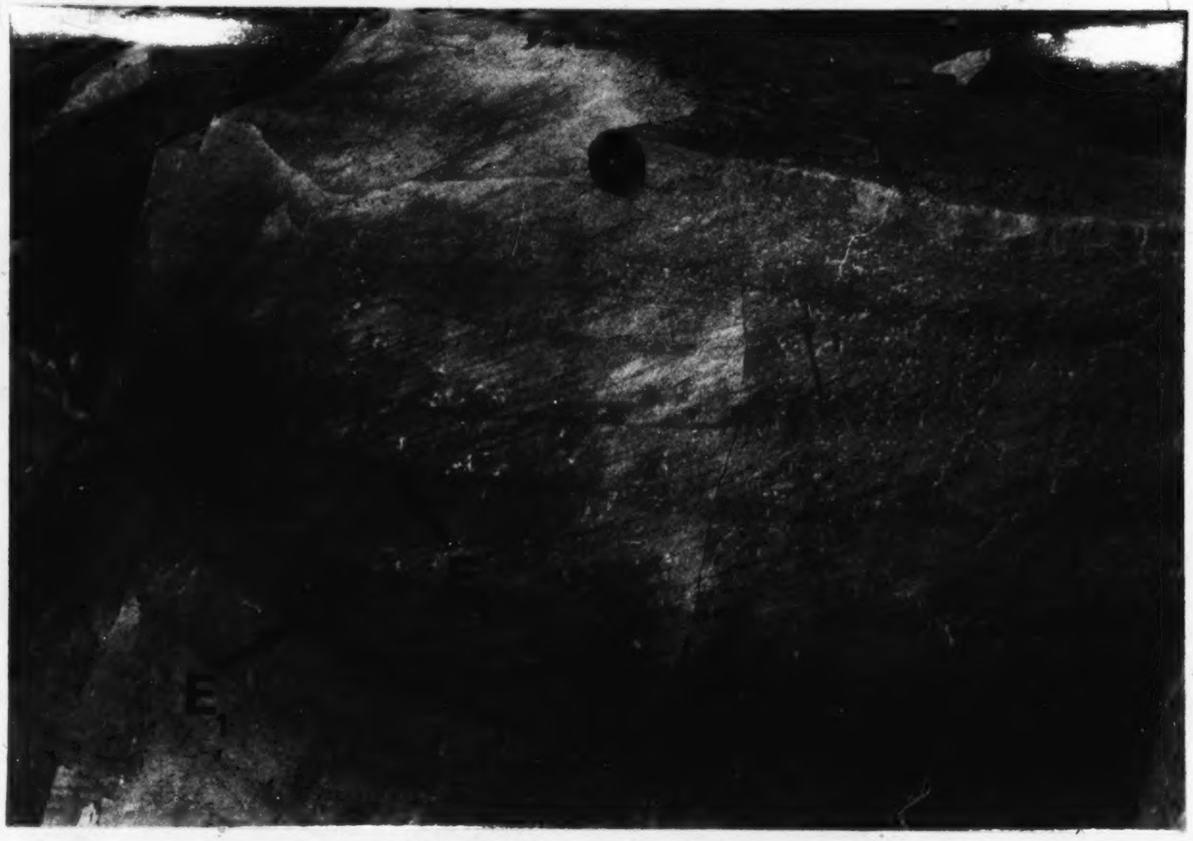

Figure 5.5. Master bedding surface. The first- and second-order bounding surfaces are indicated by arrows. The basal first-order bounding surface represents the horizontal substrate on which the sandwave migrates.

sedimentation. Therefore, this lateral relationship further emphasizes the stacked cross-stratified sequences comprising the Coarse-grained Facies Association at outcrop A.

The second lateral facies relationship occurring within the Coarse-grained Facies Association is located at outcrop D and involves Subfacies 5b units. This relationship begins with two planar tabular cross-stratified beds (Subfacies 5b), 45 cm thick, which progressively increase laterally in height and length to form part of a 2 meter thick quartzite-rich unit, with a complex internal organization of sedimentary structures as shown in Figure 5.7. The two initial planar tabular cross-beds are capped by several small-scale cross-laminated sets, which thicken laterally along the direction of transport. Detailed mapping of this 2 meter thick interval shows that reactivation surfaces are common and are usually draped by a very thin slaty shale veneer. Small-scale ripple cross-lamination rarely occurred along the reactivation surfaces. The internal cross-laminae are a maximum of 3 cm in thickness and are defined by the variation in color of adjacent cross-laminae. This 2 meter thick unit is laterally continuous and traceable up to 40 meters along strike.

The facies relationship diagram for this facies association (derived from a non-embedded Markov chain analysis) is shown in Figure 5.8 and reveals a tendency for beds of a given facies to be overlain by beds belonging to the same facies. For example, planar cross-stratification (Subfacies 5a) is usually overlain by another interval of planar cross-stratification. The preferred transition from Subfacies 5a to itself can be interpreted as representing a series of migrating and vertically aggrating two-dimensional megaripple fields. Similarly, the transition of planar cross-stratified quartzites (Subfacies 5b) into identical beds is interpreted as recording the lateral migration and aggradation of straight-crested dunes or sandwaves. The massive quartzites (Facies 8) tend to pass upward into internally structureless beds of the same facies (Facies 8) which in turn tend to be overlain by thin (<1 cm) shale beds of Facies 2. The massive quartzites beds of Facies 8 as mentioned earlier (Chapter 3) are probably not attributed to the depositional process but rather a consequence of the uniformity of grain size or a product of metamorphic recrystallization. The lateral traceability of massive quartzites into intervals of planar cross-stratification (Subfacies 5a) suggests that they were originally cross-stratified and subsequent post-depositional modification caused the massive appearence. Therefore, this transition from 8 to 8 and then into 2 probably records the lateral migration and aggradation of multiple two-dimensional megaripple fields during a period of

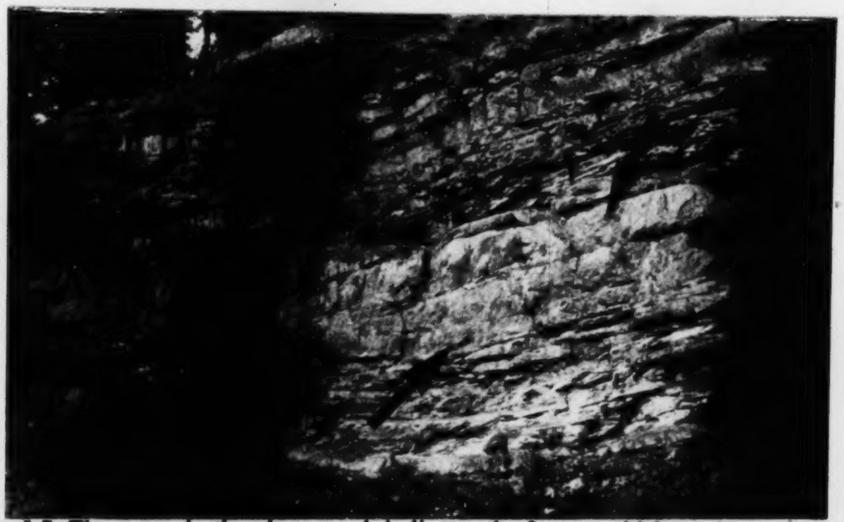

Figure 5.7. The arrow in the photograph indicates the 2 meter thick sandwave complex at outcrop D. The complicated internal arrangement of sedimentary structures in this sandwave is shown in the diagram.

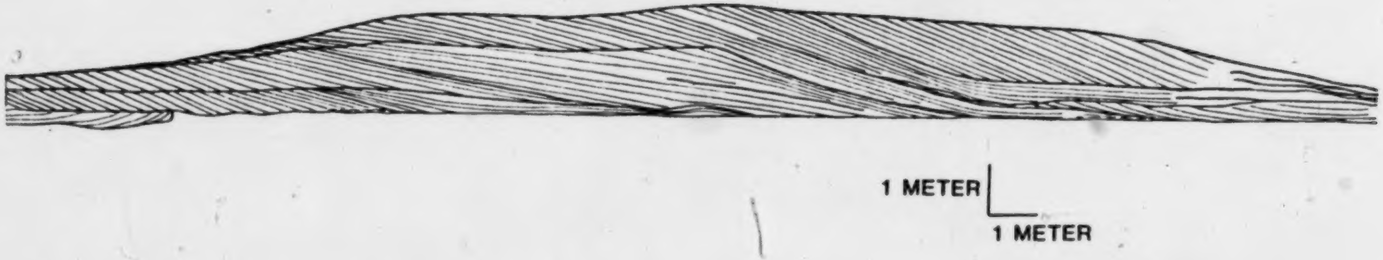

NO VERTICAL EXAGGERATION

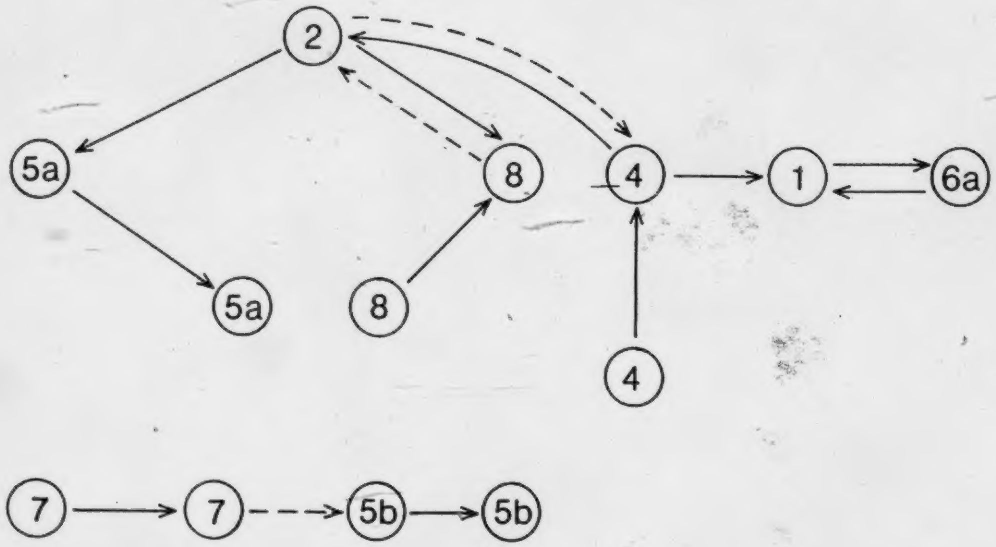
2
5a
8
4
1
6a
5a
8
4
7
7
5b
5b

Figure 5.8. Facies relationship diagram for the Coarse-grained Facies Association.

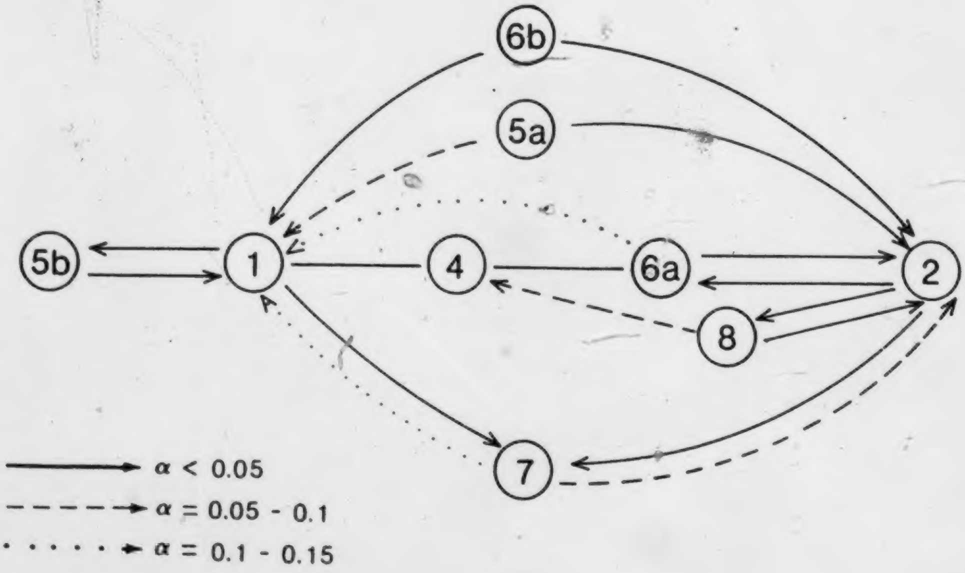
6b
5a
5b
1
4
6a
2
8
7
α < 0.05
α = 0.05 - 0.1
α = 0.1 - 0.15

Figure 5.15. Facies relationship diagram for the Coarse/Fine-grained Intercalated Facies Association.

fairly constant energy conditions which was eventually interrupted by an episode of hemipelagic sedimentation. The thin beds of shale (representing <1% of the measured Facies Association 1) tends to be succeeded by the passage of stratified facies into itself (2 into 5a→ 5a, or 4→ 4, or 8→ 8). This probably represents a progressive increase in energy conditions, resulting in diminishing mud suspension fall-out and the subsequent migration and up-building of ripple or megaripple fields. The principle transition paths of Facies 4 to 4 to 1 and then into 6a is interpreted as representing fluctuating energy conditions, in which tractional bedload movement occurred during higher flow velocities and fine-grained sedimentation existed during the lower flow conditions. The successive intervals of ripple cross-stratified quartzites (Facies 4 to 4) represents the progradation and up-building of a series of ripple fields which are subsequently draped by mud suspension fall-out recording a passage into lower energy conditions. With the reinstatement of progressively higher flow conditions the migration and vertical aggration of sinuous-crested megaripple fields (Subfacies 6a) occurs as the sand is tractionally transported. The low angle to horizontally stratified quartzites (Facies 7) usually passes upwards into either beds of the same facies or planar cross-bedded quartzites of Subfacies 5b. These transitions should be interpreted with a certain amount of caution because of the extremely low numbers of observed transition counts. This trend (7→ 7→ 5b) records the sequential deposition of very low amplitude bedforms or upper plane beds which is succeeded by slightly lower flow conditions resulting in the deposition of laterally migrating straight-crested dunes.

5.3.2 COARSE/FINE-GRAINED INTERCALATED FACIES ASSOCIATION

The second facies association identified within the Gog sediments is the Coarse/Fine-grained Intercalated Facies Association 2, which is characterized by a quartzite:shale ratio of <3:1. It is comprised of several facies with the interbedded quartzite and shale (Facies 1), trough cross-stratified quartzites (Facies 6) and planar cross-stratified quartzites (Facies 5) accounting for the majority of this association. The other facies occur in moderate to minor amounts (Table 5.2). The majority of this facies association is located at outcrops B, C and D with only a minor 2 meter interval occurring at outcrop A (section A-18-1 & A-18-2). The columnar sections of these outcrops (Appendix I) and the correlated stratigraphic sections (Fig. 5.9-5.12, in pocket) illustrate the representative facies patterns within this facies association and also the intercalated nature of the quartzite facies and fine-grained facies.

In contrast to the Gog sediments at the Spiral Tunnels sections (Hein, 1986), the lateral facies relationships at Sink Lake are easier to determine because of the good accessibility of the section and lateral continuity of individual beds along strike. This facies association contains two consistent lateral facies trends which can be recognized by tracing individual cross-stratified quartzites between measured sections. The first facies relationship involves planar cross-bedded quartzites (Subfacies 5a and 5b) which merge laterally into trough cross-stratified quartzites (Subfacies 6a and 6b). This is best illustrated in the lower part of outcrop B, where an individual planar cross-stratified quartzite bed (Subfacies 5b) changes laterally into a trough cross-stratified bed (Subfacies 6b). This laterally progressive transition from planar to trough cross-stratification is shown in Figure 5.13. Another discernable lateral facies relationship is associated with planar cross-bedded quartzites (Subfacies 5a or 5b) and small-scale cross-stratified quartzites (Facies 4). This lateral trend is characterized by individual beds of planar cross-stratification which change laterally into small-scale cross-stratified quartzites. Figure 5.14 illustrates this lateral facies relationship between Facies 5 and 4.

The facies transition diagram, derived from an embedded Markov chain analysis, reveals the significant facies relationships for this association (Fig. 5.15). Planar cross-stratified quartzites (Subfacies 5b) are usually overlain by interbedded slaty shale and quartzites (Facies 1) which in turn is succeeded by another interval of planar cross-stratification (Subfacies 5b). This relationship is interpreted as representing a migrating straight-crested dune or sandwave that is subsequently buried by an episode of hemipelagic sedimentation which occurred during a period of lower energy conditions. With the reinstatement of higher energy conditions the incremental migration of straight-crested dunes (Subfacies 5b) is initiated and advances across the previously deposited fine-grained sediments. In contrast to the Coarse-grained Facies Association the interbedded slaty shales and quartzites characterizing Facies 1 are volumetrically important (represents 38% of the measured facies association) and represent an appreciable accumulation of fine-grained material (average bed thickness is 33 cm). Alternatively, Facies 1 can pass upwards into Facies 4 which is characterized by amalgamated sets of ripple cross-stratified quartzites which in turn is overlain by multiple sets of trough cross-stratified quartzites (Subfacies 6a). This principle transition

Figure 5.13. Lateral facies relationship involving a planar cross-stratified quartzite bed (Subfacies 5b) changing laterally into a trough cross-stratified bed (Subfacies 6b).

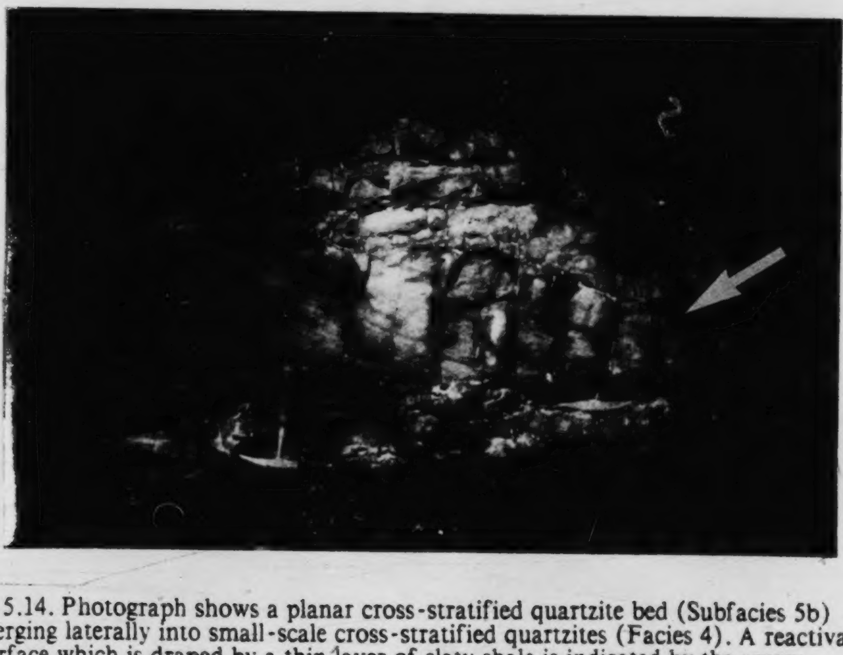

Figure 5.14. Photograph shows a planar cross-stratified quartzite bed (Subfacies 5b) merging laterally into small-scale cross-stratified quartzites (Facies 4). A reactivation surface which is draped by a thin layer of slaty shale is indicated by the arrow.

path represents the cessation of fine-grained sedimentation and a progressive increase in energy conditions resulting in the reinstatement of migrating ripple fields which are advancing over a predominately muddy substrate and are superimposed by a laterally migrating and aggrating sinuous-crested megaripple field or individual bedform. The trough cross-stratified beds (Subfacies 6a) tend to pass upwards into fine-grained sediments of either Facies 1 or 2. This records a migrating sinuous-crested dune or field which is covered by a thin layer of mud (Facies 2) or a thick accumulation of vertically accreting mud with periodic influxes of sand (Facies 1). In the case where the trough cross-stratified quartzites (Subfacies 6a) are succeeded by interbedded slaty shale (Facies 1) the flow loop between Facies 1, Facies 4, Subfacies 6a, and Facies 2 is initiated. The thin slaty shale beds of Facies 2 are overlain by a variety of lithologic facies, including planar cross-stratified quartzites (Subfacies 5b), trough cross-bedded quartzites (Subfacies 6a, 6b), low angle to horizontally stratified quartzites (Facies 7) and massive quartzites (Facies 8). All of the lithologic states return back into the fine-grained Facies of 1 or 2, indicating periods of fluctuating energy conditions, with the tractional bedload movement of sand occurring during higher flow velocities and the deposition of mud recording lower flow conditions. When slaty shale (Facies 2) passes upward into massive quartzites (Facies 8) it can be interpreted as a period of mud suspension fall-out followed by the migration of a originally cross-stratified bedform. Similarly, the transition from slaty shale to planar cross-stratified quartzites (Subfacies 5b) indicates a period of mud deposition succeeded by a migrating straight-crested megaripple field or individual bedform. The slaty shale also can be overlain by trough cross-bedded quartzites (Subfacies 6b) which in turn tends to pass into interbedded slaty shales and quartzites (Facies 1). This is interpreted as recording a short episode of hemipelagic deposition followed by a migrating sinuous-crested dune which is eventually buried by fine-grained sedimentation resulting in the reinstatement of a low-energy quiet environment. Alternatively, the slaty shale (Facies 2) or interbedded slaty shale and quartzites (Facies 1) can be overlain by low angle to horizontally stratified quartzites (Facies 7). This trend records an increase in the energy conditions where the previous mud fall-out remains in suspension and is followed by deposition of very low amplitude bedforms or upper plane beds controlled by high flow velocities.

5.4 INTERPRETATION OF THE COARSE-GRAINED FACIES ASSOCIATION

Based on the geometry and lateral and vertical arrangement of sedimentary structures, the Coarse-grained Facies Association is interpreted as a marine sandwave complex. The complex internal stratification sequences within this facies association are similar to the large-scale intraset cross-stratification and highly form-discordant internal structure in modern sandwaves (Reineck, 1963; Boersma, 1969; Dalrymple, 1984). However, it should be noted that although there is a tremendous amount of information regarding the morphology and distribution of modern sandwaves, there is still considerable uncertainty concerning the internal sedimentary structures, method of formation and migration of these large, constructive features. This inadequate understanding of the mechanisms of sandwaves genesis and maintenance has obstructed the progress towards a unifying model for sandwaves and their characteristic deposits.

Allen (1980a) has recently developed a theoretical model of sandwave development under oscillatory (reversing) flows in which the sandwave asymmetry and internal structure reflect the time-velocity asymmetry of the governing tidal currents. He recognized six classes of large bedforms developed under a wide range of current strengths and velocity asymmetries (Fig. 5.16). The bedforms characterized by his Classes I, II, and part of III are produced by essentially undirectional flow and are classified as dunes. These subaqueous dunes have slopes sufficiently steep to generate a large-scale separation of flow. The remainder of Class III, and all of Classes IV, V, and VI are categorized as sandwaves produced by flows with moderate to strong current reversals.

The internal arrangement of sedimentary sequences of the Coarse-grained Facies Association compares closely with the theoretical series of structures generated in sandwaves of Class IV and V. This facies association at outcrop A which is characterized by planar cross-stratified intrasets, separated into gently inclined cosets by master bedding surfaces (Subfacies 5a) is interpreted as small, straight-crested megaripples migrating down the lee face of a southwesterly-facing sandwave. The gentle angle of dip (10° - 15°) of the bounding surfaces enclosing the compound cross-stratified sets suggests a low degree of asymmetry of the stoss and lee faces. Flow of the dominant tidal current over the symmetrical sandwave results in bed-load transport as megaripples descending down the lee slope, which is recorded by transitions of 5a back into itself. The total absence of bidirectional cross-stratification suggests

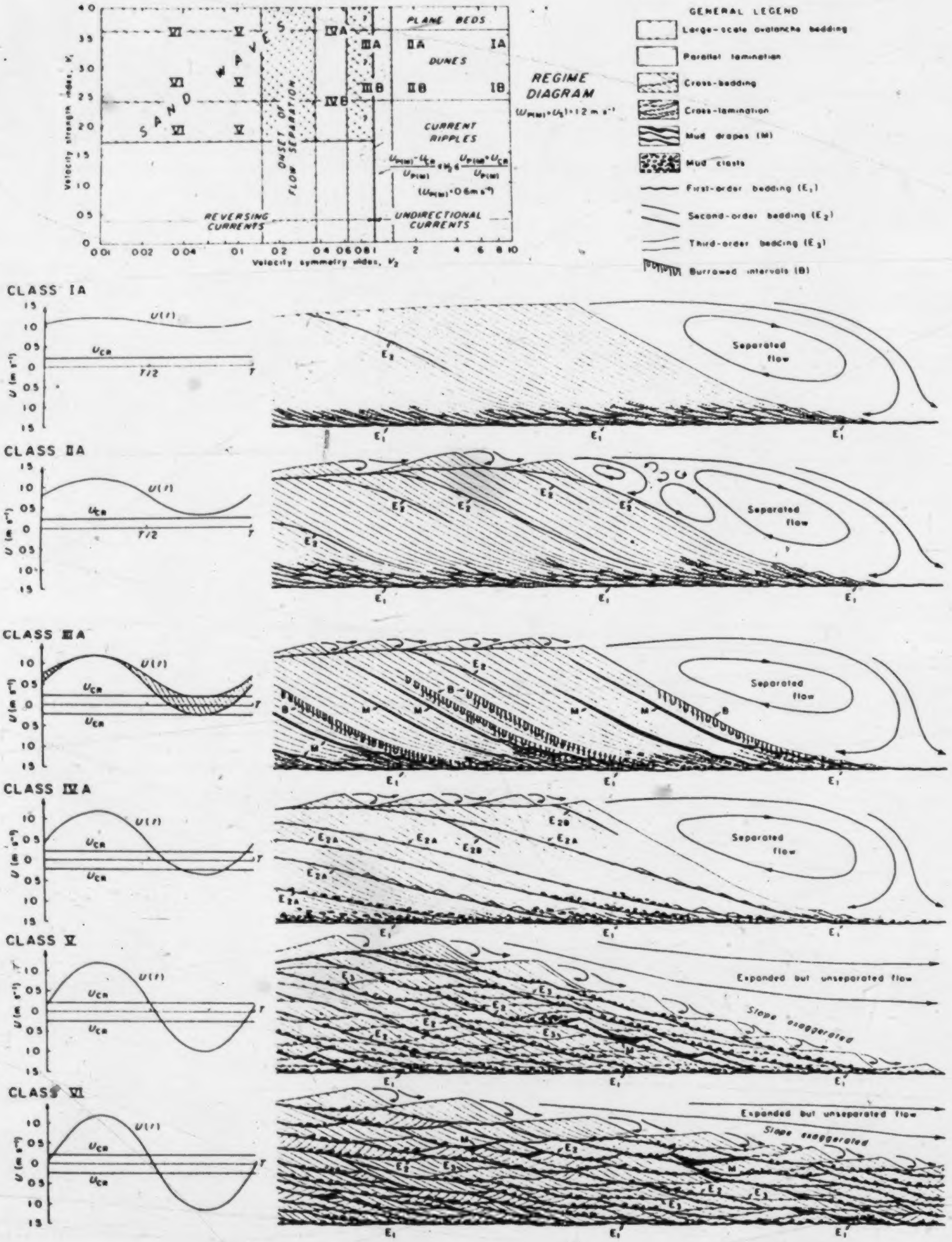
REGIME DIAGRAM
SAND WAVES
PLANE BEDS
DUNES
CURRENT RIPPLES
ONSET OF FLOW SEPARATION
REVERSING CURRENTS
UNDIRECTIONAL CURRENTS
Velocity strength index, V_1
Velocity symmetry index, V_2
GENERAL LEGEND
Large-scale avalanche bedding
Parallel lamination
Cross-bedding
Cross-lamination
Mud drapes (M)
Mud clasts
First-order bedding (E_1)
Second-order bedding (E_2)
Third-order bedding (E_3)
Burrowed intervals (B)
CLASS IA
CLASS IIA
CLASS IIIA
CLASS IVA
CLASS V
CLASS VI
$U(t)$
U_{CR}
$T/2$
T
Separated flow
Expanded but unseparated flow
Slope exaggerated

Figure 5.16. Theoretical model of the internal structure of sandwaves resulting from the different time-velocity patterns of the governing tidal currents (after Allen, 1980a, diagram obtained from Walker, 1984).

that there was no enhanced reworking of the lee side of the sandwave by the subordinate tidal current. This probably indicates that the reversing currents were not in excess of the threshold for sediment movement and therefore not strong enough to erode the dominant megaripple morphology and produce trains of subordinate-orientated ripples. Because the subordinate current is unable to erode or modify the dominant current megaripples, the cross-bedding associated with the dominant flow is preserved.

The origin of the master bedding surfaces, or second-order bounding surfaces is problematical. However, Allen (1980b) relates the gently inclined, closely spaced, master bedding surfaces (E_2) to oscillatory flow pattern of tidal currents. Due to tidal asymmetry the strength and duration of ebb and flood tidal velocities are not equal and the net bed-material transport is in the direction of the dominant current. Reversing, subordinate tidal currents rework a portion of the sandwave margin forming an erosional surface. Successive tidal events of dominant current deposition and subordinate current erosion results in these internal bounding surfaces.

The sedimentary structures within the Coarse-grained Facies Association at outcrop A are consistent with those predicted for Allen's Class V sandwaves, displaying a moderate time-velocity asymmetry. Allen's predicted numerical value for the inclined master bedding surface (4.2°) is slightly less than those measured in this facies association (10°- 15°). However, his predicted lee slope angles for symmetrical sandwaves (4.2°) are considerably less than the 10° to 20° slope values observed for symmetrical sandwaves in tidally-dominated seas (Stride, 1982).

The two meter thick interval of Coarse-grained Facies Association at outcrop D is interpreted as a solitary sandwave. The complex internal geometry and stratification sequences which were described in the second lateral facies relationship (Fig. 5.7) are similar to those formed by the Class IV sandwaves of Allen's (1980a)(Fig. 5.16). The important characteristics of this preserved sandwave which are similar to those predicted by Allen for Class IV sandwaves include: (1) An extensive, underlying first-order erosion surface (E_1, that is the surface upon which the sandwave migrated) that probably formed by the separated flow scouring ahead of the advancing sandwave. (2) Relatively steep foresets due to flow separation causing the crestward migrating megaripples to avalance just beyond the crest, resulting in the rapid steepening of the lee slope. (3) Rare examples of locally rippled bottomsets possibly formed by the reversing subordinate tidal current. (4) Gently inclined second-order erosional discontinuities which possibly record the modification of the sandwave crest during the reversal of tidal flow. (5) Thin shale drapes formed during periods of low-sediment transport probably associated with sandwave inactivity.

These internal structures suggest that the sandwave did not migrate as a single feature, but rather by superimposed megaripples advancing towards the crest which transport bed-load material to the relatively steep lee slope. The virtual lack of bidirectional cross-bedding within this sandwave indicates that the net sediment transport was largely governed by the dominant tidal current and the reversing current only caused slight modifications. The vertically stacked sequences of sandwaves are possibly due to differences in migration velocity (celerity) between individual sandwaves. The sandwaves with higher celerity will overtake and ride up the back of slower sandwaves.

5.5 INTERPRETATION FOR THE COARSE/FINE-GRAINED INTERCALATED FACIES ASSOCIATION

The increase in fine-grained facies coupled with the lateral and vertical sequence of sedimentary structures indicates that this facies association represents a relatively low energy environment which is removed from the continually tidally swept regions characterized by active, aggradational sandwave (Facies Association 1). As mentioned earlier in the interpretation for the significant facies transitions for this facies association, the depositional setting is controlled by fluctuating energy conditions, in which tractional transport of sand occurred during higher flow velocities and fine-grained sedimentation existed during the lower flow conditions. Adopting this scenario, the alternating intervals of stratified quartzites and slaty shale record the intermittently active migration of straight- and sinuous-crested bedforms generated during higher flow conditions. With the reinstatement of quiet water conditions the bedforms cease migrating and are covered by mud from suspension fall-out.

The first lateral facies relationship within this facies association, in which planar cross-stratified quartzites merge laterally into trough cross-stratified quartzites can be explained in terms of the governing hydrodynamic conditions. The change of internal cross-laminae from angular with sharp-based truncation to asymptotically-dipping with tangential basal contacts is a function of progressively increasing flow conditions. In response to the higher flow velocities the morphology of the migrating bedform changes in character from a straight-crested form to a sinuous-crested form with a developing scour pit in the trough.

The second facies association dealing with individual beds of planar cross-stratification changing laterally into small-scale ripple cross-stratified quartzites. The origin of this lateral trend is uncertain because the orientation of the small-scale ripple cross-lamination and ripple crests could not be determined due to the lack of well-exposed internal structure preventing the measurements of paleocurrents. However, in spite of this fact several possible explanations for this trend include: (1) Backflow ripples forming at the base of the slipface; (2) subordinate rippled apron or cap produced by comparatively strong reversing tidal currents flowing upslope; (3) reworking of the bedform crest and lee flank by wave-current interaction during periods of fair-weather conditions;

The presence of reactivation surfaces are often associated with this lateral variation between planar and small-scale ripple cross-stratified quartzites (Fig. 5.14) and also with thin shale drapes separating successive large-scale foresets. Reactivation surfaces are generally formed on the lee slopes of active, migrating bedforms because of flow unsteadiness, that is, fluctuations in current strength and direction with time. Such reactivation surfaces are particularly common in tidal environments. Many of the reactivation surfaces contained within beds of this facies association are in close proximity with bedding showing oppositely dipping foreset laminae (Fig. 4.3). This indicates that the genesis of the reactivation structures is possibly related to the reversal from dominant to subordinate tidal flows. Accompanying this feature are often ripples directed up the lee slope of the bedform or if the current is sufficiently weak fine-grained sedimentation may occur and drape the large-scale foresets. For a further discussion of the distinguishing criteria for recognizing reactivation surfaces in tidal deposits see De Mowbray and Visser (1984).

6. DEPOSITIONAL MODEL FOR THE LOWER CAMBRIAN GOG GROUP

The distinct assemblage of sedimentary structures within the two facies associations coupled with the vertical sequence of sedimentary structures and abundance of trace fossils indicates that the Gog Group at Sink Lake is wholly of marine origin. Within the measured sections there is no evidence of sedimentary structures or deposits suggestive of shoreline or coastal plain settings. Absent are low angle swash lamination, subareal exposure features, overbank deposits and channelling which are characteristic of coastal beach, tidal flat, lagoon or estuarine environments. This lack of any definite evidence for marginal (shoreline) sediments indicates that the entire sequence was deposited in an shallow marine shelf setting, seawards from the influence of coastal, deltaic and estuarine processes. The main depositional process active in this region was tidal currents. Rectilinear or strongly elliptical tidal flow is interpreted as the dominant sedimentation process forming the observed bimodal-bipolar paleocurrent trends in addition to the reactivation surfaces and sandwave complexes (Wolberg and Hein, 1986).

Although tidal currents largely controlled and influenced the type of sedimentation within this offshore environment, it appears that periodic storm processes were of lesser, although not necessarily negligible, importance. The hydrodynamic imprinting of storms is manifest in laterally persistent, normally graded quartzite interbeds displaying sharp, erosional basal contacts (Subfacies 1c). These thin graded layers occur within the Coarse/Fine-grained Intercalated Facies Association and are best illustrated at outcrops B and D. It should be noted that the thinly-bedded graded quartzites are volumetrically insignificant and only constitute approximately 5% of the total measured sections. Consequently the storm influences are relatively minor compared to the preeminent tidal forces. The scarcity of other storm-influenced sedimentary structures such as hummocky cross-stratification is probably attributed to the daily reworking by the omnipresent tidal currents. Observations on modern continental shelves indicate that storm-generated structures can be obliterated within several days by relatively weak (5-10 cm/sec) tidal currents (Butman *et al.*, 1979). Consequently, the storm-generated sediments have a low preservation potential on tide-dominated shelves. The model envisages the combination of tidal and minor storm processes acting in a shallow marine shelf setting and it is this interaction between these two processes which produces the characteristic sequence of sedimentary structures contained within the Lower Cambrian Gog sediments at the Sink Lake section. This interplay between storm conditions and tidal currents has been documented as an important control over sedimentation in several late Precambrian and early Cambrian tidal shelf deposits (Banks, 1973; Anderton, 1976; Johnson, 1977; Levell, 1980a; Soegaard and Eriksson, 1985).

The two facies associations identified within the measured stratigraphic succession can be interpreted as representing different parts of tidal current transport paths. As mentioned in Chapter 2, this tidal current transport path consists of a sequence of zones characterized by distinctive bedform types and is paralleled by decreases in grain size and mean tidal velocities. The following reconstruction of the early Cambrian Gog shelf is based partly on observations from modern transport paths of tidal currents (Fig. 2.3) (Stride, 1982) and on interpretations of the facies assemblages forming the two facies associations. The Coarse-grained Facies Association appears to correspond to the zone of sandwaves while the Coarse/Fine-grained Intercalated Facies Association represents offshore sand patches grading into shelf muds which occur at the distal ends of net sand transport paths (Fig. 6.1). The overall sedimentation pattern was largely controlled by tidal currents with the importance of storm deposition increasing further down the transport path.

The Coarse-grained Facies Association is interpreted as representing a series of coalescing tidal sandwaves distributed within the sandwave province occurring along the tidal transport path (Chapter 2). Documentation of the sandwave origin for this facies association was discussed in the previous chapter, where it was shown that the stratification sequences closely matched predicted forms in Allen's tidal sandwave model. This region of prograding sandwaves located on the Lower Cambrian shelf developed in response to an abundant sand supply and comparatively strong tidal currents. The predominance of a single, southwesterly mode in the paleocurrent pattern (Fig. 6.2 and 4.1) is certainly perplexing, because the majority of ancient and modern tide-dominated deposits show bipolar-bimodal paleocurrent directions which confirm the bidirectionality of bottom currents. However, the presence of unidirectional paleoflow patterns is not necessarly sufficient evidence for rejecting a tidal interpretation. Several sandstone bodies have been interpreted as tidal deposits even though they show unimodal paleocurrent patterns (Narayan, 1971; Banks, 1973; Anderton, 1976; Nio, 1976; Johnson, 1977; Levell, 1980a). There are three possibilities which might account for this unidirectional predominance of paleocurrent patterns: (1) one tidal direction is preferentially

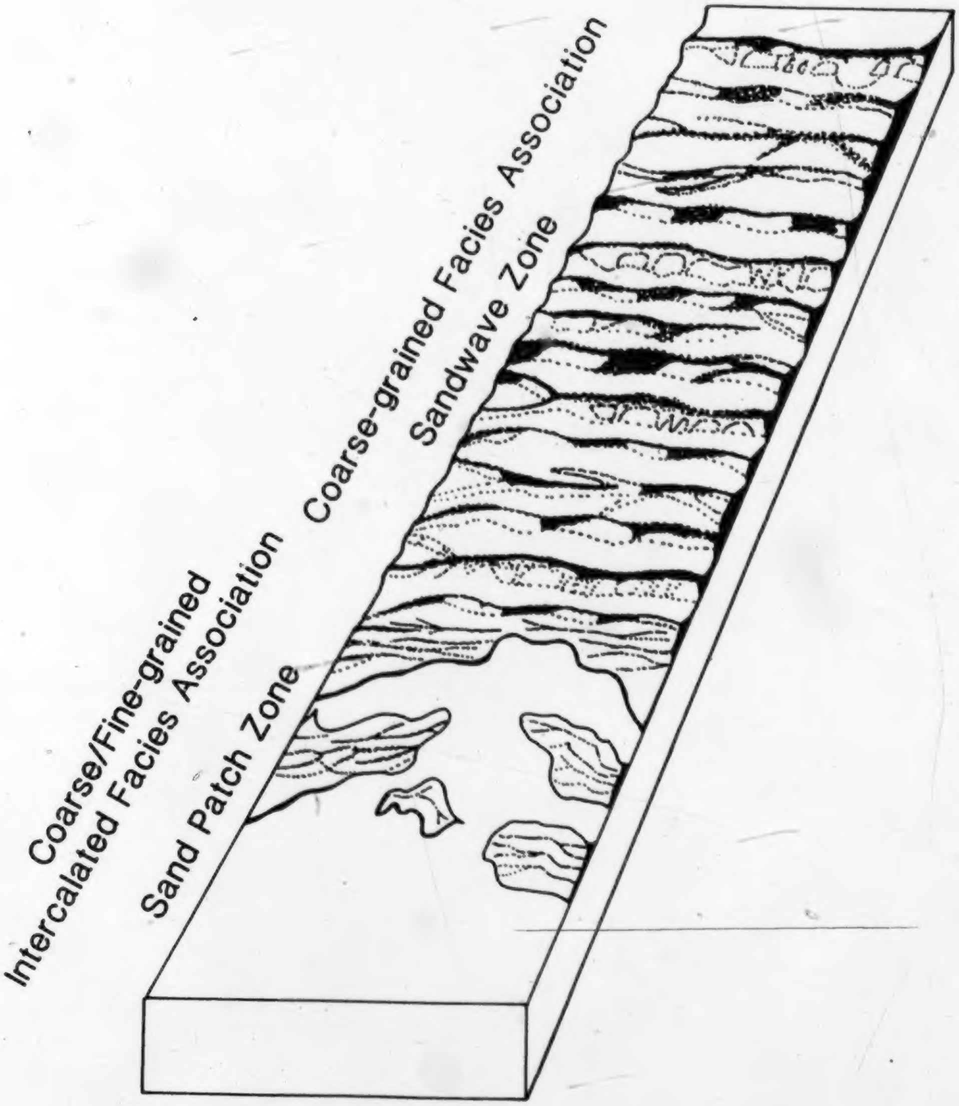
Coarse/Fine-grained
Intercalated Facies Association
Coarse-grained Facies Association
Sandwave Zone
Sand Patch Zone

Figure 6.1. Block diagram of the distal portions of the tidal transport path occurring on the early Cambrian continental shelf. The sandwave depositional zone is represented by the Coarse-grained Facies Association while the seaward zone of sand patches corresponds to the Coarse/Fine-grained Intercalated Facies Association.

reinforced by another shelf current, presumbly by a wind/wave-driven current or geostrophic current system; (2) a preservation factor in which the laterally migrating sand bodies with their internal unidirectionally inclined master bedding surfaces have the highest preservation potential (Levell, 1980a); (3) sediment transport during the dominant tidal phase systematically exceeds that during the subordinate tidal phase. This regional transport dominance results in unidirectional tidal transport paths which presently occur in the modern tidal seas of Northwest Europe (Stride, 1963; Belderson and Stride, 1966).

The interpretation of the sedimentary structures along with the lateral and vertical facies relationships within the Coarse/Fine-grained Intercalated Facies Association suggests that it developed in response to a hydraulic regime characterized predominately by tidal currents and of lesser importance the periodic influences of storms. This facies association occurs immediately downcurrent from the extensive tidal sandwave fields. This distal inner shelf zone corresponds to the outer parts of tidal current transport paths which is characterized by local sand patches grading into shelf muds. The bidirectional paleocurrent patterns of this facies association and the outcrops comprising it (Fig. 6.3 and 4.2, 4.4, 4.6) indicate a tidally-dominated offshore system. However, this Lower Cambrian shelf appears to be influenced by another shelf process, that being storm currents, with the thin interbedded sand layers of Subfacies 1c recording episodic and storm-generated deposition in the offshore shelf muds.

The near-random superposition of sand patches, storm deposits, and shelf muds identified by Markov chain analysis seems best interpreted as indicating that the processes responsible for the facies occurred in such a fashion that the various facies become intercalated in the vertical successions without cyclicity. This random order of the facies within the Coarse/Fine-grained Intercalated Facies Association may be partically attributed to the relatively short-lived, episodic nature of the storm currents. Similar examples of distal sand patches alternating randomly with offshore muds have been documented on tidally-dominated shelf environments which are influenced by intermittent storm events (Anderton, 1976; Levell, 1980b).

Although the majority of this facies association occurs at the distal end of the tidal transport path in the distal inner shelf region, there is another geographically separate area that contains a similar assemblage of sedimentary structures. This particular setting is interpreted as

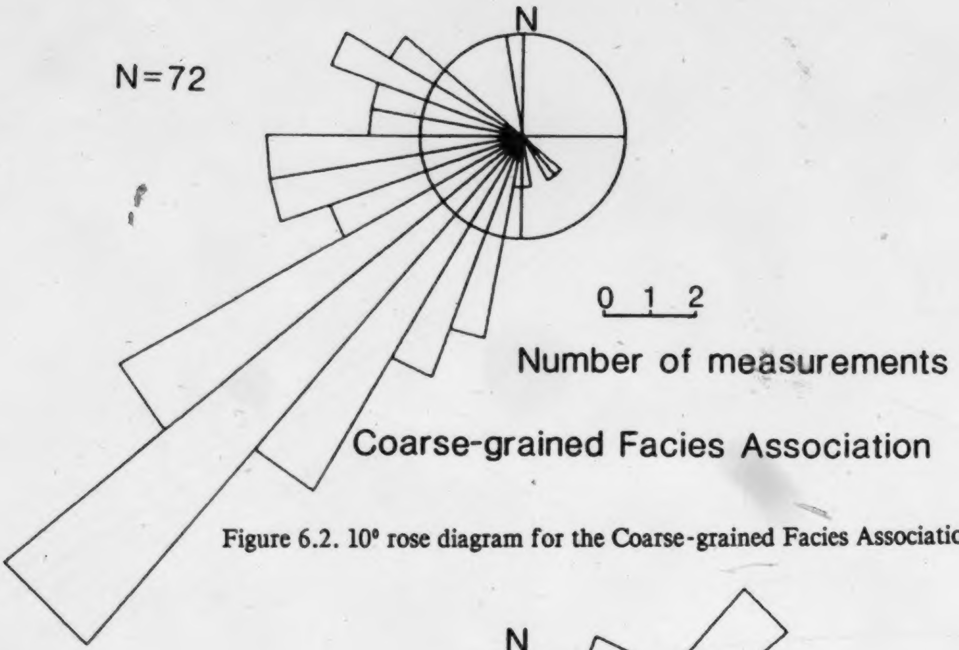

Figure 6.2. 10° rose diagram for the Coarse-grained Facies Association.

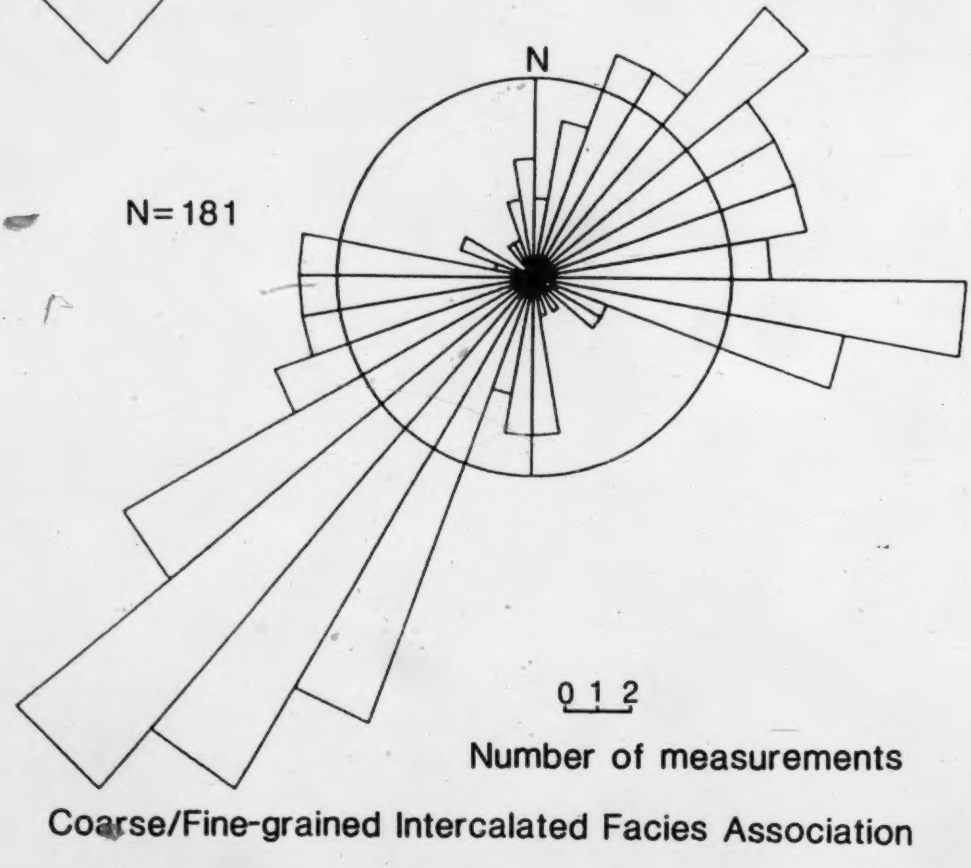

Figure 6.3. 10° rose diagram for the Coarse/Fine-grained Intercalated Facies Association.

the protected inter-sandwave-swale, a topographically depressed area between individual sandwaves. The interpretation is partly based on sections A-18-1 and A-18-2 (part of Facies Association 2) which is sandwiched between sections corresponding to the Coarse-grained Facies Association at outcrop A. This is shown in the lateral correlation diagram in Figure 5.6 (in pocket). Sedimentation within these finer grained inter-sandwave troughs probably occurred prior to or concurrent with deposition of large-scale sandwaves when less competent currents flowed between the sand bodies producing the characteristic sedimentary structures of the Coarse/Fine-grained Intercalated Facies Association.

As stated earlier in this chapter, the two facies associations are interpreted as reflecting the interaction of fair-weather and minor storm events superimposed on a tide-dominated hydraulic regime. The main depositional episode is believed to accompany strongly operative spring tidal currents which are presumbly reinforced by either storms or undirectional tidally-driven, geostrophic or littoral current systems. The spring tidal currents augmented by this intervening high energy event were directed towards the southwest which is manifested by the strongly preferential southwesterly paleocurrent direction in Facies Association 1 (Fig. 6.2 and 4.1) coupled with the slightly more dominant southwest mode in Facies Association 2 (Fig. 6.3 and 4.2, 4.4, 4.6). Maximum sediment transport probably occurred during this high energy period resulting in the extension of sandwave fields down the tidal current transport path. The adjacent zone of sand patches also temporarily shifts shedding sand further downcurrent in response to the strong spring tidal currents aided by interacting shelf currents (littoral or geostrophic) or storm processes. Fine sand placed in suspension by the high current velocities is deposited distally as thin storm-sand layers. With the reinstatement of the fair-weather period the normal bidirectional tidal currents are dominant and the shelf deposits move towards a state of equilibrium with the tidal regime. Migration of sandwaves is relatively slow and mainly directed towards the southwest. Suspension deposition of fine-grained sediment occurs in the distal inner shelf environment and covers the previously migrating offshore bedforms and sand patches generated by the high energy event. The strong and persistent tidal currents possibly destroyed or remoulded the storm-generated structures in the distal inner shelf to proximal middle shelf region.

This model envisions that the Lower Cambrian Gog sediments at Sink Lake were probably deposited in an offshore environment dominated by strong tidal currents and subjected to minor storm conditions. In addition this model allows for the intercalation of various facies within a tidally-dominated continental shelf without major fluctuations in sea level or changes in shoreline configuration.

6.1 TRACE FOSSILS OF THE LOWER CAMBRIAN GOG GROUP

Trace fossils are features representing the life activities or life-habits of organisms and provide a record of animal-sediment interactions. With each trace reflecting the behavioral adaptation of a given organism to a specific set of environmental conditions, it may be possible to infer the paleoenvironmental conditions from the particular assemblages of trace fossils present within the deposit (Frey, 1975). Environmental interpretations are not based on individual trace fossils but by the overall trace fossil assemblage, due to the fact that certain traces are found in numerous depositional settings (Frey and Pemberton, 1984). The trace fossil assemblage can be compared with body fossils and various lithologic evidence to infer a particular sedimentary environment. Since no skeletal fossils occur within the clastic sequences of the Gog Group, only the preserved sedimentary structures and trace fossils can be used to construct a model for past environments. However, trace fossils are often superior to body fossils for environmental interpretation because they are often confined to a narrow range of facies, they represent long time ranges and, are commonly found *in situ* in otherwise unfossiliferous strata and are not subject to post-mortem transport (Ekdale *et al.*, 1984).

The Lower Cambrian Gog sediments, which outcrop at Sink Lake lack hard body fossils, but contain a well preserved suite of trace fossils characteristic of a shallow marine environment. The majority of trace fossils at Sink Lake are characteristic of the *Cruziana* ichnofacies (S.G. Pemberton, 1985, personal communication). This ichnofacies consists of epi- and intrastratal crawling traces, horizontal to slightly sub-horizontal cylindrical burrows, scattered vertical burrows and inclined U-shaped burrows containing protrusive spreiten. Animals representative of this ichnofacies are mostly mobile carnivores and deposit feeders with some suspension feeders (Frey and Pemberton, 1984). The trace fossils collected at Sink Lake which are characteristic of the *Cruziana* ichnofacies include: *Cruziana* sp., *Rusophycus* sp., *Trichophycus* sp., *Diplichnites* sp., *Monomorphichus* sp., *Palaeophycus* sp. and *Planolites* sp.

Seilacher (1967) suggests that trace fossil communities occur at specific depositional localities and are controlled by water depth, which implies that they tend to have paleobathymetric significance. However, this assumption is imperfect because, water depth and distance from shore are not major factors which effect the local environment inhabited by trace fossil communities. It appears that the local availability of food, sedimentation rates and water turbulence ultimately determines the distribution of the tracemaker and thus the particular type of trace (Frey, 1975). Nevertheless, Howard (1978) maintains that these limitations should not detract from the validity of Seilacher's model and that assemblages of trace fossils are in general, distributed according to energy-depth zonations and substrate consistency.

According to this model, the trace fossil assemblage at Sink Lake indicates an open continental shelf setting located between daily wave base and storm wave base to slightly quieter offshore conditions (Frey and Pemberton, 1984). This setting inhabited by the resident ichnocoenose is removed from the high-energy inshore areas and the quiet water deep-sea environment. The *Cruziana* ichnofacies by itself is not a diagnostic feature of an offshore tidal environment but in combination with the observed sedimentary structures coupled with the absence in the sedimentary record of both foreshore and subaerial deposits aid in the interpretation of an offshore shallow marine environment.

6.2 PALEOGEOGRAPHY OF THE LOWER CAMBRIAN GOG GROUP

The effects of tides are well established in the Lower Cambrian shallow marine environment due to the presence of a suite of sedimentary structures diagnostic of tidal deposits, with the most celebrated being the ubiquitous bidirectional cross-stratification. The presence of such currents implies that the Lower Cambrian sea was connected with a deep ocean basin because as indicated in Chapter 2, tidal currents on shallow marine shelves are the result of tidal waves propagated from deep ocean basins onto adjacent shelves. Since significant tidal currents do not occur in enclosed seas or those with only a small oceanic connection, it is believed that the Gog sediments were deposited in a continental shelf type setting. The position and nature of the early Cambrian coastline is indeterminate because in the Kicking Horse Pass region no shoreline sediments are exposed. In the absence of alluvial and coastal deposits it is difficult to unequivocally state the distance from the coast and the precise orientation of the paleocurrents with respect to the shoreline. In addition there is no evidence or information on regional paleoslope, but the lack of turbidites (turbidity currents are driven by gravitational forces and require steep slopes) tentatively suggests a relatively gentle gradient. The salient points that emerge out of the paleocurrent anaylsis is that the dominant sediment transport direction was to the southwest, but a secondary paleocurrent mode directed towards the northeast supports the hypothesis of a tide-dominated current system. Another important point is that the lack of vertical variation of the southwest paleocurrent direction measured at outcrop A (Facies Association 1) suggests that the transport direction did not change drastically with time. Similarly, the vertical sections at outcrops B, C and D (Facies Association 2) show no systematic change or preferred orientation of the paleocurrent directions stratigraphically indicating that there was not a continuous and progressive change in the transport direction with time.

As mentioned earlier in Chapter 5, the genesis of the sandwave complexes in the Coarse-grained Facies Assocation is related to the prevailing tidal currents. However, an additional factor in the development of tidal sandwave complexes may be a rise of sea level (Nio, 1976). According to the global sea level curve constructed by Vail *et al.*, (1977) there was a continuous sea level rise during the early Cambrian. This progressive rise in sea level and constant sediment supply along with a continuous and uniform basin subsidence which occurred during the Lower Cambrian probably contributed to a high preservation potential for these tidal sand bodies. These factors are certainly important in explaining the excellent preservation of the sandwave complexes in the Coarse-grained Facies Association.

As previously noted, the interpretation of the sedimentary structures and paleocurrent patterns suggest that the deposition of the Lower Cambrian Gog sediments at Sink Lake took place in a shallow marine environment. These shelf deposits developed in response to a hydraulic regime characterized predominately by tidal currents and periodic storm events of secondary importance. An interesting note surrounding this sudsidiary storm influence is the paleogeographic distribution of meteorological systems during the Cambrian. Over the past few years, there has been some controversy dealing with the actual significance of tropical cyclones and winter storms affecting the shallow seas bordering Laurentia (Marsaglia and Klein, 1983, 1985; Duke, 1985a, 1985b; Hein, 1986). Paleogeographic reconstructions by Scotese *et al.* (1979) showed that in Cambrian time the continents were distributed latitudinally along or near the paleoequator (Fig. 6.4). The majority of the small landmasses were located within 45° latitude from the equator and separated by miniature seas. The area encompassed by the present day Kicking Horse Pass was situated on the north-central side of Laurentia at a

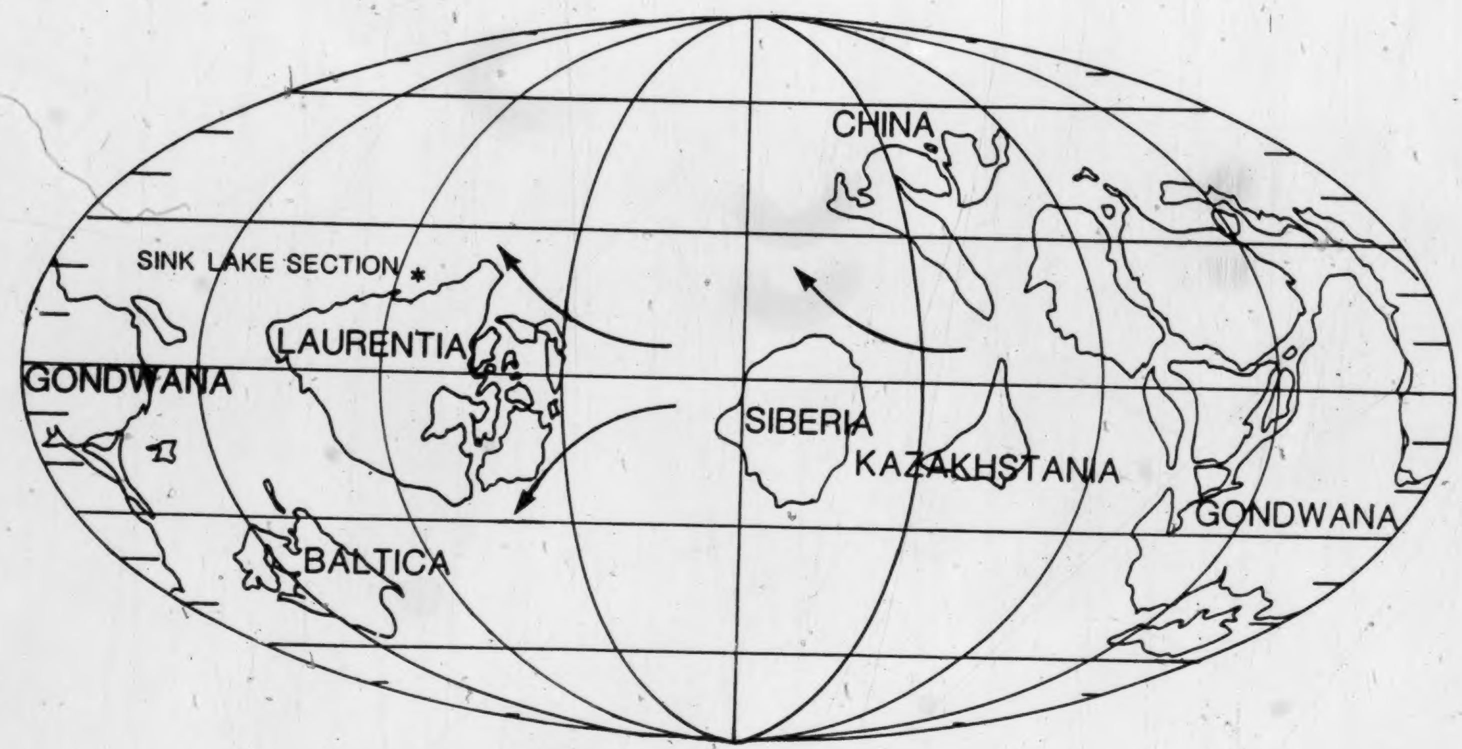
CHINA
SINK LAKE SECTION *
LAURENTIA
GONDWANA
SIBERIA
KAZAKHSTANIA
GONDWANA
BALTICA

Figure 6.4. Paleogeographic reconstruction of the Late Cambrian World (redrawn from Scotese *et al.*, 1979). Arrows indicate the proposed pathways of tropical meteorological disturbances. Note that the paleogeographic setting of Sink Lake is located in the north-central lee of Laurentia and sheltered from probable hurricane or tropical storm paths originating on the eastern side of Laurentia.

paleolatitude of 20° North (Duke, 1985b). Climatologists believe that the atmosphere circulation cells and major wind belts probably existed throughout geologic time (Dott and Batten, 1976). Assuming the same type of global atmospheric circulation and latitudinally-defined hurricane and winter storm provinces as at present, the Lake Louise-Kicking Horse Pass region was situated within a zone of mixed hurricane and winter storm influence, but slightly closer to a hurrricane-dominated paleolatitude (Marsaglia and Klein, 1983; Duke, 1985b). However, examination of the ancient paleogeographic setting for the Gog sediments in the Sink Lake region suggests that this area was situated within the north-central lee of Laurentia and possibly sheltered from low-latitude hurricane tracks (Marsaglia and Klein, 1983; Hein, 1986). Furthermore, it is noteworthy to mention that during the early Cambrian the oceanographic-atmospheric circulation system may have been influenced by the increased rotation of the earth due to the closer distance of the Moon to the Earth. The resulting increase in the centrifugal force could possibly deflect the equatorial storm system northward and away from the shallow shelf area occupying the present day Kicking Horse Pass region (Hein, 1986). In addition, the absence of permanent polar ice caps during the early Cambrian would presumably reduce the longitudinal temperature differential and thus weaken the nucleation of tropical storm systems (Hein, 1986). These are interesting points to consider and possibly explain why the Gog sections at Sink Lake are not largely storm influenced. Therefore, it should be emphasized that, although this paleogeographic setting is situated within hurricane- and winter storm- prone paleolatitudes, the specific location in the protected north-central lee of Laurentia, probably explains the tidally-dominated nature of the Gog Group at Sink Lake.

In summary, the Lower Cambrian Gog sediments, which outcrop in Yoho National Park near Sink Lake, B.C., represent deposits from an offshore, tidally-dominated shallow marine environment. This is supported by virtue of the preserved bidirectional cross-bedding, master bedding sequences, sandwave complexes, and the occurrence of reactivation surfaces and thin mud drapes in sets of cross-bedding. These sedimentary structures are characteristic of both recent and ancient tidally-dominated continental shelves. In addition the textural and mineralogical maturity of the sediments and the numerous communites of trace fossils indicate that the Gog Group is of marine origin. Futhermore, the absence of both foreshore features and evidence of emergence structures suggest that the Gog sediments were deposited in an offshore environment. All these observations support the interpretation of an offshore, tidally-dominated shallow marine paleogeographic setting for the Gog Group strata located at Sink Lake.

7. REFERENCES CITED

Allan, J.A., 1914, Geology of Field map area, B.C. and Alberta: Geological Survey of Canada Memoir 55, geological series no. 46, 312 p.

Allen, J.R.L., 1980a, Sand waves: a model of origin and internal structure: Sedimentary Geology, v. 26, p. 281-328.

Allen, J.R.L., 1980b, Sand-wave immobility and the internal master bedding of sand-wave deposits: Geology Magazine, v. 117, p. 437-446.

Aitken, J.D., 1968, Cambrian sections in the easternmost southern Rocky Mountains and the adjacent subsurface, Alberta: Geological Survey of Canada Paper 66-23, 96 p.

Aitken, J.D., 1969, Sub-Cambrian unconformity, Rocky Mountains, Main Ranges: Canadian Journal of Earth Sciences, v. 6, p. 193-200.

Anderton, R., 1976, Tidal-shelf sedimentation: an example from the Scottish Dalradian: Sedimentology, v. 23, p. 429-458.

Arnott, R.W., and Hein, F.J., 1986, Submarine canyon fills of the Hector Formation, Lake Louise, Alberta: Late Precambrian syn-rift deposits of the proto-Pacific miogeocline: Bulletin of Canadian Petroleum Geology, 22 p. (in press)(Dec. issue, v. 34, No.4).

Balkwill, H.R., 1972, Structural geology, Lower Kicking Horse River region, Rocky Mountains, British Columbia: Bulletin of Canadian Petroleum Geology, v. 20, p. 608-633.

Banks, N.L., 1973, Tide-dominated offshore sedimentation, Lower Cambrian, North Norway: Sedimentology, v. 20, p. 213-228.

Belderson, R.H., and Stride, A.H., 1966, Tidal current fashioning of a basal bed: Marine Geology, v. 4, p. 237-257.

Blatt, H., Middleton, G., and Murray, R.C., 1980, Origin of Sedimentary Rocks: Prentice-Hall Inc., New Jersey, second edition, 782 p.

Boersma, J.R., 1969, Internal structure of some tidal mega-ripples on a shoal in the Westerschelde Estuary, the Netherlands, report of a preliminary investigation: Geologie en Mijnbouw, v. 48, p. 409-414.

Bond, G.C., and Kominz, M.A., 1984, Construction of tectonic subsidence curves for the early Paleozoic miogeocline, southern Canadian Rocky Mountains: Implications for subsidence mechanisms, age of breakup, and crustal thinning: Geological Society of America Bulletin, v. 95, p. 155-173.

Burling, L.D., 1914, Early Cambrian stratigraphy in the North American Cordillera, with discussion of Albertella and related faunas: Geological Survey of Canada Museum Bulletin, no. 2, Geological Survey no. 17, p. 93-129.

Burling, L.D., 1922, A Cambro-Ordovician section in the Beaverfoot Range, near Golden, British Columbia: Geological Magazine v. 59, p. 452-461.

Butman, B., Noble, M., and Folger, D.W., 1979, Long-term observations of bottom current and bottom sediment movement on the Mid-Atlantic Continental Shelf: Journal of Geophysical Research, v. 84, p. 1187-1205.

Cant, D.J., and Walker, R.G., 1976, Development of a braided-fluvial facies model for the Devonian Battery Point Sandstone, Quebec: Canadian Journal of Earth Science, v. 3,

p. 102-119.

Carr, T.R., 1982, Log-linear models, Markov chain and cyclic sedimentation: Journal of Sedimentary Petrology, v. 52, p. 905-912.

Caston, V.N.D., 1972, Linear sand banks in the North Sea: Sedimentology, v. 18, p. 63-78.

Cluckey, E., Cacchione, D.A., and Nelson, C.H., 1980, Liquefaction potential of the Yukon prodelta, Bering Sea: Offshore Technology Conference, 12. Houston 1980. Proceedings, v. 2, p. 315-325.

Coleman, J.M., 1969, Brahmaputra River: channel processes and sedimentation: Sedimentary Geology v. 3, p. 131-239.

Charlesworth, H.A.K., Weiner, J.L., Akehurst, A.J., Bielenstein, H.U., Evans, C.R., Griffiths, R.E., Remington, D.B., Stauffer, M.R., and Steiner, J., 1967, Precambrian geology of the Jasper region, Alberta: Research Council of Alberta, Bulletin 23, 74 p.

Cluckey, E., Cacchione D.A., and Nelson, C.H., 1980, Liquefaction potential of the Yukon prodelta, Bering Sea: Offshore Technology Conference, 12., Houston 1980. Proceedings, v. 2, p. 315-325.

Cook, D.G., 1975, Structural style influenced by lithofacies, Rocky Mountain Main Ranges, Alberta-British Columbia: Geological Survey of Canada Bulletin 233, 73 p.

Curray, J.R., 1956, The analysis of two-dimensional orientation data: The Journal of Sedimentary Petrology, v. 44, p. 158-168.

Davis, J.C., 1973, Statistics and Data Analysis in Geology: John Wiley and Sons, Inc., New York, 550 p.

Dalrymple, R.W., Knight, J.R., and Lambiase, J.J., 1978, Bedforms and their hydraulic stability relationships in a tidal environment, Bay of Fundy, Canada: Nature, v. 275, p. 100-104.

Dalrymple, R.W., 1984, Morphology and internal structure of sandwaves in the Bay of Fundy: Sedimentology, v. 31, p. 365-382.

Dawson, G.M., 1901, Geological record of the Rocky Mountain region in Canada; Geological Society of America Bulletin, v. 12, p. 57-92.

De Mowbray, T., and Visser, M.T., 1984, Reactivation surfaces in subtidal channel deposits, Oosterschelde, southwest Netherlands: Journal of Sedimentary Petrology, v. 54, p. 811-824.

de Raaf, J.F.M., Reading, H.G., and Walker, R.G., 1965, Cyclic sedimentation in the Lower Westphalian of North Devon, England: Sedimentology, v. 4, p. 1-52.

Deiss, Charles, 1939, Cambrian formations of southwestern Alberta and southeastern British Columbia: Geological Society of America Bulletin, v. 50, p. 951-1026.

Deiss, Charles, 1940, Lower and Middle Cambrian stratigraphy of southwestern Alberta and southeastern British Columbia: Geological Society of America Bulletin, v. 51, p. 731-794.

Dott, R.H., Jr., 1973, Paleocurrent analysis of trough cross stratification: Journal of Sedimentary Petrology, v. 43, p. 779-783.

Dott, R.H., Jr. and Batten, R.L., 1976, Evolution of the Earth: New York, McGraw-Hill, 649 p.

Dott, R.H., Jr., and Bourgeois, J., 1982, Hummocky stratification: significance of its variable bedding sequences: Geological Society of America Bulletin, v. 93, p. 663-680.

Duke, W.L., 1985a, The paleogeography of Paleozoic and Mesozoic storm depositional systems: a discussion: Journal of Geology, v. 93, p. 88-90.

Duke, W.L., 1985b, Hummocky cross-stratification, tropical hurricanes, and intense winter storms: Sedimentology, v. 32, p. 167-194.

Ekdale, A.A., Bromley, R.G., and Pemberton, S.G., 1984, Ichnology: Trace Fossils in Sedimentology and Stratigraphy: Society of Economic Paleontologists and Mineralogists, Short Course Notes 15, 315 p.

Ethier, V.G., 1975, Application of Markov analysis to the Banff Formation (Mississippian), Alberta: Mathematical Geology, v. 7, p. 47-61.

Evans, C.S., 1933, Brisco-Dogtooth map-area, British Columbia: Geological Survey of Canada Summary Report, 1932, Pt. AII, p. 106-176.

Field, M.E., and Roy, P.S., 1984, Large storm and current shaped sandbodies on the southern Australian shelf: Calgary, Alberta, Canadian Society of Petroleum Geologists, Research Symposium on the Sedimentology of Shelf Sands and Sandstones, Programs with Abstracts, p. 36.

Flemming, B.W., 1978, Underwater sand dunes along the southeast African Continental Margin - observations and implication: Marine Ecology, v. 26, p. 177-198.

Flemming, B.W., 1980a, Factors controlling shelf sediment dispersal along the southeastern African continental margin: *In* Nittrouer, C.A., *ed.*, Sedimentary Dynamics of Continental Shelves, No. 32, Elsevier, p. 259-277.

Flemming, B.M., 1980b, Sand transport and bedform patterns on the continental shelf between Durban and Port Elizabeth (southeast African continental margin): Sedimentary Geology, v. 26, p. 179-205.

Flemming, B.M., and Stride, A.H., 1967, Basal sand and gravels patches with separate indications of tidal currents and storm-wave paths, near Plymouth: Journal of the Marine Biological Association of the United Kingdom, v. 47, p. 433-444.

Frey, R.W., 1975, The Study of Trace Fossils: New York, Heidelberg, Berlin, Springer-Verlag, 562 p.

Frey, R.W. and Pemberton, S.G., 1984, Trace fossils facies models: *In* Walker, R.G. *ed.*, Facies Models: Geoscience Canada, Reprint series I, second edition, p. 189-207.

Fritz, W.H., 1980a, Two new formations in the Lower Cambrian Atan Group, Cassiar Mountains, north-central British Columbia: *In* Current Research, Part B, Geological Survey of Canada Paper 80-1B, p. 217-225.

Fritz, W.H., 1980b, International Precambrian-Cambrian Boundary Working Group's 1979 field study to MacKenzie Mountains, Northwest Territories, Canada: *In* Current Research, Part A, Geological Survey of Canada Paper 80-1A, p. 41-45.

Fritz, W.H., 1982, Vampire Formation, a new Upper Precambrian(?)/Lower Cambrian formation, Mackenzie Mountains, Yukon and N.W.T.: *In* Current Research, Part B, Geological Survey of Canada, Paper 82-1B, p. 83-92.

Fritz, W.H., 1985, Lithology, trace fossils, and correlation of Precambrian-Cambrian boundary beds, Cassiar Mountains, north-central British Columbia: Geological Survey of Canada Paper 83-13, 24 p.

Gabrielse, H., 1975, Geology of the Fort Grahame E 1/2 map-area, British Columbia:

Geological Survey of Canada Paper 75-33, 28 p.

Gingerich, P.D., 1969, Markov analysis of cyclic alluvial sediments: Journal of Sedimentary Petrology, v. 39, p. 330-332.

Gross, G.M., 1977, Oceanography: A View of the Earth: Prentice-Hall Inc., New Jersey, 497 p.

Harms, J.C., Southard, J.B., and Walker, R.G., 1982, Structures and Sequences in Clastic Rocks: Society of Economic Paleontologists and Mineralogists, Short Course Notes, No. 9, variously paginated.

Harper, C.W., Jr., 1984, Improved methods of facies sequence analysis: *In* Facies Models, R.G. Walker, *ed.*, Geoscience Canada, Reprint Series I, second edition, p. 11-13.

Harper, C.W., Jr., 1985, Facies models revisited: an examination of quantitative methods: Geoscience Canada, v. 11, p. 203-206.

Hayes, M.O., 1967, Hurricanes as geological agents: case studies of hurricane Carla, 1961, and Cindy, 1963: Report of Investigations No. 61, 54 p. The University of Texas at Austin, Bureau of Economic Geology.

Heezen, B.C., and Ewing, M., 1952, Turbidity current and submarine slumps and the 1929 Grand Banks earthquake: American Joural of Science v. 250, p. 849-873.

Hein, F.J., 1982, Slope-to-shelf transition: Precambrian Miette Group to Lower Cambrian Gog Group, Kicking Horse Pass/ Spiral Tunnels, B.C. and Alberta: *In* Walker, R.G., and Rahmani, R.A.,*eds.*, Clastic units of the Front Ranges, Foothills and Plains in the area between Field, B.C. and Drumheller, Alberta: International Association of Sedimentologists Field Trip Guide 21A, p. 117-136.

Hein, F.J., and Arnott, R.W., 1983, Precambrian Miette conglomerates, Lower Cambrian Gog quartzites and modern braided outwash deposits, Kicking Horse Pass area: Canadian Society of Petroleum Geologists Field Guidebook, 46 p.

Hein, F.J., 1986, Tidal/littoral offshore shelf deposits: Lower Cambrian Gog Group, southern Canadian Rocky Mountains: Sedimentary Geology [Submitted]

Henkel, D.J., 1970, The role of waves in causing submarine landslides: Geotechnique, v. 20, p. 75-80.

High, L.R., Jr., and Picard, M.D., 1974, Reliability of cross-stratification types as paleocurrent indicators in fluvial rocks: Journal of Sedimentary Petrology, v. 44, p. 158-168.

Houbolt, J.J.H.C., 1968, Recent sediments in the Southern Bight of the North Sea: Geologie en Mijnbouw, v. 47, p. 245-273.

Howard, J.D., 1978, Sedimentology and trace fossils: *In* Basan, P.B., *ed.*, Trace Fossil Concepts: Society of Economic Paleontologists and Mineralogists., Short Course Notes 5, p. 13-47.

Hughes, R.D., 1955, Geology of portions of Sunwapta and Southesk Map-areas, Jasper National Park, Alberta, Canada: Alberta Society of Petroleum Geologists, Guide Book, Fifth Annual, Field Conference p. 69-116.

Johnson, H.D., 1977, Shallow marine sand bar sequences: an example from the late Precambrian of North Norway: Sedimentology, v. 24, p. 245-270.

Johnson, H.D., 1978, Shallow Siliciclastic Seas: *In* Reading, H.G., *ed.*, Sedimentary Environments and Facies, Elsevier, New York, p. 207-259

Johnson, S.Y., 1984, Cyclic fluvial sedimentation in a rapidly subsiding basin, northwest Washington: Sedimentary Geology, v. 38, p. 361-391.

Jopling, A.V., 1965, Hydraulic factors controlling the slope of laminae in laboratory deltas: Journal of Sedimentary Petrology, v. 35, No. 4, p. 777-791.

Karl, H.A., Carlson, P.R., and Cacchione, D.A., 1983, Factors that influence sediment transport at the shelfbreak: *In* Stanley, D.J., and Moore G.T., *eds.*, The Shelfbreak: Critical Interface on Continental Margins: Society of Economic Paleontologists and Mineralogists Special Publication No. 33, p. 219-231.

Karlsrud, K., and Edgers, L., 1982, Some aspects of submarine slope stability: *In* Saxov, S., and Nieuwenhuis, J.K., *eds.*, Marine Slides and Other Mass Movement, NATO conference series, Series IV, marine sciences, Plenum Press, New York, p. 21-49.

Kenyon, N.H., 1970, Sand ribbons of European tidal seas: Marine Geology, v. 9, p. 25-39.

Kenyon, N.H., Belderson, R.H., Stride, A.H., and Johnson M.A., 1981, Offshore tidal sand-banks as indicators of net sand transport and as potential deposits: *In* Holocene Marine Sedimentation in the North Sea Basin. Special Publication International Association of Sedimentologists, v. 5, p. 257-268, Blackwell Scientific Publications, Oxford, 524 p.

Klein, G. De V., 1970, Depositional and dispersal dynamics of intertidal sand bars: Journal of Sedimentary Petrology, v. 40 p. 1095-1127.

Kumar, N., and Sanders, J.E., 1976, Characteristics of shoreface storm deposits: modern and ancient examples: Journal of Sedimentary Petrology, v. 46, p. 145-162.

Levell, B.K., 1980a, A late Precambrian tidal shelf deposit, the Lower Sandfjord Formation, Finnmark, North Norway: Sedimentology, v. 27, p. 539-557.

Levell, B.K., 1980b, Evidence for currents associated with waves in Late Precambrian shelf deposits from Finnmark, North Norway: Sedimentology, v. 27, p. 153-166.

Marsaglia, K.M., and Klein, G. De V., 1983, The paleogeography of Paleozoic and Mesozoic storm depositional systems: The Journal of Geology, v. 91, p. 117-142.

Marsaglia, K.M., and Klein, G. De V., 1985, The paleogeography of Paleozoic and Mesozoic storm depositional systems: The Journal of Geology, v. 93, p. 91-94.

McCave, I.N., 1971, Sand waves in the North Sea off the coast of Holland: Marine Geology, v. 10, p. 199-225.

McCave, I.N., and Langhorne, D.N., 1982, Sand waves and sediment transport around the end of a tidal sand bank: Sedimentology, v. 29, p. 95-110.

McConnell, R.G., 1887, On the geological structure of a portion of the Rocky Mountains: Geological Survey of Canada Annual Report. 1886, v. 2, pt. D. 41 p.

McConnell, R.G., 1889, Note on the geology of Mt. Stephen, British Columbia: American Geology, v. 3, p. 22-25.

McCormick, J.M., and Thiruvathukal, J.V., 1976, Elements of Oceanography: Sanders, W.B., Philadelphia, 346 p.

Miall, A.D., 1973, Markov chain analysis applied to an ancient alluvial plain succession: Sedimentology, v. 20, p. 347-364.

Michelson, P.C., and Dott, R.H., Jr., 1973, Orientation analysis of trough cross stratification in Upper Cambrian sandstones of western Wisconsin: Journal of Sedimentary Petrology, v. 43, p. 784-794.

Middleton, G.V., and Hampton, M.A., 1976, Subaqueous sediment transport and deposition by sediment gravity flows: *In* Stanley, D.J., and Swift, D.J.P., *eds.*, Marine Sediment Transport and Environmental Management: Wiley Interscience, New York, p. 197-218.

Monger, J.W.H., Souther, J.G., and Gabrielse, H., 1972, Evolution of the Canadian Cordillera: A plate tectonic model: American Journal of Science, v. 272, p. 577-602.

Morton, R.A., 1981, Formation of storm deposits by wind-forced currents in the Gulf of Mexico and the North Sea: *In* Nio, S.D. *et al., eds.*, Holocene Marine Sedimentation in the North Sea Basin. Special Publication International Association of Sedimentologists, v. 5, p. 385-396. Blackwell Scientific Publications, Oxford, 524 p.

Mountjoy, E.W., 1962, Mount Robson (southeast) Map-area, Rocky Mountains of Alberta and British Columbia 83 E/SE: Geological Survey of Canada Paper 61-31, 114 p.

Mountjoy, E.W., and Aitken, J.D., 1963, Early Cambrian and Late Precambrian paleocurrents, Banff and Jasper National Parks: Bulletin of Canadian Petroleum Geology, v. 11, p. 161-168.

Narayan, J., 1971, Sedimentary structures in the Lower Greensand of the Weald England and the Bas-Boullonais France: Sedimentary Geology, v. 6, p. 73-109.

Nelson, C.H., 1982, Modern shallow water graded sand layers from storm surges, Bering Shelf: a mimic of Bouma sequences and turbidite systems: Journal of Sedimentary Petrology, v. 52, p. 537-545.

Nio, S.-D., 1976, Marine transgressions as a factor in the formation of sandwave complexes: Geologie en Mijnbouw, v. 55, p. 18-40.

North, F.K., and Henderson, G.G.L., 1954, Summary of the geology of the southern Rocky Mountains of Canada: Alberta Society of Petroleum Geologists, 4 th Annual Field Conference Guildbook, p. 15-81.

Okulith, V.J., 1949, Geology of part of the Selkirk Mountains in the vicinity of the main line of the Canadian Pacific Railway, British Columbia: Geological Survey of Canada Bulletin, No. 14.

Okulitch, V.J., 1956, The Lower Cambrian of western Canada and Alaska: *In* El Sistema Cambrico, Paleogeografia y el Problema de su Base-Symposium Pt. 2, p. 701-734, XX Congreso Geologico International.

Off, T., 1963, Rhythmic linear sand bodies caused by tidal currents: Bulletin of American Association of Petroleum Geologists v. 47, p. 324-341.

Palonen, P., 1976, Sedimentology and stratigraghy of Gog Group sandstones in southern Canadian Rockies: University of Calgary, Ph.D. thesis, 201 p.

Pietrafesa, L.J., 1983, Shelfbreak circulation, fronts and physical oceanography: East and west coast perspectives: *In* Stanley, D.J., and Moore, G.T., *eds.*, The Shelfbreak: Critical Interface on Continental Margins: Society of Economic Paleontologists and Mineralogists Special Publication No. 33 p. 233-250.

Poulton, T.P., and Simony, P.S., 1980, Stratigraphy, sedimentology, and regional correlation of the Horsethief Creek Group (Hadrynian, Late Precambrian) in the northern Purcell and Selkirk Mountains, British Columbia: Canadian Journal of Earth Science, v. 17, p. 1708-1724.

Powers, D.W., and Easterling, R.G., 1982, Improved methodology for using embedded Markov chains to describe cyclical sediments: Journal of Sedimentary Petrology, v. 52, p. 913-923.

Powers, M.C., and Kinsman, B., 1953, Shell accumulations in underwater sediments and their relation to the thickness of the traction zone: Journal of Sedimentary Petrology, v. 23, p. 229-234.

Price, R.A., Balkwill, H.R., Charlesworth, H.A.K., Cook, D.G., and Simony, P.S., 1972, The Canadian Rockies and tectonic evolution of the southeastern Canadian Cordillera: International Geological Congress no. 24, Montreal, Field Excursion A15-C15 128 p.

Price, R.A., and Mountjoy E.W., 1970, Geologic structure of the Canadian Rocky Mountains between Bow and Athabasca rivers- a progress report: *In* Wheeler, J.O., *ed.*, Structure of the southern Canadian Cordillera: Geological Association of Canada Special Paper no. 6, p. 7-25.

Price, R.A., Cook, D.G., Aitken, J.D., and Mountjoy, E.W., 1980a, Lake Louise (East Half), 1:50,000 Geological Map: Geological Survey of Canada, Map 1482A.

Price, R.A., Cook, D.G., Aitken, J.D., and Mountjoy, E.W., 1980b, Lake Louise (West Half), 1:50,000 Geological Map: Geological Survey of Canada, Map 1483A.

Prior, D.B. and Coleman, J.M., 1982, Active slides and flows in underconsolidated marine sediments on the slopes of the Mississippi delta: *In* Saxov, S., and Nieuwenhuis, J.K., *eds.*, Marine Slides and Other Mass Movements, NATO conference series, Series IV, marine science., Plenum Press, New York, p. 21-49.

Pugh, D.C., 1971, Subsurface Cambrian stratigraphy in southern and central Alberta: Geological Survey of Canada Paper 70-10, 33 p.

Pugh, D.C., 1973, Subsurface lower Paleozoic stratigraphy in northern and central Alberta: Geological Survey of Canada Paper 72-12, 54 p.

Pugh, D.C., 1975, Cambrian stratigraphy from western Alberta to northeastern British Columbia: Geological Survey of Canada Paper 74-37, 31 p.

Rasetti, F., 1951, Middle Cambrian stratigraphy and Faunas of the Canadian Rocky Mountains: Smithsonian Miscellaneous Collections, v. 116, no. 5, 277 p.

Read, W.A., 1969, Analysis and simulation of Namurian sediments in central Scotland using a Markov-process model: Mathematical Geology, v. 1, p. 199-219.

Reineck, H.E., 1963, Sedimentgefuge in Bereich der sudlichen Nordsee: Adhandlungen der Senckenbergischen Naturforschen den Gesellschaft, No 505.

Reineck, H.G., and Singh, I.B., 1972, Genesis of laminated sand and graded rhythmites in storm-sand layers of shelf muds: Sedimentology, v. 18, p. 123-128.

Reineck, H.G., and Singh, I.B., 1980, Depositional Sedimentary Environments: Berlin, Springer-Verlag, 549 p.

Ross, D.A., 1982, Introduction to Oceanography: Prentice-Hall Inc., New Jersey, third edition, 544 p.

Seilacher, A., 1967, Bathymetry of trace fossils: Marine Geology, v. 5, p. 413-428.

Selley, R.C., 1970, Studies of sequence in sediments using a simple mathematical devise: Quarterly Journal Geological Society of London, v. 125, p. 557-581.

Scotese, C.R., Bamback, R.K., Barton, C., Van Der Voo, R., and Ziegler, A.M., 1979, Paleozoic base maps: Journal of Geology, v. 87, p. 217-277.

Slind, O.L., and Perkins, G.D., 1966, Lower Paleozoic and Proterozoic sediments of the Rocky Mountains between Jasper, Alberta and Pine River, British Columbia: Bulletin of Canadian Petroleum Geology, v. 14, p. 442-468.

Smith, J.D., and Hopkins, T.S., 1972, Sediment transport on the continental shelf off of Washington and Oregon in light of recent current measurement: *In* Swift, D.J.P., Duane, D.B., and Pilkey, O.H., *eds.*, Shelf Sediment Transport: Process and Pattern, Dowden, Hutchinson and Ross Inc., Pennsylvania p. 143-181.

Soegaard, K., and Eriksson, K.A., 1985, Evidence of tide, storm, and wave interaction on a Precambrian siliciclastic shelf: The 1,700 m.y. Ortega Group, New Mexico: Journal of Sedimentary Petrology, v. 55, p. 672-684.

Stelck, C.R., and Hedinger, A.S., 1975, Archaeocyathids and the Lower Cambrian continental shelf of the Canadian Cordillera: Canadian Journal of Earth Science, v. 12, p. 2014-2020.

Stewart, J.H., 1972, Initial deposits in the Cordilleran geosyncline: Evidence of a Late Precambrian (< 850 m.y.) continental separation: Geological Society of America Bulletin, v. 83, p. 1345-1360.

Stride, A.H., 1963, Current swept floors near the southern half of Great Britain: Quarterly Journal Geological Society of London, v. 119, p. 175-199.

Stride, A.H., 1982, Offshore Tidal Sands: Processes and Deposits. Chapman and Hall Ltd., New York., 222 p.

Swift, D.J.P., 1975, Tidal sand ridges and shoal retreat massifs: Marine Geology, v. 18, p. 105-134.

Taylor, R.S., Mathews, W.H., and Kupsch, W.O., 1964, Tertiary; Chapter 13, *In* Geological history of Western Canada: Alberta Society of Petroleum Geology, p. 190-194.

Teitz, M., and Mountjoy, E.W., 1985, The Yellowhead and Astoria carbonate platforms in the Late Proterozoic Upper Miette Group, Jasper, Alberta: *In* Current Research, Part A, Geological Survey of Canada Paper 85-1A, p. 341-348.

Terwindt, J.H.J., 1971, Litho-facies of inshore estuarine and tidal-inlet deposits: Geologie en Mijnbouw, v. 50, p. 515-526.

Thompson, W.O., 1937, Original structures of beaches, bars, and dunes: Bulletin of the Geological Society of America, v. 48, p. 723-752.

Thurman, H.V., 1981, Introductory Oceanography: Charles E. Merrill Publishing Company, Columbus, Ohio, third edition, 464 p.

Twichwell, D.C., 1983, Bedforms distributions and inferred sand transport on Georges Bank, United States Atlantic Continental Shelf: Sedimentology, v. 30 p. 695-710.

Vail, P.R., Mitchum, R.M. Jr., and Thompson, S., III, 1977, Seismic stratigraphy and global changes of sea level, Part 4: Global cycles of relative changes of sea level: *In*, Payton, C.E., *ed.*, Seismic Stratigraphy -- Applications to Hydrocarbon Exploration: Tulsa, American Association of Petroleum Geologists, Memoir 26, p. 83-97.

Walcott, C.D., 1908a, Cambrian sections of the Cordilleran area: Smithsonian Miscellaneous Collections, v. 53, p. 167-230.

Walcott, C.D., 1908b, Nomenclature of some Canadian Cordilleran formations: Smithsonian Miscellaneous Collections, v. 53 p. 1-12.

Walcott, C.D., 1910, Pre-Cambrian rocks of the Bow River Valley, Alberta, Canada: Smithsonian Miscellaneous Collections, v. 53, p. 423-431.

Walcott, C.D., 1912, Cambrian Brachipoda: U.S. Geological Survey Monographs 51, 872 p.

Walcott, C.D., 1913, Cambrian formations of the Robson Peak District, British Columbia and

Alberta, Canada: Smithsonian Miscellaneous Collections, v. 57, p. 327-343.

Walcott, C.D., 1927, Pre-Devonian sedimentation in southern Canadian Rocky Mountains: Smithsonian Miscellaneous Collections, v. 75, p. 147-173.

Walcott, C.D., 1928, Pre-Devonian Paleozoic formations of the Cordilleran provinces of Canada: Smithsonian Miscellaneous Collections, v. 75, p. 185-367.

Walker, R.G., 1975, Generalized facies models for resedimented conglomerates of turbidite association: Bulletin of the Geological Society of America, v. 86, p. 737-748.

Walker, R.G., 1979, Facies Models 7: Shallow Marine Sands: *In* Walker, R.G., *ed.*, Facies Models: Geoscience Canada, Reprint series I, p. 75-89.

Walker, R.G., 1984, Shelf and shallow marine sands: *In* Walker, R.G., *ed.*, Facies Models: Geoscience Canada, Reprint series I, second edition, p. 141-169.

Wolberg, A.C., and Hein, F.J., 1986, Sedimentology of the Lower Cambrian Gog Group, Yoho Park, B.C.,: *In* National Parks, Natural Sciences Research Digest (Accepted).

Young, F.G., 1979, The lowermost Paleozoic McNaughton Formation and equivalent Cariboo Group of eastern British Columbia: Piedmont and tidal complex: Geological Survey of Canada Bulletin 288, 60 p.

8. APPENDIX I

Appendix I contains columnar sections drawn from field notes. Figure 7.1 indicates the lithologic symbols and sedimentary structures used in the drafted sections. Paleocurrent directions for the individual cross-stratified beds are shown to the right of the columnar sections. North is orientated to the top of the page. The appropriate facies for each bed is also indicated to the right of the sections. The abbreviations for different grain sizes shown at the bottom of the sections are as follows:
c= shale or slaty shale
s=silty shale
vfs= very-fine sand
fs= fine sand
ms= medium sand
cs= coarse sand
vcs= very coarse sand

Lithologic Symbols and Sedimentary Structures

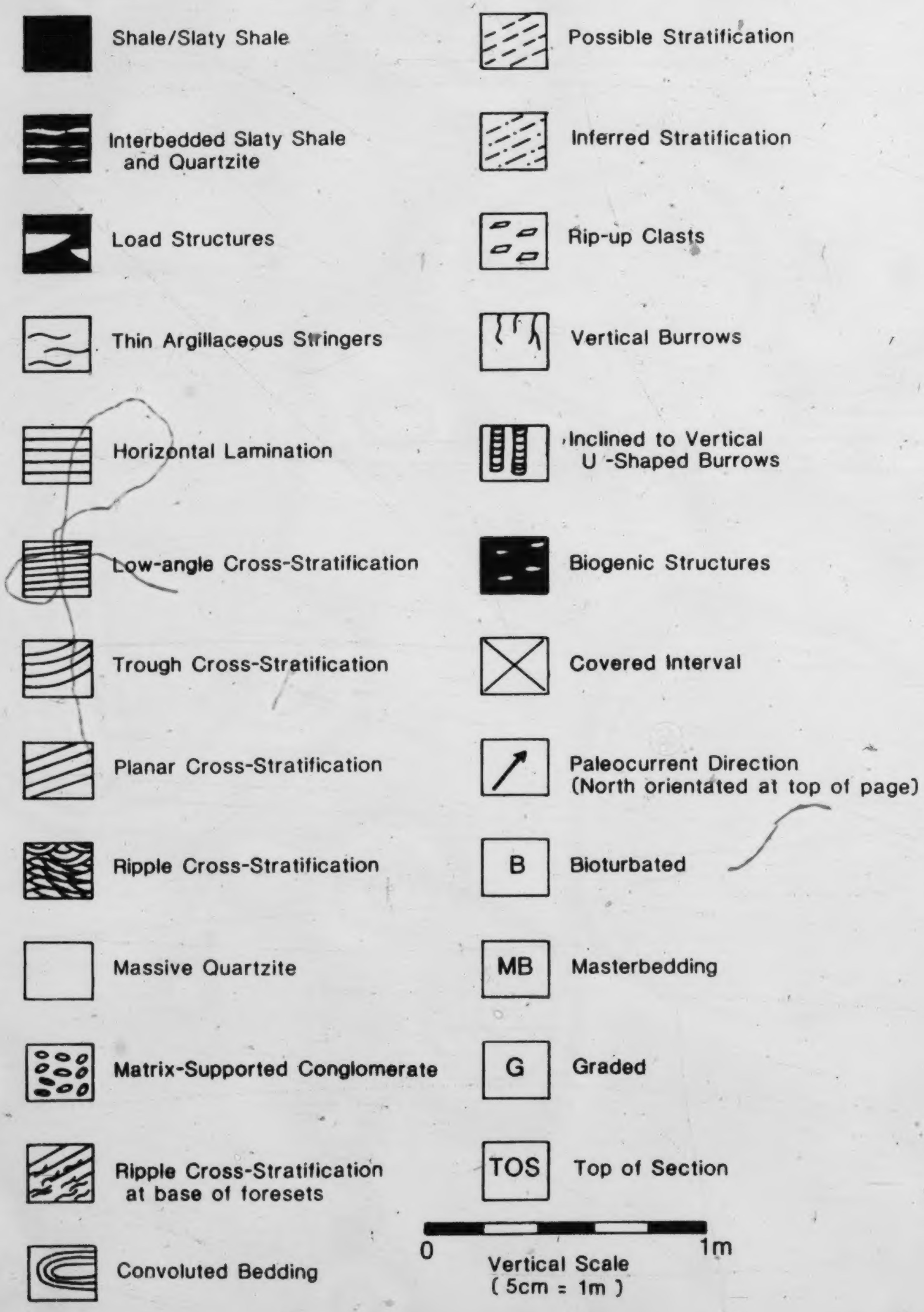
Shale/Slaty Shale
Interbedded Slaty Shale and Quartzite
Load Structures
Thin Argillaceous Stringers
Horizontal Lamination
Low-angle Cross-Stratification
Trough Cross-Stratification
Planar Cross-Stratification
Ripple Cross-Stratification
Massive Quartzite
Matrix-Supported Conglomerate
Ripple Cross-Stratification at base of foresets
Convoluted Bedding
Possible Stratification
Inferred Stratification
Rip-up Clasts
Vertical Burrows
Inclined to Vertical U -Shaped Burrows
Biogenic Structures
Covered Interval
Paleocurrent Direction (North orientated at top of page)
B
Bioturbated
MB
Masterbedding
G
Graded
TOS
Top of Section
0
1m
Vertical Scale (5cm = 1m)

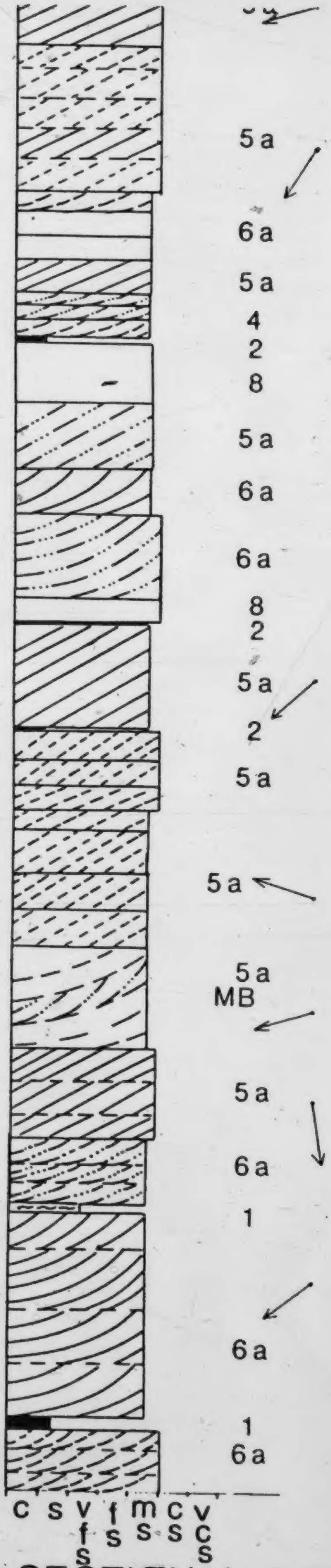
2
5a
6a
5a
4
2
8
5a
6a
6a
8
2
5a
2
5a
5a
5a
MB
5a
6a
1
6a
1
6a
c
s
vfs
fs
ms
cs
vcs

SECTION A-1

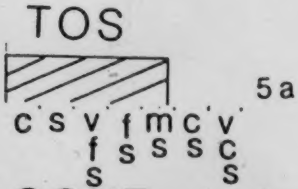
TOS
5a
c
s
vfs
fs
ms
cs
vcs

CONT. A-1

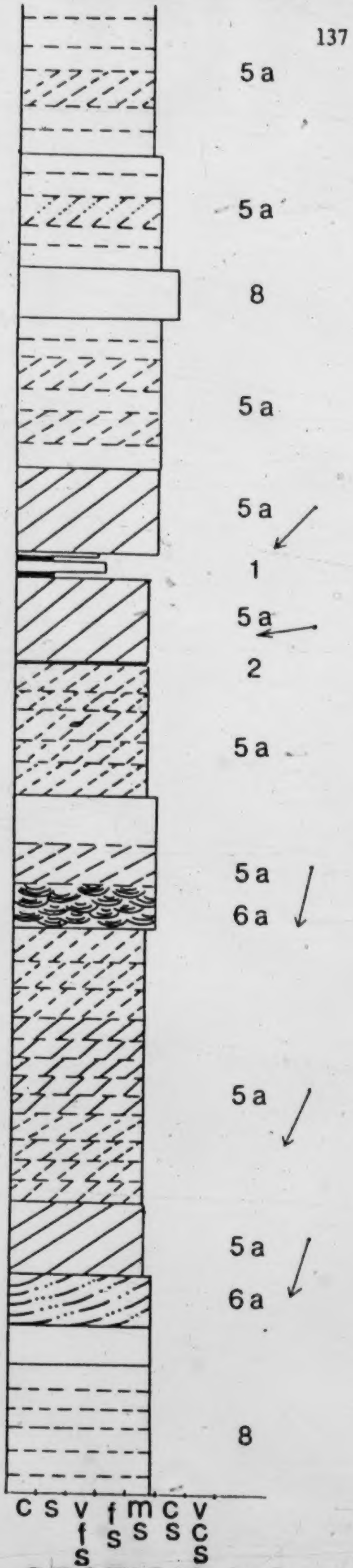
5a
5a
8
5a
5a
1
5a
2
5a
5a
6a
5a
5a
6a
8
c
s
vfs
fs
ms
cs
vcs

SECTION A-2

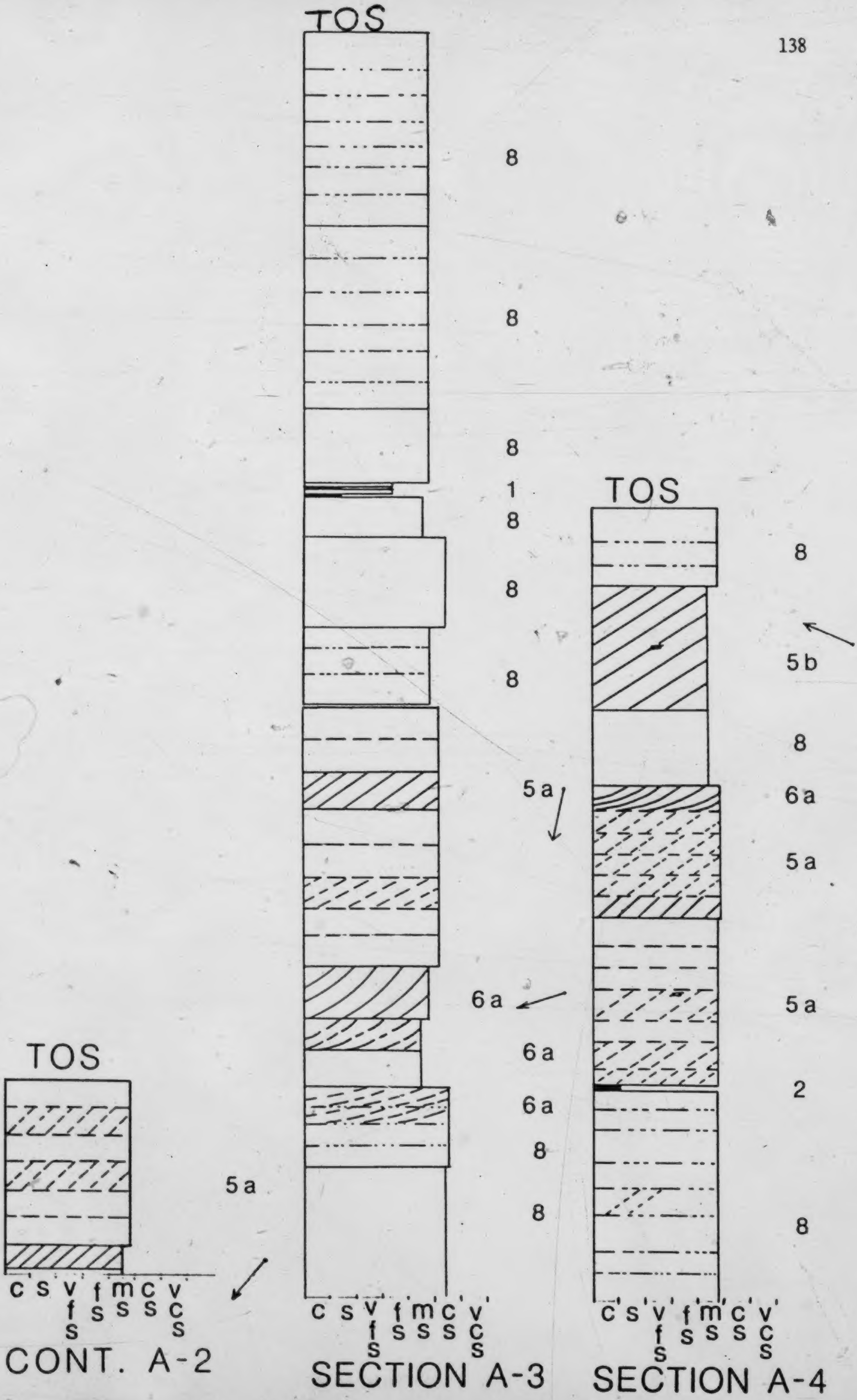
TOS
8
8
8
1
8
8
8
5a
6a
6a
6a
8
8
TOS
8
5b
8
6a
5a
5a
2
8
TOS
5a
c s vfs fs ms cs vcs
CONT. A-2
SECTION A-3
SECTION A-4

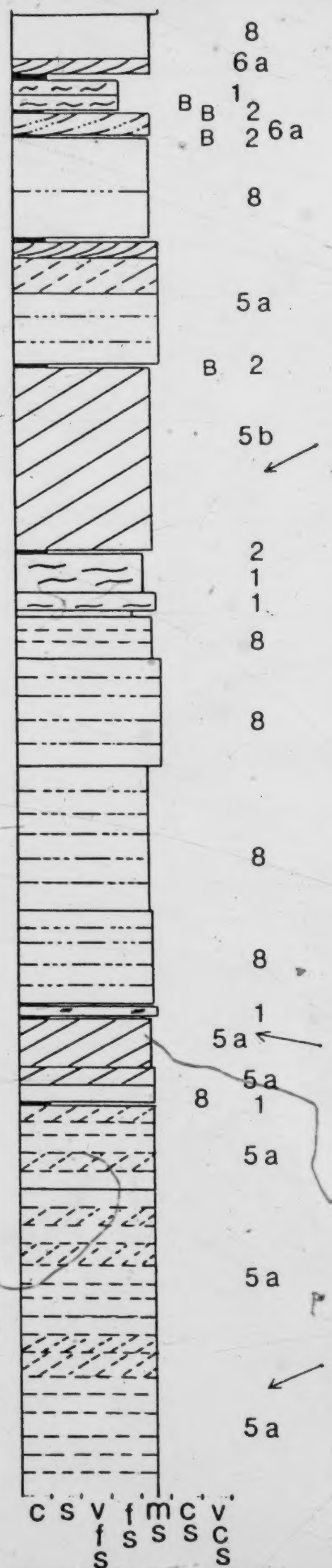
8
6a
1
B B 2
B 2 6a
8
5a
B 2
5b
2
1
1
8
8
8
8
1
5a
5a
8 1
5a
5a
5a
c s vfs fs ms cs vcs

SECTION A-5

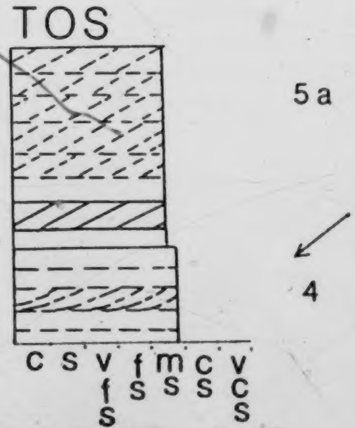
TOS
5a
4
c s vfs fs ms cs vcs

CONT. A-5

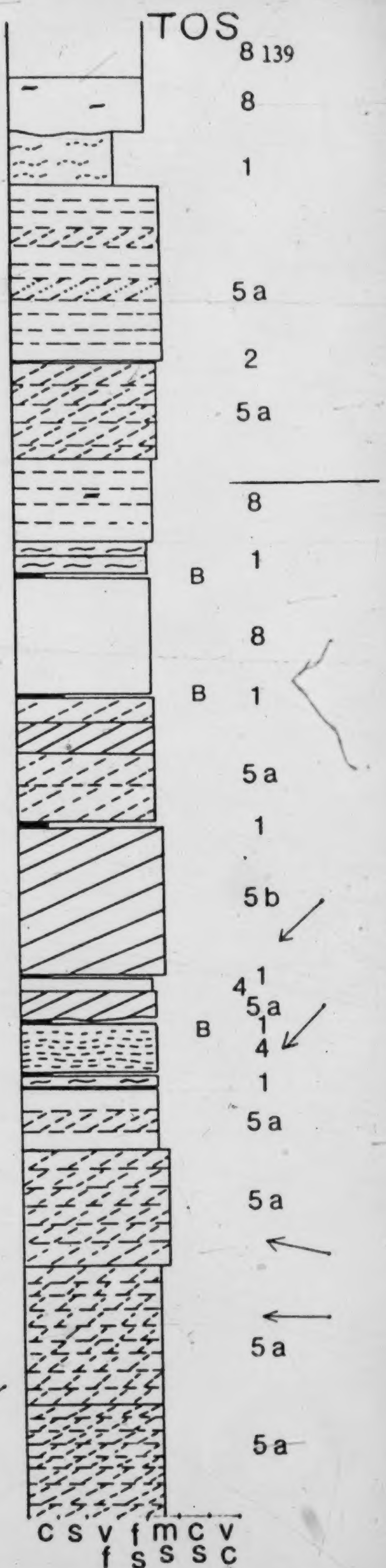
TOS
8
8
1
5a
2
5a
8
B 1
8
B 1
5a
1
5b
4 1
5a
B 1
4
1
5a
5a
5a
5a
c s vfs fs ms cs vcs

SECTION A-6

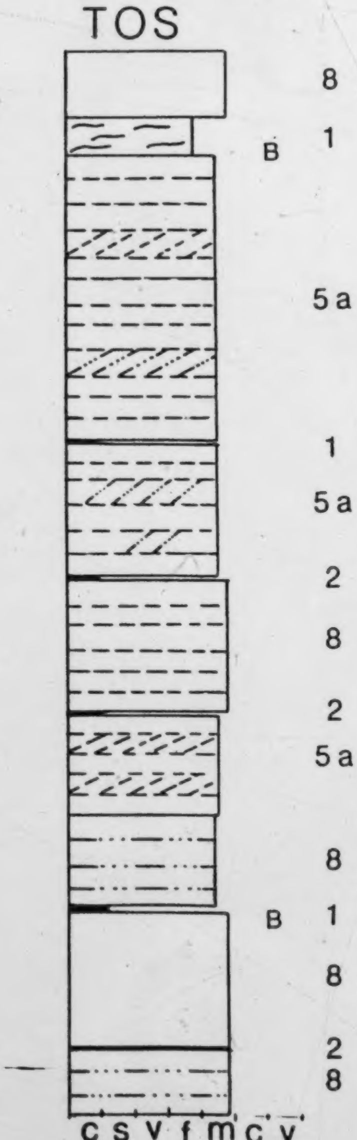
TOS
8
B 1
5 a
1
5 a
2
8
2
5 a
8
B 1
8
2
8
c s v f s
f s
m s
c s
v c s

SECTION A-7

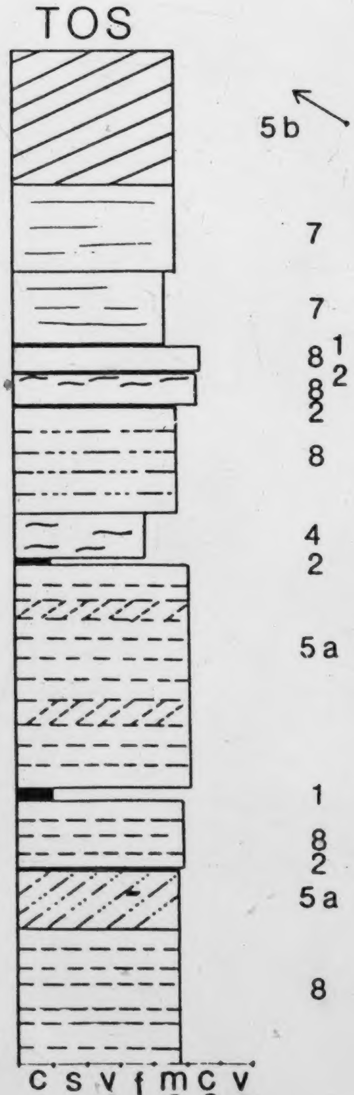
TOS
5 b
7
7
8 1
8 2
2
8
4
2
5 a
1
8
2
5 a
8
c s v f s
f s
m s
c s
v c s

SECTION A-8

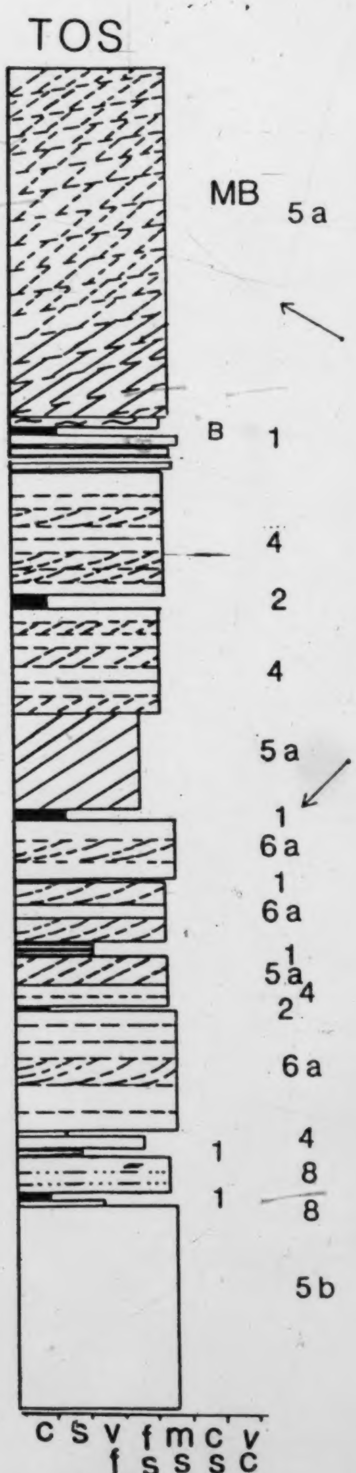
TOS
MB 5 a
B 1
4
2
4
5 a
1
6 a
1
6 a
1
5 a 4
2
6 a
1 4
8
1 8
5 b
c s v f s
f s
m s
c s
v c s

SECTION A-9

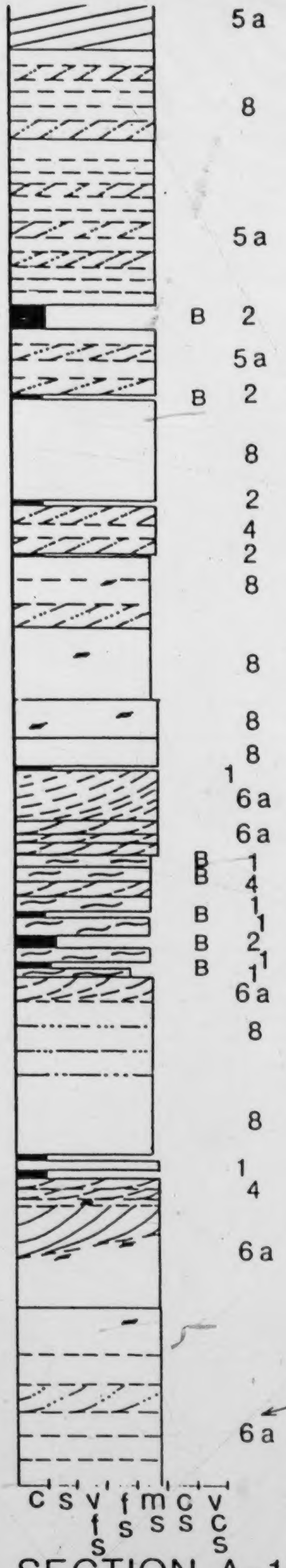
5a
8
5a
B 2
5a
B 2
8
2
4
2
8
8
8
8
1
6a
6a
B 1
B 4
B 1
1
B 2
1
B 1
6a
8
8
1
4
6a
6a
c s vfs fs ms cs vcs

SECTION A-10

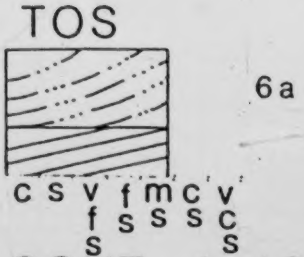
TOS
6a
c s vfs fs ms cs vcs

CONT. A-10

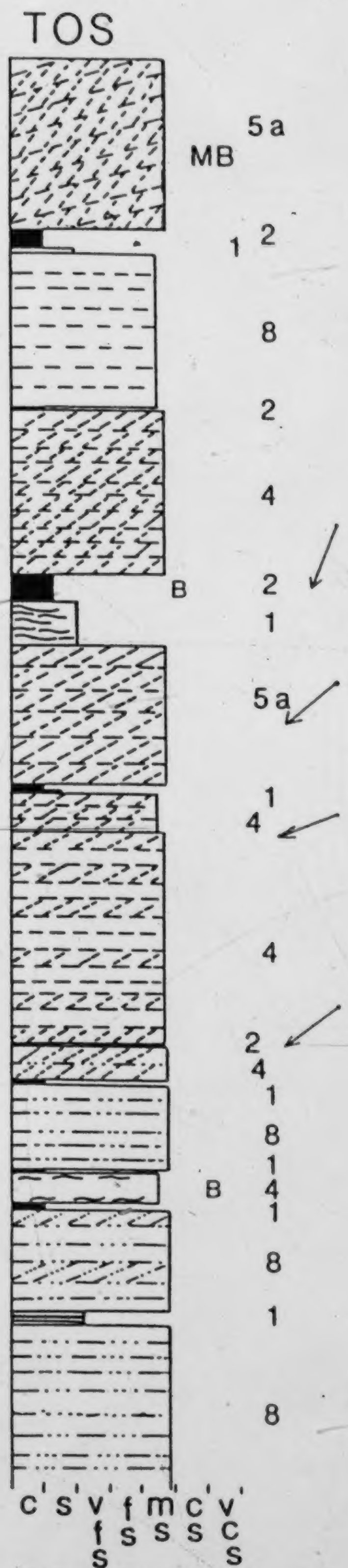
TOS
5a
MB
1 2
8
2
4
B 2
1
5a
1
4
4
2
4
1
8
1
B 4
1
8
1
8
c s vfs fs ms cs vcs

SECTION A-11

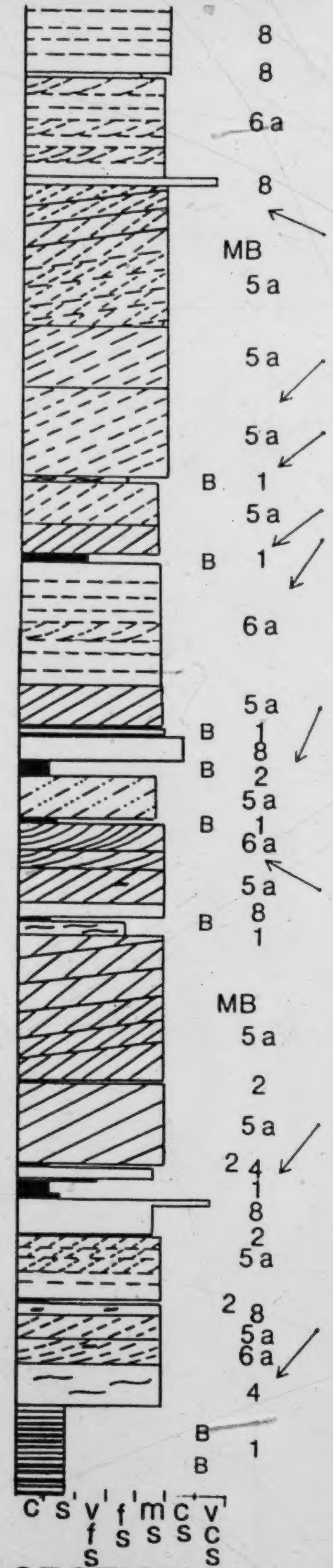
8
8
6a
8
MB
5a
5a
5a
B 1
5a
B 1
6a
5a
B 1
8
B 2
5a
B 1
6a
5a
8
B 1
MB
5a
2
5a
2 4
1
8
2
5a
2 8
5a
6a
4
B
1
B
c s vfs fs ms cs vcs

SECTION A-12

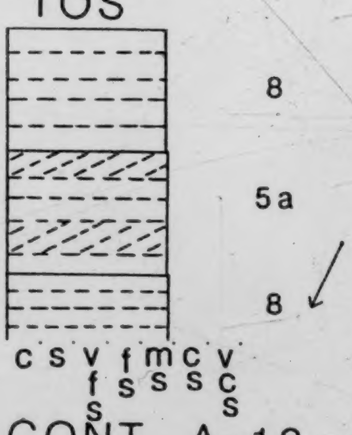
TOS
8
5a
8
c s vfs fs ms cs vcs

CONT. A-12

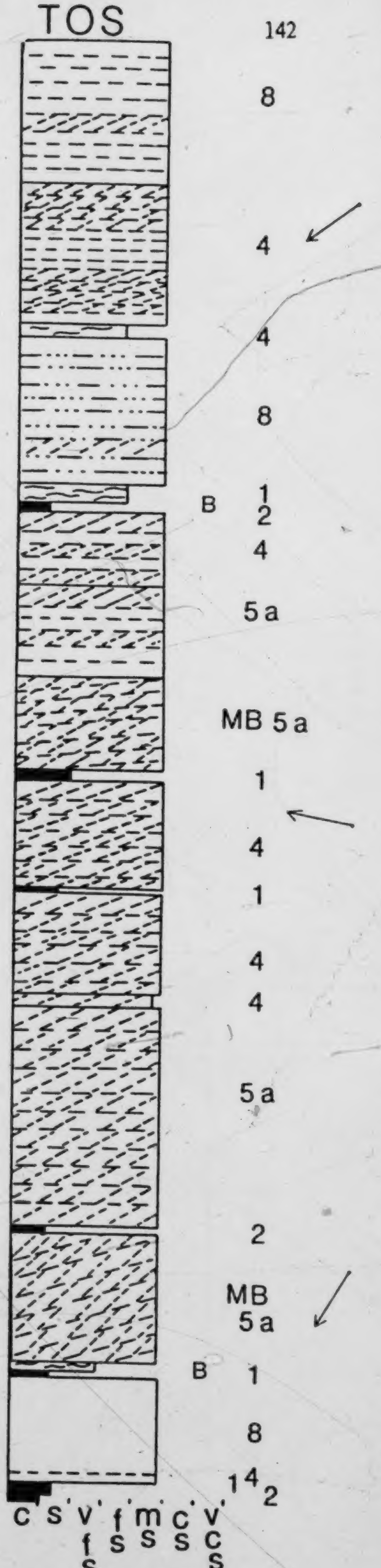
TOS
8
4
4
8
1
B 2
4
5a
MB 5a
1
4
1
4
4
5a
2
MB
5a
B 1
8
1 4 2
c s vfs fs ms cs vcs

SECTION A-13

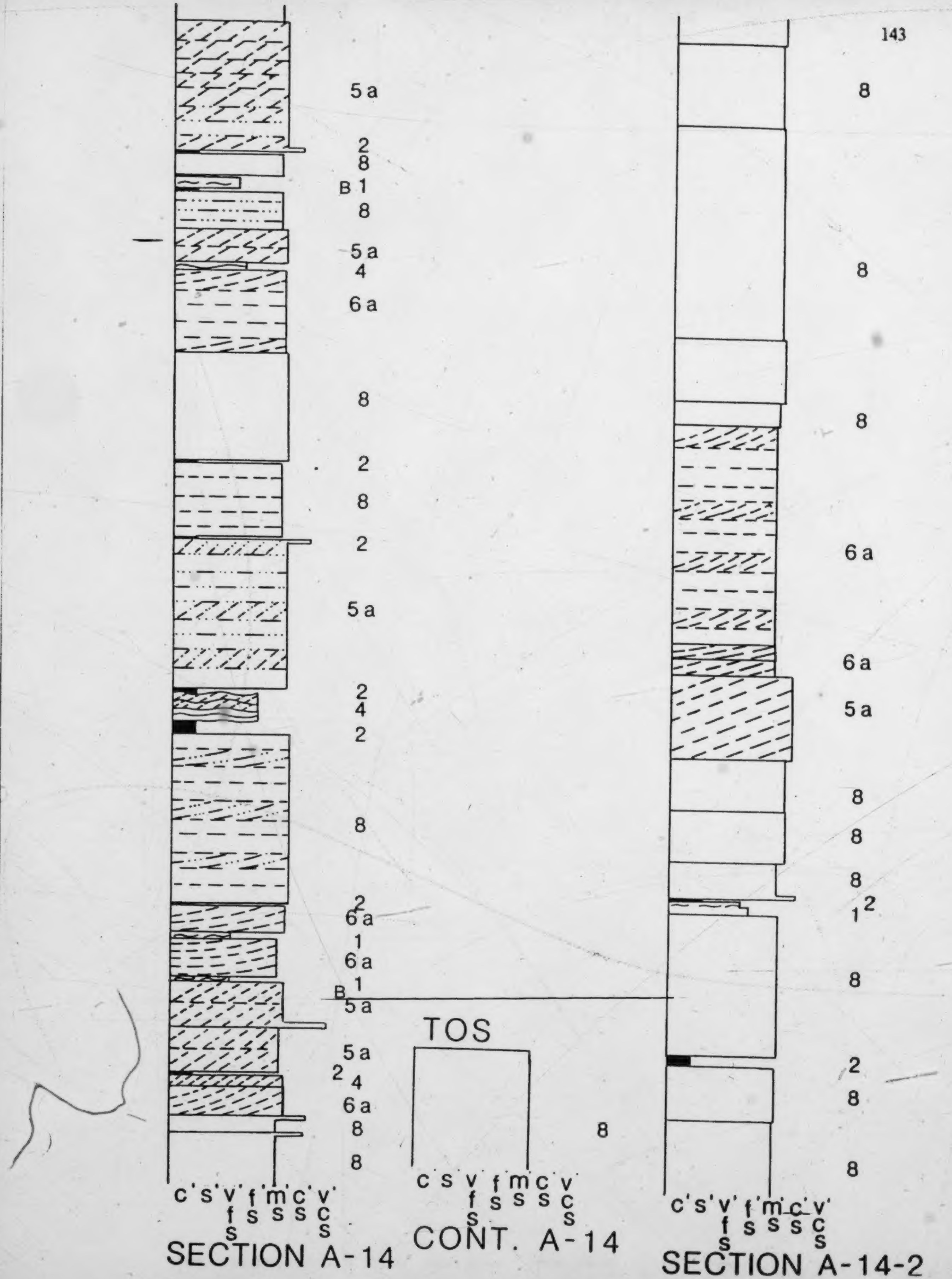
5a
2
8
B 1
8
5a
4
6a
8
2
8
2
5a
2
4
2
8
2
6a
1
6a
B 1
5a
5a
2
4
6a
8
8
c s vfs fs ms cs vcs
SECTION A-14
TOS
8
c s vfs fs ms cs vcs
CONT. A-14
8
8
8
6a
6a
5a
8
8
8
1 2
8
2
8
8
c s vfs fs ms cs vcs
SECTION A-14-2

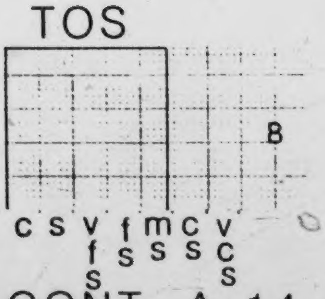
TOS
B
c s vfs fs ms cs vcs

CONT. A-14-2

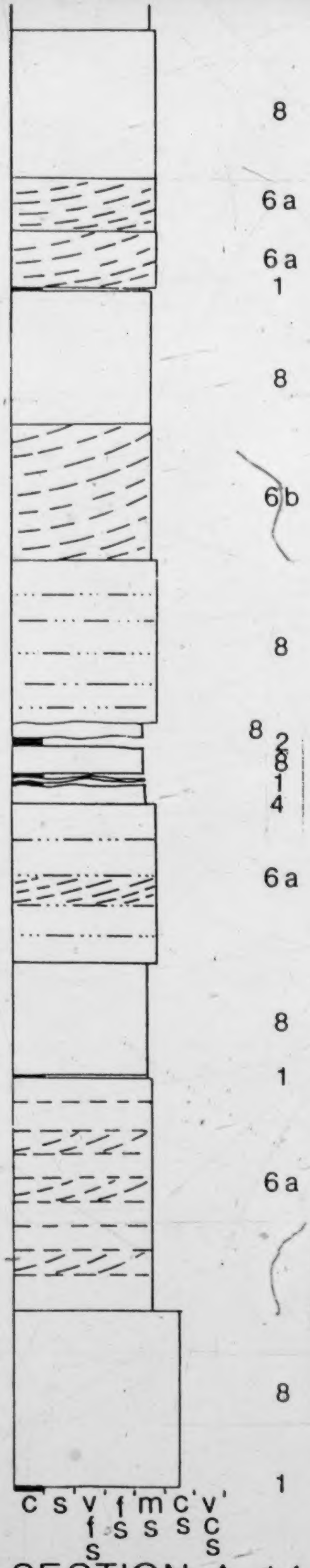
8
6a
6a
1
8
6b
8
8
2
8
1
4
6a
8
1
6a
8
1
c s vfs fs ms cs vcs

SECTION A-14-3

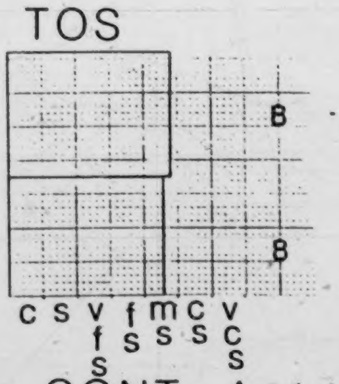
TOS
B
B
c s vfs fs ms cs vcs

CONT. A-14-3

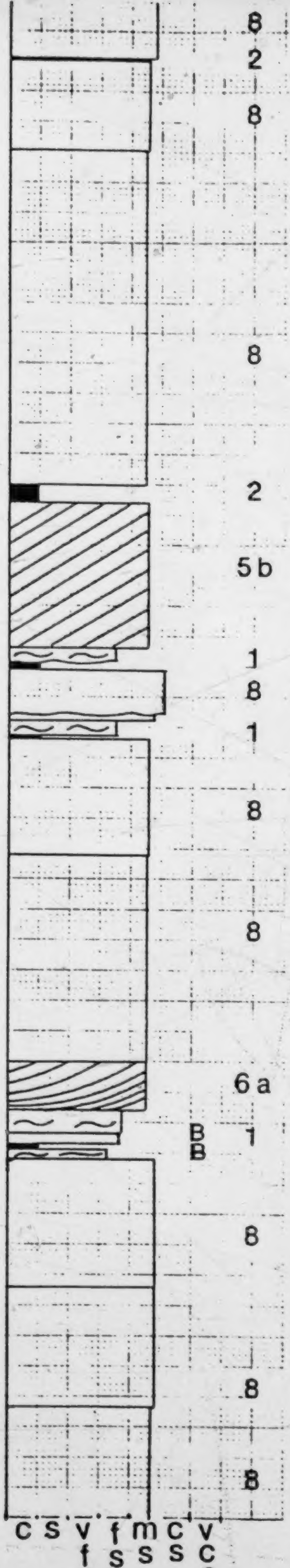
8
2
8
8
2
5 b
1
8
1
8
8
6 a
B
1
B
8
8
8
c s v f s f s m s c s v c s

SECTION A-14-4

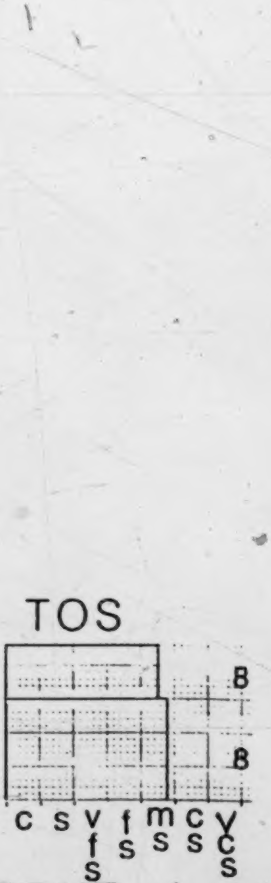
TOS
8
8
c s v f s f s m s c s v c s

CONT. A-14-4

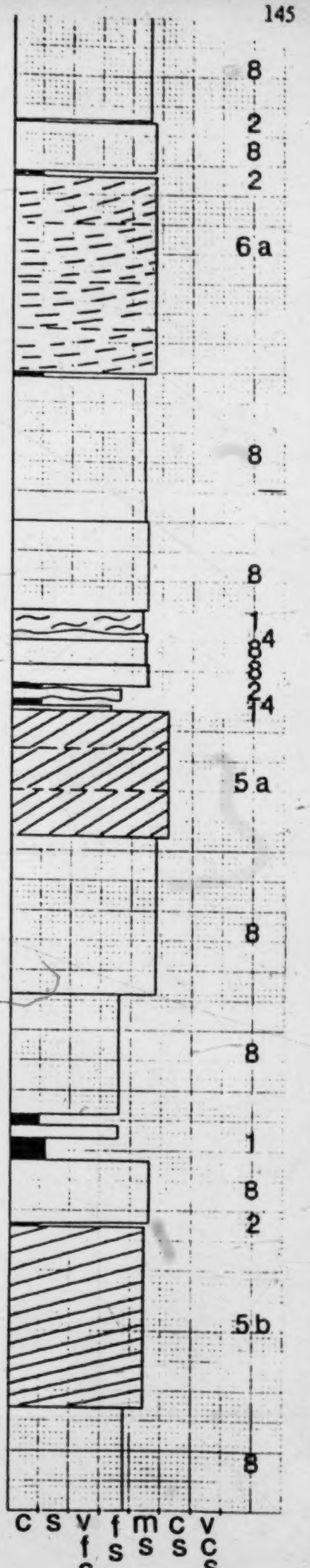
8
2
8
2
6 a
8
8
1
4
8
8
2
1
4
5 a
8
8
1
8
2
5 b
8
c s v f s f s m s c s v c s

SECTION A-14-5

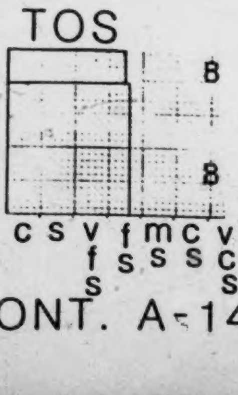
TOS
8
8
c s vfs fs ms cs vcs

CONT. A-14-5

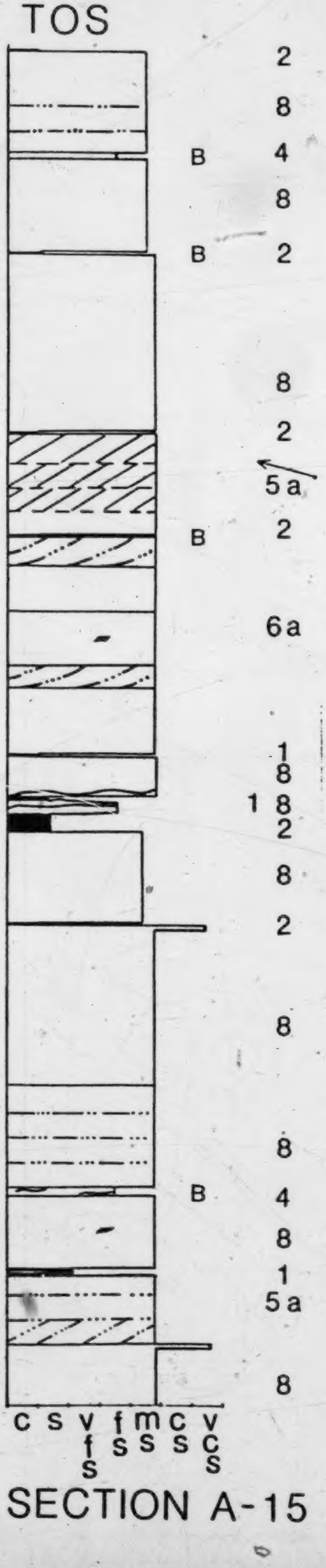
TOS
2
8
B 4
8
B 2
8
2
5a
B 2
6a
1
8
1 8
2
8
2
8
8
B 4
8
1
5a
8
c s vfs fs ms cs vcs

SECTION A-15

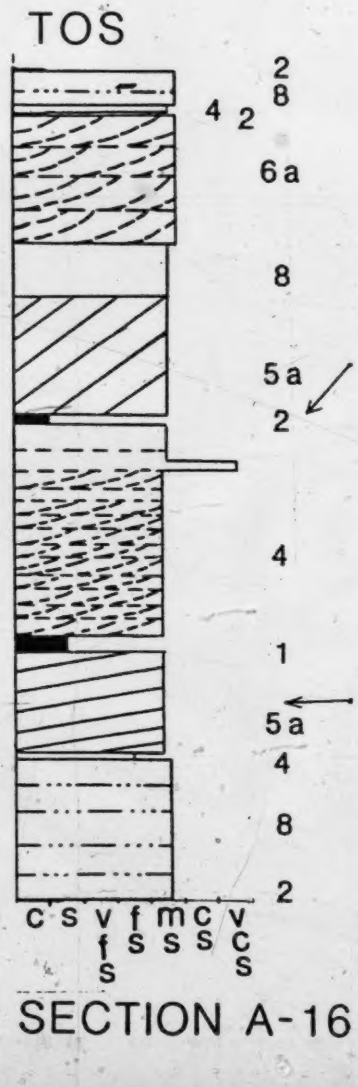
TOS
2
8
4 2
6a
8
5a
2
4
1
5a
4
8
2
c s vfs fs ms cs vcs

SECTION A-16

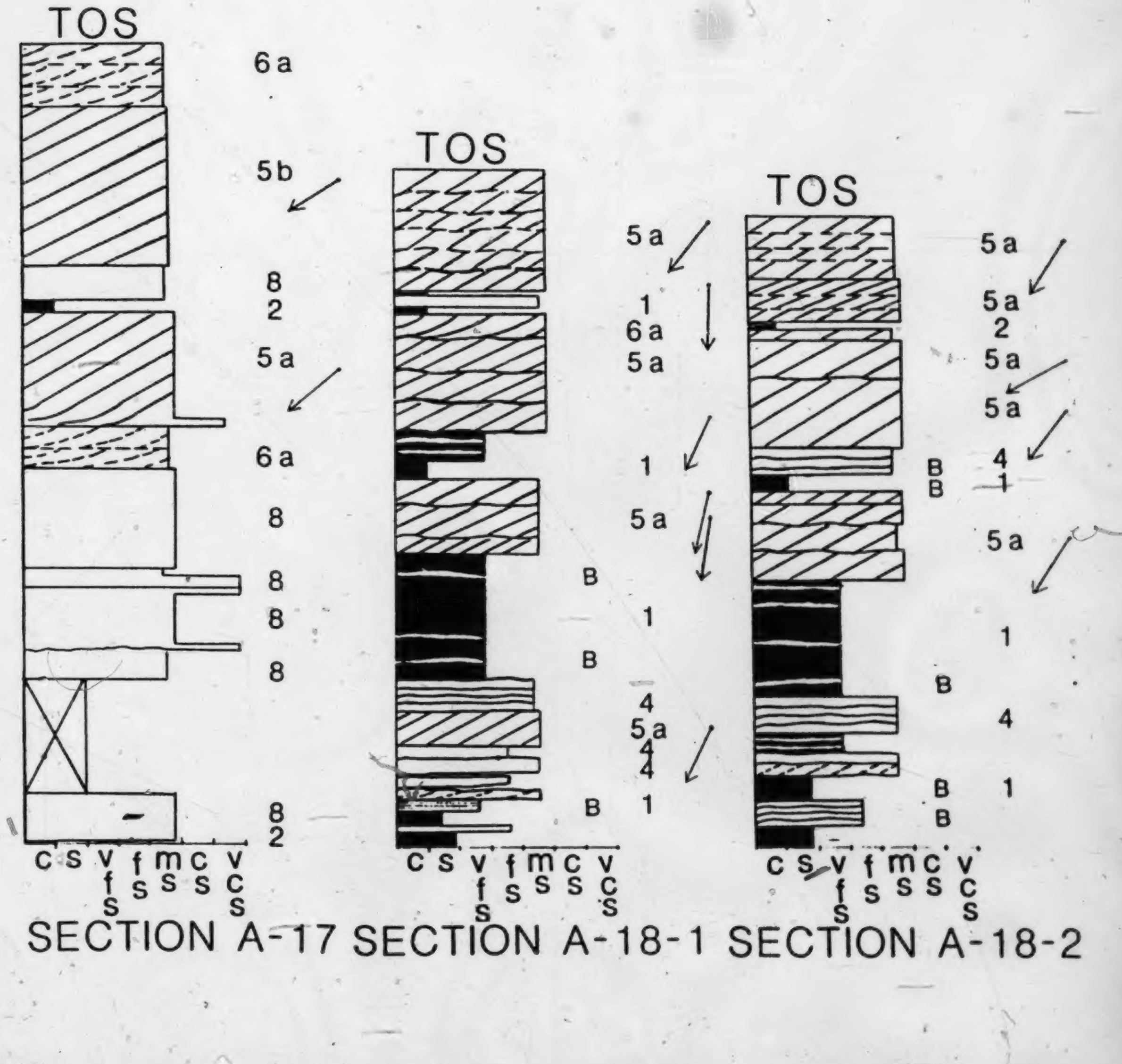
TOS
6a
5b
8
2
5a
6a
8
8
8
8
8
2
c s vfs fs ms cs vcs
TOS
5a
1
6a
5a
1
5a
B
1
B
4
5a
4
4
B 1
c s vfs fs ms cs vcs
TOS
5a
5a
2
5a
5a
B 4
B 1
5a
1
B
4
B 1
B
c s vfs fs ms cs vcs

SECTION A-17 SECTION A-18-1 SECTION A-18-2

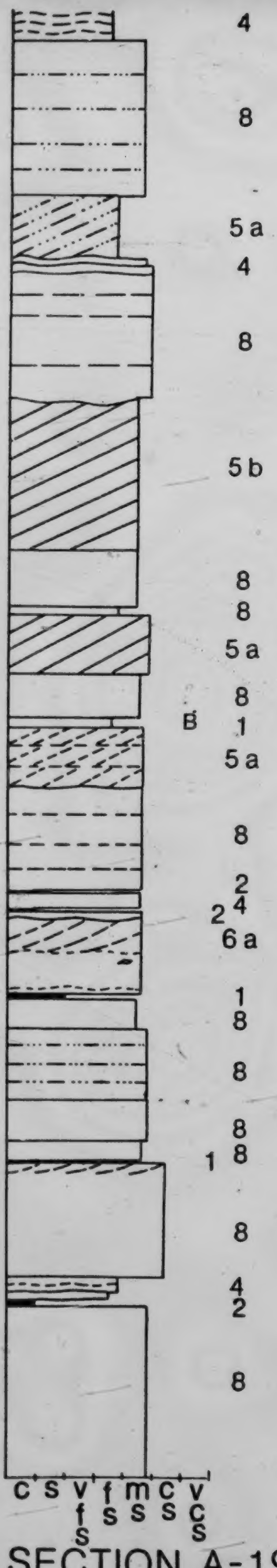
4
8
5 a
4
8
5 b
8
8
5 a
8
B 1
5 a
8
2
2 4
6 a
1
8
8
8
1 8
8
4
2
8
c s vfs fs ms cs vcs

SECTION A-19

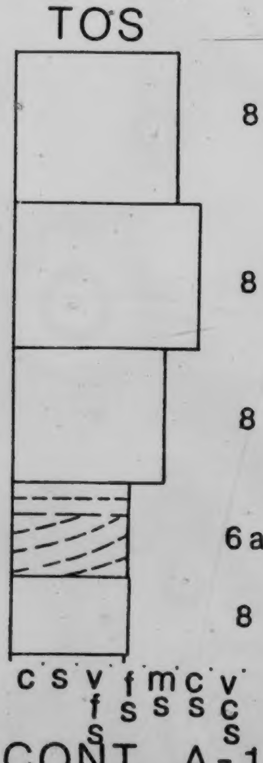
TOS
8
8
8
6 a
8
c s vfs fs ms cs vcs

CONT. A-19

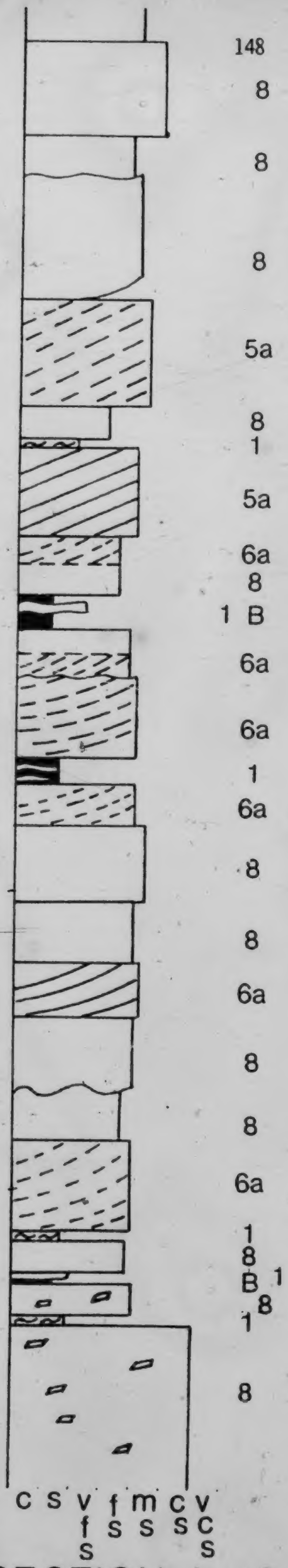
8
8
8
5a
8
1
5a
6a
8
1 B
6a
6a
1
6a
8
8
6a
8
8
6a
1
8
B 1
8
1
8
c s vfs fs ms cs vcs

SECTION A-19-2

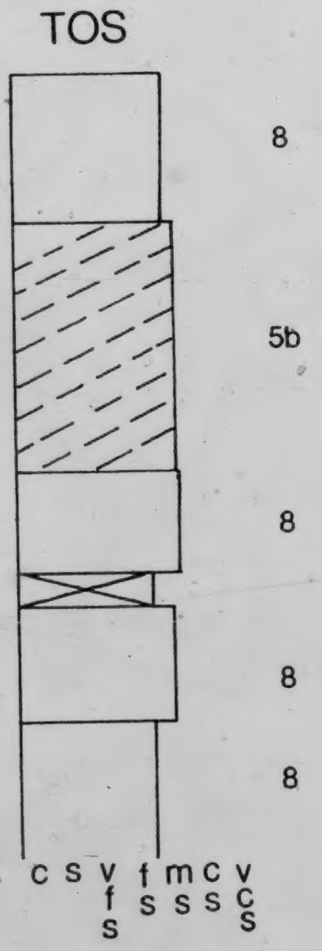
TOS
8
5b
8
8
8
c s v f m c v
f s s s c
s s

CONT. A-19-2

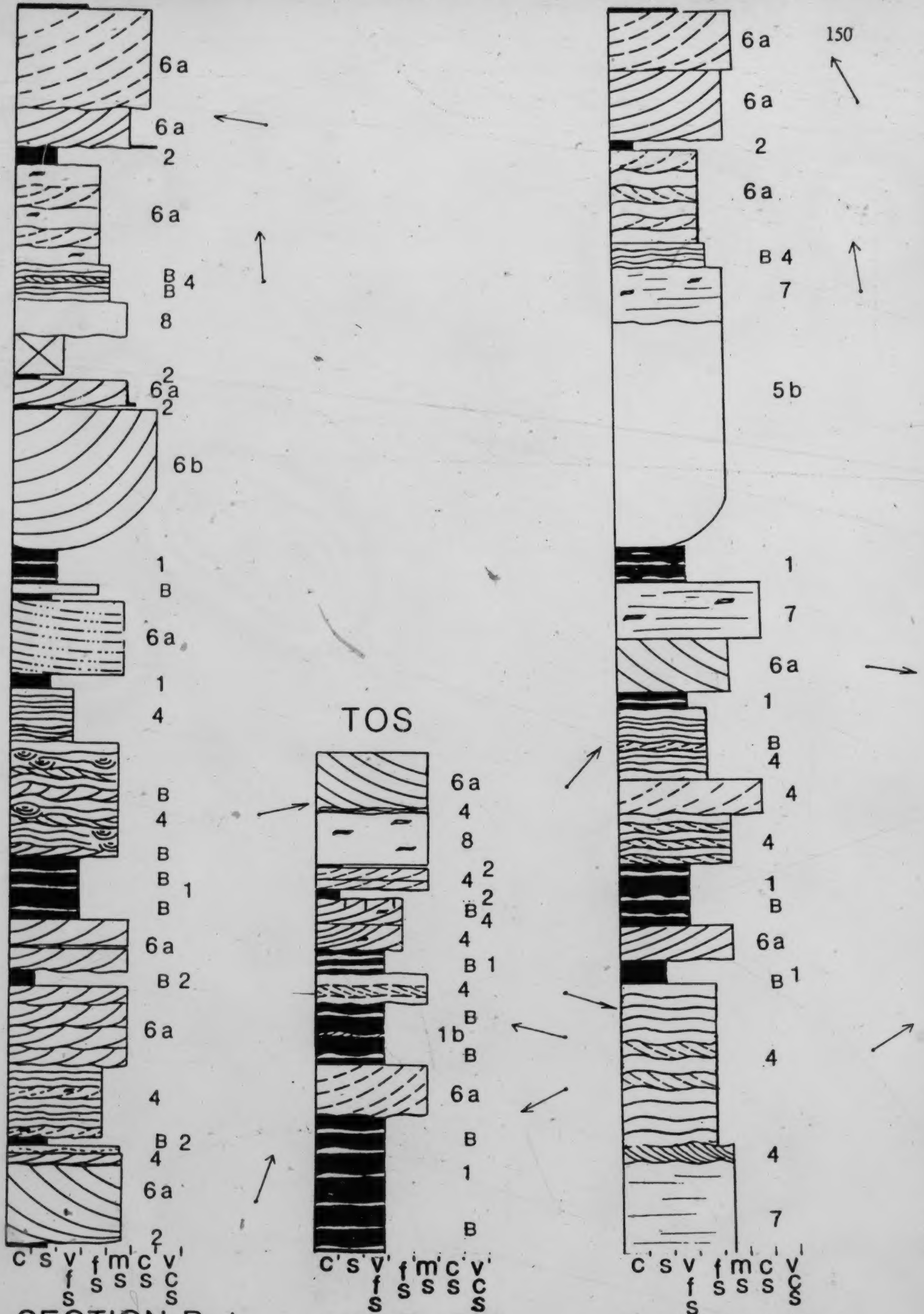
6a
6a
2
6a
B 4 B
8
2
6a
2
6b
1
B
6a
1
4
B
4
B
B 1
B
6a
B 2
6a
4
B 2
4
6a
2
c s vfs fs ms cs vcs
TOS
6a
4
8
4 2
2
B 4
4
B 1
4
B
1b
B
6a
B
1
B
c s vfs fs ms cs vcs
150
6a
6a
2
6a
B 4
7
5b
1
7
6a
1
B 4
4
4
1 B
6a
B 1
4
4
7
c s vfs fs ms cs vcs

SECTION B-1 CONT. B-1 SECTION B-2

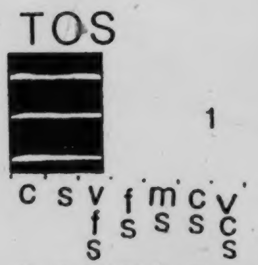
TOS
1
c s vfs fs ms cs vcs

CONT. B-2

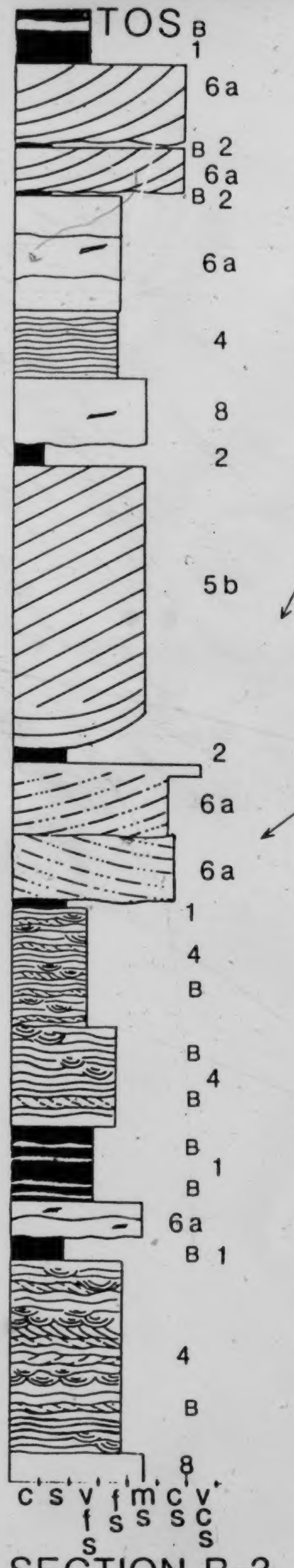
TOS
B 1
6a
B 2
6a
B 2
6a
4
8
2
5b
2
6a
6a
1
4
B
B
4
B
B
1
B
6a
B 1
4
B
8
c s vfs fs ms cs vcs

SECTION B-3

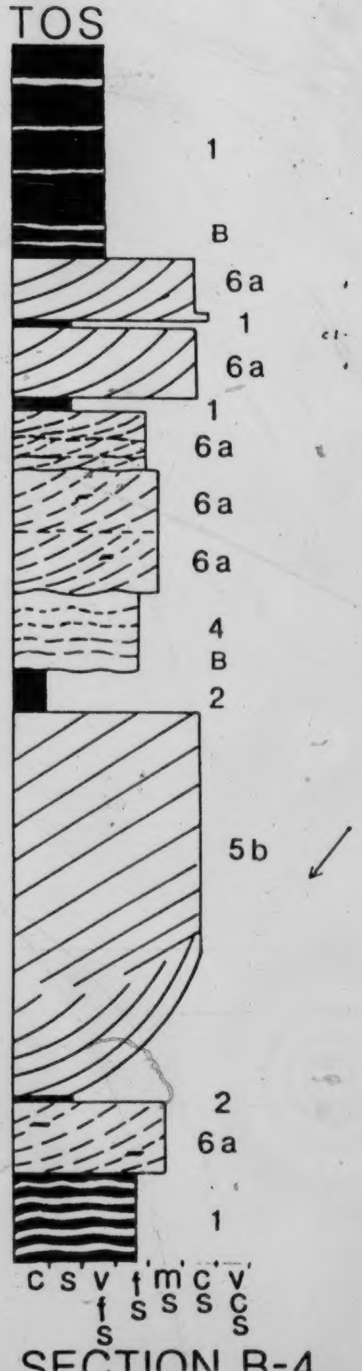
TOS
1
B
6a
1
6a
1
6a
6a
6a
4
B
2
5b
2
6a
1
c s vfs fs ms cs vcs

SECTION B-4

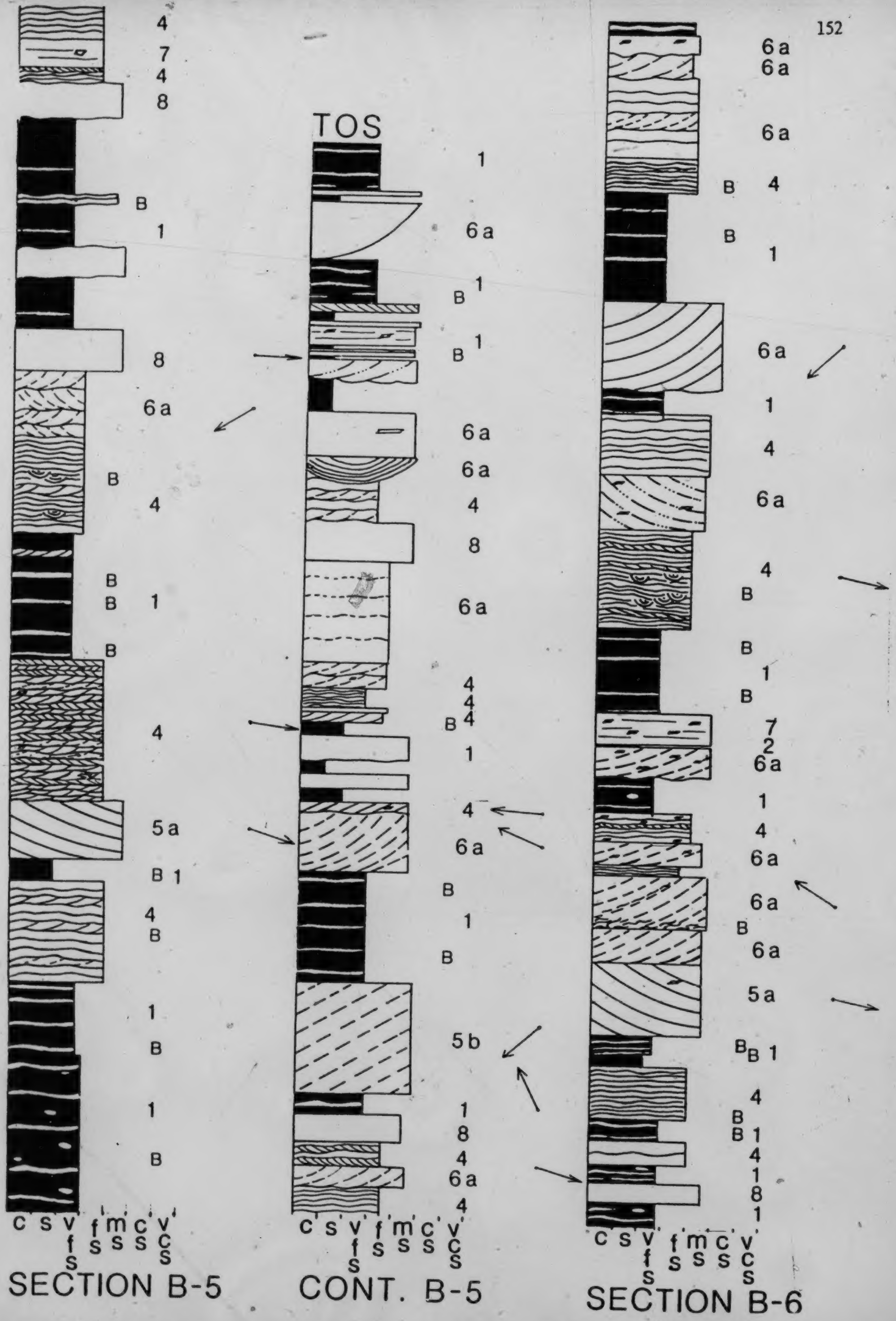
4
7
4
8
B
1
8
6a
B
4
B
B 1
B
4
5a
B 1
4
B
1
B
1
B
c s vf fs ms cs vc
s s s s s
TOS
1
6a
1
B
1
B
6a
6a
4
8
6a
4
4
B 4
1
4
6a
B
1
B
5b
1
8
4
6a
4
c s vf fs ms cs vc
s s s s s
6a
6a
6a
B 4
B
1
6a
1
4
6a
4
B
B
1
B
7
2
6a
1
4
6a
6a
B
6a
5a
B B 1
4
B
B 1
4
1
8
1
c s vf fs ms cs vc
s s s s s

SECTION B-5

CONT. B-5

SECTION B-6

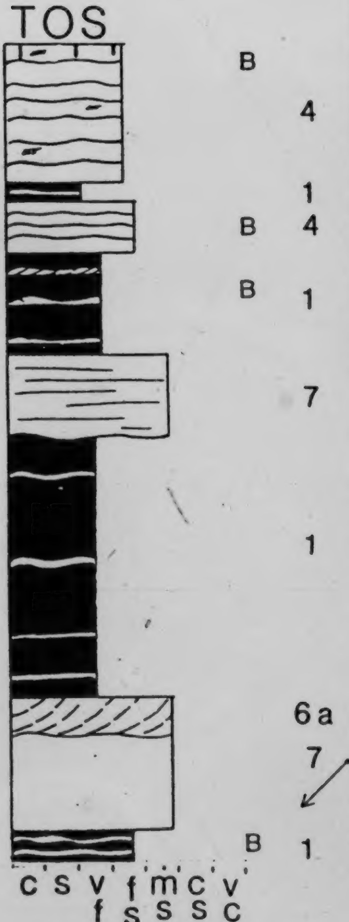
TOS
B
4
1
B 4
B 1
7
1
6a
7
B 1
c s vfs fs ms cs vcs

CONT. B-6

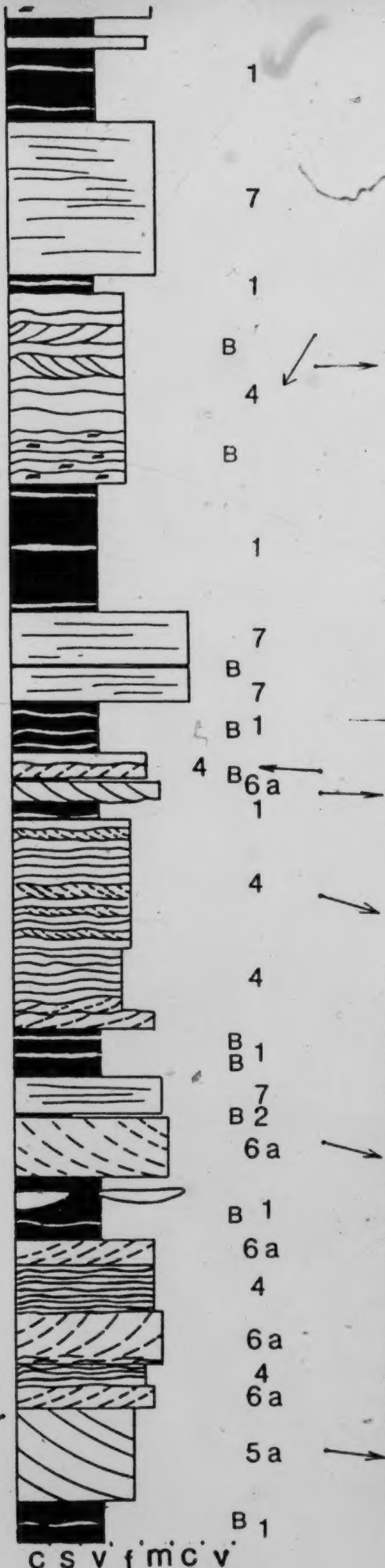
1
7
1
B
4
B
1
7
B
7
B 1
4 B
6a
1
4
4
B 1
B
7
B 2
6a
B 1
6a
4
6a
4
6a
5a
B 1
c s vfs fs ms cs vcs

SECTION B-7

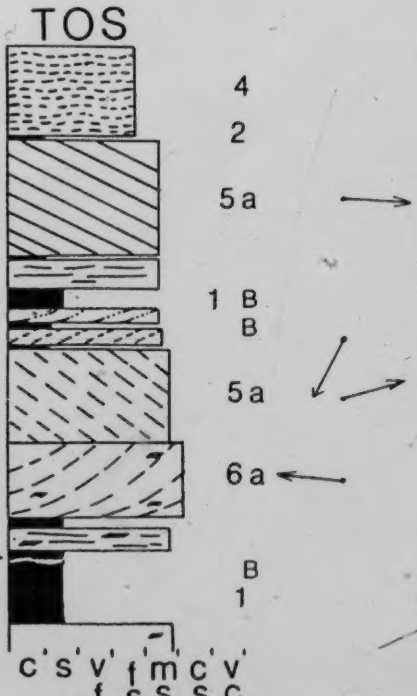
TOS
4
2
5a
1 B
B
5a
6a
B
1
c s vfs fs ms cs vcs

CONT. B-7

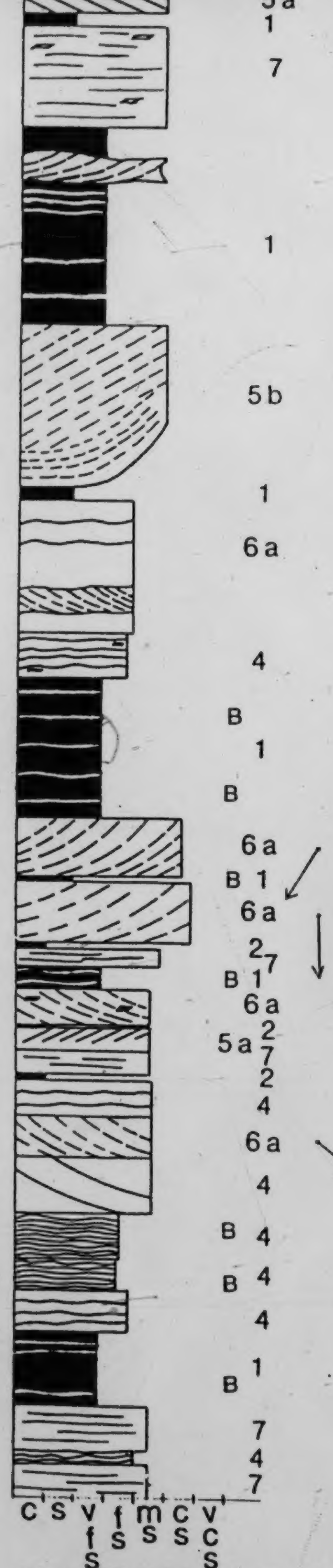
5a
1
7
1
5b
1
6a
4
B
1
B
6a
B 1
6a
2
7
B 1
6a
5a 2
7
2
4
6a
4
B 4
B 4
4
B 1
7
4
7
c s vfs fs ms cs vcs

SECTION B-8

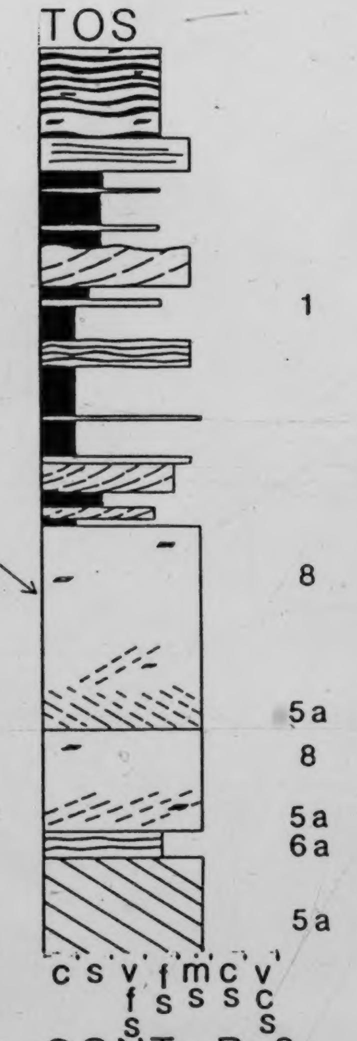
TOS
1
8
5a
8
5a
6a
5a
c s vfs fs ms cs vcs

CONT. B-8

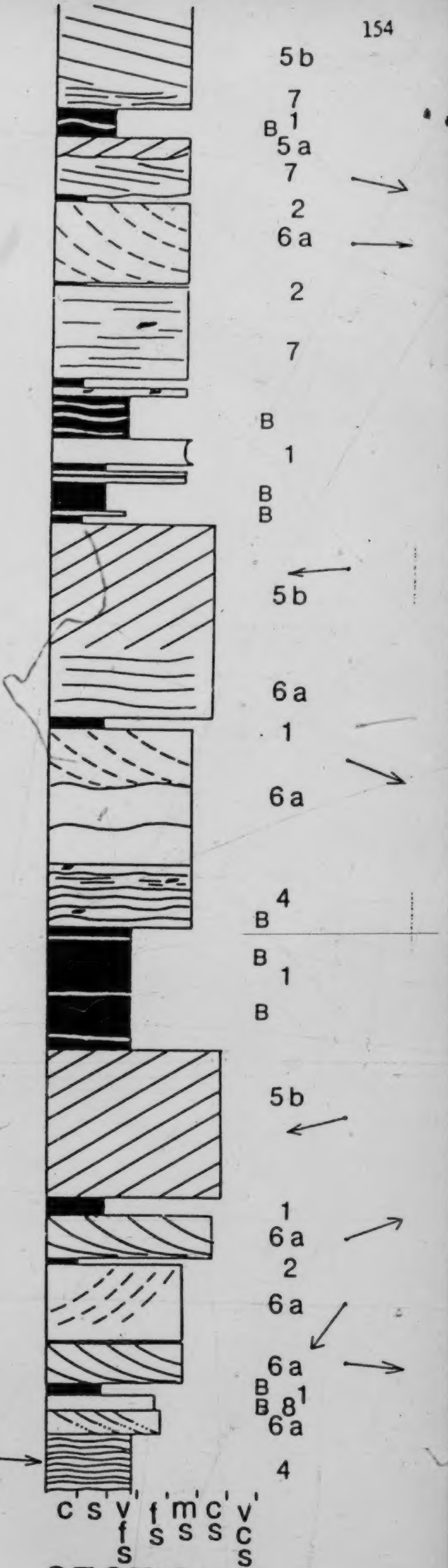
5b
7
B 1
5a
7
2
6a
2
7
B
1
B
B
5b
6a
1
6a
4
B
B 1
B
5b
1
6a
2
6a
6a
B 1
B 8
6a
4
c s vfs fs ms cs vcs

SECTION B-9

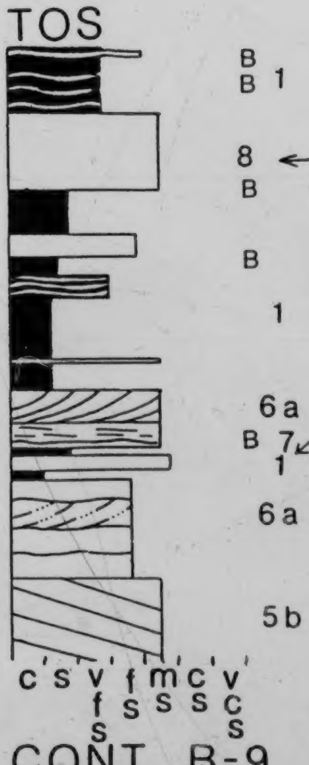
TOS
B
B 1
8
B
B
1
6a
B 7
1
6a
5b
c s v f m c v
f s s s c
s s

CONT. B-9

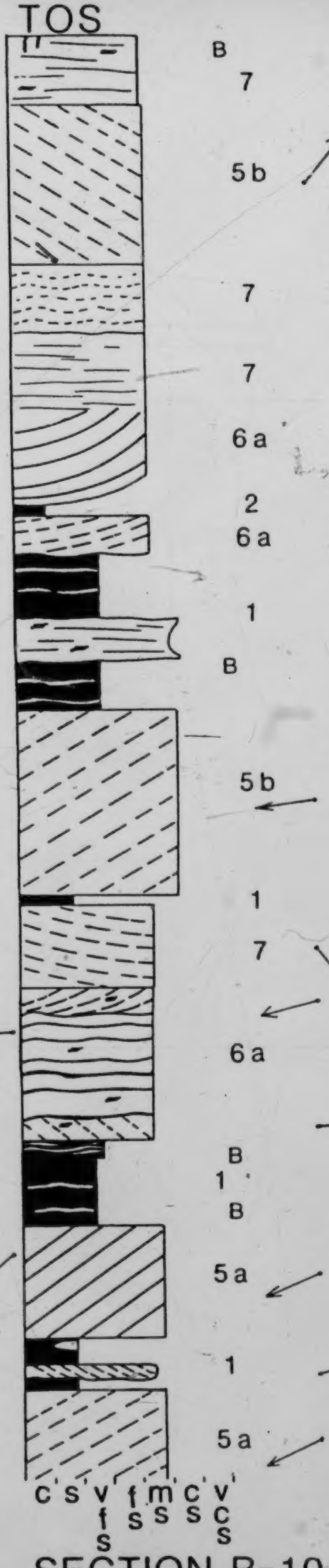
TOS
B
7
5b
7
7
6a
2
6a
1
B
5b
1
7
6a
B
1
B
5a
1
5a
c s v f m c v
f s s s c
s s

SECTION B-10

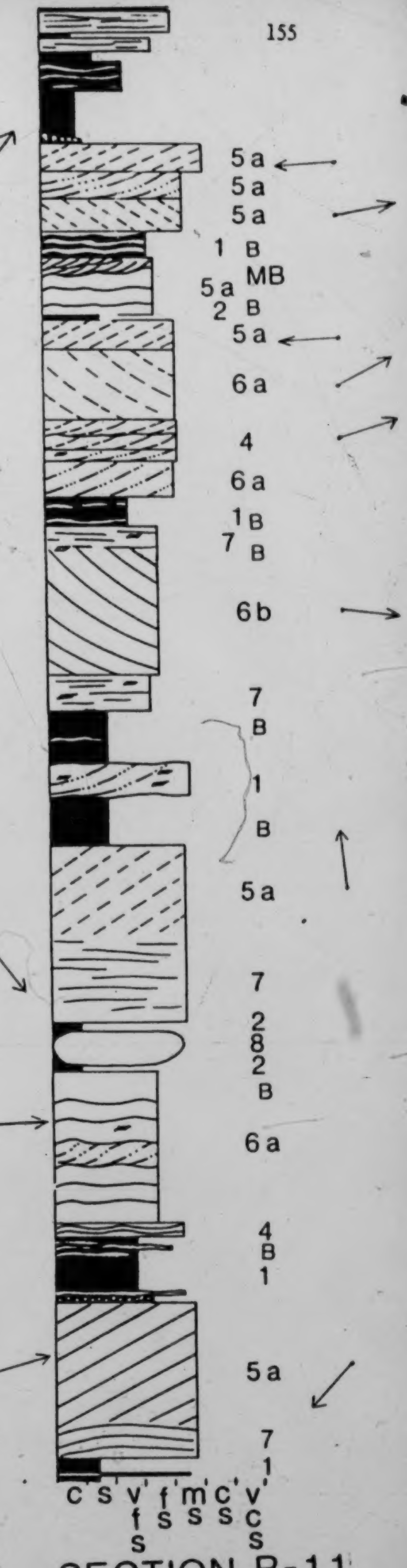
5a
5a
5a
1 B
5a MB
2 B
5a
6a
4
6a
1 B
7 B
6b
7
B
1
B
5a
7
2
8
2
B
6a
4
B
1
5a
7
1
c s v f m c v
f s s s c
s s

SECTION B-11

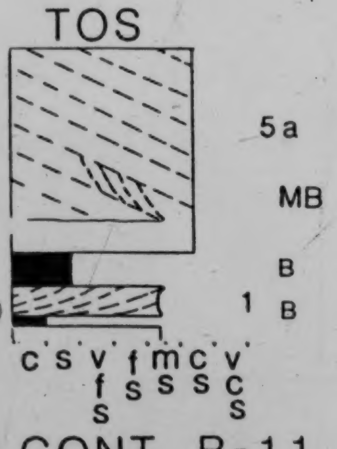
TOS
5a
MB
B
1
B
c s v f m c v
f s s s c
s s

CONT. B-11

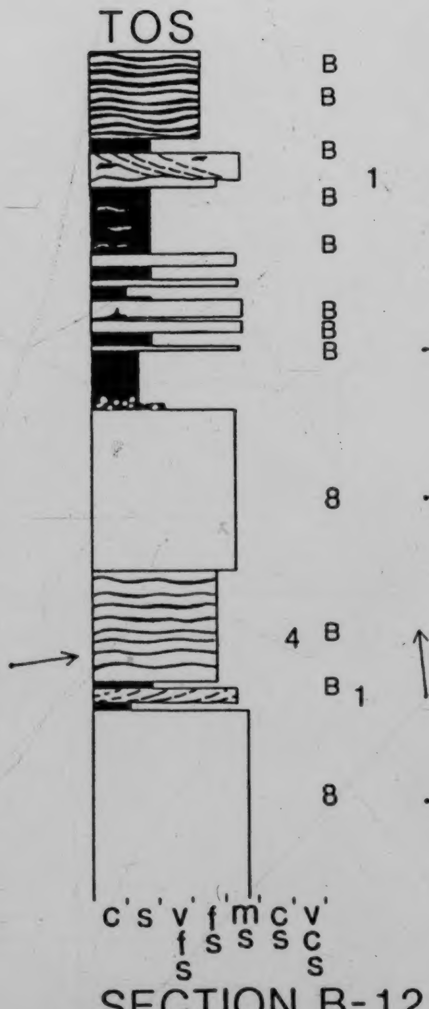
TOS
B
B
B
1
B
B
B
B
B
8
4 B
B 1
8
c s v f m c v
f s s s c
s s

SECTION B-12

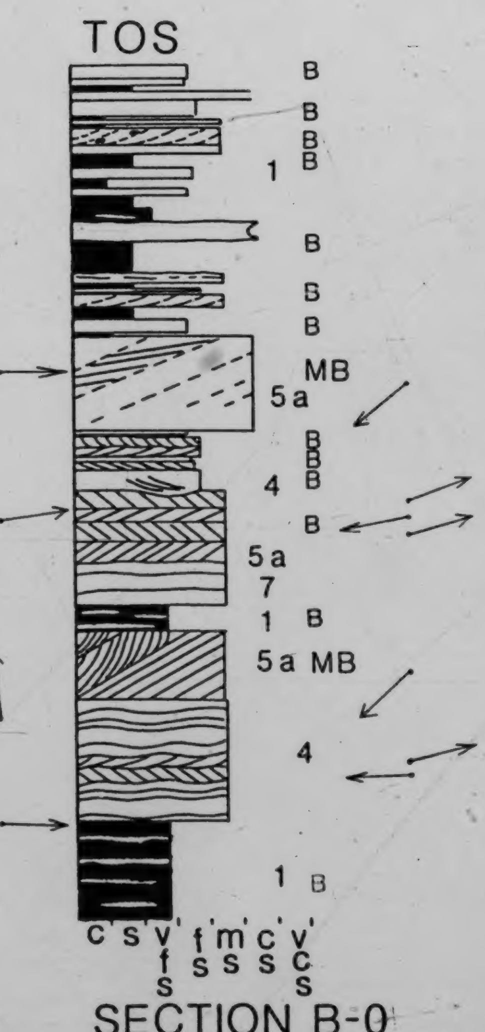
TOS
B
B
B
1 B
B
B
B
MB
5a
B
B
4 B
B
5a
7
1 B
5a MB
4
1 B
c s v f m c v
f s s s c
s s

SECTION B-0

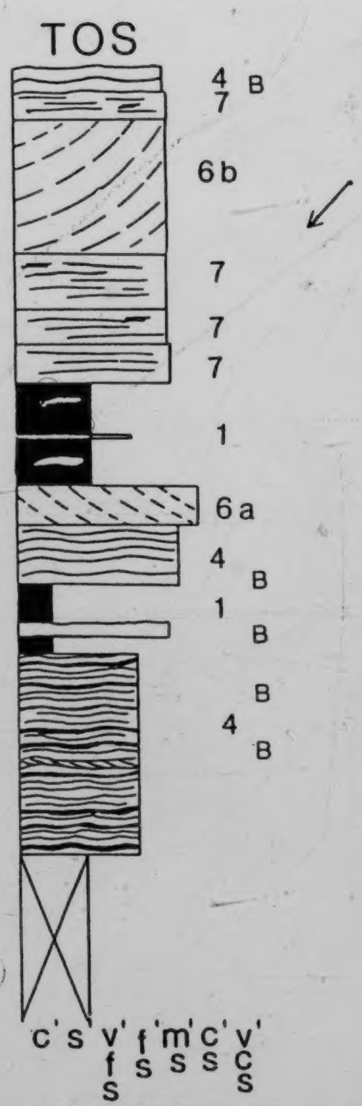
TOS
4 B
7
6b
7
7
7
1
6a
4
B
1
B
B
4
B
c s vfs fs ms cs vcs

SECTION B-0-1

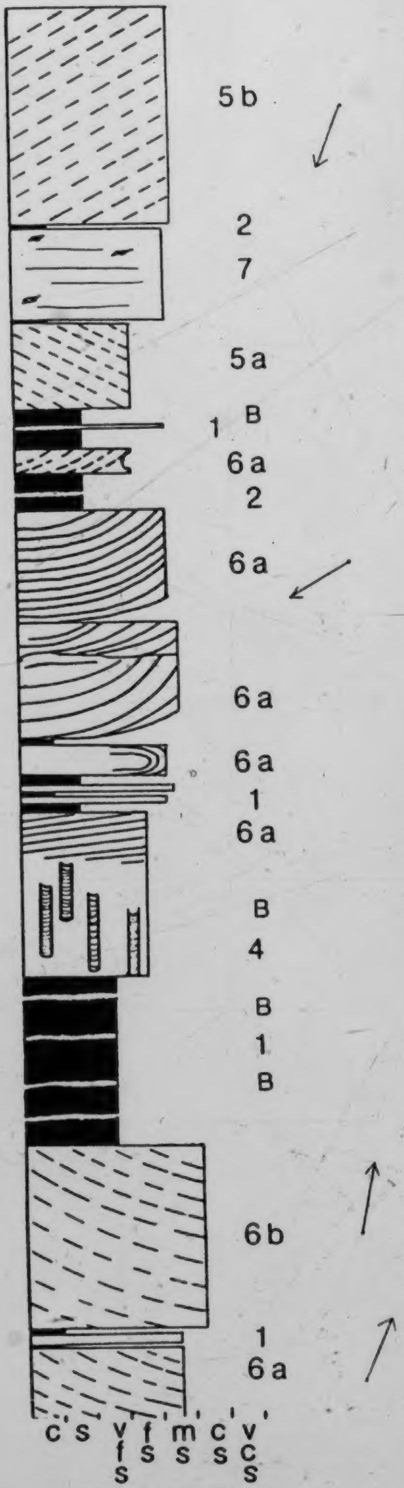
5b
2
7
5a
B
1
6a
2
6a
6a
6a
1
6a
B
4
B
1
B
6b
1
6a
c s vfs fs ms cs vcs

SECTION C-1

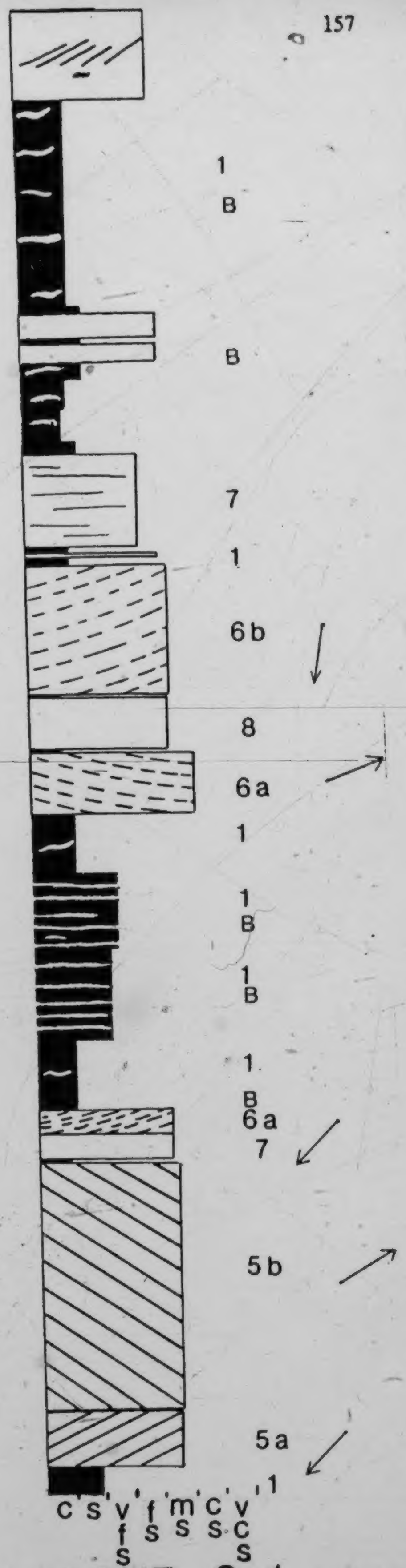
1
B
B
7
1
6b
8
6a
1
1
B
1
B
1
B
6a
7
5b
5a
1
c s vfs fs ms cs vcs

CONT. C-1

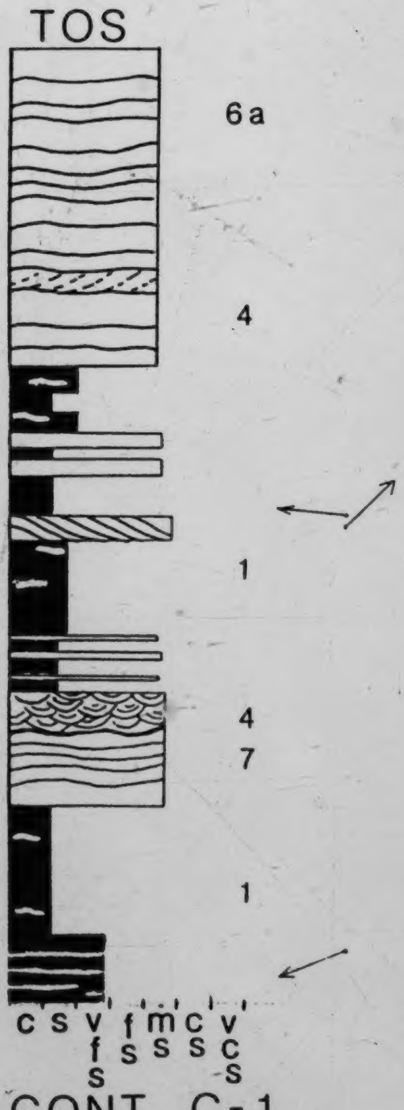
TOS
6a
4
1
4
7
1
c s vfs fs ms cs vcs

CONT. C-1

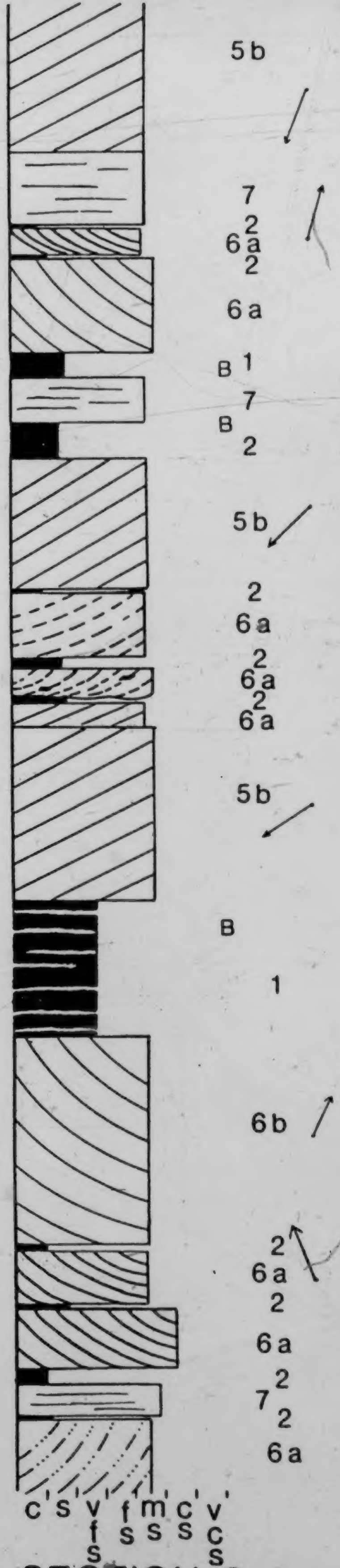
5b
7
2
6a
2
6a
B 1
7
B 2
5b
2
6a
2
6a
2
6a
5b
B
1
6b
2
6a
2
6a
2
7
2
6a
c s vfs fs ms cs vcs

SECTION C-2

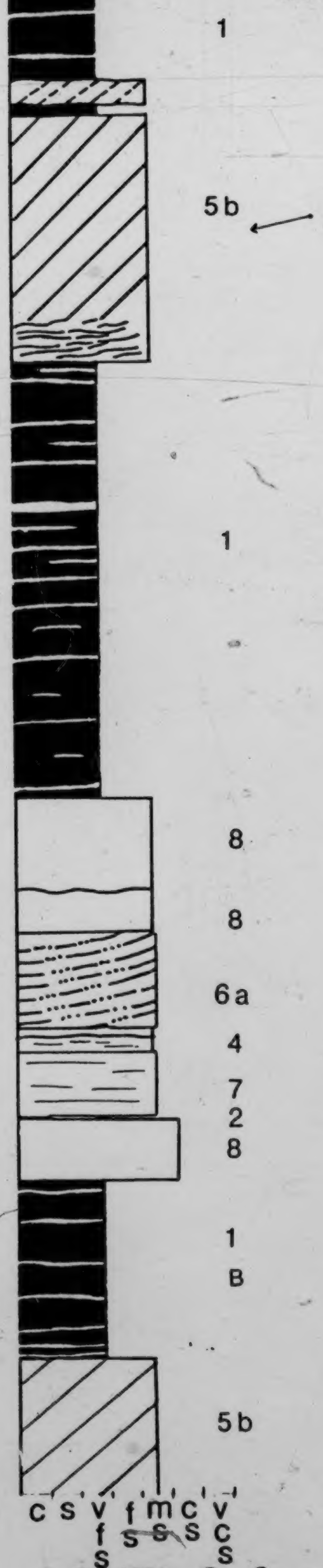
1
5b
1
8
8
6a
4
7
2
8
1
B
5b
c s vfs fs ms cs vcs

CONT. C-2

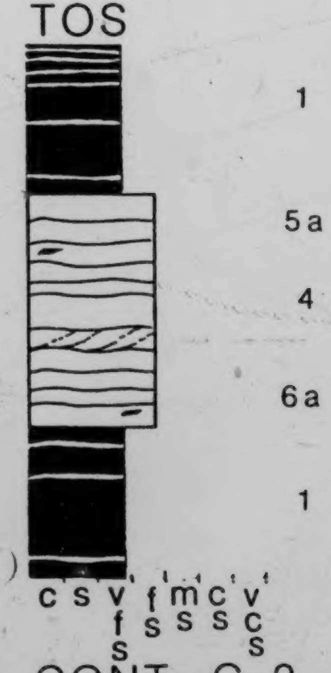
TOS
1
5a
4
6a
1
c s vfs fs ms cs vcs

CONT. C-2

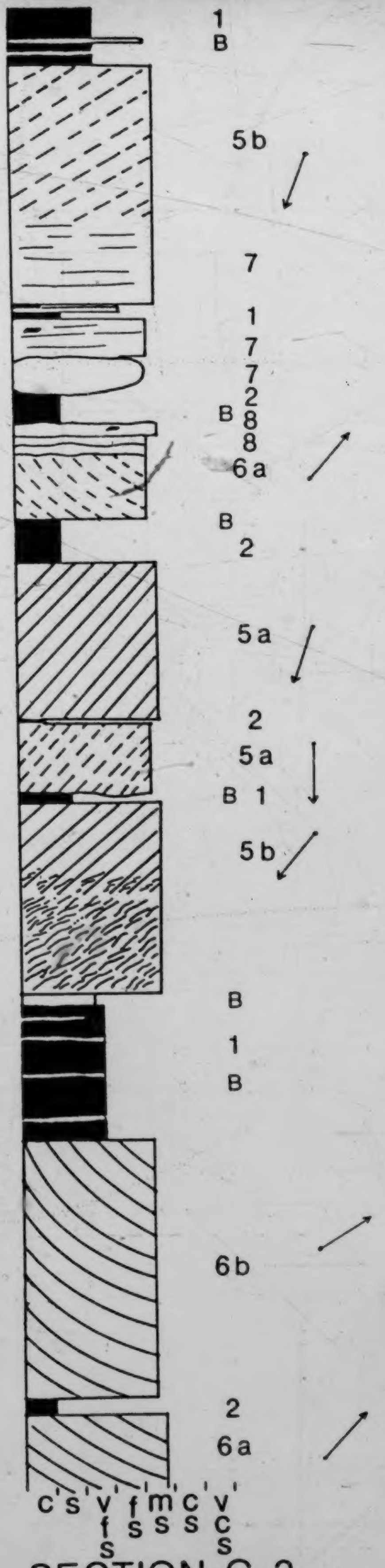
1
B
5b
7
1
7
7
2
B 8
8
6a
B
2
5a
2
5a
B 1
5b
B
1
B
6b
2
6a
c s vfs fs ms cs vcs

SECTION C-3

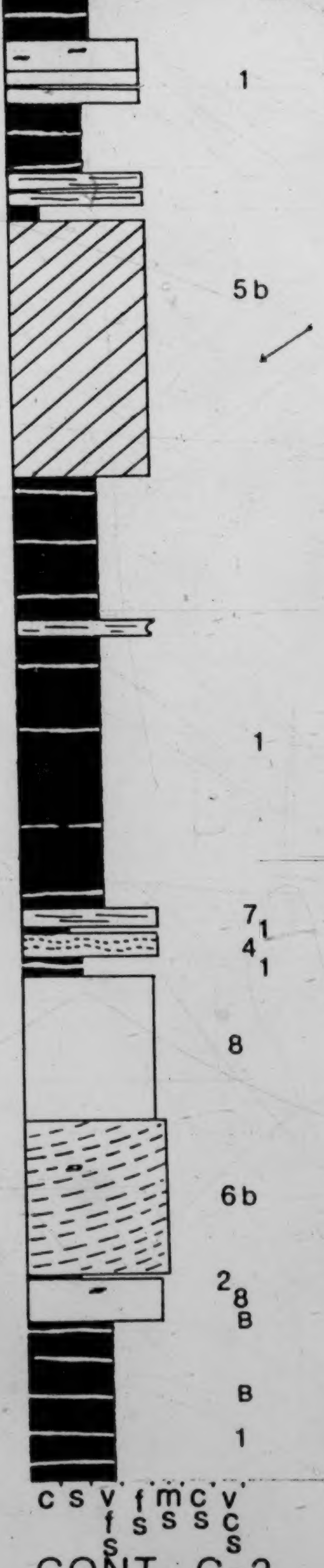
1
5b
1
7
1
4
1
8
6b
2
8
B
B
1
c s vfs fs ms cs vcs

CONT. C-3

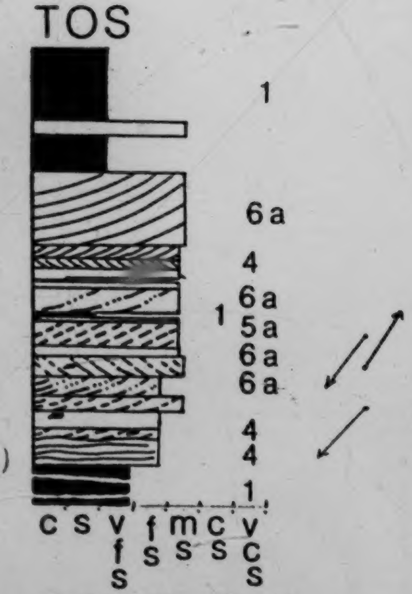
TOS
1
6a
4
6a
1
5a
6a
6a
4
4
1
c
s
vfs
fs
ms
cs
vcs

CONT. C-3

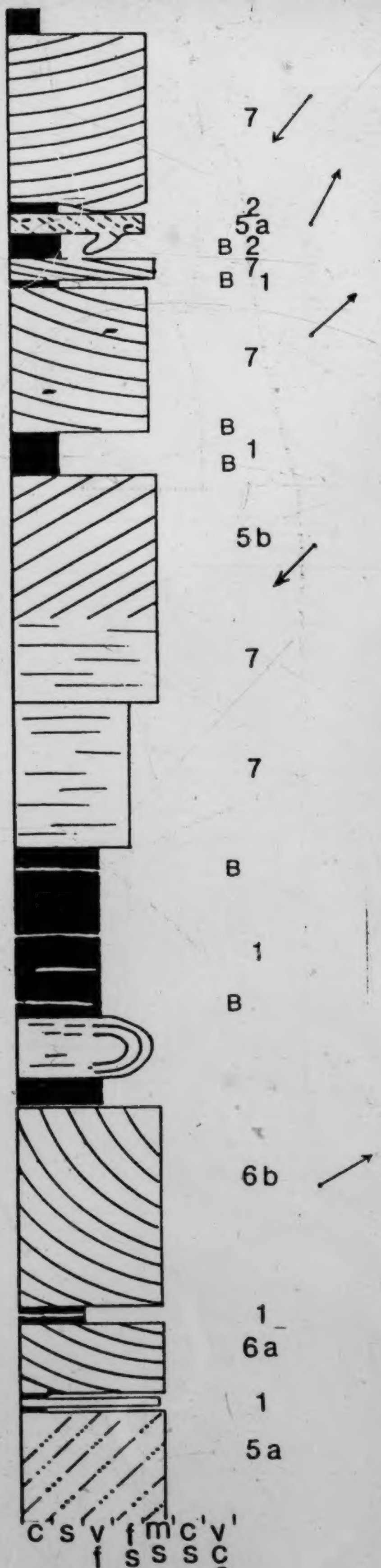
7
2
5a
B 2
B 7 1
7
B
1
B
5b
7
7
B
1
B
6b
1
6a
1
5a
c
s
vfs
fs
ms
cs
vcs

SECTION C-4

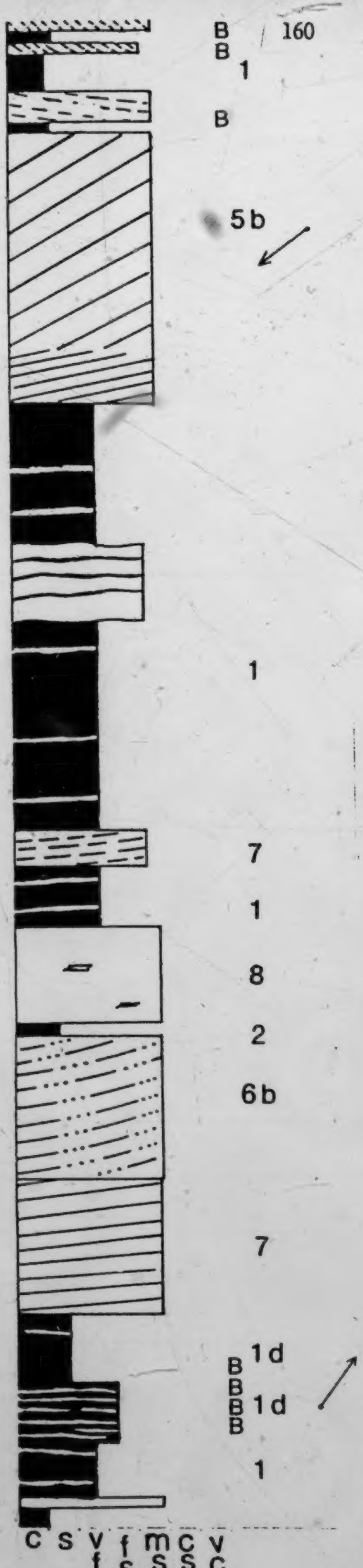
B
B
1
B
5b
1
7
1
8
2
6b
7
B 1d
B
B 1d
B
1
c
s
vfs
fs
ms
cs
vcs

CONT. C-4

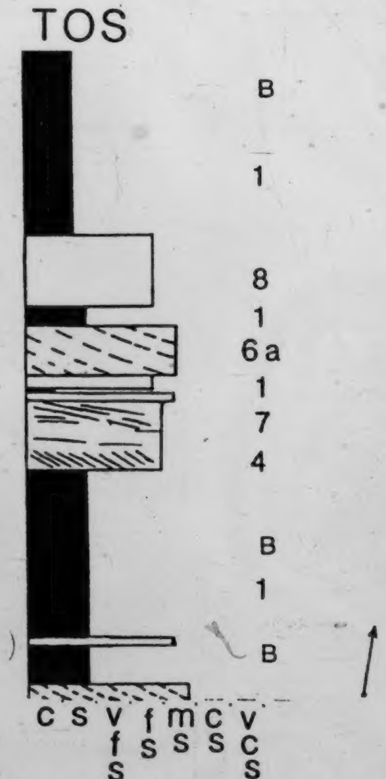
TOS
B
1
8
1
6a
1
7
4
B
1
B
c s vfs fs ms cs vcs

CONT. C-4

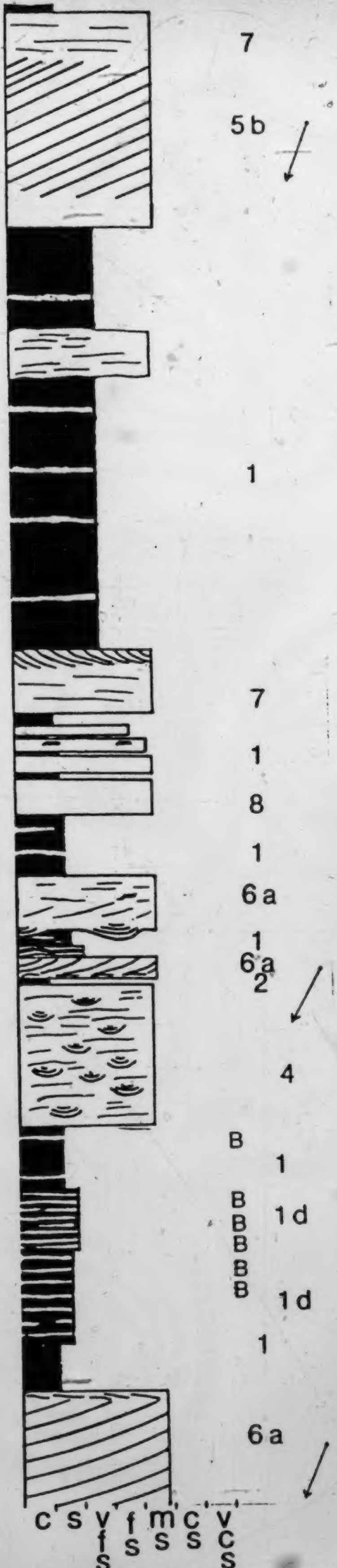
7
5b
1
7
1
8
1
6a
1
6a
2
4
B
1
B
B
1d
B
B
B
1d
1
6a
c s vfs fs ms cs vcs

SECTION C-5

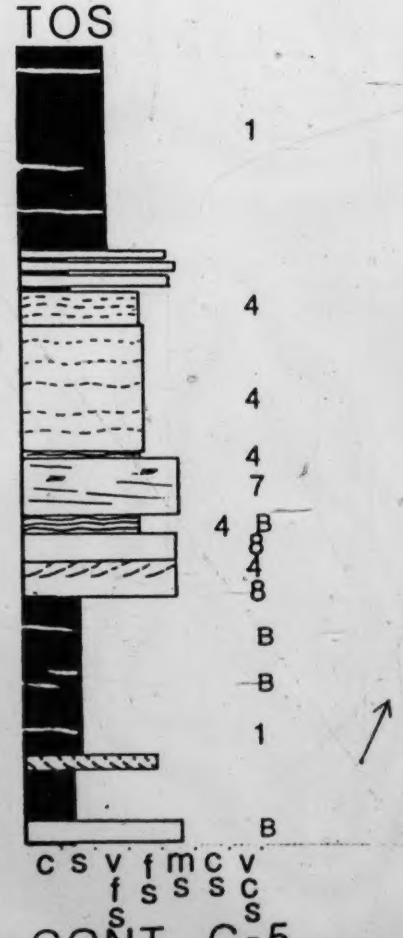
TOS
1
4
4
4
7
4
B
8
4
8
B
B
1
B
c s vfs fs ms cs vcs

CONT. C-5

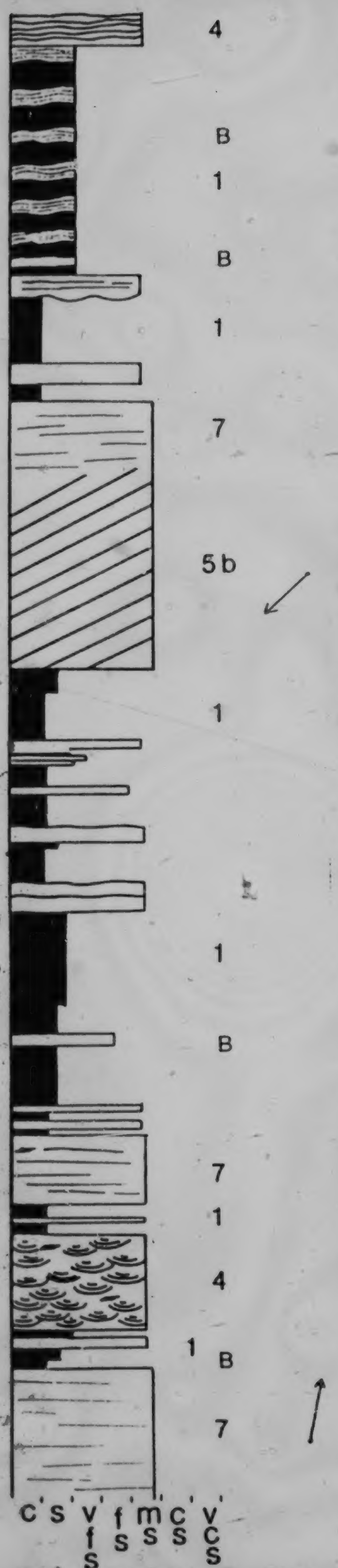
4
B
1
B
1
7
5b
1
1
B
7
1
4
1
B
7
c s vfs fs ms cs vcs

SECTION C-6

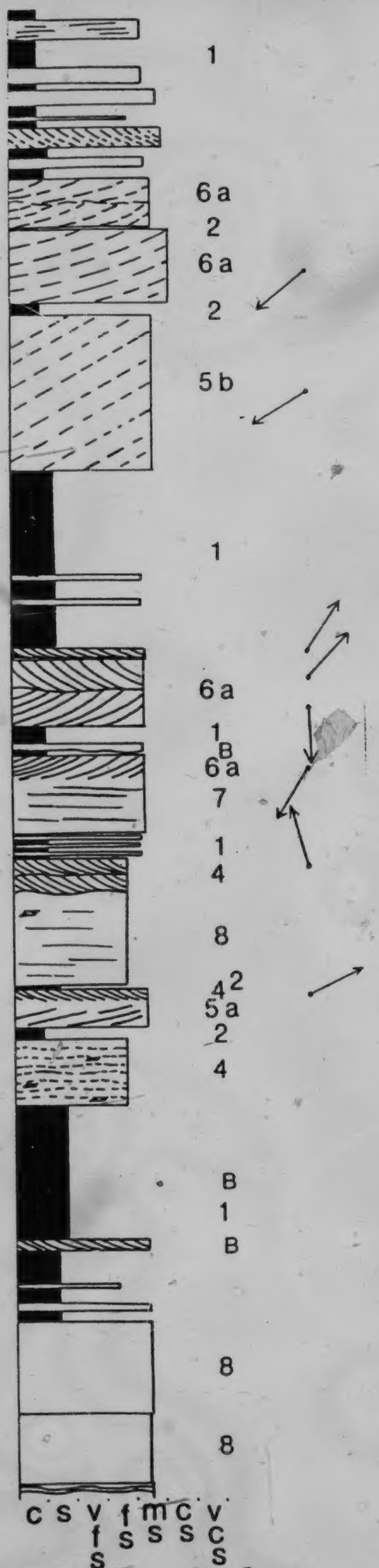
1
6a
2
6a
2
5b
1
6a
1
B
6a
7
1
4
8
4
2
5a
2
4
B
1
B
8
8
c s vfs fs ms cs vcs

CONT. C-6

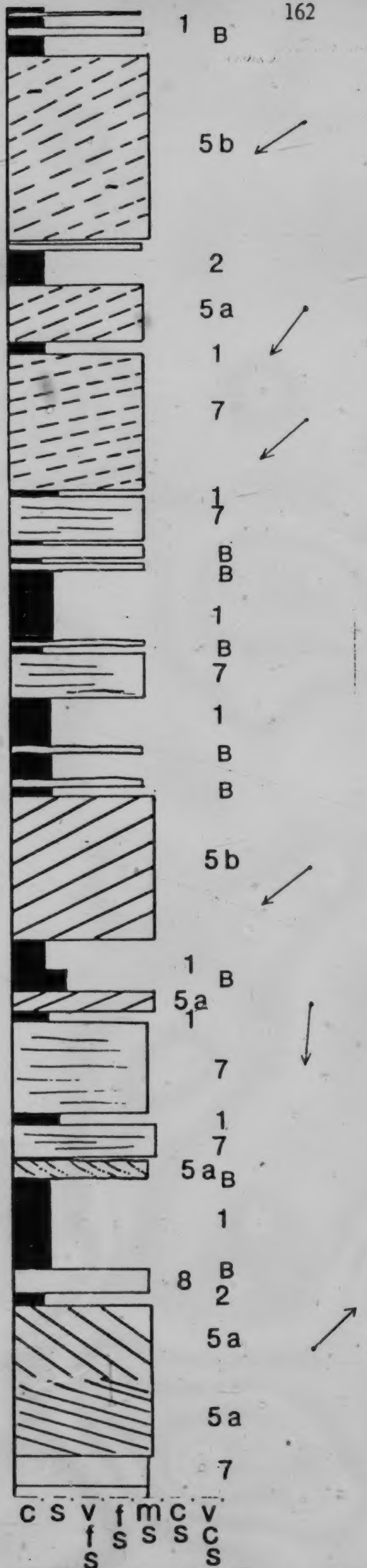
1
B
5b
2
5a
1
7
1
7
B
B
1
B
7
1
B
B
5b
1
B
5a
1
7
1
7
5a
B
1
B
8
2
5a
5a
7
c s vfs fs ms cs vcs

CONT. C-6

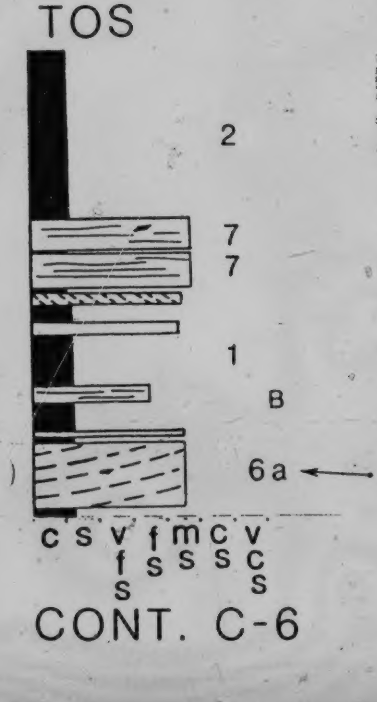
TOS
2
7
7
1
B
6a
c s v f s f s m s c s v c s

CONT. C-6

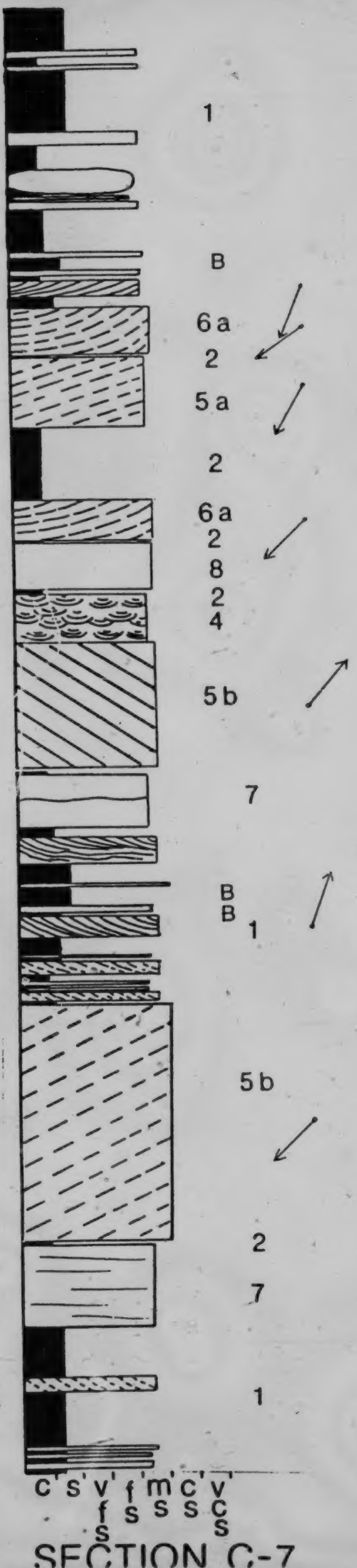
1
B
6a
2
5a
2
6a
2
8
2
4
5b
7
B
B
1
5b
2
7
1
c s v f s f s m s c s v c s

SECTION C-7

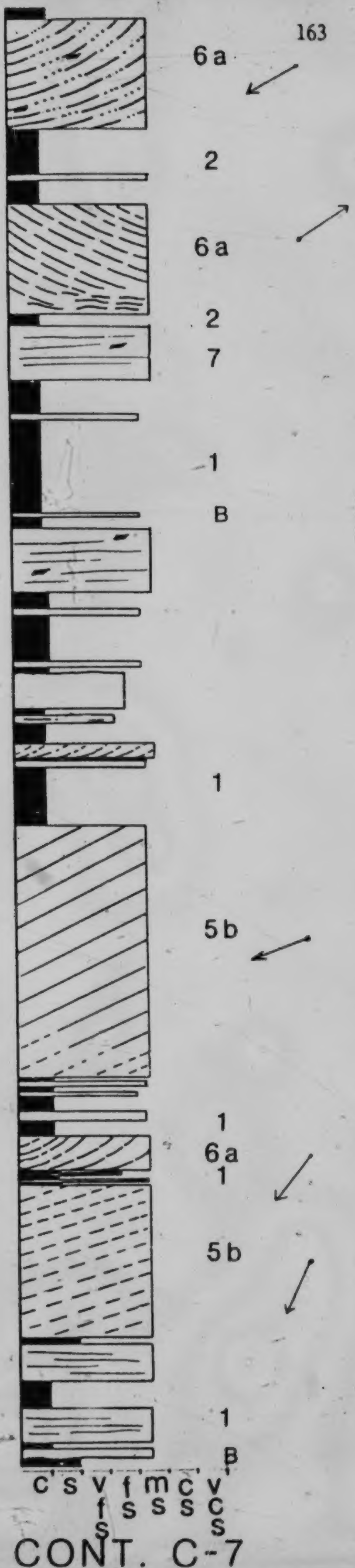
6a
2
6a
2
7
1
B
1
5b
1
6a
1
5b
1
B
c s v f s f s m s c s v c s

CONT. C-7

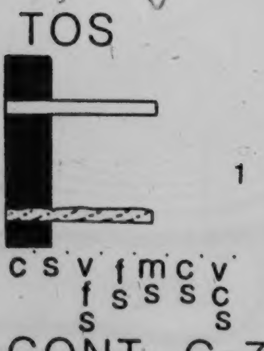
TOS
1
c s v f m c v
f s s s c
s s

CONT. C-7

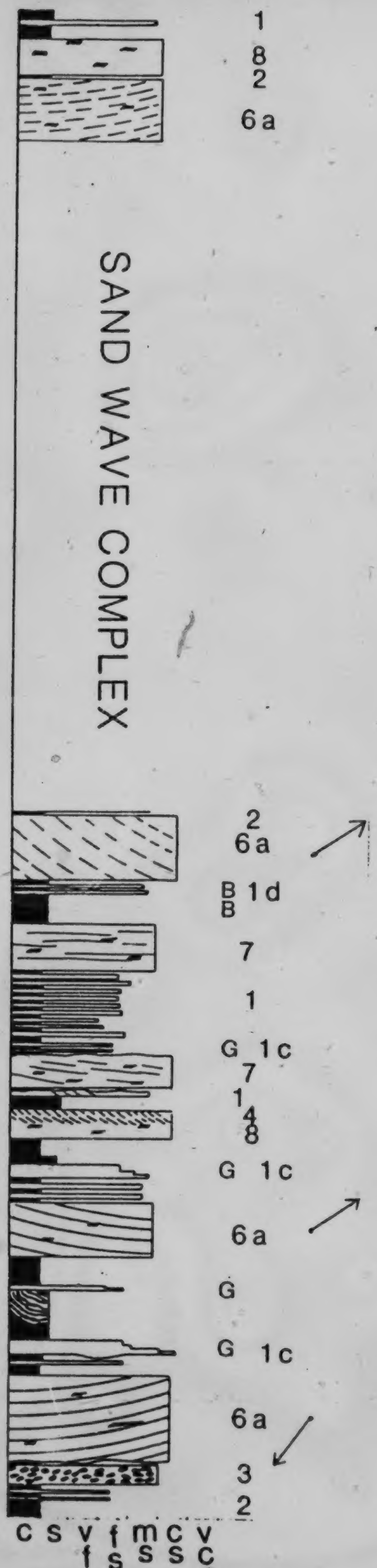
1
8
2
6a
SAND WAVE COMPLEX
2
6a
B 1d
B
7
1
G 1c
7
1
4
8
G 1c
6a
G
G 1c
6a
3
2
c s v f m c v
f s s s c
s s

SECTION D-1

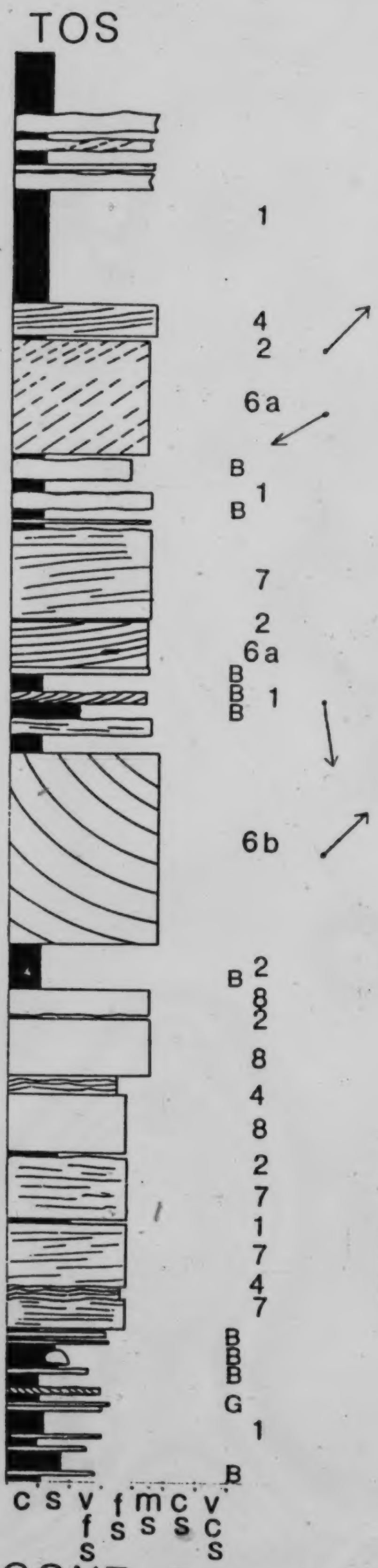
TOS
1
4
2
6a
B
1
B
7
2
6a
B
B 1
B
6b
B 2
8
2
8
4
8
2
7
1
7
4
7
B
B
B
G
1
B
c s v f m c v
f s s s c
s s

CONT. D-1

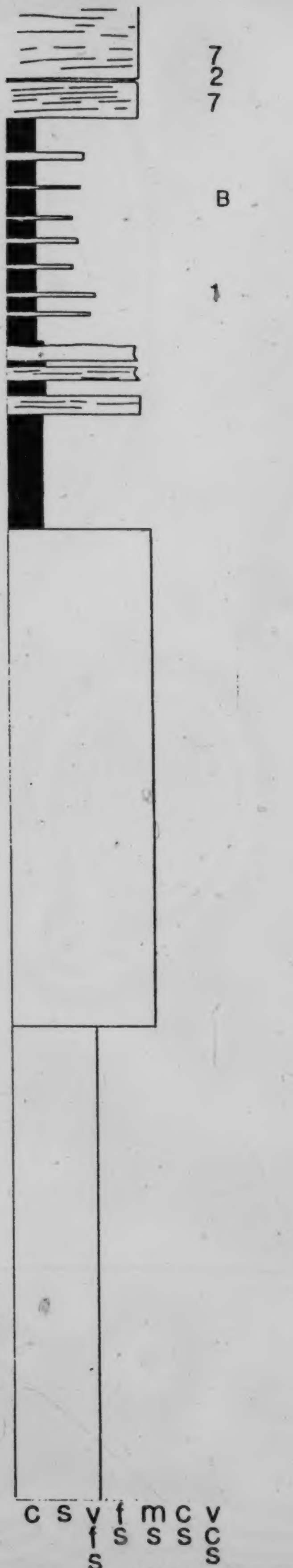
7
2
7
B
1
c
s
vfs
fs
ms
cs
vcs

SECTION D-2

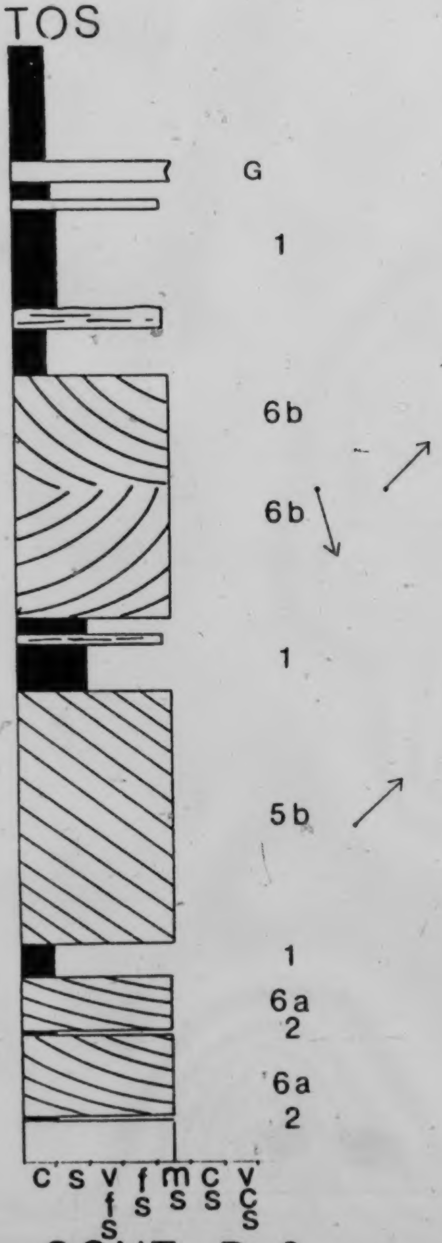
TOS
G
1
6b
6b
1
5b
1
6a
2
6a
2
c
s
vfs
fs
ms
cs
vcs

CONT. D-2

9. APPENDIX II

Appendix II contains 10° rose diagrams recording the rotated paleocurrent data for the various facies and subfacies at each of the four major outcrops.

10 DEG ROSE HISTOGRAM. N = 5

ROTATED PALEOCURRENT DATA
FOR FACIES 4 AT OUTCROP A

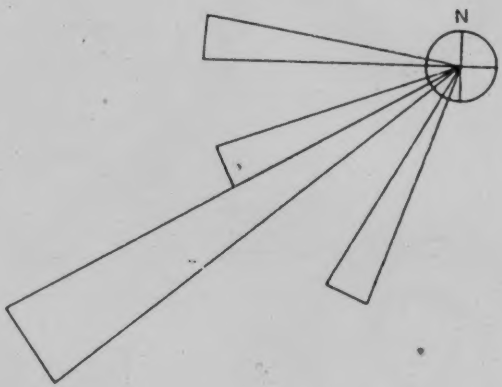

10 DEG ROSE HISTOGRAM. N = 53

ROTATED PALEOCURRENT DATA
FOR SUBFACIES 5A AT OUTCROP A

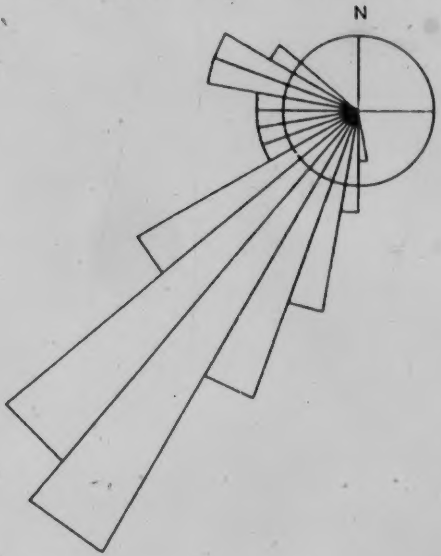

10 DEG ROSE HISTOGRAM. N = 10

ROTATED PALEOCURRENT DATA
FOR SUBFACIES 5B AT OUTCROP A

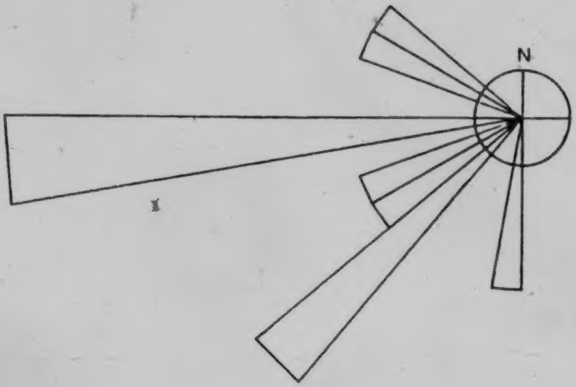

10 DEG ROSE HISTOGRAM. N = 5

ROTATED PALEOCURRENT DATA
FOR SUBFACIES 6A AT OUTCROP A

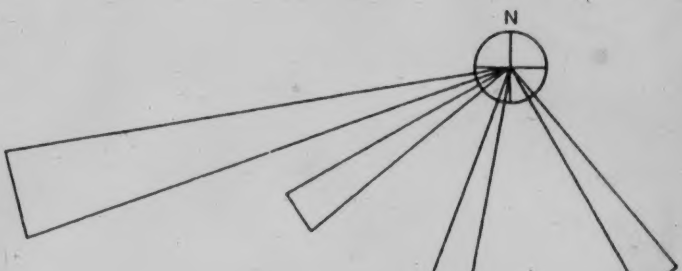

10 DEG ROSE HISTOGRAM. N = 5

ROTATED PALEOCURRENT DATA FOR SUBFACIES 1B AT OUTCROP B

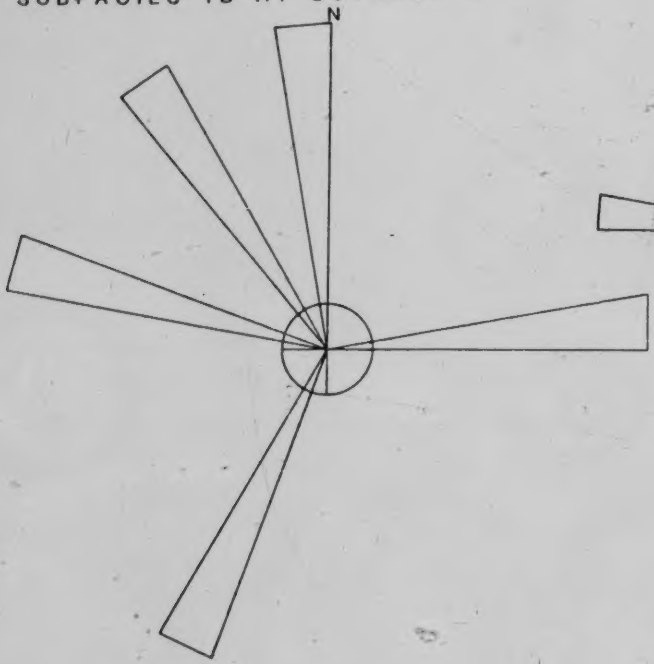

10 DEG ROSE HISTOGRAM. N = 19

ROTATED PALEOCURRENT DATA FOR FACIES 4 AT OUTCROP B

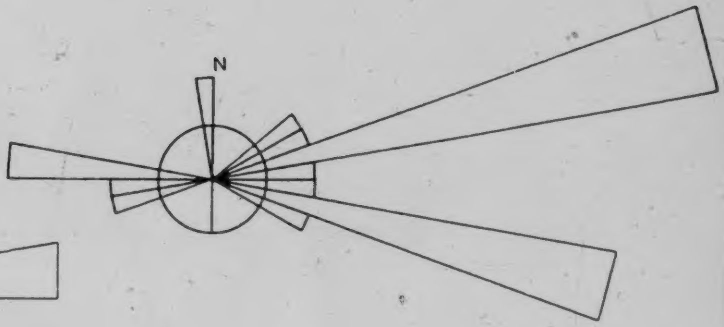

10 DEG ROSE HISTOGRAM. N = 18

ROTATED PALEOCURRENT DATA FOR SUBFACIES 5A AT OUTCROP B

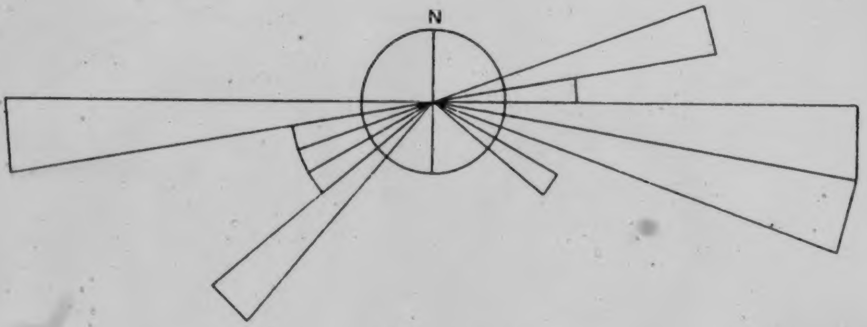

10 DEG ROSE HISTOGRAM. N = 9

ROTATED PALEOCURRENT DATA FOR SUBFACIES 5B AT OUTCROP B

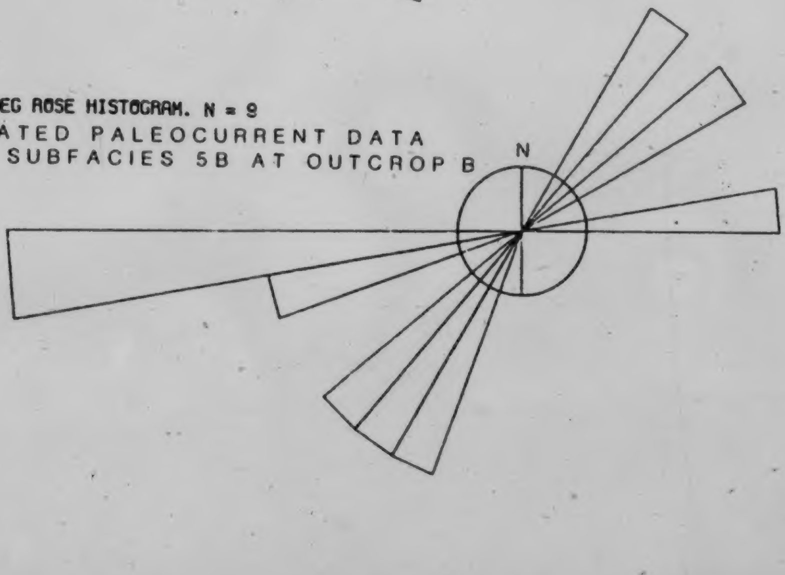

10 DEG ROSE HISTOGRAM. N = 32

ROTATED PALEOCURRENT DATA
FOR SUBFACIES 6A AT OUTCROP B

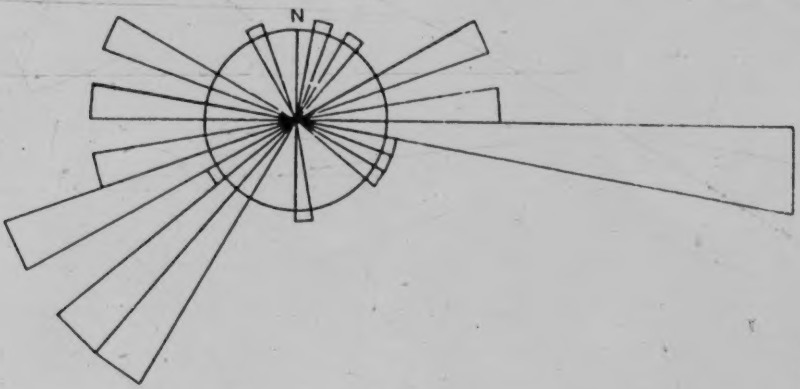

10 DEG ROSE HISTOGRAM. N = 3

ROTATED PALEOCURRENT DATA
FOR SUBFACIES 6B AT OUTCROP B

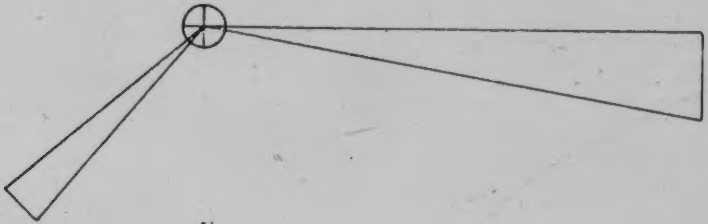

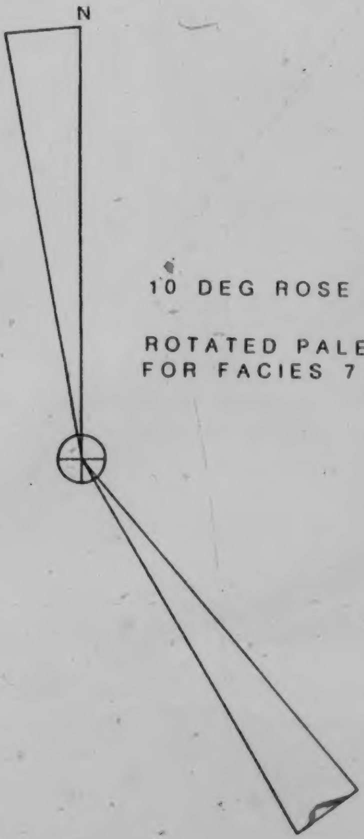

10 DEG ROSE HISTOGRAM N=2

ROTATED PALEOCURRENT DATA
FOR FACIES 7 AT OUTCROP B

10 DEG ROSE HISTOGRAM. N = 9

ROTATED PALEOCURRENT DATA
FOR SUBFACIES 1B AT OUTCROP C

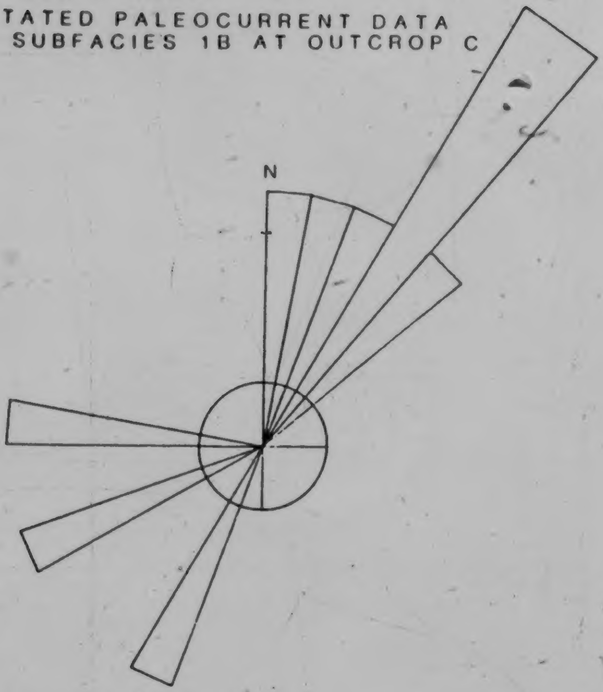

10 DEG ROSE HISTOGRAM. N = 1

ROTATED PALEOCURRENT DATA
FOR FACIES 4 AT OUTCROP C

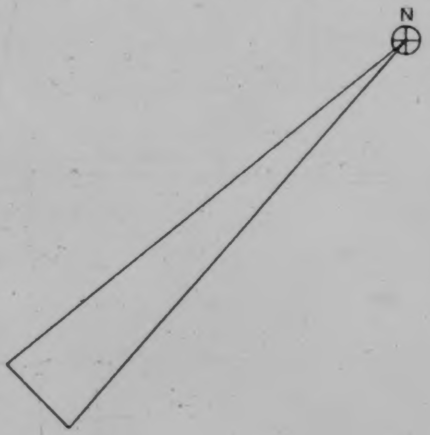

10 DEG ROSE HISTOGRAM. N = 11

ROTATED PALEOCURRENT DATA
FOR SUBFACIES 5A AT OUTCROP C

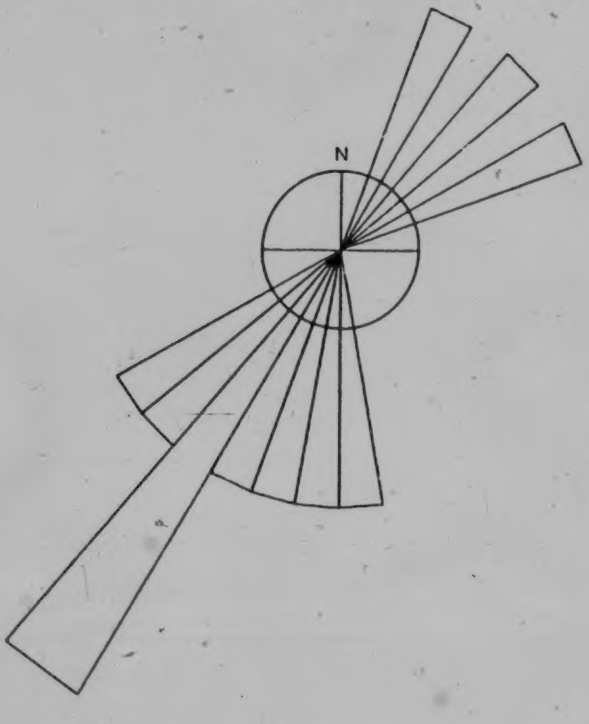

10 DEG ROSE HISTOGRAM. N = 20

ROTATED PALEOCURRENT DATA
FOR SUBFACIES 5B AT OUTCROP C

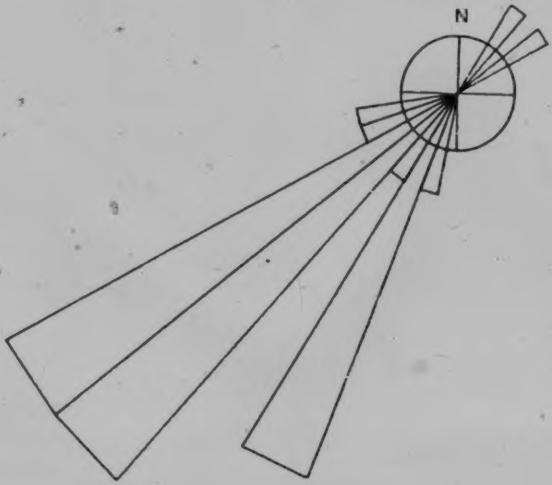

10 DEG ROSE HISTOGRAM. N=22

ROTATED PALEOCURRENT DATA
FOR SUBFACIES 6A AT OUTCROP C

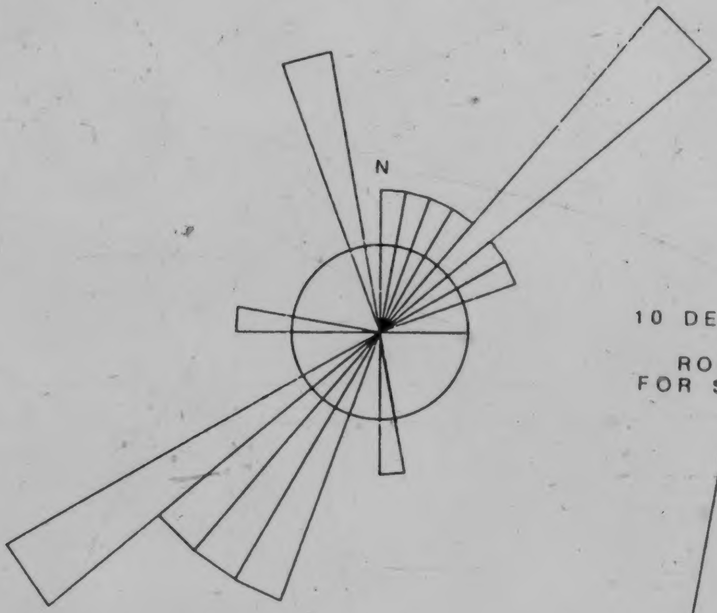

10 DEG ROSE HISTOGRAM. N=6

ROTATED PALEOCURRENT DATA
FOR SUBFACIES 6B AT OUTCROP C

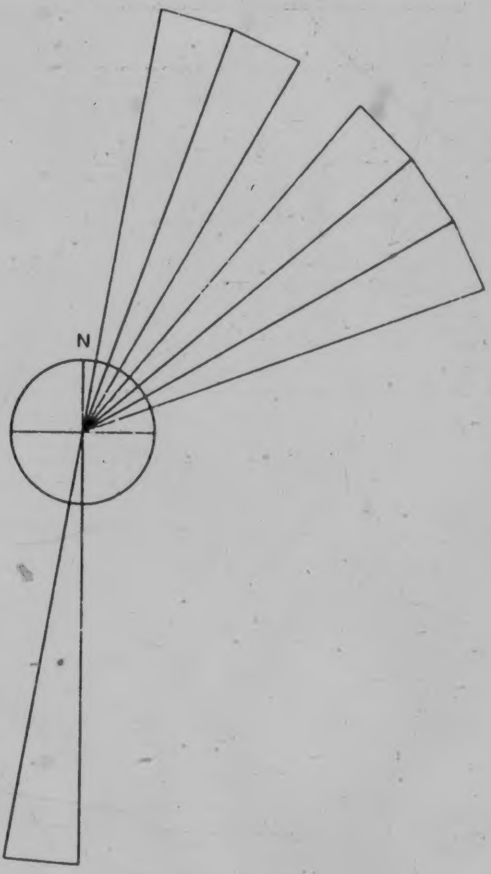

10 DEG ROSE HISTOGRAM. N = 2

ROTATED PALEOCURRENT DATA
FOR FACIES 7 AT OUTCROP C

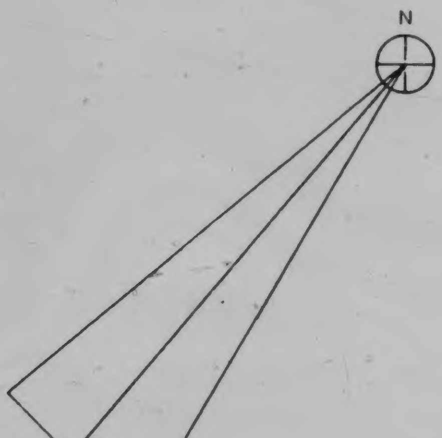

10 DEG ROSE HISTOGRAM. N = 1

ROTATED PALEOCURRENT DATA FOR SUBFACIES 1B AT OUTCROP D

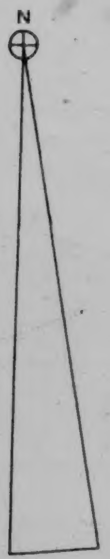

10 DEG ROSE HISTOGRAM. N = 1

ROTATED PALEOCURRENT DATA FOR SUBFACIES 5A AT OUTCROP D

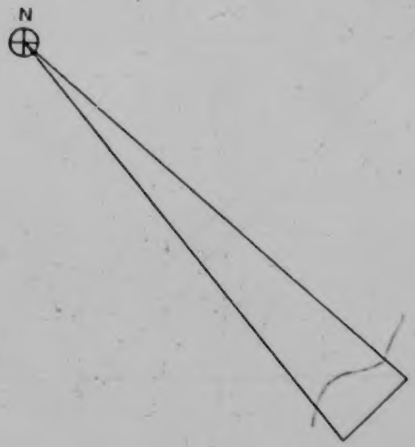

10 DEG ROSE HISTOGRAM. N = 8

ROTATED PALEOCURRENT DATA FOR SUBFACIES 5B AT OUTCROP D

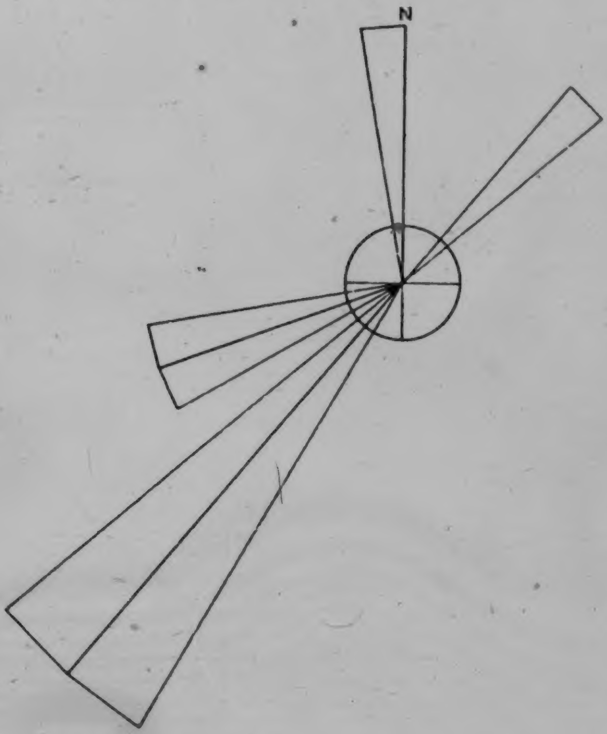

10 DEG ROSE HISTOGRAM. N = 7

ROTATED PALEOCURRENT DATA FOR SUBFACIES 6A AT OUTCROP D

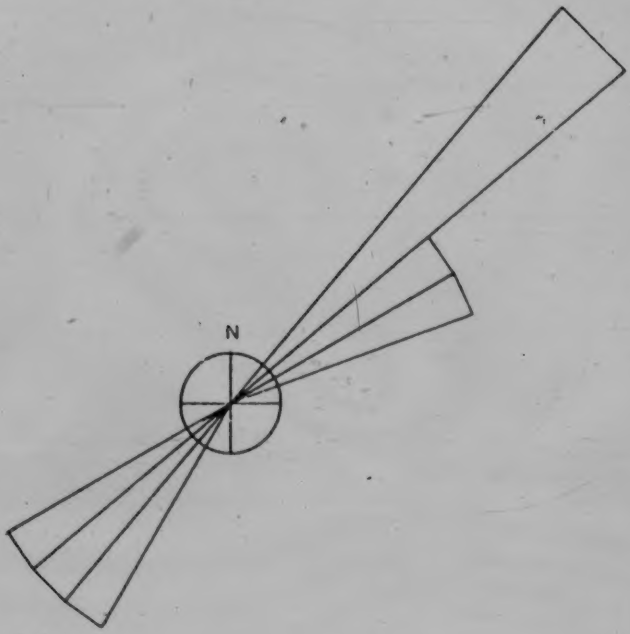

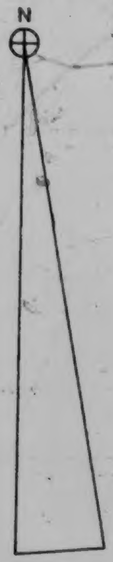

10 DEG ROSE HISTOGRAM. N = 1

ROTATED PALEOCURRENT DATA FOR SUBFACIES 1B AT OUTCROP D

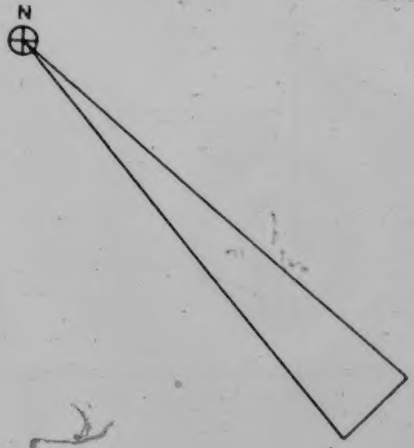

10 DEG ROSE HISTOGRAM. N = 1

ROTATED PALEOCURRENT DATA FOR SUBFACIES 5A AT OUTCROP D

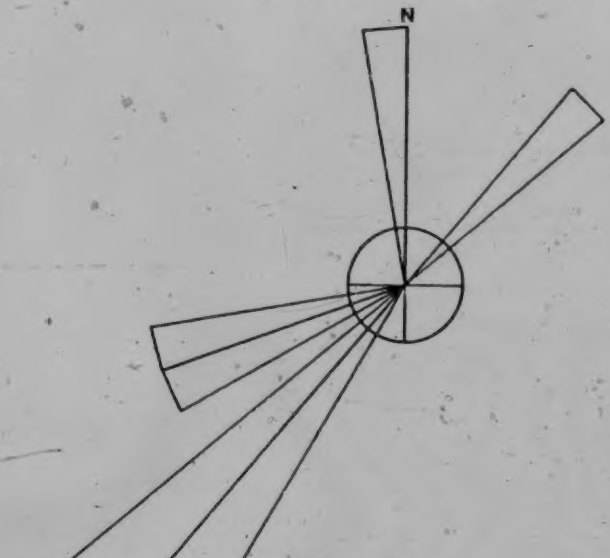

10 DEG ROSE HISTOGRAM. N = 8

ROTATED PALEOCURRENT DATA FOR SUBFACIES 5B AT OUTCROP D

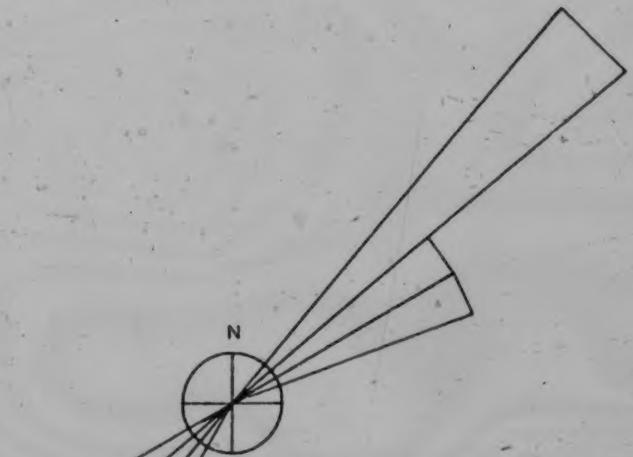

10 DEG ROSE HISTOGRAM. N = 7

ROTATED PALEOCURRENT DATA FOR SUBFACIES 6A AT OUTCROP D

10 DEG ROSE HISTOGRAM. N = 3

ROTATED PALEOCURRENT DATA FOR SUBFACIES 6B AT OUTCROP D

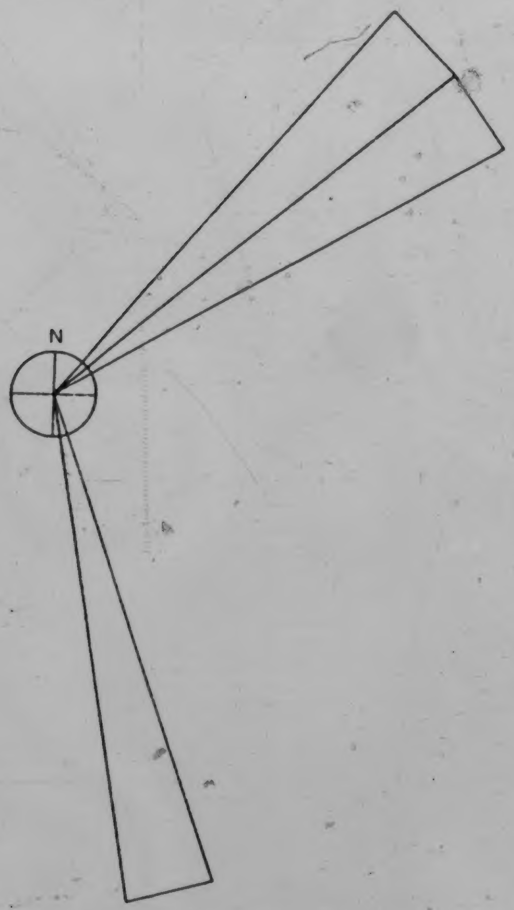

10. APPENDIX III

Appendix III contains the tally, observed probablity, random and difference matrices for the four outcrops and two facies associations.

Table 5.3. Non-embedded tally matrix for the Coarse-grained Facies Association.

	1	2	3	4	5a	5b	6a	6b	7	8	SUM
1	10	4	0	12	12	4	14	0	1	25	82
2	4	0	0	12	20	1	4	0	0	29	70
3	0	0	0	0	0	0	0	0	0	0	
4	14	13	0	11	8	0	1	0	0	10	57
5a	14	15	0	8	28	0	7	0	0	15	87
5b	1	2	0	0	0	6	1	0	0	4	14
6a	12	6	0	4	9	0	6	0	0	10	47
6b	0	0	0	0	0	0	0	0	0	0	0
7	0	0	0	0	0	1	0	0	1	0	2
8	22	25	0	10	14	5	16	0	0	50	142
SUM	77	65	0	57	91	17	49	0	2	143	501

Table 5.4. Non-embedded observed probability matrix for the Coarse-grained Facies Association

	1	2	3	4	5a	5b	6a	6b	7	8
1	0.121	0.048	0	0.146	0.146	0.048	0.172	0	0.012	0.304
2	0.057	0	0	0.171	0.286	0.014	0.057	0	0	0.414
3	0	0	0	0	0	0	0	0	0	0
4	0.245	0.228	0	0.193	0.140	0	0.017	0	0	0.175
5a	0.161	0.172	0	0.092	0.322	0	0.080	0	0	0.172
5b	0.071	0.142	0	0	0	0.430	0.071	0	0	0.285
6a	0.255	0.127	0	0.085	0.191	0	0.127	0	0	0.212
6b	0	0	0	0	0	0	0	0	0	0
7	0	0	0	0	0	0.500	0	0	0.500	0
8	0.154	0.176	0	0.070	0.099	0.035	0.112	0	0	0.352

Table 5.5. Non-embedded random probability matrix for the Coarse-grained Facies Association

	1	2	3	4	5a	5b	6a	6b	7	8
1	0.153	0.130	0	0.113	0.181	0.034	0.098	0	0.004	0.285
2	0.153	0.130	0	0.113	0.181	0.034	0.098	0	0.004	0.285
3	0.153	0.130	0	0.113	0.181	0.034	0.098	0	0.004	0.285
4	0.153	0.130	0	0.113	0.181	0.034	0.098	0	0.004	0.285
5a	0.153	0.130	0	0.113	0.181	0.034	0.098	0	0.004	0.285
5b	0.153	0.130	0	0.113	0.181	0.034	0.098	0	0.004	0.285
6a	0.153	0.130	0	0.113	0.181	0.034	0.098	0	0.004	0.285
6b	0	0	0	0	0	0	0	0	0	0
7	0.153	0.130	0	0.113	0.181	0.034	0.098	0	0.004	0.285
8	0.153	0.130	0	0.113	0.181	0.034	0.098	0	0.004	0.285

Table 5.6. Non-embedded difference matrix for the Coarse-grained Facies Association

	1	2	3	4	5a	5b	6a	6b	7	8
1	-0.032	-0.082	0	+0.033	-0.035	+0.014	+0.074	0	+0.008	+0.019
2	-0.096	-0.130	0	+0.058	+0.105	-0.020	-0.041	0	-0.004	+0.129
3	0	0	0	0	0	0	0	0	0	0
4	+0.092	+0.098	0	+0.080	-0.041	-0.034	-0.081	0	-0.004	-0.110
5a	+0.008	+0.042	0	-0.021	+0.141	-0.034	-0.018	0	-0.004	-0.113
5b	-0.082	+0.012	0	-0.113	-0.181	+0.396	-0.027	0	-0.004	+0.001
6a	+0.102	-0.003	0	-0.028	+0.010	-0.034	+0.029	0	-0.004	-0.073
6b	0	0	0	0	0	0	0	0	0	0
7	-0.153	-0.130	0	-0.113	-0.181	+0.466	-0.098	0	+0.496	-0.285
8	+0.001	+0.046	0	-0.043	-0.082	+0.001	+0.014	0	-0.004	+0.067

Table 5.7. Embedded tally matrix for the Coarse/Fine-grained Intercalated Facies Association.

	1	2	3	4	5a	5b	6a	6b	7	8	SUM
1	---	2	0	38	16	18	36	3	40	13	166
2	3	---	1	7	7	10	30	6	22	18	104
3	0	1	---	0	0	0	0	0	0	0	1
4	30	10	0	---	3	0	29	0	5	6	83
5a	17	12	0	4	---	0	3	0	0	2	38
5b	18	6	0	3	0	---	3	0	3	0	33
6a	45	40	0	13	3	1	---	0	4	5	111
6b	7	2	0	0	0	0	0	---	2	1	12
7	31	19	0	8	7	4	5	3	---	1	78
8	19	14	0	10	2	1	2	0	0	---	48
SUM	170	106	1	83	38	34	108	12	76	46	674

Table 5.8. Embedded observed probability matrix for the Coarse/Fine-grained Intercalated Facies Association

	1	2	3	4	5a	5b	6a	6b	7	8
1	---	0.012	0	0.229	0.096	0.108	0.217	0.018	0.240	0.078
2	0.028	---	0.009	0.067	0.067	0.096	0.288	0.057	0.211	0.173
3	0	1.00	---	0	0	0	0	0	0	0
4	0.361	0.120	0	---	0.036	0	0.350	0	0.060	0.072
5a	0.447	0.316	0	0.105	---	0	0.079	0	0	0.052
5b	0.545	0.181	0	0.090	0	---	0.090	0	0.090	0
6a	0.405	0.360	0	0.117	0.027	0.009	---	0	0.036	0.045
6b	0.583	0.166	0	0	0	0	0	---	0.166	0.083
7	0.397	0.243	0	0.102	0.089	0.051	0.064	0.038	---	0.012
8	0.396	0.291	0	0.208	0.041	0.021	0.041	0	0	---

Table 5.9. Embedded random probability matrix for the Coarse/Fine-grained Intercalated Facies Association

	1	2	3	4	5a	5b	6a	6b	7	8
1	---	0.219	0.002	0.164	0.070	0.062	0.226	0.021	0.149	0.086
2	0.349	---	0.001	0.137	0.058	0.052	0.188	0.017	0.124	0.072
3	0.296	0.154	---	0.116	0.049	0.044	0.159	0.015	0.105	0.060
4	0.334	0.174	0.001	---	0.056	0.049	0.180	0.017	0.119	0.068
5a	0.311	0.162	0.001	0.122	---	0.046	0.167	0.016	0.110	0.064
5b	0.309	0.161	0.001	0.121	0.051	---	0.166	0.016	0.109	0.063
6a	0.351	0.183	0.001	0.137	0.058	0.052	---	0.018	0.125	0.072
6b	0.300	0.156	0.001	0.117	0.050	0.044	0.161	---	0.106	0.061
7	0.330	0.172	0.001	0.129	0.055	0.049	0.178	0.016	---	0.067
8	0.315	0.164	0.001	0.123	0.052	0.046	0.169	0.016	0.112	---

Table 5.10. Embedded difference matrix for the Coarse/Fine-grained Intercalated Facies Association

	1	2	3	4	5a	5b	6a	6b	7	8
1	---	-0.210	-0.001	+0.065	+0.026	+0.046	-0.009	-0.003	+0.091	-0.008
2	-0.321	---	+0.007	-0.070	+0.009	+0.044	+0.100	+0.040	+0.087	+0.101
3	-0.296	+0.846	---	-0.116	-0.049	-0.044	-0.159	-0.015	-0.105	-0.060
4	+0.027	-0.054	-0.001	---	-0.020	-0.049	+0.170	-0.017	-0.059	+0.004
5a	+0.136	+0.154	-0.001	-0.017	---	-0.046	-0.088	-0.016	-0.110	-0.012
5b	+0.236	+0.020	-0.001	-0.031	-0.051	---	-0.076	-0.016	-0.019	-0.063
6a	+0.054	+0.177	-0.001	-0.020	-0.031	-0.043	---	-0.018	-0.089	-0.027
6b	+0.283	+0.010	-0.001	-0.117	-0.050	-0.044	-0.161	---	+0.060	+0.022
7	+0.067	+0.071	-0.001	-0.027	+0.034	+0.002	-0.114	+0.022	---	-0.055
8	+0.081	+0.127	-0.001	+0.085	-0.011	-0.025	-0.128	-0.016	-0.112	---

Table 5.11. Non-embedded tally matrix for outcrop A.

	1	2	3	4	5a	5b	6a	6b	7	8	SUM
1	27	6	0	16	17	2	14	0	1	27	110
2	6	0	0	12	20	1	4	0	0	29	72
3	0	0	0	0	0	0	0	0	0	0	
4	17	13	0	8	8	0	1	0	0	10	57
5a	19	15	0	8	27	0	7	0	0	15	91
5b	1	2	0	0	0	0	1	0	0	4	8
6a	13	7	0	4	9	0	6	0	0	10	49
6b	0	0	0	0	0	0	0	0	0	0	0
7	0	0	0	0	0	1	0	0	1	0	2
8	24	25	0	10	14	5	16	0	0	50	144
SUM	107	68	0	58	95	9	49	0	2	145	533

Table 5.12. Non-embedded observed probability matrix for outcrop A.

	1	2	3	4	5a	5b	6a	6b	7	8
1	0.245	0.054	0	0.145	0.154	0.018	0.127	0	0.010	0.245
2	0.083	0	0	0.166	0.277	0.014	0.055	0	0	0.403
3	0	0	0	0	0	0	0	0	0	0
4	0.298	0.228	0	0.140	0.140	0	0.017	0	0	0.175
5a	0.208	0.165	0	0.088	0.297	0	0.077	0	0	0.165
5b	0.125	0.250	0	0	0	0	0.125	0	0	0.500
6a	0.265	0.143	0	0.082	0.184	0	0.122	0	0	0.204
6b	0	0	0	0	0	0	0	0	0	0
7	0	0	0	0	0	0.500	0	0	0.500	0
8	0.167	0.173	0	0.069	0.097	0.035	0.111	0	0	0.347

Table 5.13. Non-embedded random probability matrix for outcrop A.

	1	2	3	4	5a	5b	6a	6b	7	8
1	0.200	0.127	0	0.108	0.178	0.016	0.091	0	0.003	0.272
2	0.200	0.127	0	0.108	0.178	0.016	0.091	0	0.003	0.272
3	0	0	0	0	0	0	0	0	0	0
4	0.200	0.127	0	0.108	0.178	0.016	0.091	0	0.003	0.272
5a	0.200	0.127	0	0.108	0.178	0.016	0.091	0	0.003	0.272
5b	0.200	0.127	0	0.108	0.178	0.016	0.091	0	0.003	0.272
6a	0.200	0.127	0	0.108	0.178	0.016	0.091	0	0.003	0.272
6b	0	0	0	0	0	0	0	0	0	0
7	0.200	0.127	0	0.108	0.178	0.016	0.091	0	0.003	0.272
8	0.200	0.127	0	0.108	0.178	0.016	0.091	0	0.003	0.272

Table 5.14. Non-embedded difference matrix for outcrop A.

	1	2	3	4	5a	5b	6a	6b	7	8
1	+0.045	-0.073	0	+0.037	-0.024	+0.002	+0.036	0	+0.007	-0.027
2	-0.117	-0.127	0	+0.058	+0.099	-0.002	-0.036	0	-0.003	+0.131
3	0	0	0	0	0	0	0	0	0	0
4	+0.098	+0.101	0	+0.032	-0.038	-0.016	-0.074	0	-0.003	-0.097
5a	+0.008	+0.038	0	-0.020	+0.119	-0.016	-0.014	0	-0.003	-0.107
5b	-0.075	+0.123	0	-0.108	-0.178	-0.016	+0.034	0	-0.003	+0.228
6a	+0.065	-0.016	0	-0.026	+0.006	-0.016	+0.031	0	-0.003	-0.068
6b	0	0	0	0	0	0	0	0	0	0
7	-0.200	-0.127	0	-0.108	-0.178	+0.484	-0.091	0	+0.497	-0.272
8	-0.033	+0.046	0	-0.038	-0.081	+0.019	+0.020	0	-0.003	+0.075

Table 5.15. Embedded tally matrix for outcrop B.

	1	2	3	4	5a	5b	6a	6b	7	8	SUM
1	---	0	0	24	7	5	23	1	12	4	76
2	0	---	0	4	1	2	12	1	7	5	31
3	0	0	---	0	0	0	0	0	0	0	0
4	18	4	0	---	1	0	23	0	2	3	51
5a	9	3	0	2	---	0	3	0	0	2	19
5b	5	2	0	1	0	---	1	0	1	0	10
6a	27	16	0	10	3	1	---	0	4	3	64
6b	0	1	0	0	0	0	0	---	2	0	3
7	11	2	0	5	6	1	2	2	---	0	29
8	8	2	0	6	2	0	1	0	0	---	19
SUM	78	30	0	52	20	9	65	3	28	17	302

Table 5.16. Embedded observed probability matrix for outcrop B.

	1	2	3	4	5a	5b	6a	6b	7	8
1	---	0	0	0.316	0.092	0.066	0.303	0.013	0.158	0.053
2	0	---	0	0.129	0.032	0.064	0.387	0	0.226	0.161
3	0	0	---	0	0	0	0	0	0	0
4	0.353	0.078	0	---	0.020	0	0.451	0	0.040	0.059
5a	0.473	0.158	0	0.105	---	0	0.158	0	0	0.105
5b	0.500	0.200	0	0.100	0	---	0.100	0	0.100	0
6a	0.422	0.250	0	0.156	0.047	0.015	---	0	0.063	0.047
6b	0	0.330	0	0	0	0	0	---	0.667	0
7	0.379	0.069	0	0.172	0.207	0.034	0.069	0.069	---	0
8	0.421	0.105	0	0.316	0.105	0	0.053	0	0	---

Table 5.17. Embedded random probability matrix for outcrop B.

	1	2	3	4	5a	5b	6a	6b	7	8
1	---	0.126	0	0.239	0.081	0.035	0.320	0.012	0.117	0.069
2	0.326	---	0	0.184	0.063	0.027	0.247	0.009	0.090	0.053
3	0	0	---	0	0	0	0	0	0	0
4	0.356	0.107	0	---	0.068	0.030	0.271	0.010	0.100	0.060
5a	0.315	0.090	0	0.178	---	0.026	0.239	0.009	0.087	0.051
5b	0.304	0.091	0	0.172	0.058	---	0.231	0.008	0.085	0.050
6a	0.383	0.115	0	0.217	0.074	0.032	---	0.010	0.106	0.063
6b	0.300	0.090	0	0.170	0.057	0.025	0.227	---	0.083	0.050
7	0.323	0.097	0	0.183	0.062	0.027	0.245	0.009	---	0.053
8	0.312	0.094	0	0.176	0.060	0.026	0.237	0.008	0.087	---

Table 5.18. Embedded difference matrix for outcrop B.

	1	2	3	4	5a	5b	6a	6b	7	8
1	---	-0.126	0	+0.077	+0.011	+0.030	-0.017	+0.001	+0.041	-0.016
2	-0.326	---	0	-0.055	-0.030	+0.036	+0.140	-0.009	+0.136	+0.108
3	0	0	---	0	0	0	0	0	0	0
4	-0.003	-0.029	0	---	-0.048	-0.030	+0.180	-0.010	-0.060	-0.001
5a	+0.158	+0.068	0	-0.073	---	-0.026	-0.081	-0.009	-0.087	+0.054
5b	+0.196	+0.109	0	-0.072	-0.058	---	-0.131	-0.008	+0.015	-0.050
6a	+0.039	+0.135	0	-0.061	-0.027	-0.016	---	-0.01	-0.043	-0.016
6b	-0.300	+0.240	0	-0.170	-0.057	-0.025	-0.227	---	+0.584	-0.050
7	+0.056	-0.028	0	-0.011	+0.145	+0.007	-0.176	+0.060	---	-0.053
8	+0.109	+0.011	0	+0.140	+0.045	-0.026	-0.184	-0.008	-0.087	---

Table 5.19. Embedded tally matrix for outcrop C.

	1	2	3	4	5a	5b	6a	6b	7	8	SUM
1	---	0	0	9	4	10	8	1	23	6	61
2	0	---	0	2	6	6	16	5	13	10	58
3	0	0	---	0	0	0	0	0	0	0	0
4	5	6	0	---	2	0	5	0	2	2	22
5a	3	9	0	2	---	0	0	0	0	0	14
5b	12	4	0	1	0	---	1	0	2	0	20
6a	15	17	0	3	0	0	---	0	0	2	37
6b	5	1	0	0	0	0	0	---	0	1	7
7	17	13	0	2	1	3	3	1	---	1	41
8	8	10	0	2	0	1	1	0	0	---	22
SUM	65	60	0	21	13	20	34	7	40	22	282

Table 5.20. Embedded observed probability matrix for outcrop C.

	1	2	3	4	5a	5b	6a	6b	7	8
1	---	0	0	0.147	0.065	0.164	0.131	0.016	0.377	0.098
2	0	---	0	0.034	0.103	0.103	0.276	0.086	0.224	0.172
3	0	0	---	0	0	0	0	0	0	0
4	0.227	0.272	0	---	0.030	0	0.227	0	0.090	0.090
5a	0.214	0.643	0	0.143	---	0	0	0	0	0
5b	0.600	0.200	0	0.050	0	---	0.050	0	0.100	0
6a	0.405	0.459	0	0.081	0	0	---	0	0	0.054
6b	0.714	0.143	0	0	0	0	0	---	0	0.143
7	0.415	0.317	0	0.049	0.024	0.073	0.073	0.024	---	0.024
8	0.363	0.454	0	0.091	0	0.045	0.045	0	0	---

Table 5.21. Embedded random probability matrix for outcrop C.

	1	2	3	4	5a	5b	6a	6b	7	8
1	---	0.308	0	0.090	0.054	0.085	0.155	0.028	0.185	0.094
2	0.331	---	0	0.087	0.052	0.082	0.149	0.027	0.179	0.091
3	0	0	---	0	0	0	0	0	0	0
4	0.273	0.246	0	---	0.043	0.068	0.123	0.023	0.148	0.075
5a	0.265	0.239	0	0.069	---	0.066	0.120	0.022	0.144	0.073
5b	0.272	0.245	0	0.071	0.043	---	0.123	0.023	0.147	0.075
6a	0.288	0.259	0	0.075	0.045	0.071	---	0.024	0.156	0.079
6b	0.260	0.234	0	0.068	0.041	0.065	0.118	---	0.141	0.072
7	0.296	0.266	0	0.078	0.047	0.073	0.134	0.024	---	0.081
8	0.274	0.247	0	0.072	0.043	0.068	0.124	0.023	0.148	---

Table 5.22. Embedded difference matrix for outcrop C.

	1	2	3	4	5a	5b	6a	6b	7	8
1	---	-0.308	0	+0.057	+0.011	+0.079	-0.024	-0.012	+0.192	+0.004
2	-0.331	---	0	-0.053	+0.051	+0.021	+0.127	+0.058	+0.045	+0.081
3	0	0	---	0	0	0	0	0	0	0
4	-0.046	+0.026	0	---	+0.047	-0.068	+0.104	-0.023	-0.06	+0.014
5a	-0.051	+0.404	0	+0.074	---	-0.066	-0.120	-0.022	-0.144	-0.073
5b	+0.328	-0.045	0	-0.021	-0.043	---	-0.073	-0.023	-0.047	-0.075
6a	+0.117	+0.200	0	+0.006	-0.045	-0.071	---	-0.024	-0.156	-0.025
6b	+0.454	-0.091	0	-0.068	-0.041	-0.065	-0.118	---	-0.141	+0.071
7	+0.120	+0.051	0	-0.030	-0.023	0	-0.061	-0.001	---	-0.057
8	+0.089	+0.207	0	+0.019	-0.043	-0.023	-0.079	-0.023	-0.148	---

Table 5.23. Non-embedded tally matrix for outcrop D.

	1	2	3	4	5a	5b	6a	6b	7	8	SUM
1	3	0	0	1	0	1	5	1	5	1	17
2	1	0	1	1	0	2	2	1	2	3	13
3	0	1	0	0	0	0	0	0	0	0	1
4	4	0	0	2	0	0	0	0	1	1	8
5a	0	0	0	0	0	0	0	0	0	0	0
5b	1	0	0	1	0	5	1	0	0	0	0
6a	2	6	0	0	0	0	0	0	0	0	8
6b	2	0	0	0	0	0	0	0	0	0	2
7	3	4	0	1	0	0	0	0	0	0	8
8	1	2	0	2	0	0	0	0	0	0	5
SUM	17	13	1	8	0	8	8	2	8	5	70

Table 5.24. Non-embedded observed probability matrix for outcrop D.

	1	2	3	4	5a	5b	6a	6b	7	8
1	0.176	0	0	0.059	0	0.059	0.294	0.059	0.294	0.059
2	0.077	0	0.077	0.077	0	0.154	0.154	0.077	0.154	0.231
3	0	1.000	0	0	0	0	0	0	0	0
4	0.500	0	0	0.250	0	0	0	0	0.125	0.125
5a	0	0	0	0	0	0	0	0	0	0
5b	0.125	0	0	0.125	0	0.625	0.125	0	0	0
6a	0.250	0.750	0	0	0	0	0	0	0	0
6b	1.000	0	0	0	0	0	0	0	0	0
7	0.375	0.500	0	0.125	0	0	0	0	0	0
8	0.200	0.400	0	0.400	0	0	0	0	0	0

Table 5.25. Non-embedded random probability matrix for outcrop D.

	1	2	3	4	5a	5b	6a	6b	7	8
1	0.242	0.185	0.014	0.114	0	0.114	0.114	0.028	0.114	0.071
2	0.242	0.185	0.014	0.114	0	0.114	0.114	0.028	0.114	0.071
3	0.242	0.185	0.014	0.114	0	0.114	0.114	0.028	0.114	0.071
4	0.242	0.185	0.014	0.114	0	0.114	0.114	0.028	0.114	0.071
5a	0.242	0.185	0.014	0.114	0	0.114	0.114	0.028	0.114	0.071
5b	0.242	0.185	0.014	0.114	0	0.114	0.114	0.028	0.114	0.071
6a	0.242	0.185	0.014	0.114	0	0.114	0.114	0.028	0.114	0.071
6b	0.242	0.185	0.014	0.114	0	0.114	0.114	0.028	0.114	0.071
7	0.242	0.185	0.014	0.114	0	0.114	0.114	0.028	0.114	0.071
8	0.242	0.185	0.014	0.114	0	0.114	0.114	0.028	0.114	0.071

Table 5.26. Non-embedded difference matrix for outcrop D.

	1	2	3	4	5a	5b	6a	6b	7	8
1	-0.060	-0.185	-0.014	-0.055	0	-0.055	+0.180	+0.031	+0.180	-0.012
2	-0.165	-0.185	+0.063	-0.037	0	+0.040	+0.040	+0.050	+0.040	+0.160
3	-0.242	+0.815	-0.014	-0.114	0	-0.114	-0.114	-0.028	-0.114	-0.071
4	+0.258	-0.185	-0.014	+0.136	0	-0.114	-0.114	-0.028	+0.011	+0.054
5a	-0.242	-0.185	-0.014	-0.114	0	-0.114	-0.114	-0.028	-0.114	-0.071
5b	-0.117	-0.185	-0.014	+0.011	0	+0.511	+0.011	-0.028	-0.114	-0.071
6a	+0.008	+0.565	-0.014	-0.114	0	-0.114	-0.114	-0.028	-0.114	-0.071
6b	+0.758	-0.185	-0.014	-0.114	0	-0.114	-0.114	-0.028	-0.114	-0.071
7	+0.133	+0.315	-0.014	+0.011	0	-0.114	-0.114	-0.028	-0.114	-0.071
8	-0.042	+0.215	-0.014	+0.286	0	-0.114	-0.114	-0.028	-0.114	-0.071

1 OF/DE

LOCATION OF SECTIONS AT OUTCROP A

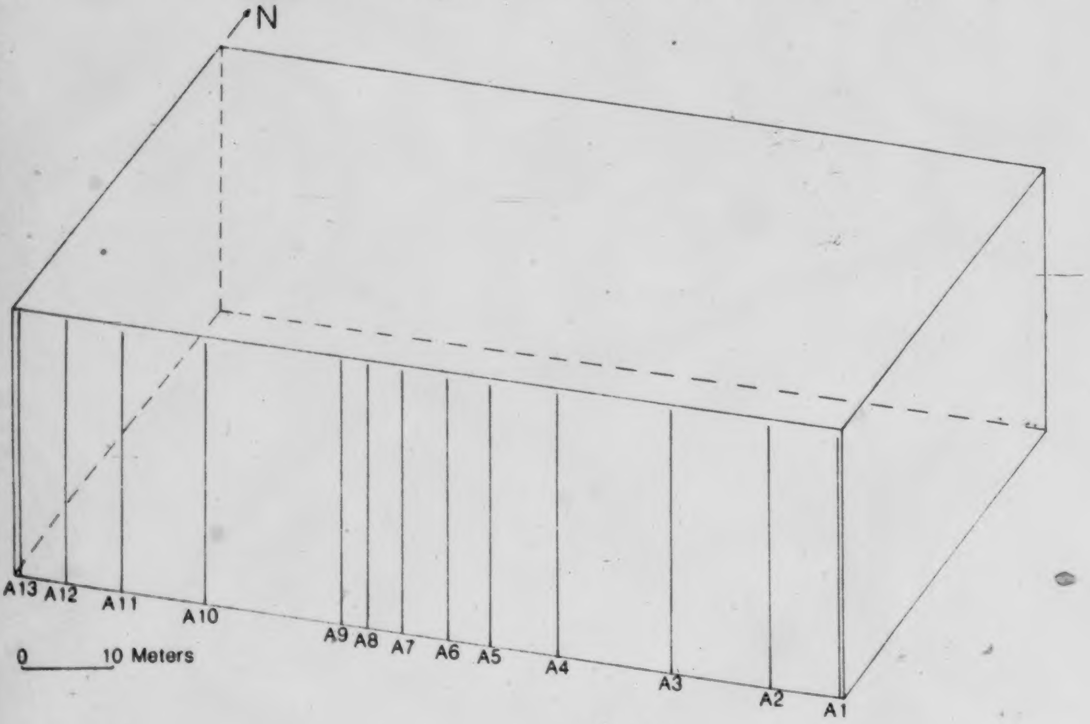
N
A13
A12
A11
A10
A9
A8
A7
A6
A5
A4
A3
A2
A1
0
10 Meters

LOCATION OF SECTIONS AT OUTCROP A

2

OF/DE

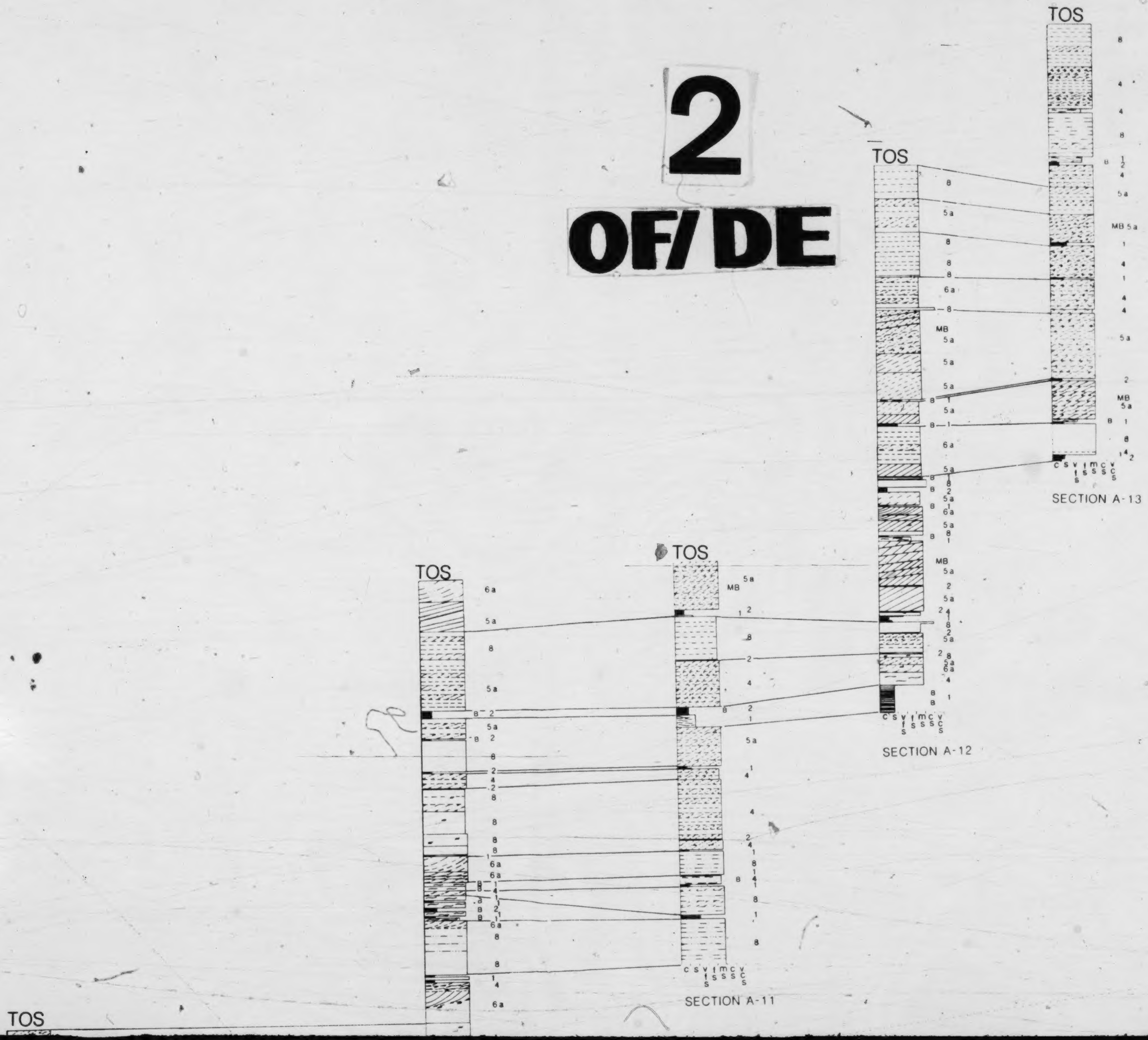
TOS
TOS
TOS
TOS
MB
5a
6a
8
4
1
2
c s vf f m c vc
s s s s s
SECTION A-11
SECTION A-12
SECTION A-13

LOCATION OF SECTIONS AT OUTCROP A

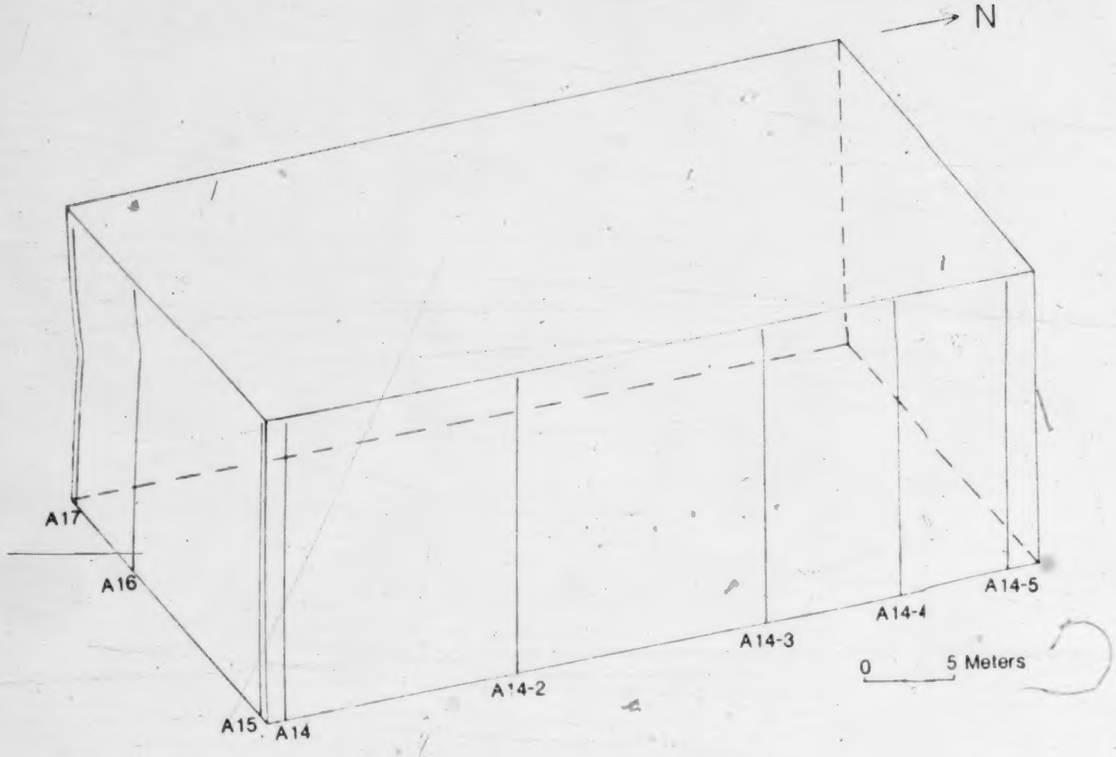
N
A17
A16
A15
A14
A14-2
A14-3
A14-4
A14-5
0 5 Meters

LOCATION OF SECTIONS AT OUTCROP A

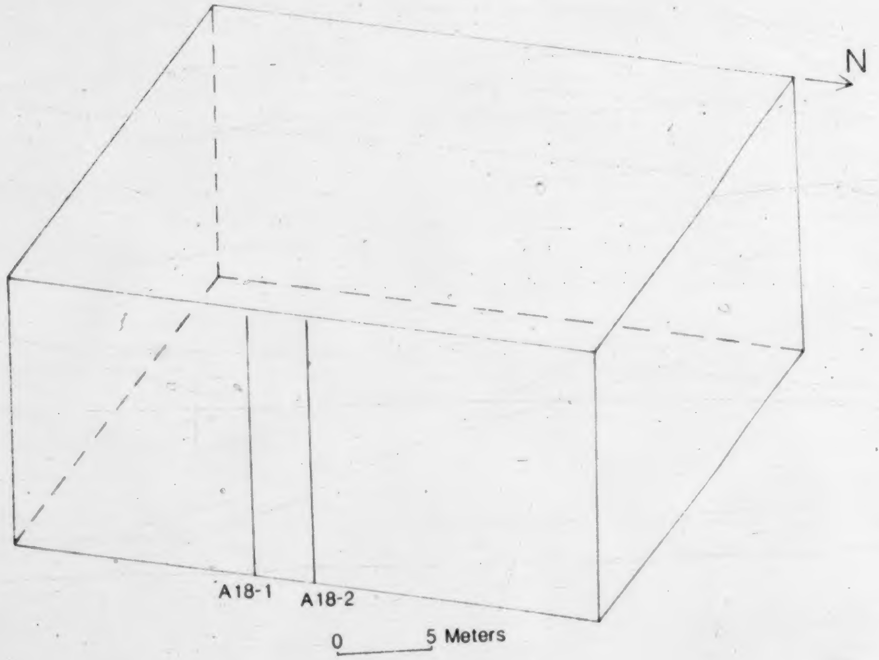
N
A18-1
A18-2
0 5 Meters

LOCATION OF SECTIONS AT OUTCROP A

COARSE-GRAINED FACIES ASSOCIATION

3
OF/DE

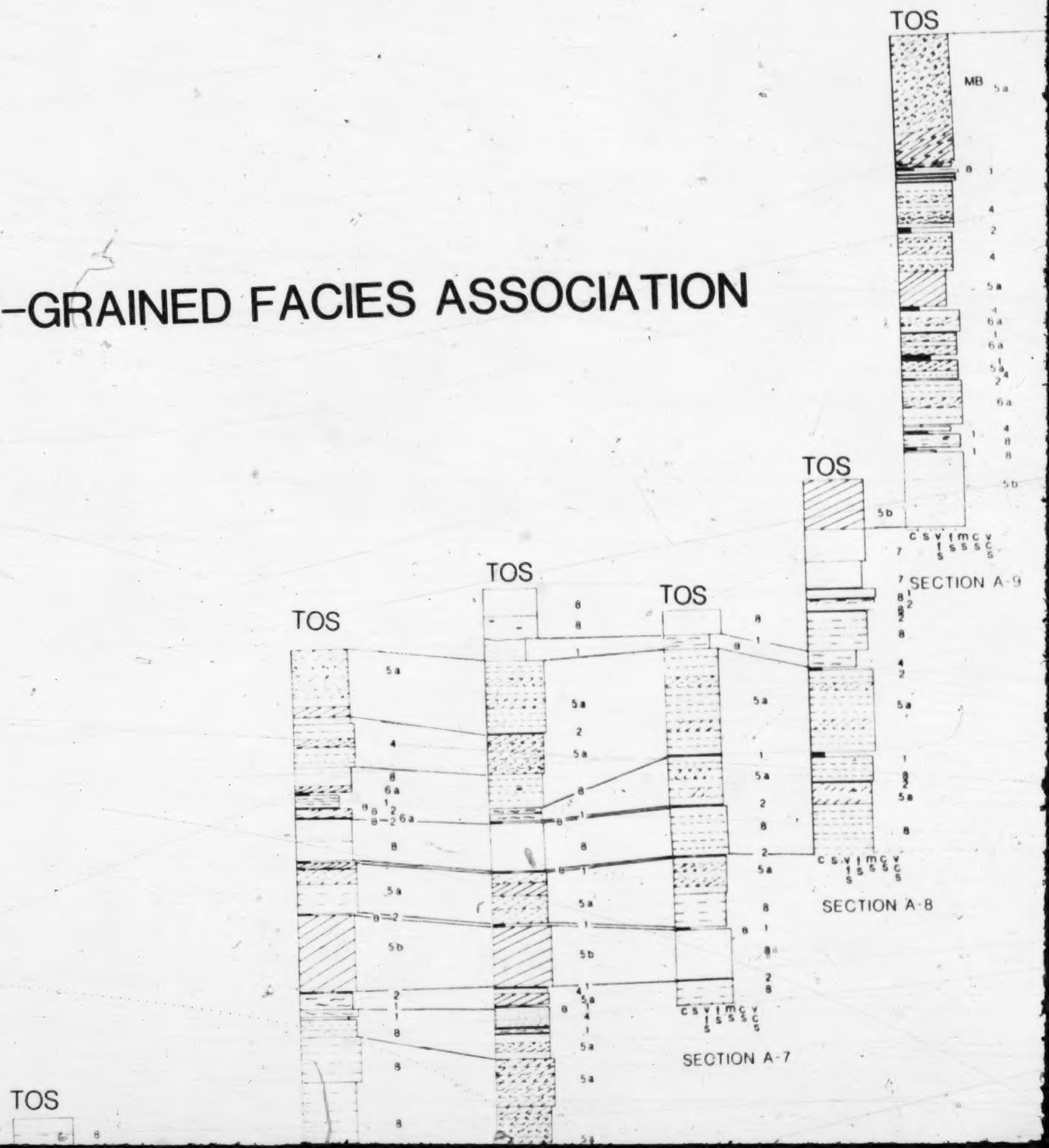
TOS
TOS
TOS
TOS
TOS
TOS
MB
5a
5b
6a
c s v f m c v f s s s c s
SECTION A-9
SECTION A-8
SECTION A-7

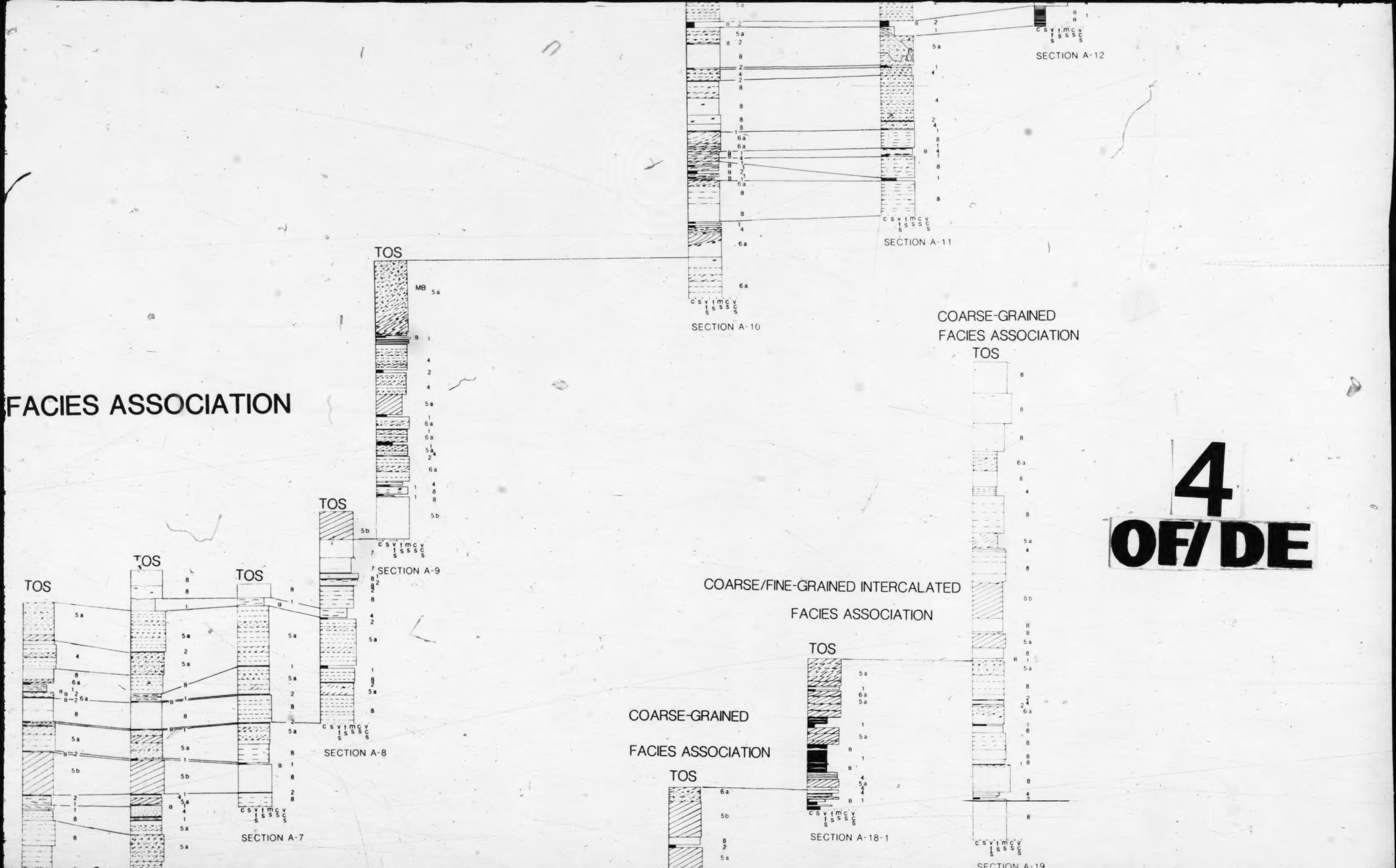
FACIES ASSOCIATION
COARSE-GRAINED FACIES ASSOCIATION
COARSE/FINE-GRAINED INTERCALATED FACIES ASSOCIATION
COARSE-GRAINED FACIES ASSOCIATION
TOS
MB
c s vf f m c vc s s s s
SECTION A-7
SECTION A-8
SECTION A-9
SECTION A-10
SECTION A-11
SECTION A-12
SECTION A-18-1
SECTION A-19
1
2
4
5a
5b
6a
7
8

4
OF/DE

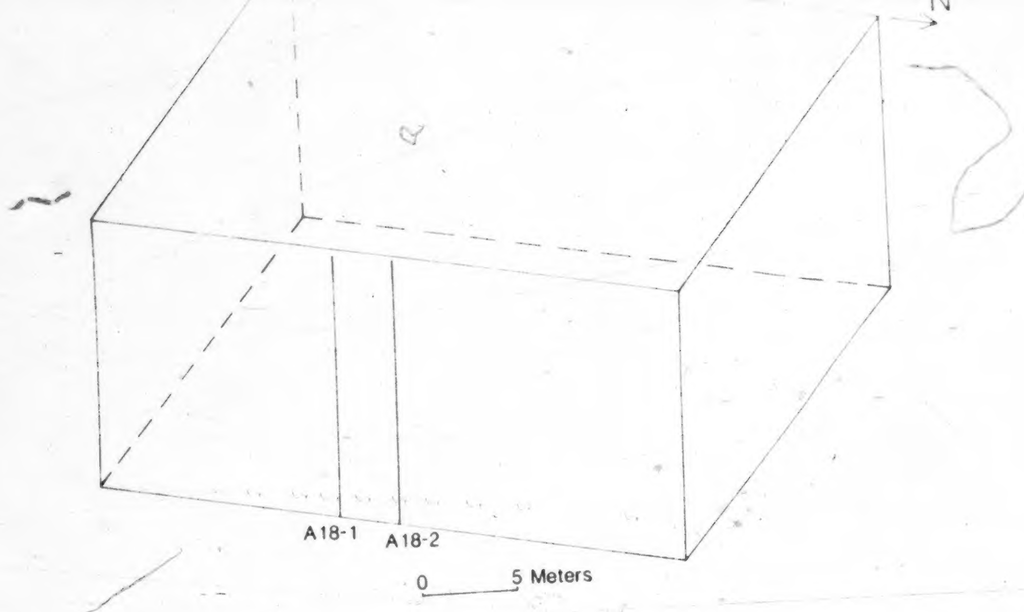
N
A18-1
A18-2
0
5 Meters

LOCATION OF SECTIONS AT OUTCROP A

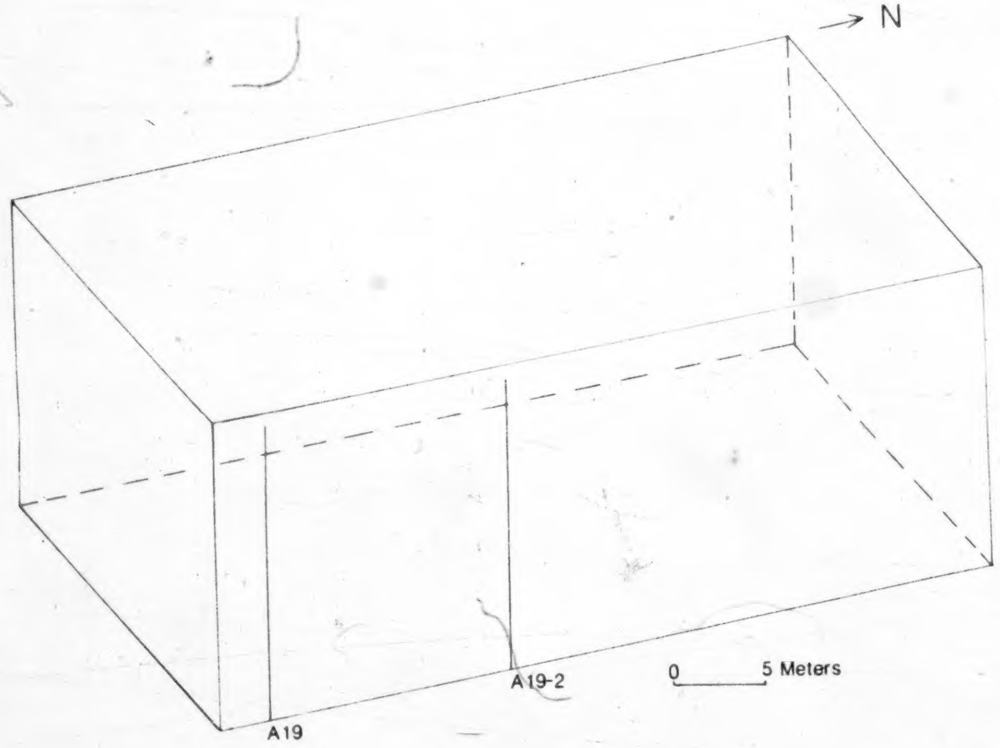
N
A19
A19-2
0
5 Meters

5
OF/DE

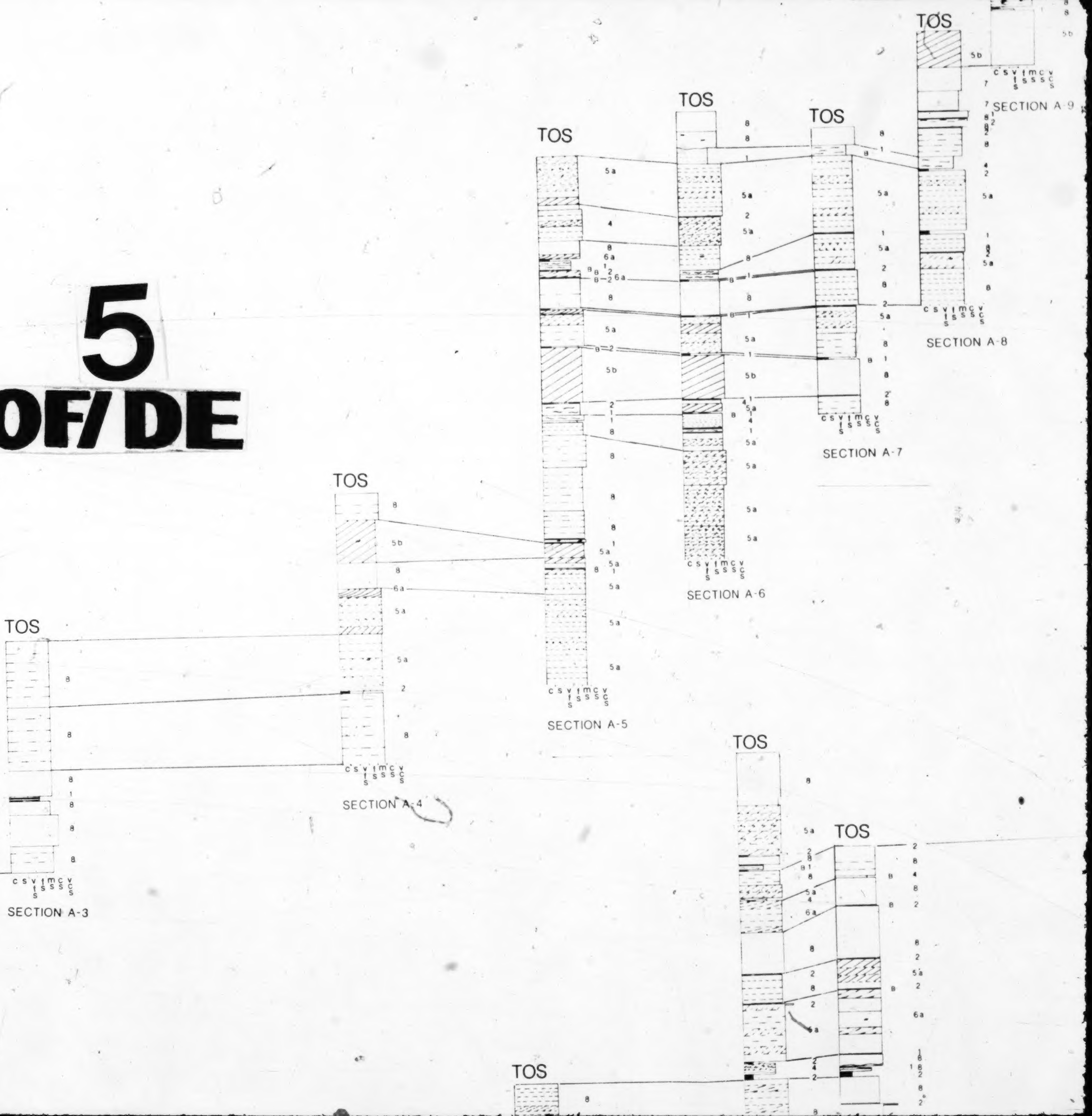
TOS
c s vf f m c vc
s s s s s
5a
5b
6a
8
1
2
4

SECTION A-3

SECTION A-4

SECTION A-5

SECTION A-6

SECTION A-7

SECTION A-8

SECTION A-9

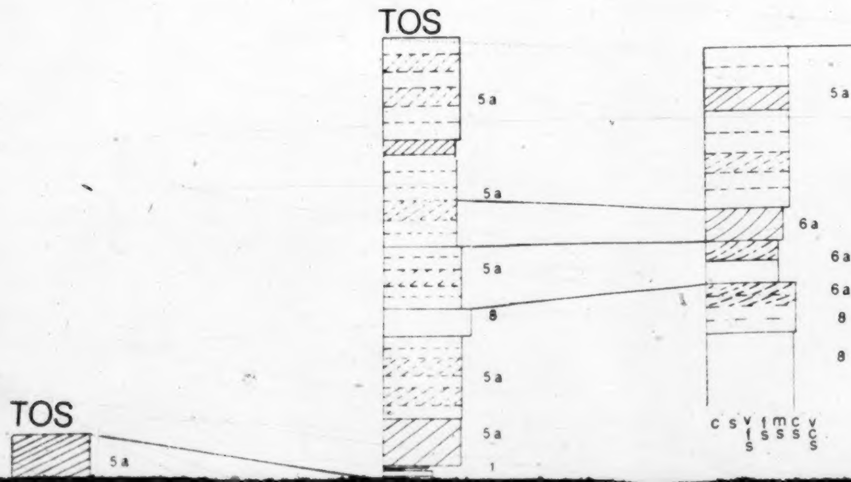
TOS
5a
6a
8
1
c s vf f m c vc
s s s s s

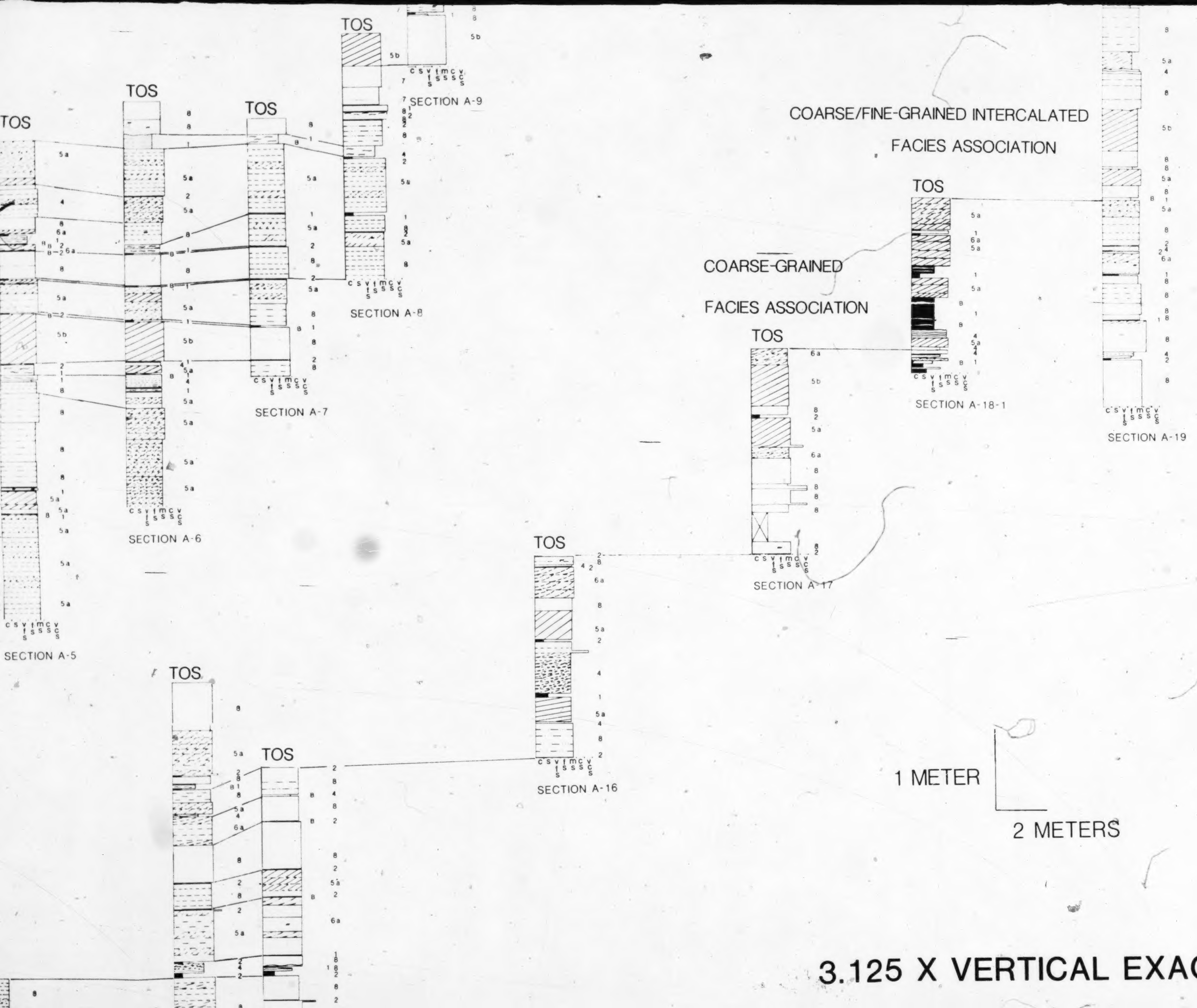
TOS
SECTION A-5
SECTION A-6
SECTION A-7
SECTION A-8
SECTION A-9
SECTION A-16
SECTION A-17
SECTION A-18-1
SECTION A-19
COARSE/FINE-GRAINED INTERCALATED FACIES ASSOCIATION
COARSE-GRAINED FACIES ASSOCIATION
c s vf f m c vc
s s s s s
1 METER
2 METERS

6 OF/DE

3.125 X VERTICAL EXAGGERATION

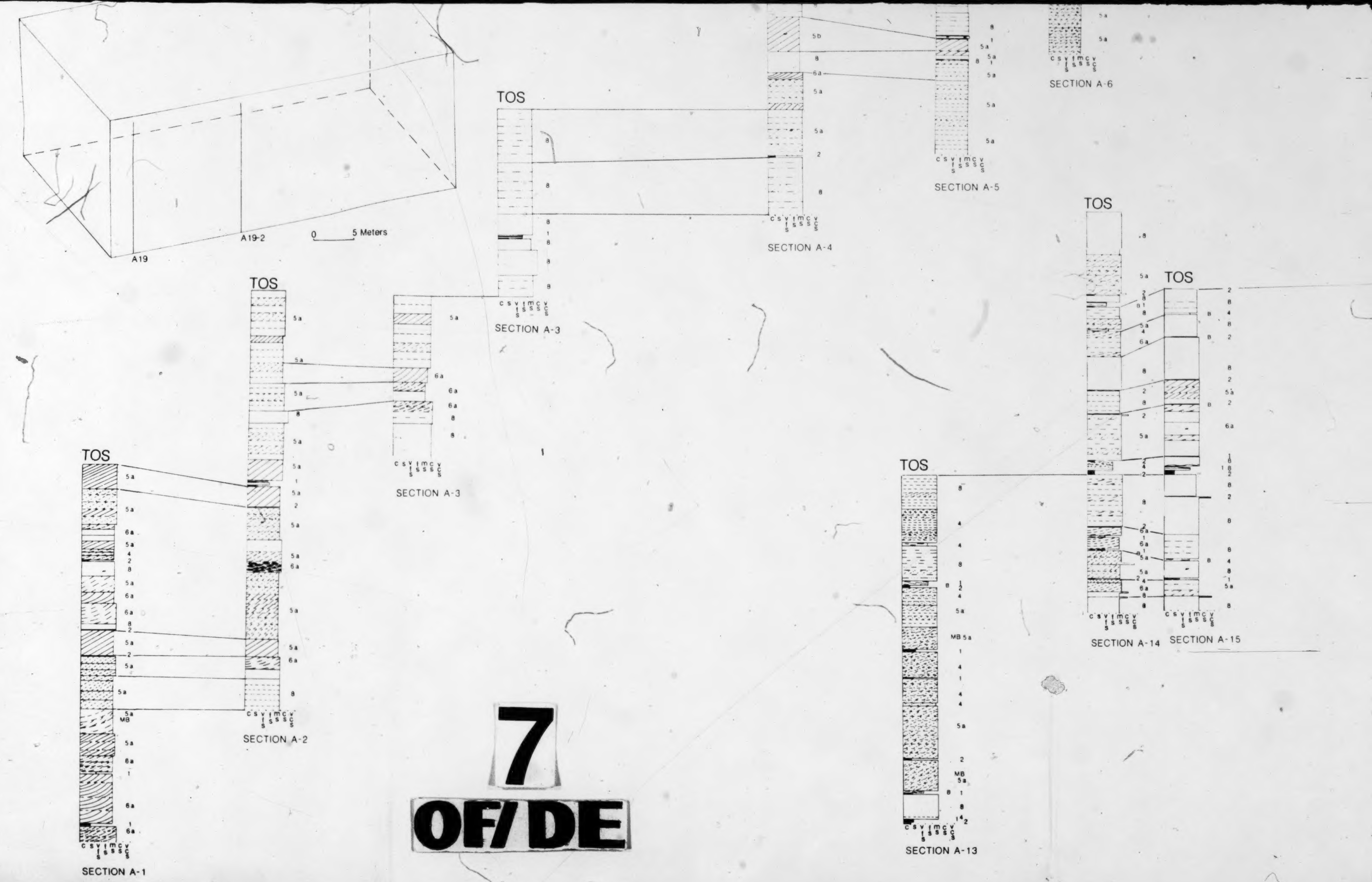
A19
A19-2
0 5 Meters
TOS
SECTION A-1
SECTION A-2
SECTION A-3
SECTION A-3
SECTION A-4
SECTION A-5
SECTION A-6
SECTION A-13
SECTION A-14
SECTION A-15
c s vf f m c vc s s s s s
5a
5b
6a
MB
1
2
4
8

7

OF/DE

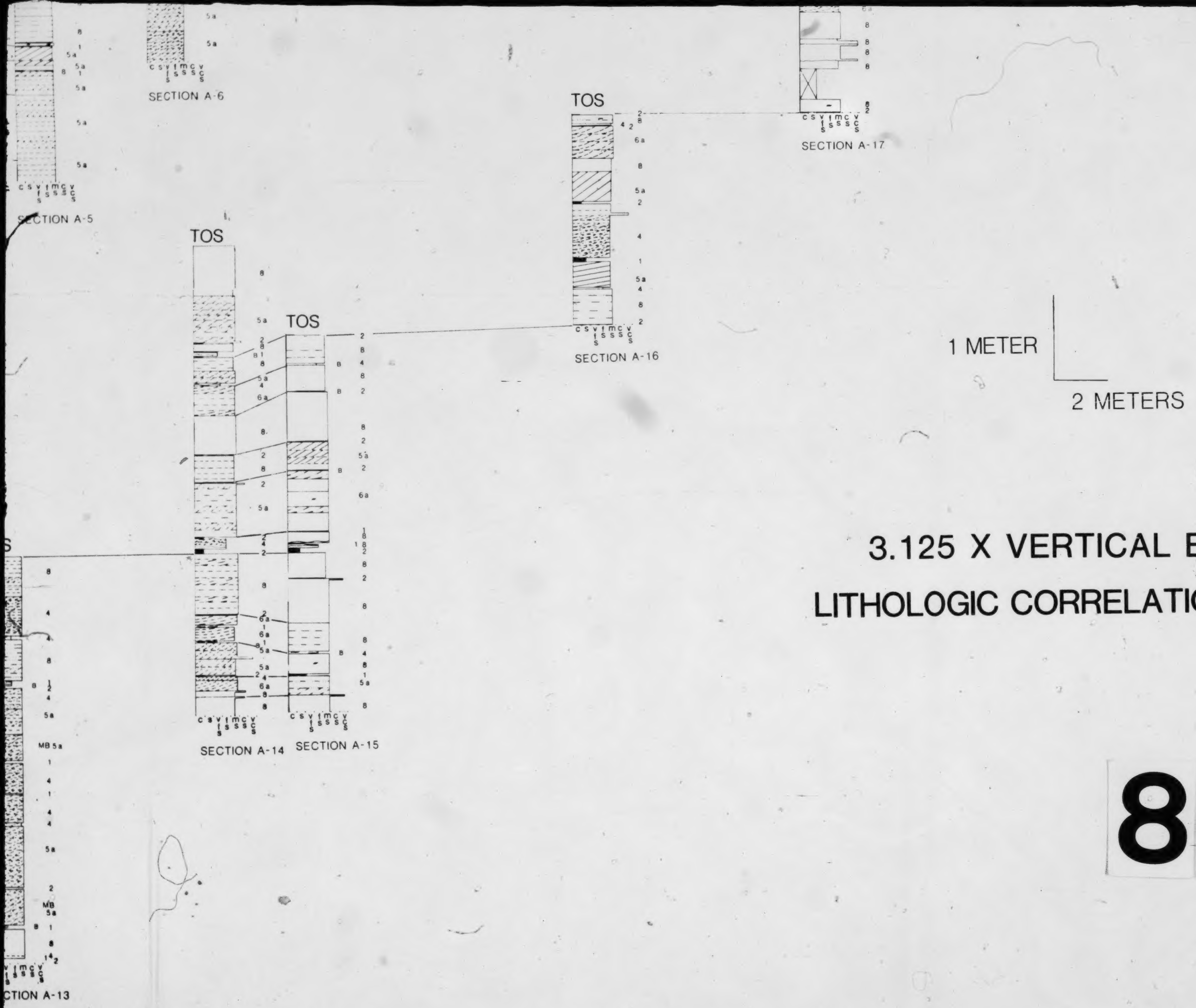
SECTION A-5
SECTION A-6
SECTION A-17
TOS
SECTION A-16
TOS
TOS
SECTION A-14
SECTION A-15
CTION A-13
c s v f m c v
1 METER
2 METERS

3.125 X VERTICAL EXAGGERATION

LITHOLOGIC CORRELATIONS FOR OUTCROP A

8 OF/DE 8

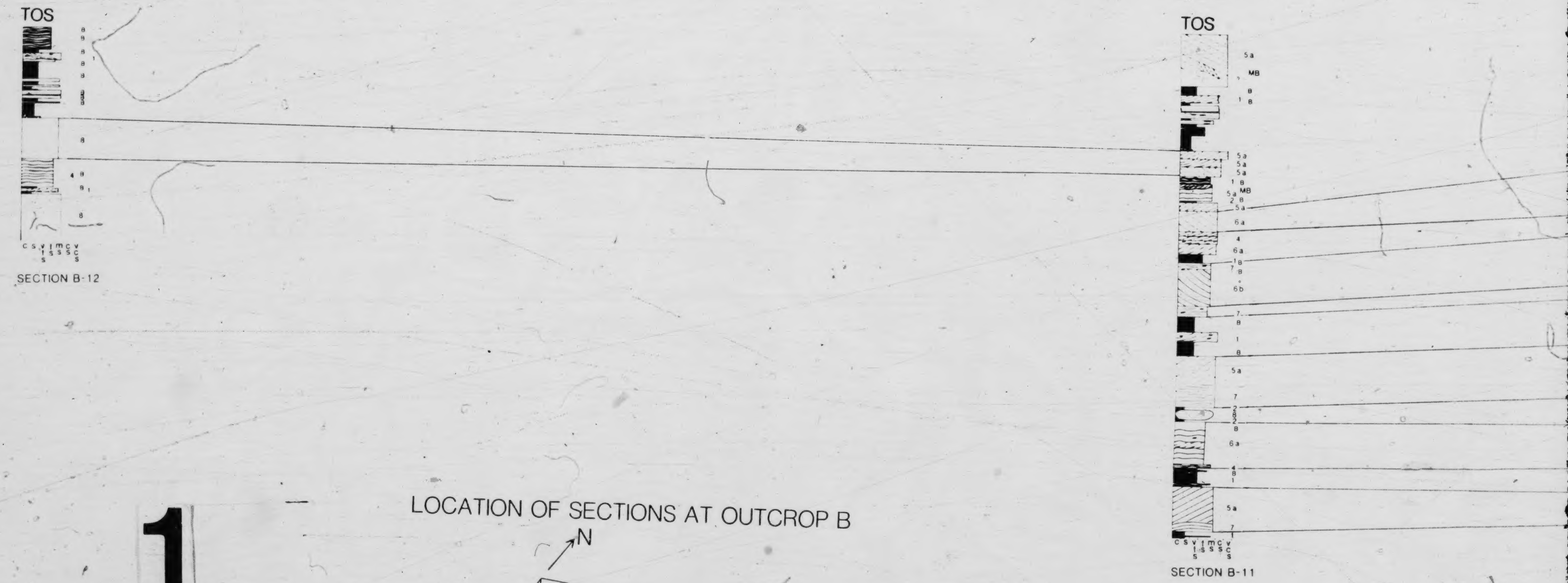
TOS
8
8
8
8
8
8
8
1
8
4 8
8 1
8
c s vf f m c vc
SECTION B-12
TOS
5a
MB
8
1 8
5a
5a
5a
1 8
MB
5a
2 8
5a
6a
4
6a
1 8
7 8
6b
7
8
1
8
5a
7
2
8
2
8
6a
4
8
1
5a
7
c s vf f m c vc
SECTION B-11

LOCATION OF SECTIONS AT OUTCROP B

1

OF/DE

2

OF/DE

COARSE/FINE-GRAINED INTERCALATED FACIES ASSOCIATION

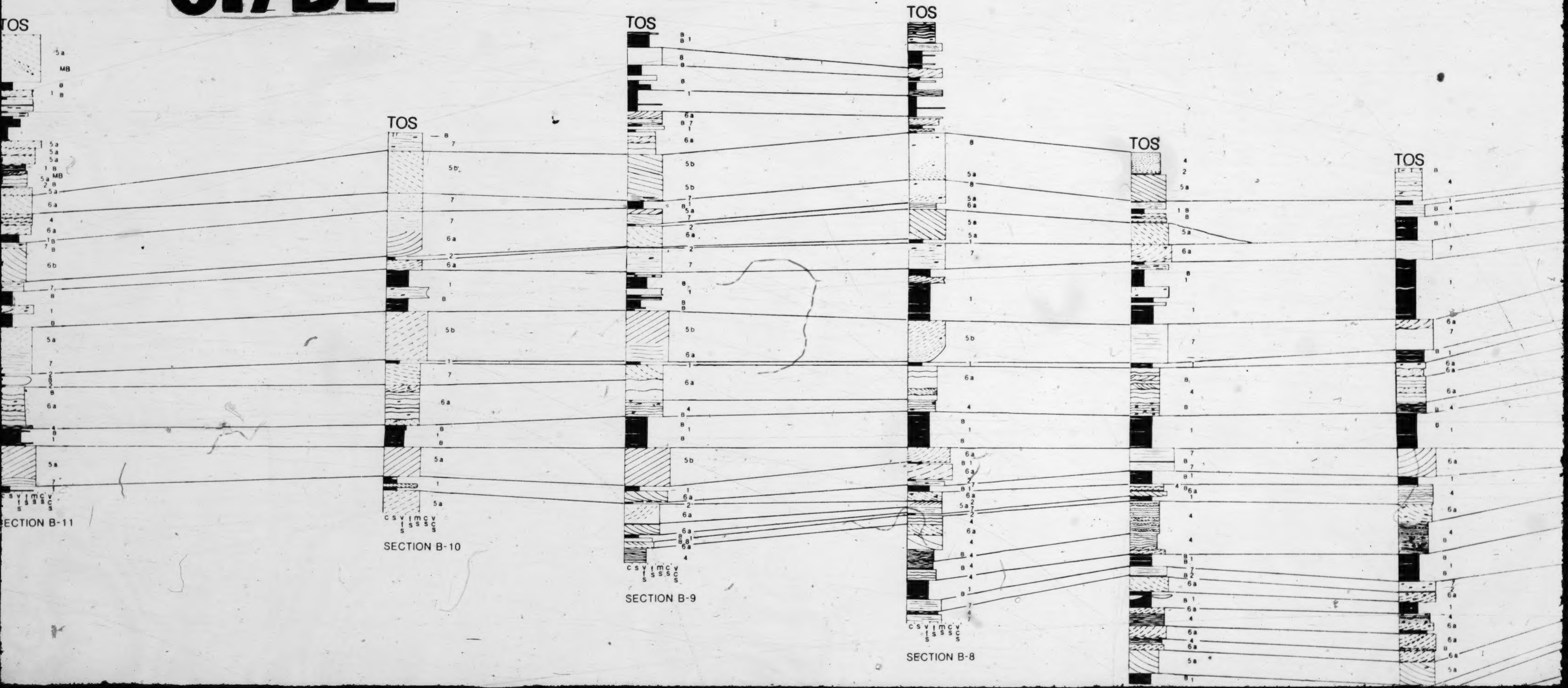
TOS
TOS
TOS
TOS
TOS
TOS
c s vf f m c vc
s s s s s
ECTION B-11
SECTION B-10
SECTION B-9
SECTION B-8
1
2
4
5a
5b
6a
6b
7
8
MB

TERCALATED FACIES ASSOCIATION

3
OF/DE

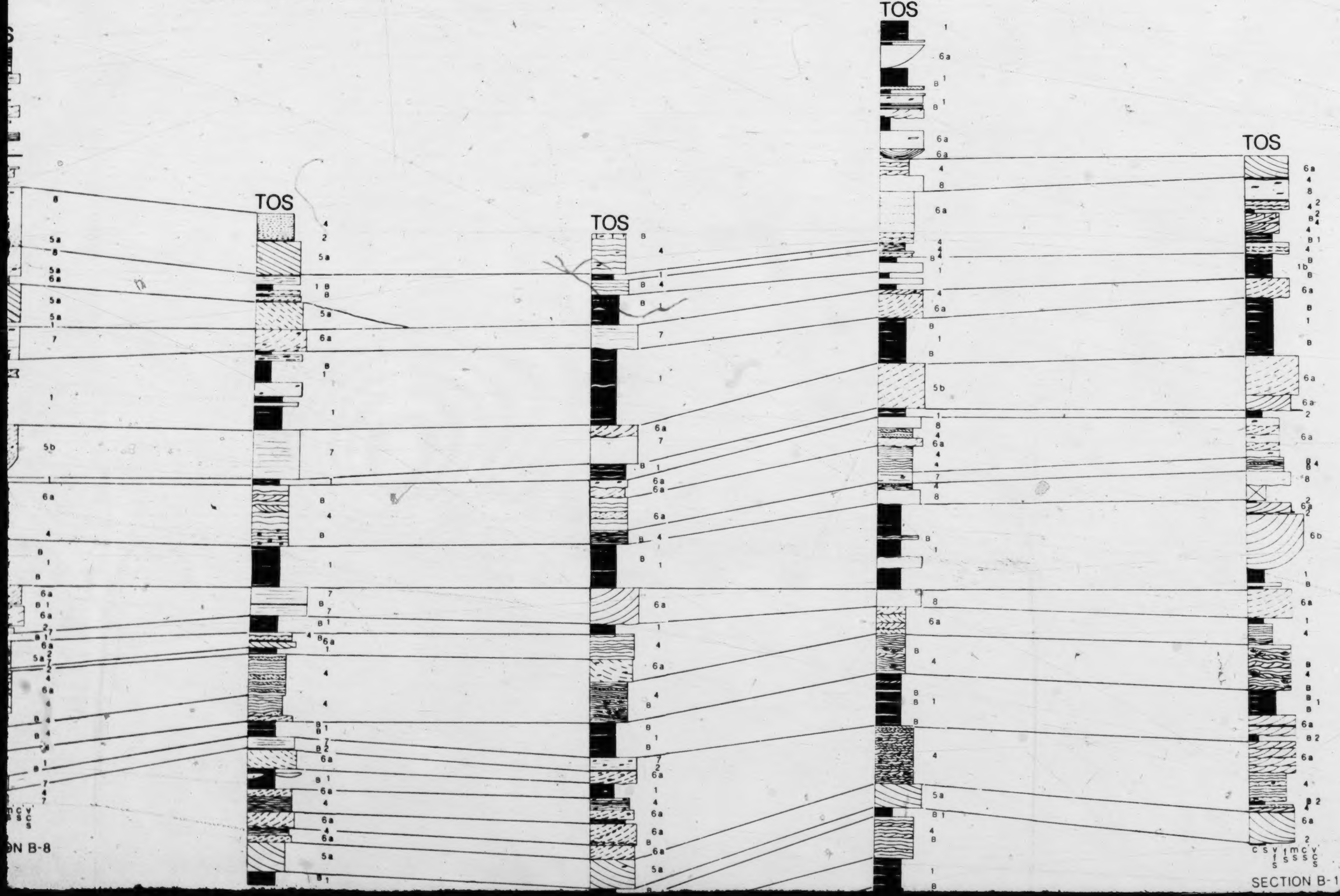
TOS
TOS
TOS
TOS
ON B-8
c s vf f m c vc s s s s s
SECTION B-1

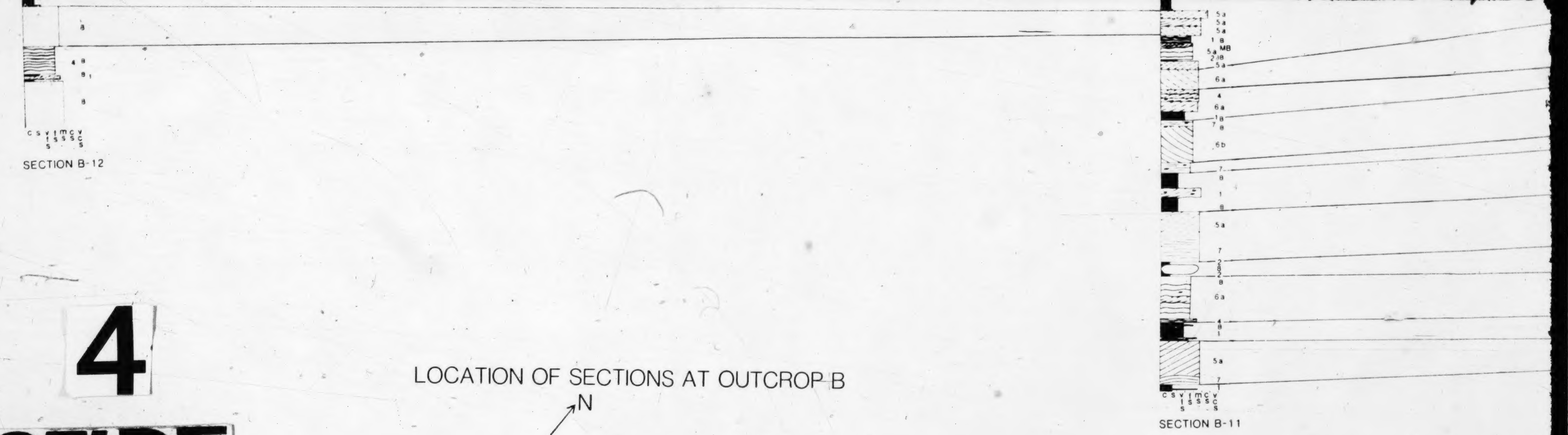
8
4 8
8 1
8
c s vf f m c vc
s s s s s
SECTION B-12
5a
5a
5a
1 8
5a MB
2 8
5a
6a
4
6a
1 8
7 8
6b
7
8
1
8
5a
7
2
8
2
8
6a
4
8
1
5a
7
1
c s vf f m c vc
s s s s s
SECTION B-11

4
OF/DE

LOCATION OF SECTIONS AT OUTCROP B

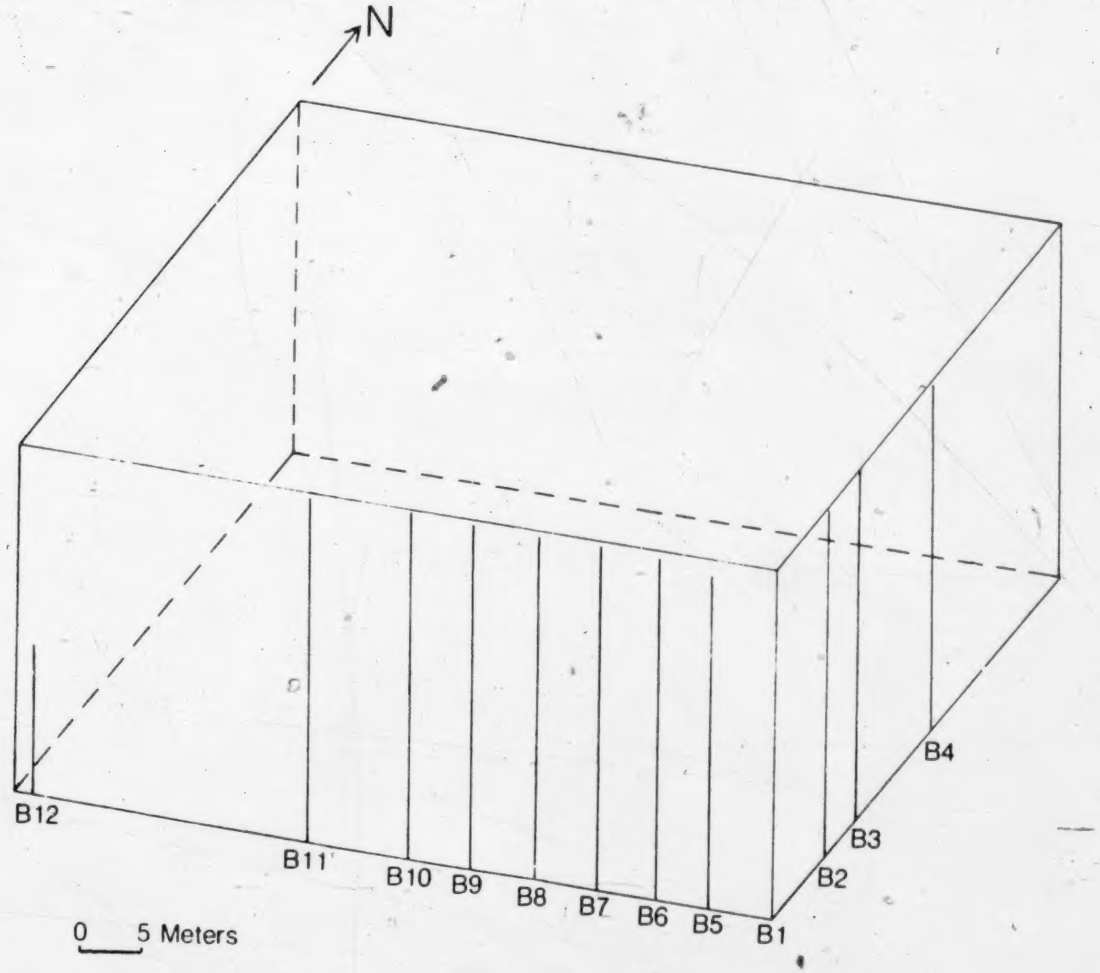
N
B12
B11
B10
B9
B8
B7
B6
B5
B1
B2
B3
B4
0 5 Meters

CORRELATIONS FOR OUTCROP A

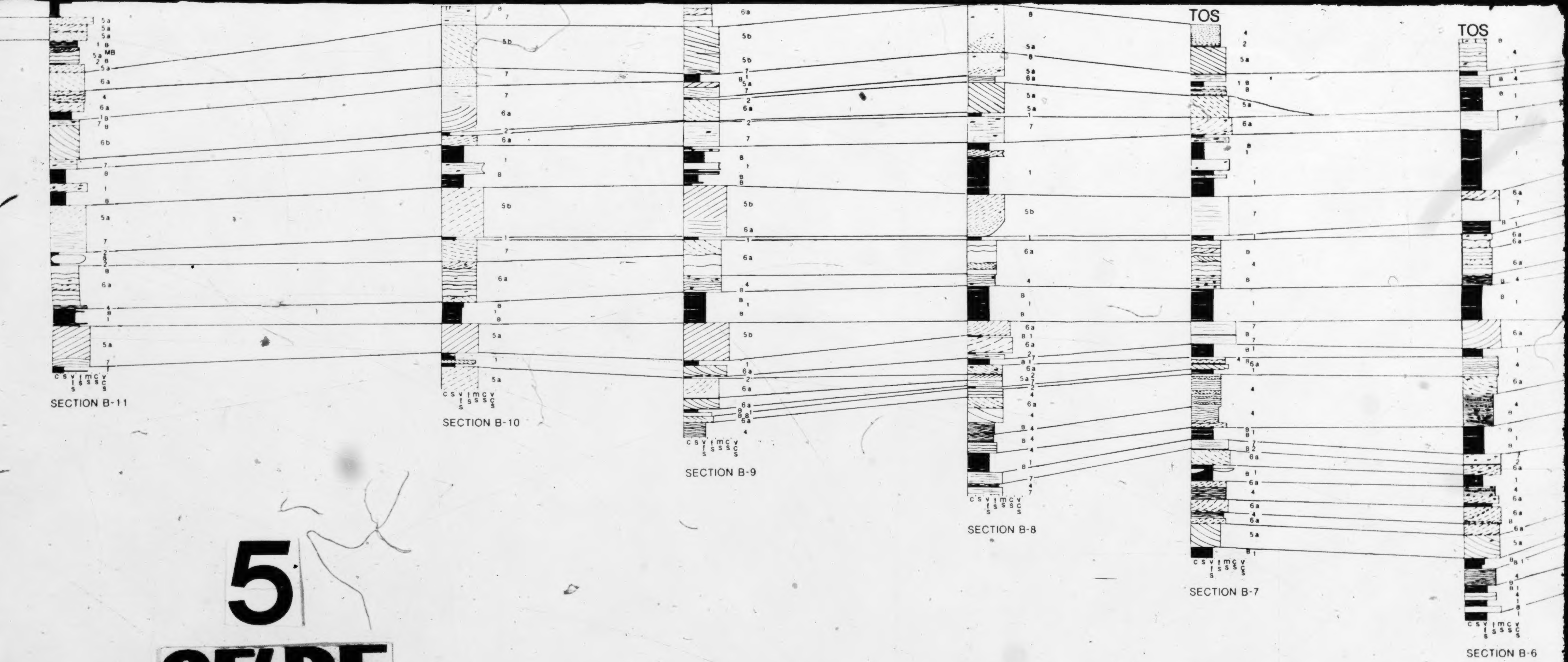
TOS
TOS
c s v f m c v
f s s s c
s s
SECTION B-11
SECTION B-10
SECTION B-9
SECTION B-8
SECTION B-7
SECTION B-6

5

OF/DE

6 OF/DE 6

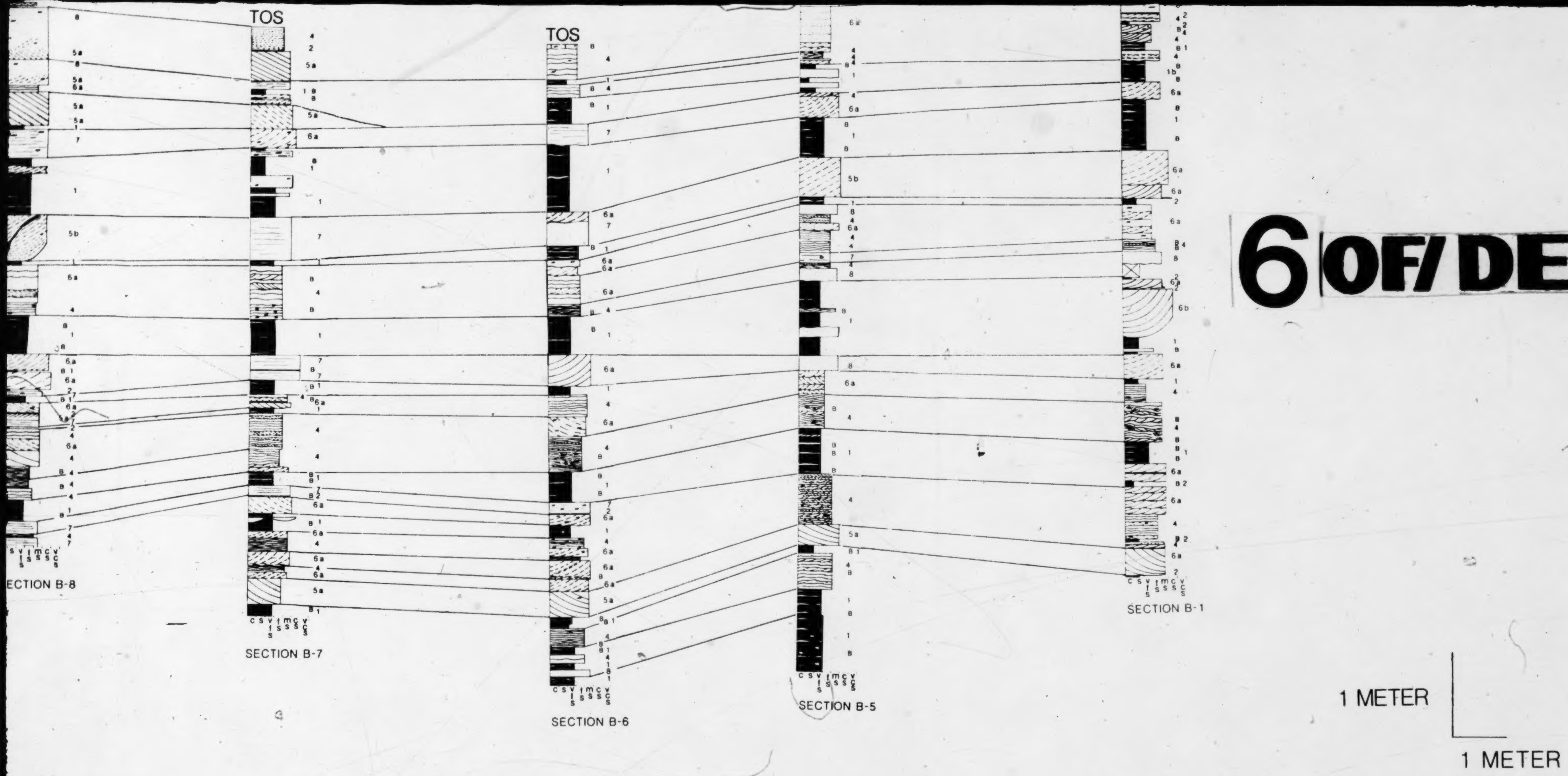
TOS
TOS
c s vf m c vc
f s s s c
s s
ECTION B-8
SECTION B-7
SECTION B-6
SECTION B-5
SECTION B-1
1 METER
1 METER

1.56 X VERTICAL EXAGGERATION

LITHOLOGIC CORRELATIONS FOR OUTCROP B

COARSE/FINE-GRAINED INTERCALATED FACIES ASSOCIATION

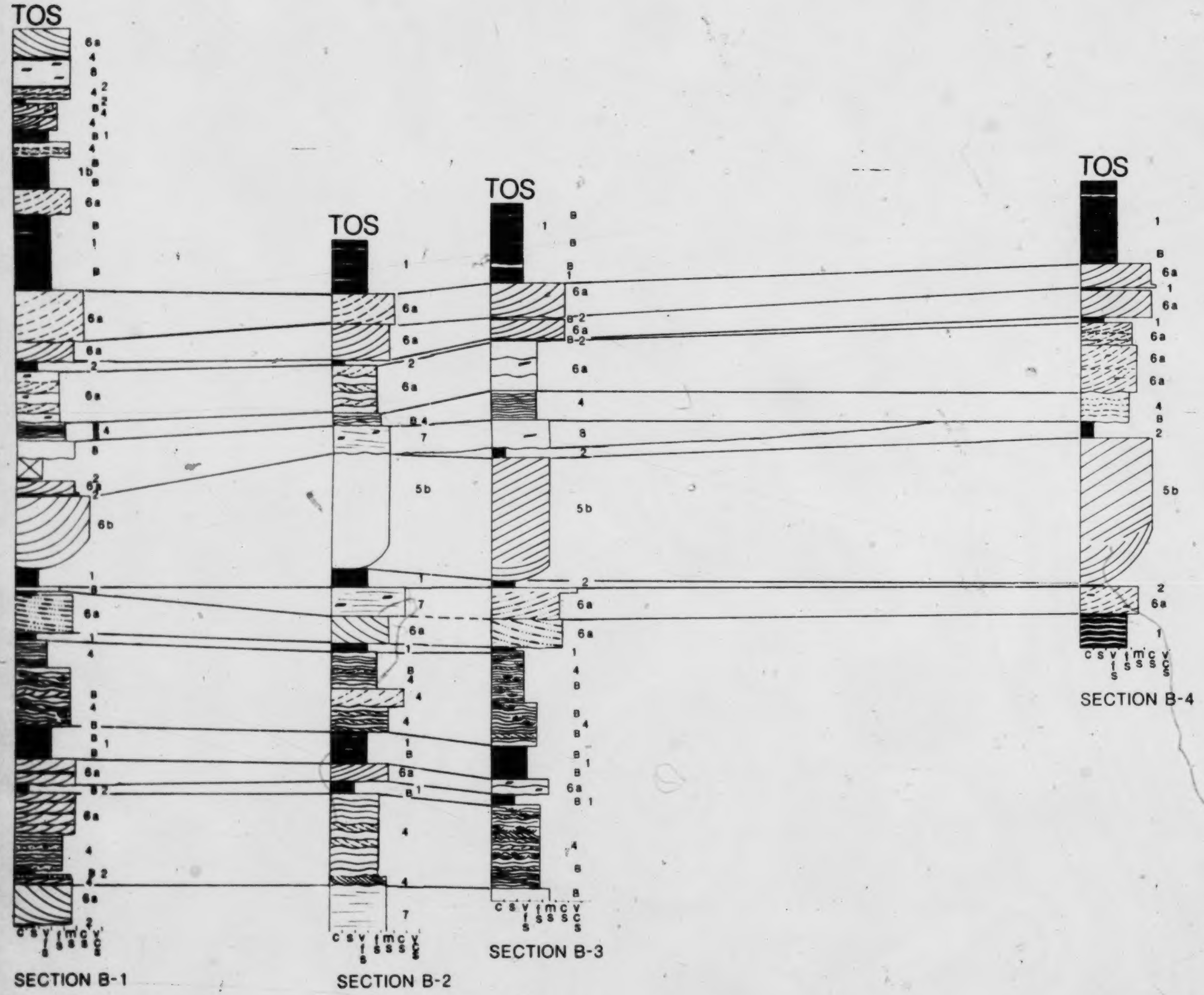
TOS
TOS
TOS
TOS
6a
4
8
1b
5b
6b
7
2
1
c s v f m c v
s s s s c s
SECTION B-1
SECTION B-2
SECTION B-3
SECTION B-4

LOCATION OF SECTIONS AT OUTCROP B

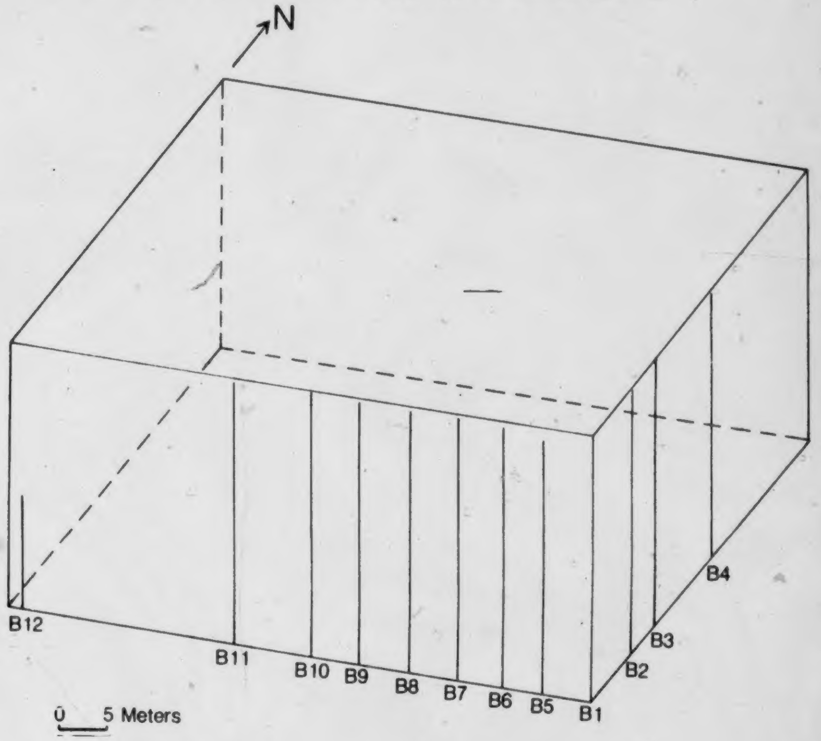
N
B12
B11
B10
B9
B8
B7
B6
B5
B1
B2
B3
B4
0 5 Meters

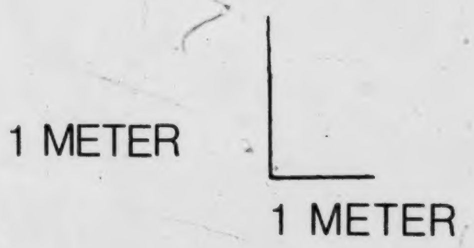
1 METER
1 METER

1.56 X VERTICAL EXAGGERATION

LITHOLOGIC CORRELATIONS FOR OUTCROP B

1

OF/DE

LOCATION OF SECTION

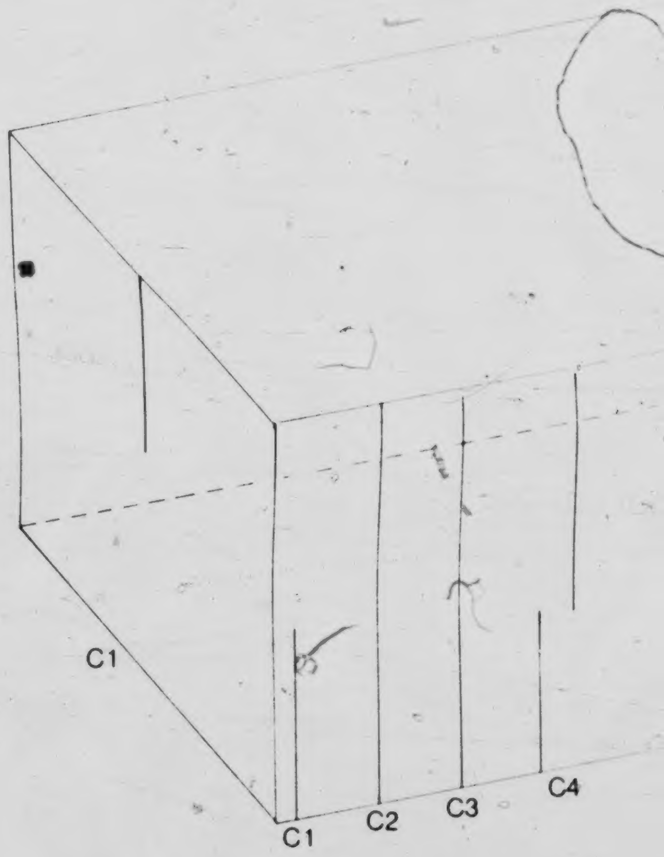
C1
C1
C2
C3
C4

2

OF/DE

LOCATION OF SECTIONS AT OUTCROP C

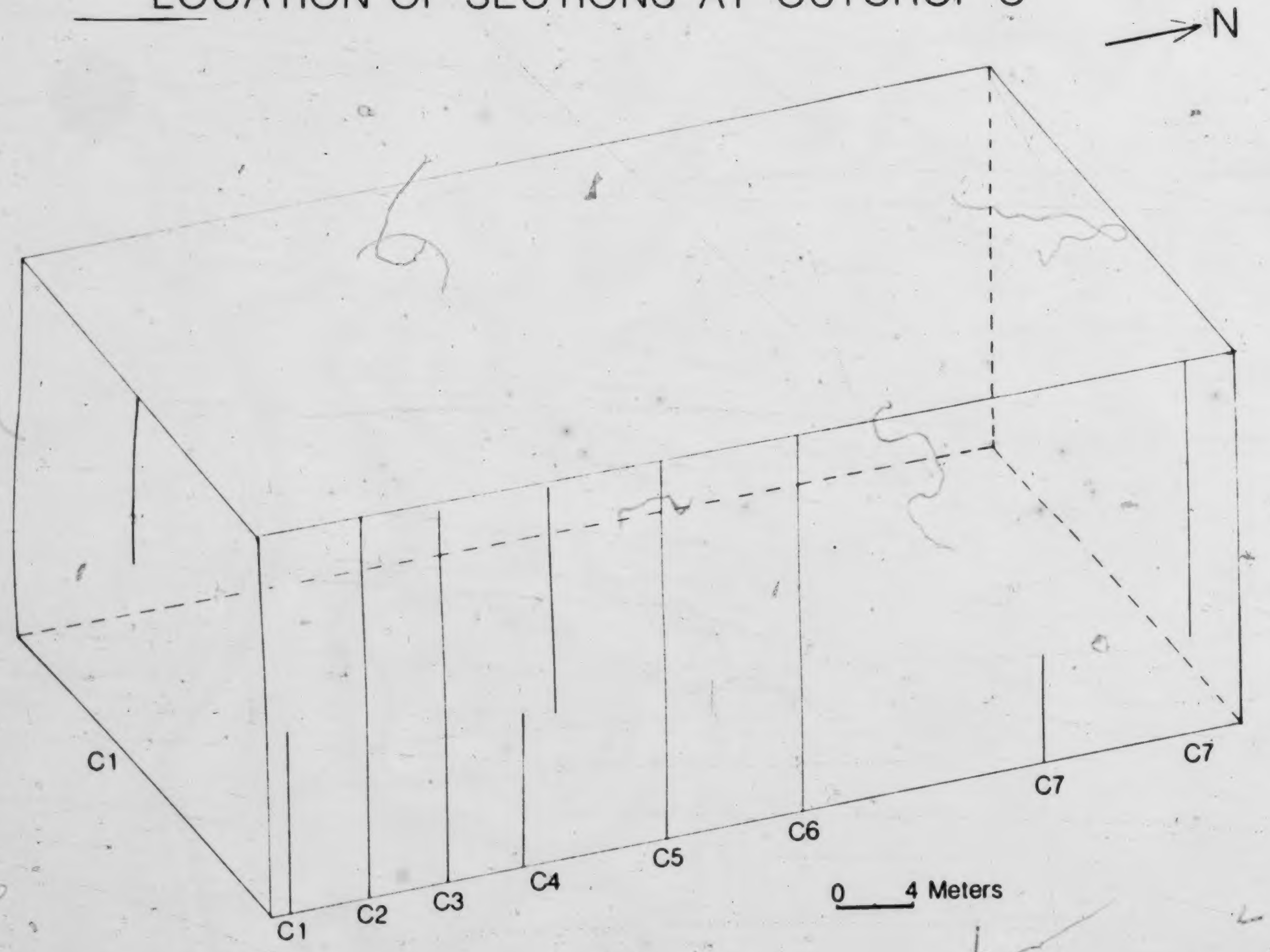
N
C1
C1
C2
C3
C4
C5
C6
C7
C7
0 4 Meters

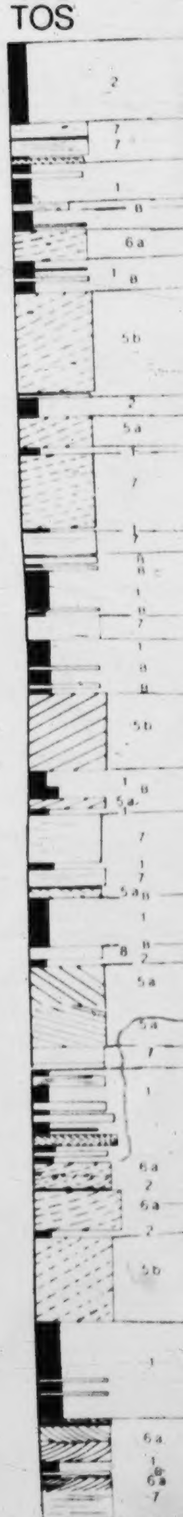
TOS
2
7
7
1
8
6a
1 8
5b
2
5a
7
8
1
8
7
1
8
8
5b
1 8
5a
7
1
7
5a
1
8
2
5a
5a
7
1
6a
2
6a
2
5b
1
6a
1
8
6a
7

COARSE/FINE-GRAINED INTERCALATED FACIES ASSOCIATION

ON

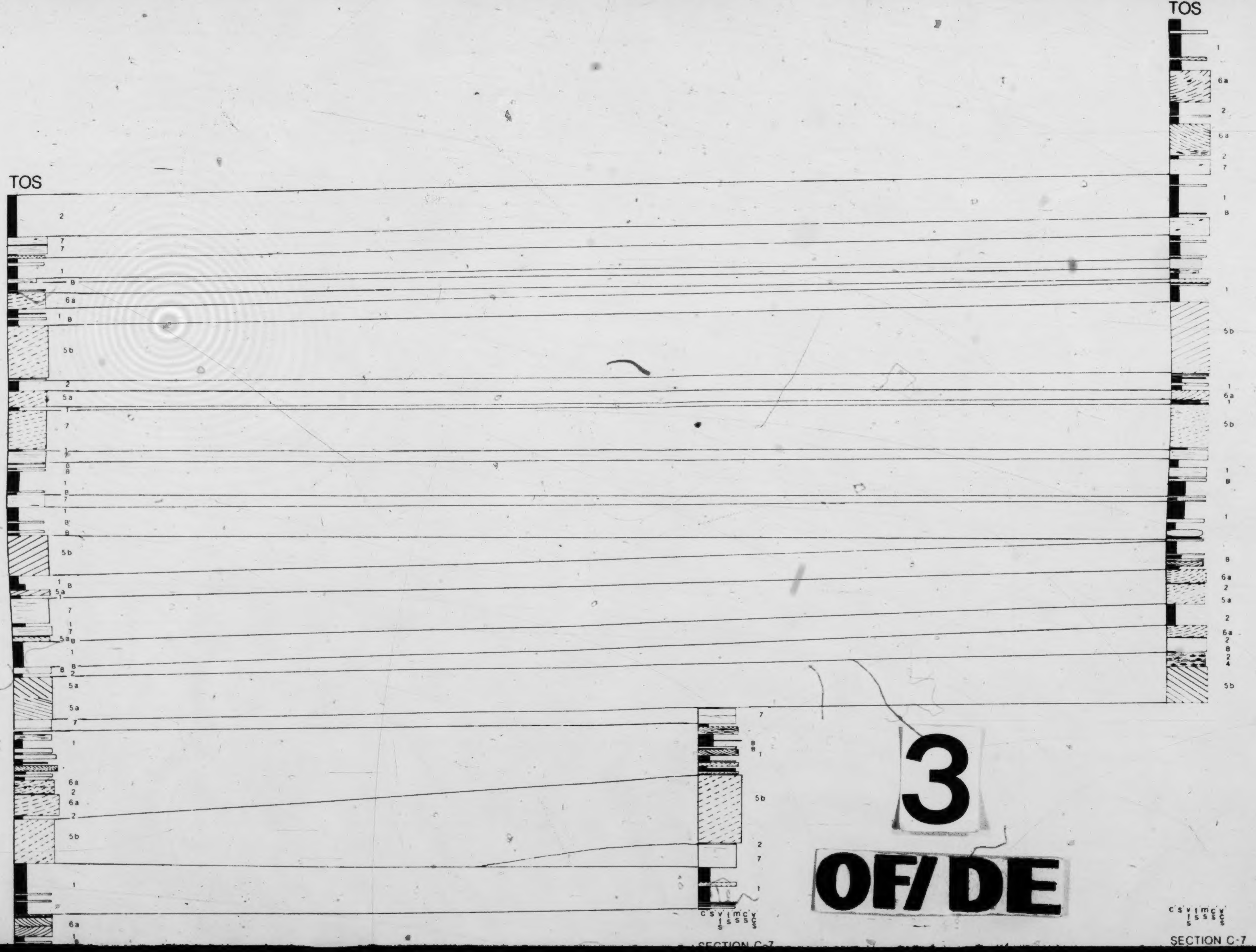

TOS
6a
5b
5a
5b
5a
5a
5a
5a
6a
6a
5b
6a
5b
c s v f m c v
SECTION C-7
TOS
6a
6a
5b
6a
5b
6a
5a
6a
5b
c s v f m c v
SECTION C-7

3

OF/DE

4

OF/DE

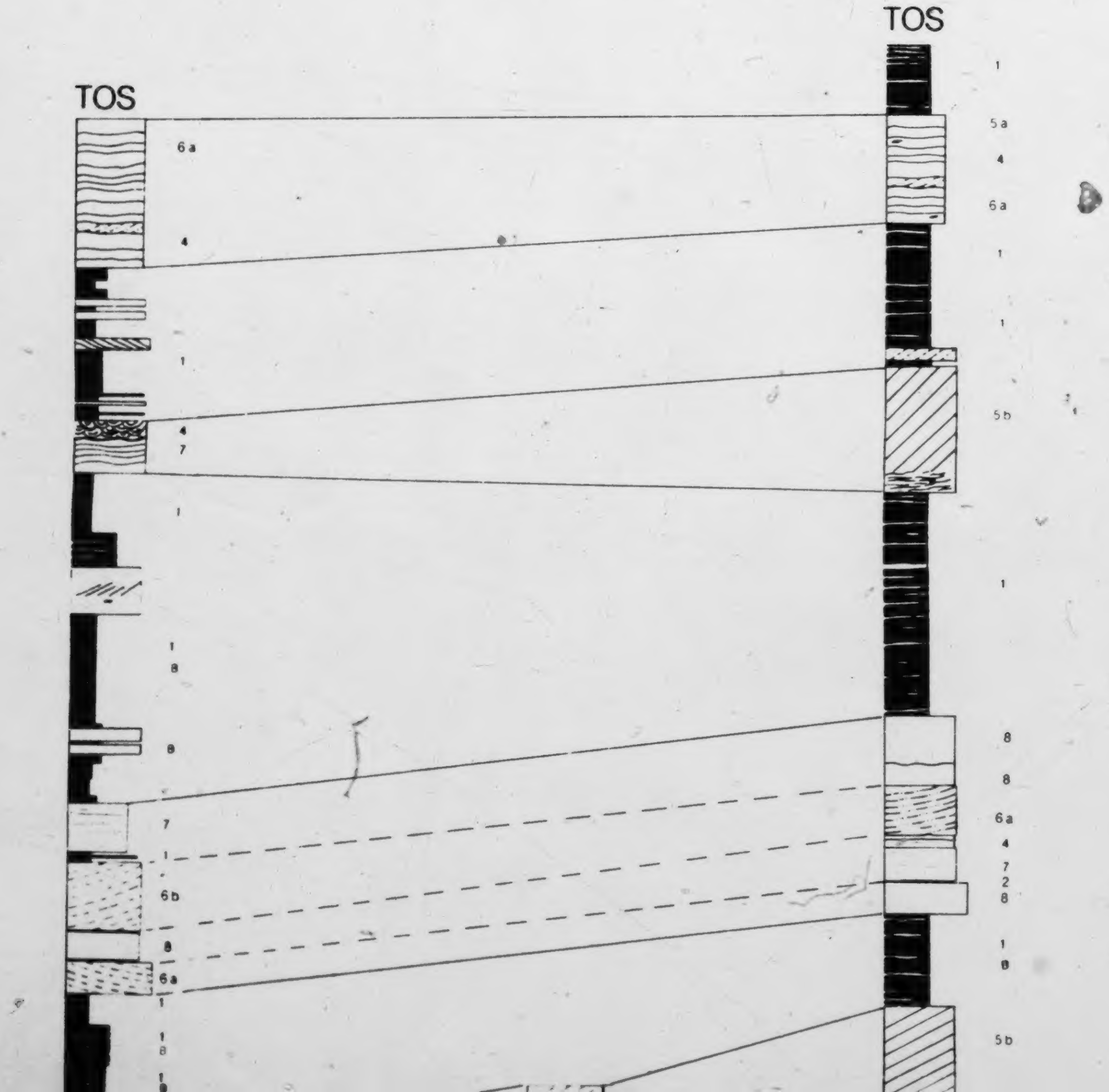
TOS
6a
4
1
4
7
1
1
8
8
7
1
6b
8
6a
1
1
8
TOS
1
5a
4
6a
1
1
5b
1
8
8
6a
4
7
2
8
1
8
5b

C1
C1
C2
C3
C4
C5

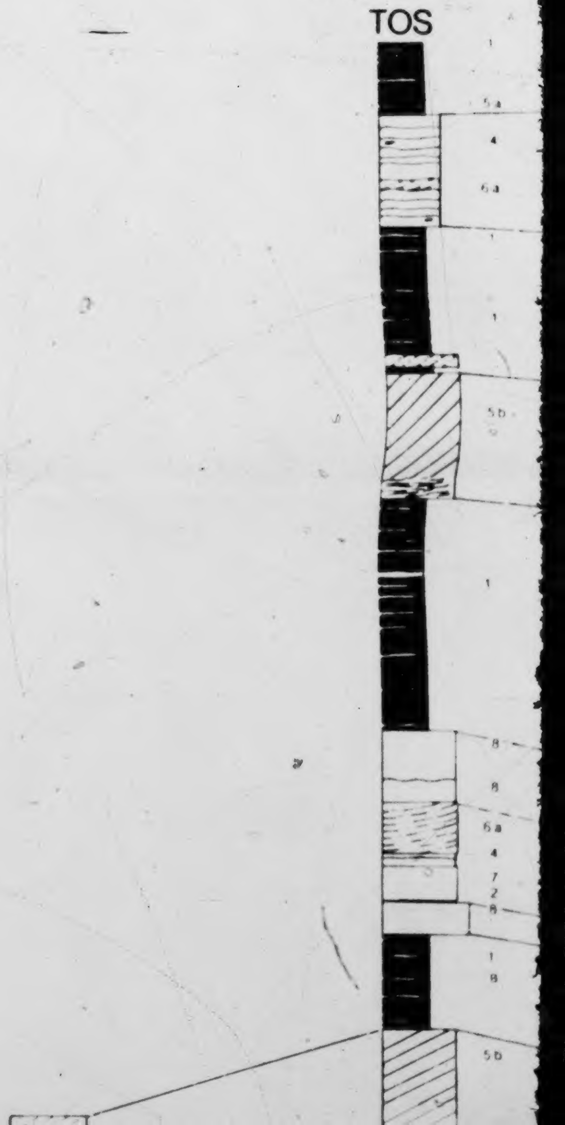
TOS
1
5a
4
6a
1
1
5b
1
8
8
6a
4
7
2
8
1
8
5b

COARSE/FINE-GRAINED INTERCALATED FACIES ASSOCIATION

5

OF/DE

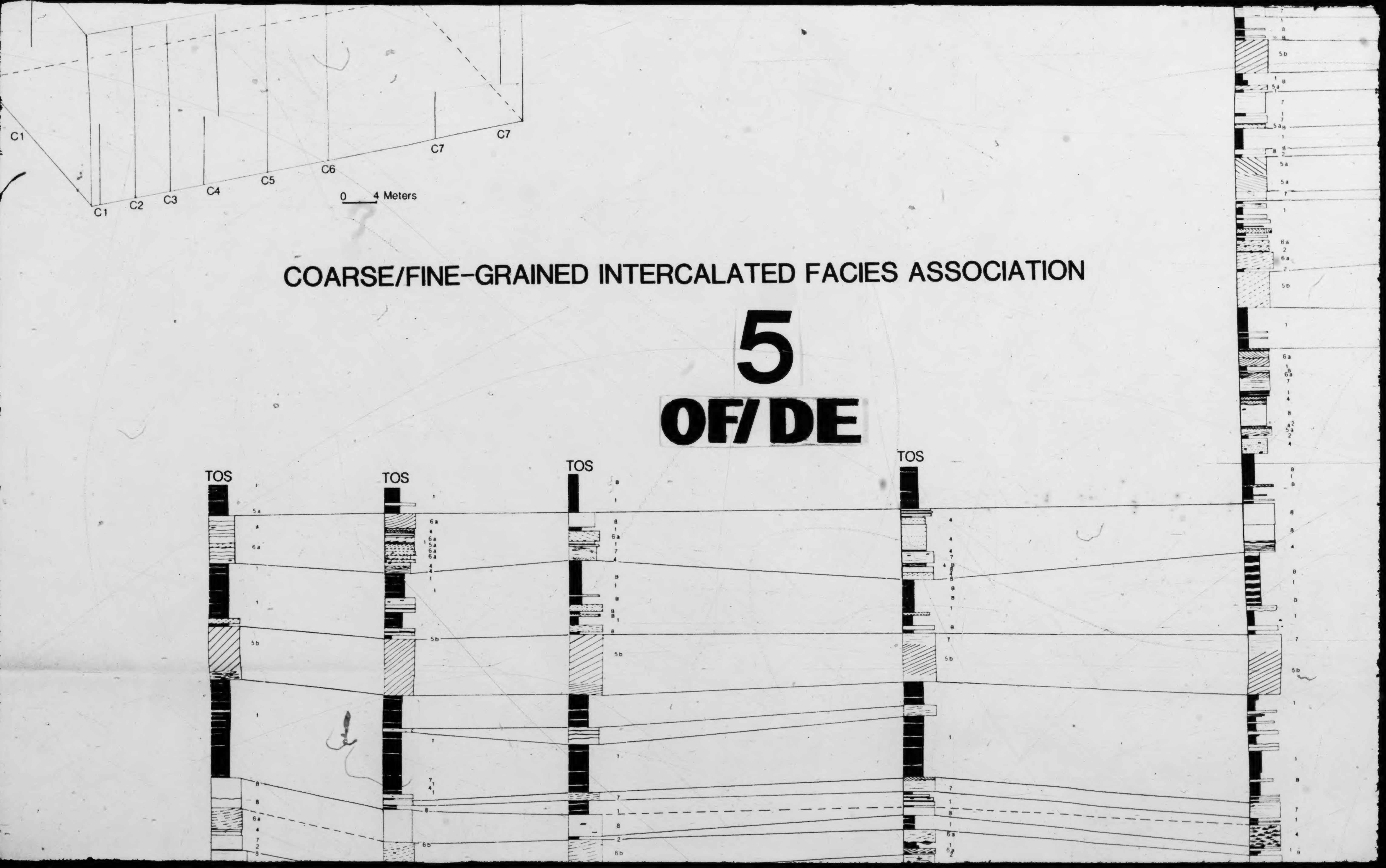
C1
C1
C2
C3
C4
C5
C6
C7
C7
0 4 Meters
TOS
TOS
TOS
TOS
1
5a
4
6a
5b
6b
7
8
2

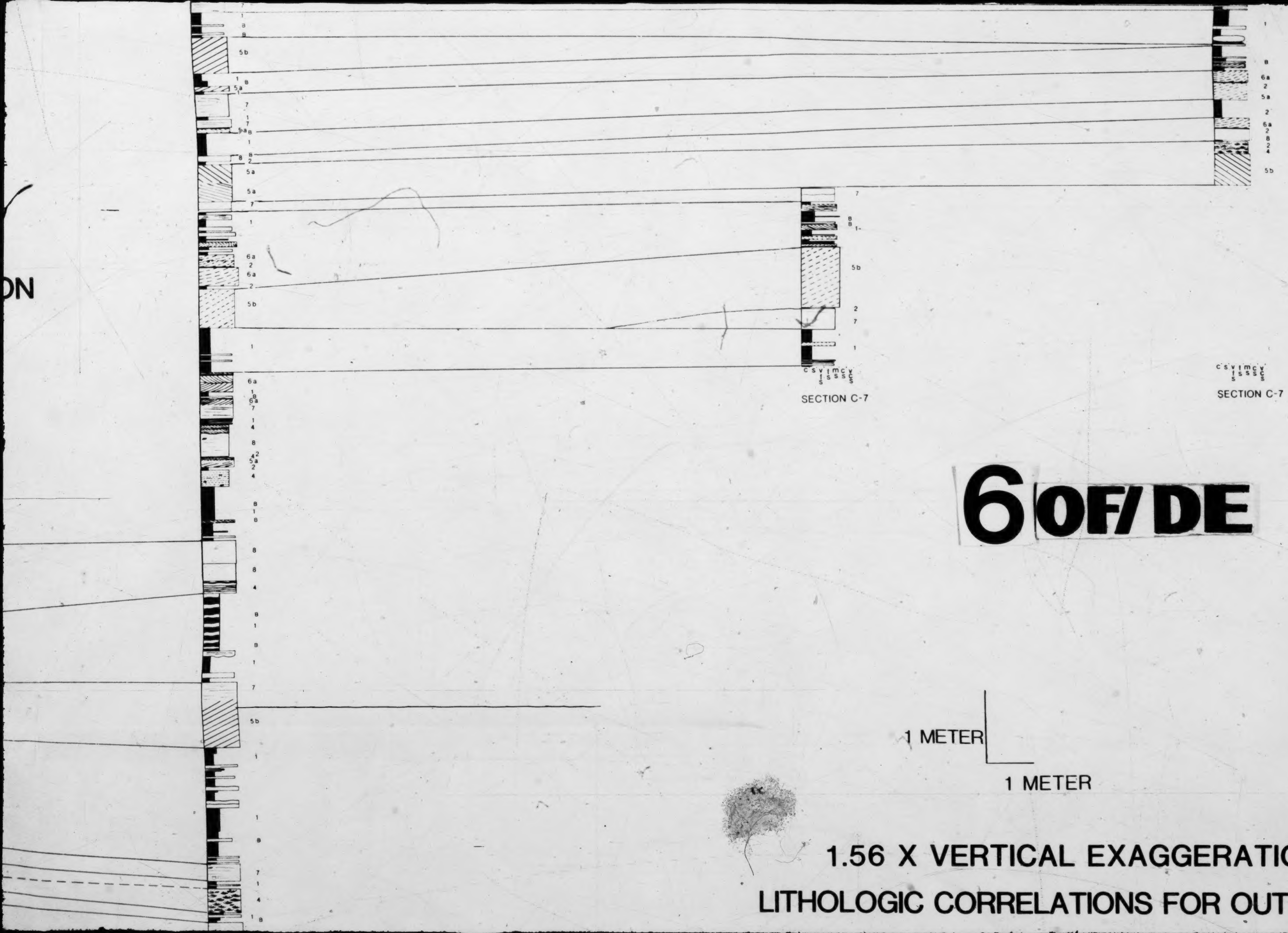
ON
1
8
5b
5a
7
6a
2
4
c s v l m c v
f s s s c
s s s
SECTION C-7
SECTION C-7
1 METER
1 METER

6 OF/DE

1.56 X VERTICAL EXAGGERATION

LITHOLOGIC CORRELATIONS FOR OUTCROP C

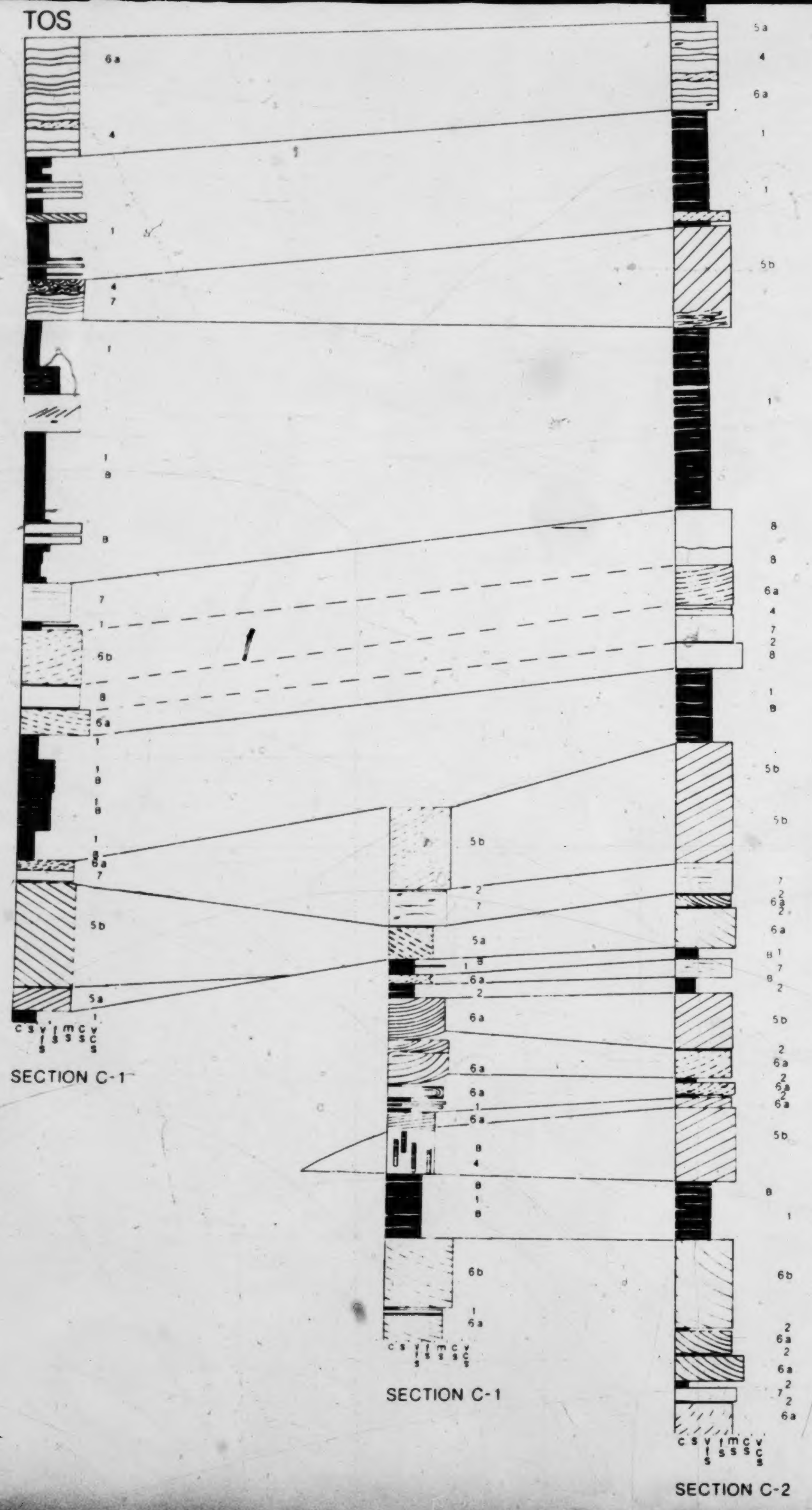
TOS
6a
4
1
4
7
1
1
8
8
7
1
6b
8
6a
1
1
8
1
8
1
8
6a
7
5b
5a
1
c s vf f m c v
s s s s c
s
SECTION C-1
5b
2
7
5a
8
1
6a
2
6a
6a
6a
1
6a
8
4
8
1
8
6b
1
6a
c s vf f m c v
s s s s c
s
SECTION C-1
5a
4
6a
1
1
5b
1
8
8
6a
4
7
2
8
1
8
5b
5b
7
2
6a
2
6a
8
7
8
2
5b
2
6a
6a
2
6a
5b
8
1
6b
2
6a
2
6a
7
2
6a
c s vf f m c v
s s s s c
s
SECTION C-2

7
OF/DE

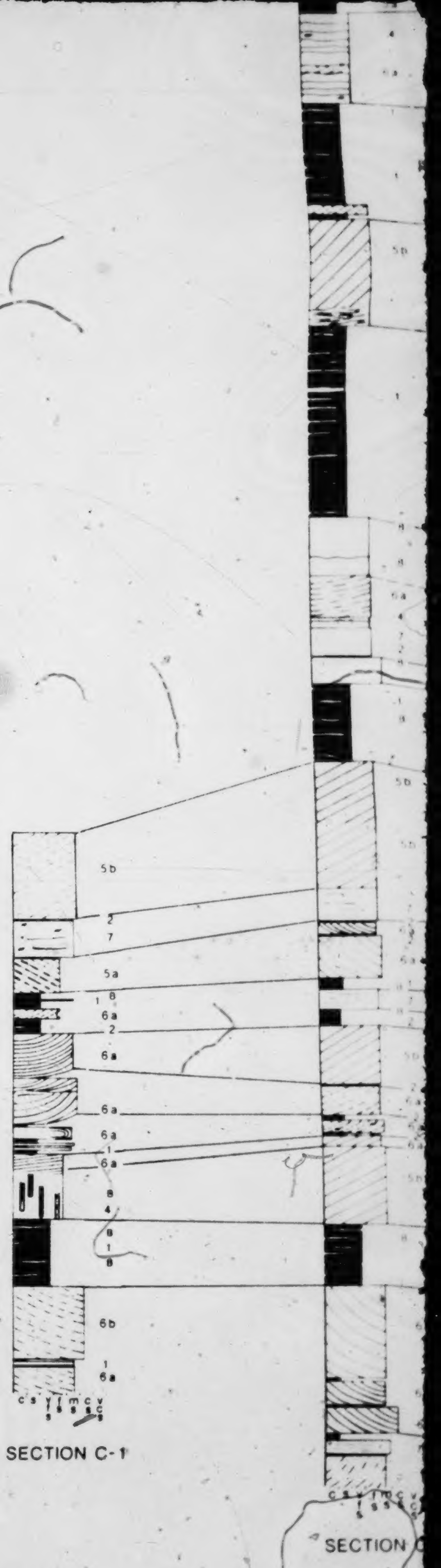
5b
2
7
5a
8
1
6a
2
6a
6a
6a
1
6a
8
4
8
1
8
6b
1
6a
c s vf f m c v
s s s s c
s
SECTION C-1
SECTION C

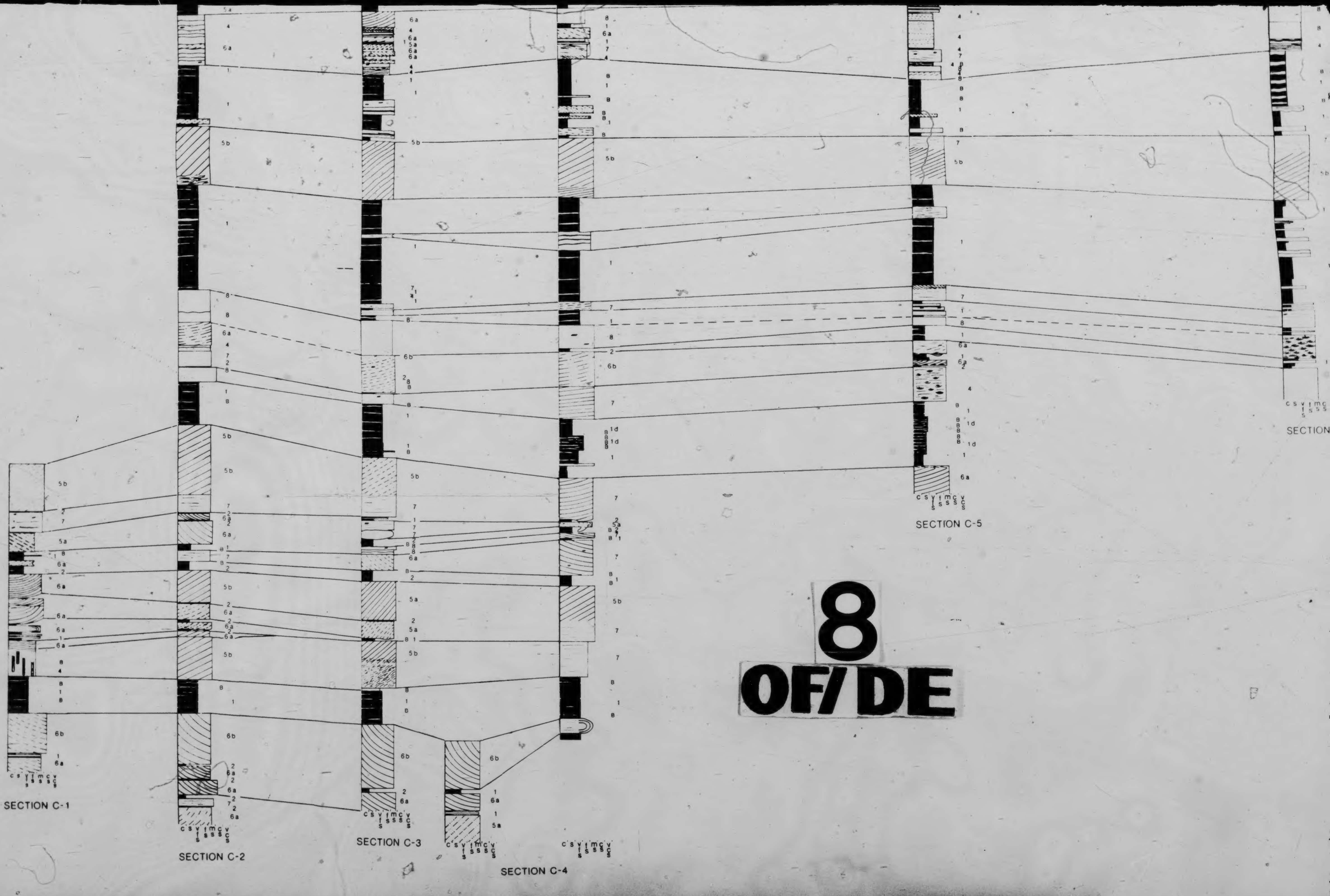
c s vf f m c vc
SECTION C-1
SECTION C-2
SECTION C-3
SECTION C-4
SECTION C-5
SECTION

8
OF/DE

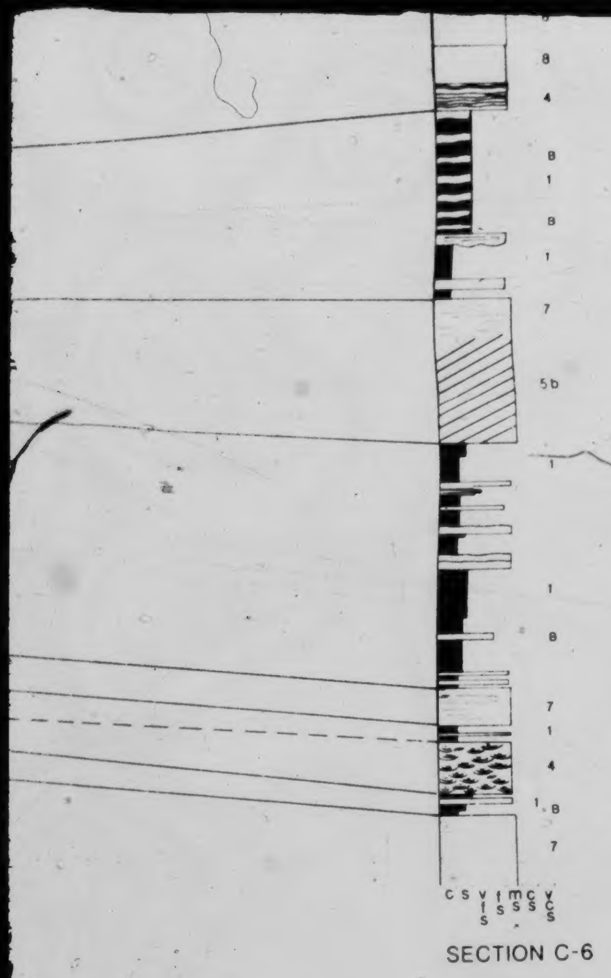
8
4
8
1
8
1
7
5b
1
1
8
7
1
4
1
8
7
c s vfs fs ms cs vcs
SECTION C-6

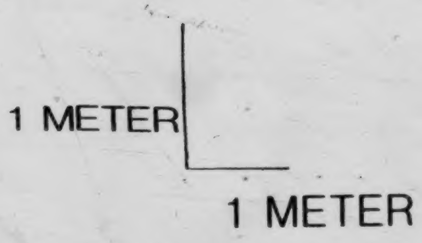
1 METER
1 METER

1.56 X VERTICAL EXAGGERATION

LITHOLOGIC CORRELATIONS FOR OUTCROP C

9 OF/DE 9

1
OF/DE

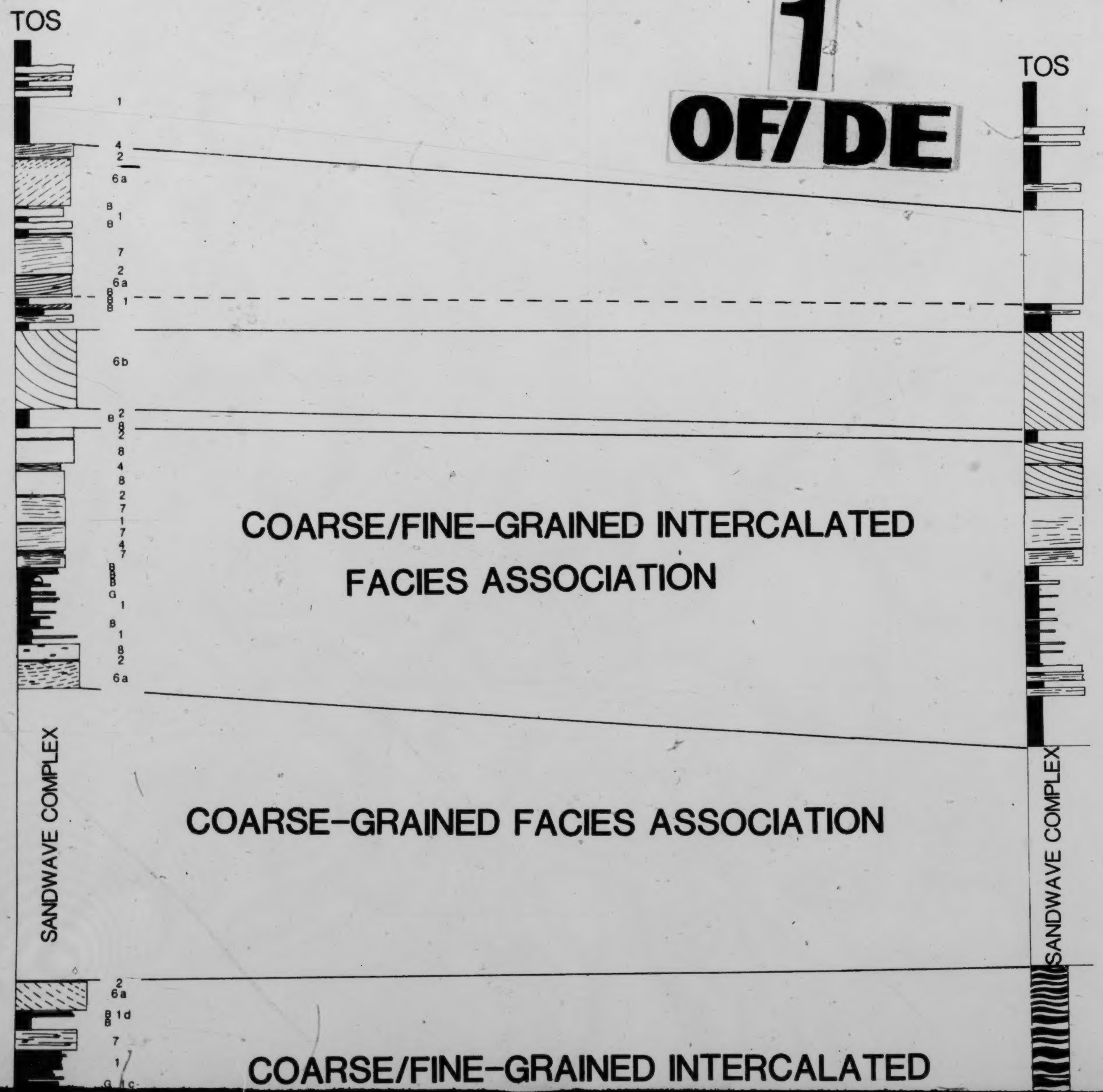
TOS
TOS
SANDWAVE COMPLEX
SANDWAVE COMPLEX
COARSE/FINE-GRAINED INTERCALATED FACIES ASSOCIATION
COARSE-GRAINED FACIES ASSOCIATION
COARSE/FINE-GRAINED INTERCALATED
1
4
2
6a
B
1
B
7
2
6a
1
6b
2
8
2
8
4
8
2
7
1
7
4
7
G
1
B
1
8
2
6a
2
6a
1d
7
1
G
1
6b
6b
1
5b
1
6a
2
6a
2
7
2
7
B
1
B
1

LOCATION OF SECTIONS AT OUTCROP D

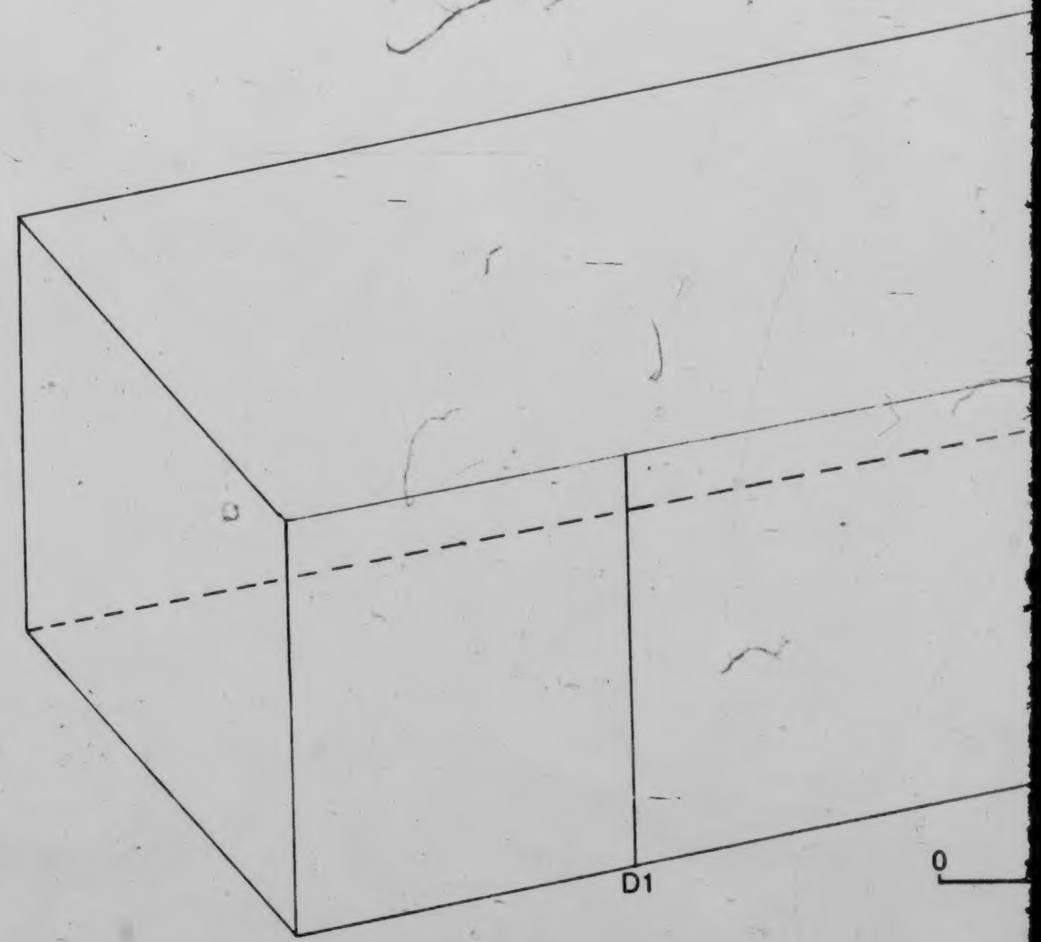

2
OF/DE

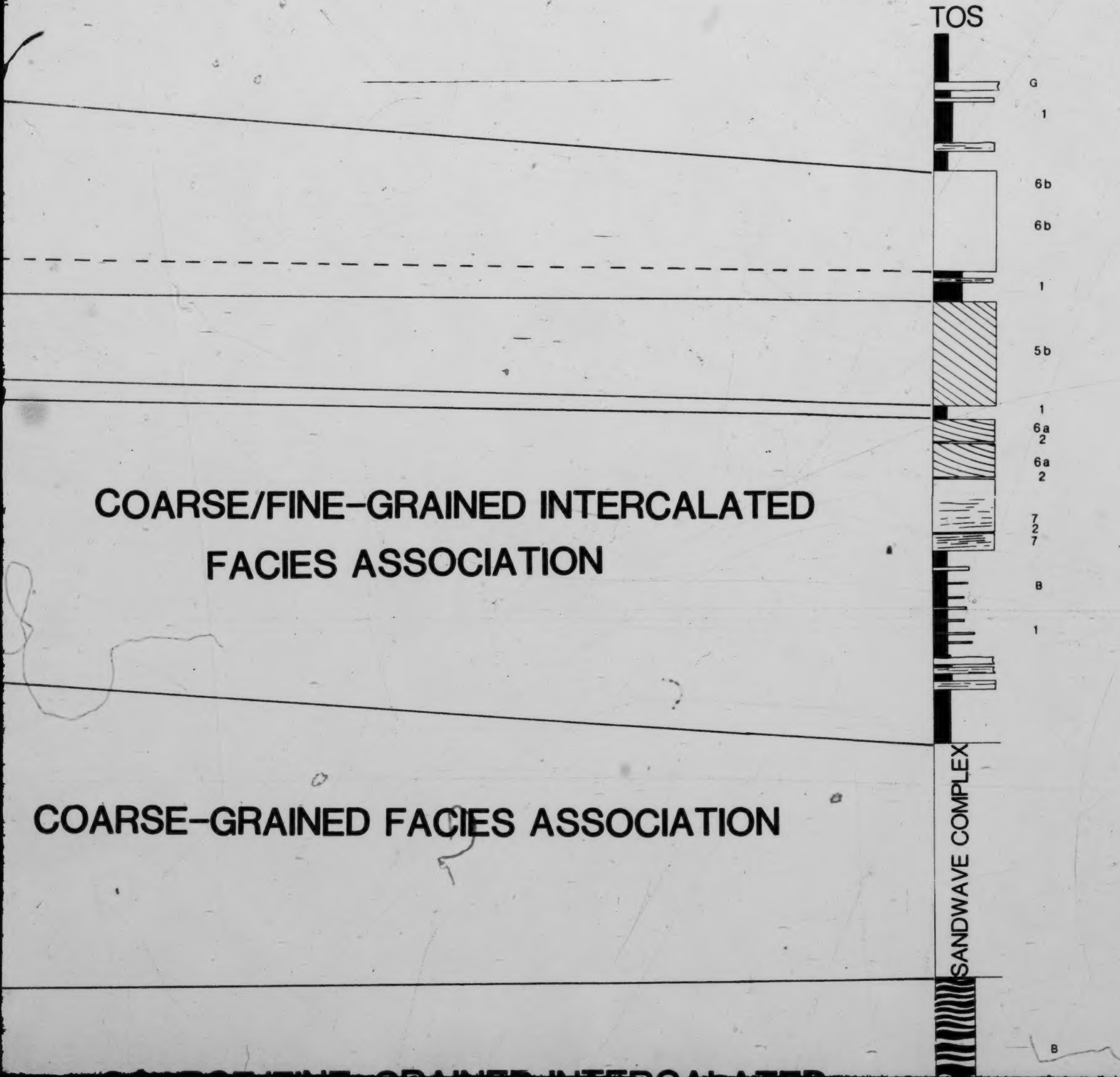
TOS
G
1
6b
6b
1
5b
1
6a
2
6a
2
7
2
7
B
1
COARSE/FINE-GRAINED INTERCALATED FACIES ASSOCIATION
SANDWAVE COMPLEX
COARSE-GRAINED FACIES ASSOCIATION
B

LOCATION OF SECTIONS AT OUTCROP D

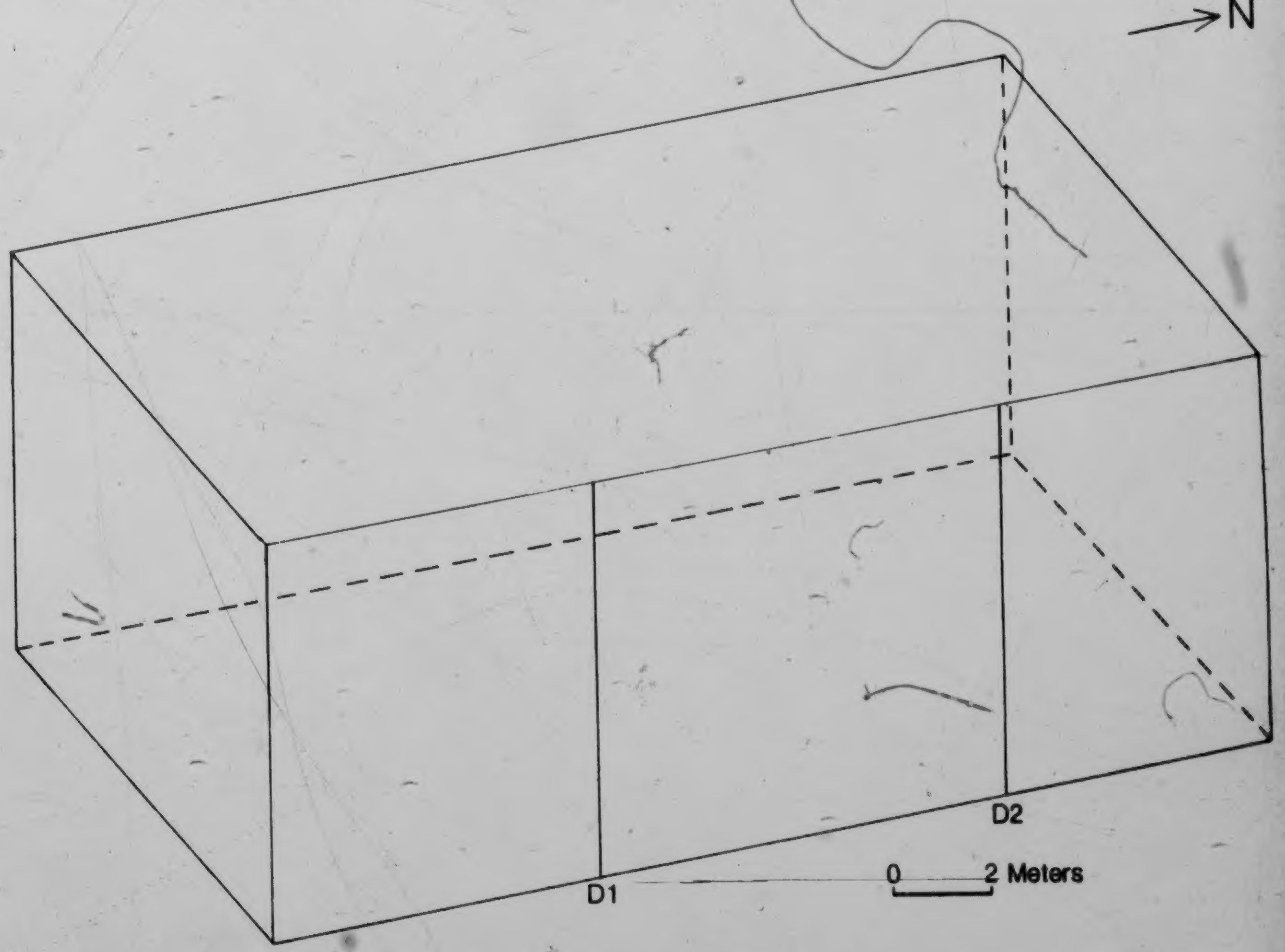
N
D1
D2
0
2 Meters

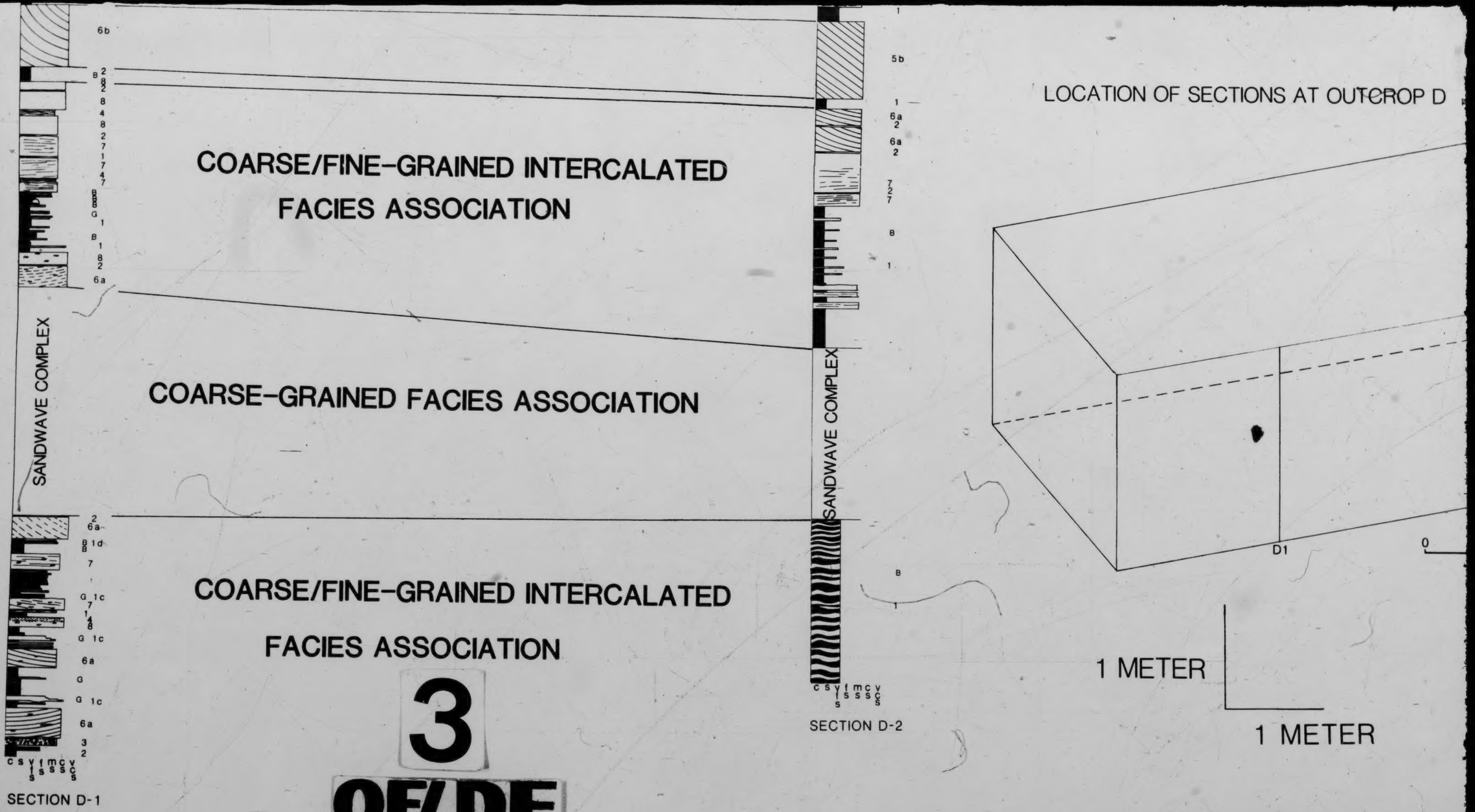
6b
B 2
8
2
8
4
8
2
7
1
7
4
7
B
B
B
G
1
B
1
8
2
6a
5b
1
6a
2
6a
2
7
2
7
B
1
COARSE/FINE-GRAINED INTERCALATED FACIES ASSOCIATION
SANDWAVE COMPLEX
COARSE-GRAINED FACIES ASSOCIATION
SANDWAVE COMPLEX
2
6a
B 1d
B
7
G 1c
7
1
4
8
G 1c
6a
G
G 1c
6a
3
2
COARSE/FINE-GRAINED INTERCALATED FACIES ASSOCIATION
B
1
c s vf m c v
f s s s c
s s
SECTION D-1
c s vf m c v
f s s s c
s s
SECTION D-2
LOCATION OF SECTIONS AT OUTCROP D
D1
0
1 METER
1 METER

3

OF/DE

1.04 X VERTICAL EXAGGERA

LITHOLOGIC CORRELATIONS FOR OUTC

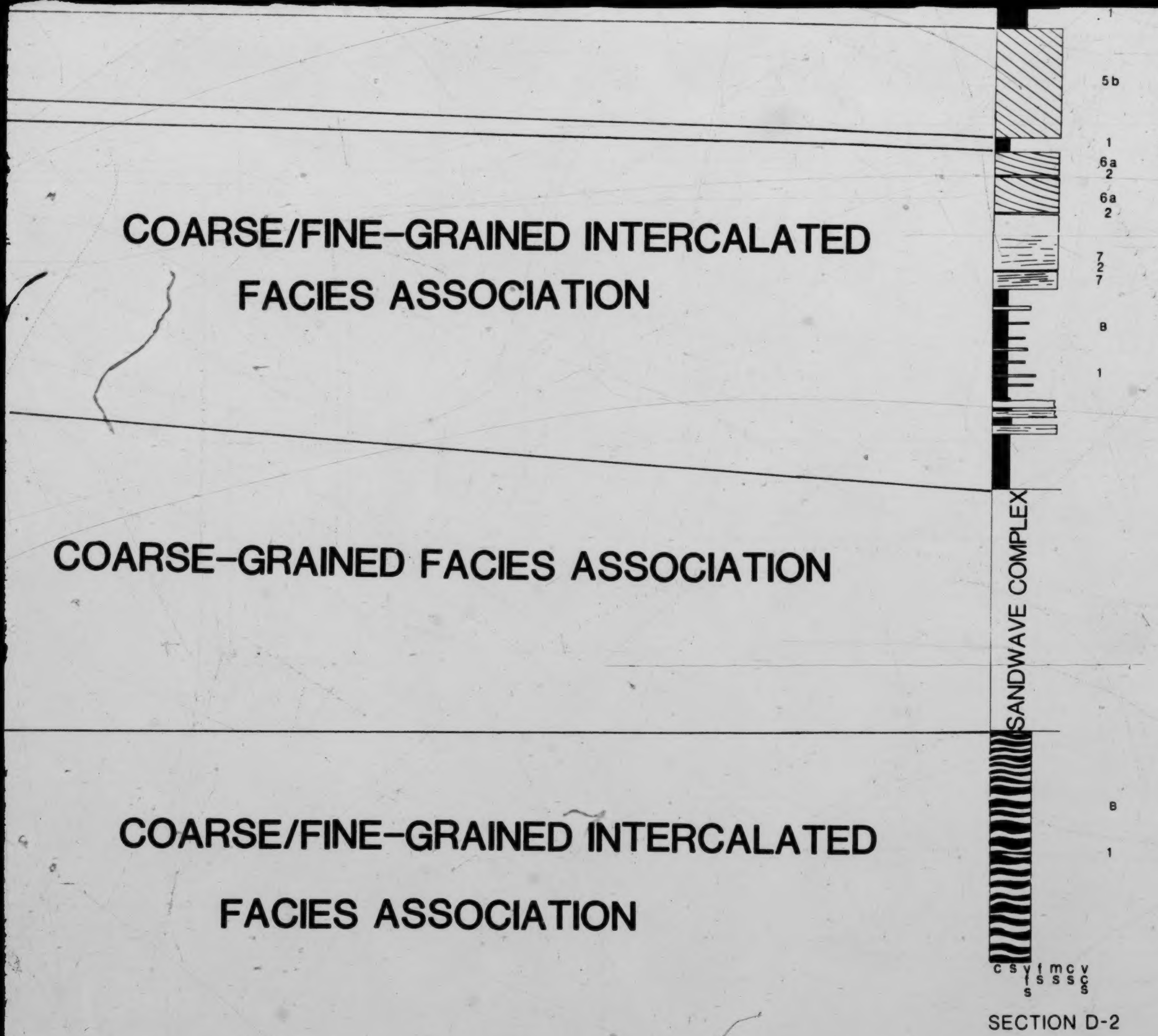
5b
1
6a
2
6a
2
7
2
7
8
1
COARSE/FINE-GRAINED INTERCALATED FACIES ASSOCIATION
SANDWAVE COMPLEX
COARSE-GRAINED FACIES ASSOCIATION
8
1
COARSE/FINE-GRAINED INTERCALATED FACIES ASSOCIATION
c s vf f m c vc
s s s s s s
SECTION D-2

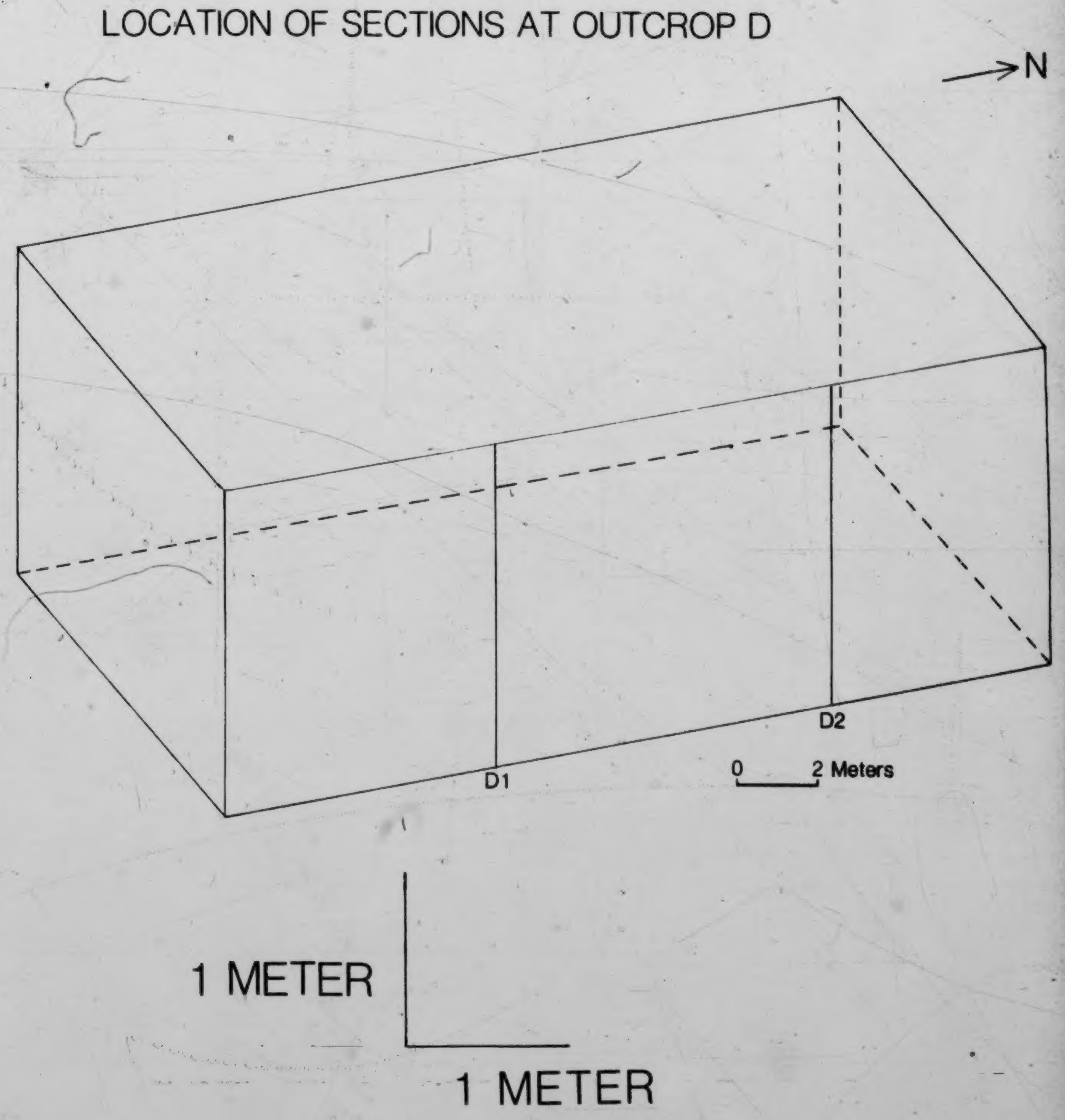
LOCATION OF SECTIONS AT OUTCROP D
N
D1
D2
0 2 Meters
1 METER
1 METER

4 OF/DE 4

1.04 X VERTICAL EXAGGERATION

LITHOLOGIC CORRELATIONS FOR OUTCROP D